

Techno-Economic Assessment of Steam Recovery Integration in the Bayer Process for Low-carbon Alumina Production

Siyun Ning

Thesis submitted for the degree of Doctor of Philosophy

School of Chemical Engineering

Faculty of Sciences, Engineering and Technology

Adelaide University, Australia

Dec 2025

Table of contents

ABSTRACT ..... **V**

DECLARATION ..... **IX**

ACKNOWLEDGEMENTS ..... **X**

CHAPTER 1-INTRODUCTION **1**

1.1 Background **2**

1.2 Significance of the work **5**

1.3 Scope and structure of the thesis **5**

CHAPTER 2-LITERATURE REVIEW **8**

2.1 Bayer process **9**

Digestion 9

Clarification 11

Precipitation and Evaporation 11

Calcination 12

2.2 Waste vapour recovery as a decarbonisation pathway **16**

2.3 Steam recovery or heat recovery technologies **16**

2.3.1 Multi-stage mechanical vapour recompression (MVR) 18

2.3.2 Multi-stage thermal vapour recompression (TVR) 20

2.3.3 System efficiencies and economic analysis.....21

2.4 Electric boilers as a decarbonisation pathway 22

2.5 Low carbon calcination technologies integrated with steam recovery.....24

2.5.1 Concentrated solar thermal energy.....25

2.5.2 Pressurised two-stage calcination with steam recovery 25

2.5.3 Hydrogen calcination 26

2.5.4 Electrified calcination 28

2.6 Alumina calcination process under steam environment.....29

2.6.1 The effects of air and steam environments on the calcination performance 29

2.6.2 The effects of steam environment on overall energy consumption 29

2.6.3 The effects of steam environment on alumina quality 30

2.7 Challenges in steam recovery from the calcination process.....31

2.7.1 High-concentration steam recovery from steam calcination.....31

2.7.2 Heat and steam recovery from the exit gas from air calcination.....34

2.8 Steam recovery from both calcination and Bayer circuit.....35

2.9 Objectives of the thesis.....36

2.10 References 37

CHAPTER 3 45

Techno-economic Assessment of Decarbonising Alumina Calcination Using Hydrogen Combustion with Steam Recovery 45

Preface **46**

CHAPTER 4 ..... **92**

Techno-economic Assessment of Integrated Steam Cleaning and Recovery from Alumina Calcination for various decarbonisation scenarios **92**

Preface **93**

CHAPTER 5 ..... **111**

Techno-economic Assessment of Multi-stage Mechanical Vapour Recompression (MVR), Thermal Vapour Recompression (TVR) and Integrated TVR-MVR Systems for Net-zero Steam Generation in Alumina Refineries **111**

Preface **112**

CHAPTER 6 ..... **142**

Optimisation of Steam Recovery from Calcination and the Bayer circuit using Multi-stage Mechanical Vapour Recompression **142**

Preface **143**

CHAPTER 7-CONCLUSIONS **154**

7.1 Applying hydrogen combustion in calcination while increasing the viability of steam recovery **154**

7.2 Integrated steam cleaning and recovery from various calcination scenarios **155**

7.3 Comparison of various steam compression technologies.....155

7.4 Optimisation of steam recovery from the Bayer circuit and calcination 156

CHAPTER 8-FUTURE WORK RECOMMENDATION.....158

SUPPLEMENTARY APPENDIX FOR CHAPTER 4 162

Process Modelling for Retrofitting Alumina Calcination for Fully electrification 162

Preface 162

Abstract

Recovering available waste water vapour from the alumina refining process presents a promising method to improve overall energy efficiency and reduce reliance on fossil fuel steam generation. This study conducted a comprehensive techno-economic assessment to understand the viability of recovering waste vapour (typically at ~1 atmospheric pressure or 0.14 bar) from the Bayer process. Various steam recovery technologies, including multi-stage MVR (mechanical vapour recompression), multi-stage TVR (thermal vapour recompression), and integrated TVR-MVR systems were assessed in terms of their energy consumption and coefficient of performance (COP) for recompressing vapour to high-pressure (typically 5-15 bar, 175°C to 230°C), representative of low-temperature digestion condition in the refining process. In particular, steam-cleaning and recovery from the steam calcination (H_2 in oxygen-steam combustion or fully electrified calcination) was analysed, which eliminates the direct CO_2 emissions from natural gas combustion during calcination while generates high-concentration steam that can be recovered for the Bayer process.

Firstly, this study assessed the technical viability of a novel retrofitted calciner design that accommodates H_2 in oxygen-steam combustion integrated with steam recovery. A detailed calcination model was developed in Aspen Plus to estimate the heat utilisation efficiency, calciner units such as cyclones' performance and overall energy consumption under steam environment, and to compare with conventional natural gas/air combustion. Energy consumption under H_2 in oxygen-steam calcination was calculated to be slightly higher than natural gas/air combustion, at 2.89-2.96 GJ/$t_{Al_2O_3}$ (LHV) compared with 2.88 GJ/$t_{Al_2O_3}$ (LHV). This increase is caused by the inhibited pre-calcination reaction, which indirectly lowers the heat transfer efficiency under a steam-rich environment than in an air environment. However,

it produces high-concentration steam for recovery, enabling efficient recovery of its latent energy. Cyclone performance under the steam environment was found to remain comparable pressure drop and separation efficiency (>97%) using recirculated superheated steam as carrier gas.

Secondly, this study estimated an integrated steam cleaning and recovery process for high-concentration steam recovery from steam calcination (H_2 in oxygen-steam combustion and fully electrified calcination), with an integrated venturi scrubber removing fine particles prior to multi-stage MVR system. The work also examined the recovery of diluted steam mixed with N_2 and CO_2 from air calcination (including H_2/air and natural gas/air combustion) by adopting gas separation process prior multi-stage MVR system. Results show that the associated energy penalty for gas separation and steam cleaning accounts for 5%-9% of the energy consumption in steam recovery, with remaining 91-95% for MVR systems. Steam recovery from fully electrified calcination or H_2 in oxy-steam combustion achieves recovery rates of 0.64 $t_{steam}/t_{Al_2O_3}$ and 0.86 $t_{steam}/t_{Al_2O_3}$, respectively, with an energy consumption of 0.54 GJ/t_{steam}. Steam recovery from air-fired calcination achieves lower recovery rate of 0.54-0.55 $t_{steam}/t_{Al_2O_3}$, consuming 0.71 GJ/t_{steam} energy. The recovered steam from various calcination pathways was estimated to offset 27%, 32%, and 43% of the total steam demand in the Bayer circuit, assuming an average steam consumption of 2 $t_{steam}/t_{Al_2O_3}$, which is presently supplied by natural gas boilers. This leads to corresponding reductions in overall energy consumption for steam supply by 21%, 27% and up to 36%, respectively.

Thirdly, the study assessed various steam recovery technologies, including multi-stage MVR, multi-stage TVR, and proposed integrated TVR-MVR by developing comprehensive models in Aspen Plus and MATLAB. Among the options, MVR system achieves the highest efficiency, achieving COP values of 3.2 (for the vapour inlet pressure at 0.14 bar) and 5.7 (For

the vapour inlet pressure at 1 bar) for recompressing steam to 8 bar, representative of steam condition in the low-temperature digestion, whereas natural gas boilers operate at a COP of 0.8. The integrated TVR-MVR configuration reduces the MVR stage and thereby lowers the operational risk. However, the COP decreases to 1.9 when compressing from ~1 bar to 8 bar. Multi-stage TVR is less technically feasible, with COP reducing to 1.0 (for the case of 0.14 bar) and 1.4 (for the case of ~1 bar) for recompressing to 8 bar.

Finally, the study assessed the optimisation of steam recovery from both calcination and the Bayer circuit using multi-stage MVR systems. The results demonstrate the 100 % of steam demand for Bayer circuit usage can potentially be met via internal recovery, with contributions of 43% from the proposed scenario of H_2 in oxygen-steam calcination, 9% from digestion, 37% from evaporation, and 11% from precipitation. The proposed steam recovery enables energy reduction from 6.64 to 1.41 GJ/$t_{Al_2O_3}$, representing 79% energy conservation relative to steam generation from natural gas boilers. In addition, transitioning from fossil fuel steam generation to electricity-powered steam recovery could eliminate direct carbon emissions. Economically, in comparison with natural gas boilers at a gas price of 7.5 US$/GJ plus a carbon capture and storage cost (CCS) of 179 US$/$t_{CO_2}$, the estimated levelised cost of decarbonised steam for the Bayer circuit ($LCOS_B$) decreases by 50 % at a fixed 70 US$/MWh electricity price, reducing from 110.2 to 55.1 US$/$t_{Al2O3}$. This reduction is accompanied by a significant increase in capital investment for the MVR systems, accounting for 50 % of $LCOS_B$.

This study evaluates key decarbonisation technologies that could be implemented in the Bayer process, including hydrogen combustion for calcination, mechanical and thermal vapour recompression for steam recovery, and electric boilers for steam generation, with particular emphasis on the technical and economic viability of steam recovery. The results demonstrate

the potential of these technologies from both technical and economic perspectives to support low-carbon alumina production.

Declaration

I certify that this work contains no material which has been accepted for the award of any other degree or diploma in my name, in any university or other tertiary institution and, to the best of my knowledge and belief, contains no material previously published or written by another person, except where due reference has been made in the text. In addition, I certify that no part of this work will, in the future, be used in a submission in my name, for any other degree or diploma in any university or other tertiary institution without the prior approval of the University of Adelaide and where applicable, any partner institution responsible for the joint award of this degree. The author acknowledges that copyright of published works contained within the thesis resides with the copyright holder(s) of those works. I give permission for the digital version of my thesis to be made available on the web, via the University's digital research repository, the Library Search and also through web search engines, unless permission has been granted by the University to restrict access for a period of time.

Siyun Ning Date

03/12/2025

Acknowledgements

I am deeply grateful for the support that has carried me through this journey. I acknowledge with appreciation the University of Adelaide Research Scholarship and the Heavy Industry Low-carbon Transition Cooperative Research Centre (HILT CRC) top-up scholarship, which made this work possible.

I would like to express my heartfelt gratitude to my supervisors, Dr. Woei Saw, Prof. Peter Ashman, and Prof. Graham Nathan, for their invaluable supervision, guidance, and encouragement throughout the challenges and achievements of the past few years. I am especially grateful to Dr. Saw for his constant support, motivation, and for introducing me to the HILT CRC program. I sincerely thank Prof. Ashman and Prof. Nathan for their expert advice in academic and technical writing, and for their significant contributions to the publications arising from this work.

I also acknowledge the opportunities provided through HILT CRC, which enabled collaboration with experienced industry advisors from alumina refineries. I am deeply grateful to David Cochrane, Ray Chatfield, and Andrew Furlong for their valuable insights and feedback, and for generously sharing their experience and extensive knowledge in alumina refining. I also thank HILT CRC for supporting students and creating opportunities to present our work, which helped me strengthen my presentation skills, an experience that will be invaluable for my future career. To my colleagues at the University of Adelaide, Dr. Gule Li, Dr. Peijun Guo, Dr. Nguyet Ky Ngo, Dr. Daniel Jin Tung Ang, and Dr. Nikhil Kirti, I am sincerely thankful for the valuable discussions, advice, and encouragement you have shared with me. Finally, and above all, I thank my beloved parents, Mr. Zhongyi Ning and Ms. Xiaolan Li. Your endless patience, faith, and love have been the quiet foundation of my life.

Chapter 1-Introduction

1.1 Background

In alignment with the Paris Agreement that limits the global warming to below 2°C and achieves net-zero emissions by around 2050-2070 [1-3], it is important to reduce associated CO_2 emissions in heavy industries such as cement, iron ore, alumina and aluminium [4, 5]. Australia produces 19 million tonnes of alumina annually, generating 14 million tonnes of CO_2 equivalent emissions [6, 7]. This emission accounts for approximately 24% of Australia's scope one manufacturing emissions, and 3% of nation's total emissions [8-10]. Therefore, it is essential to pursue decarbonisation of alumina refining to advance broader sustainable production objective [3, 11].

The alumina refining process, known as the Bayer process, is highly energy-intensive, consuming approximately 10.0-15.9 $GJ/t_{Al_2O_3}$ across different regions, depending on bauxite ore quality and technologies employed [12, 13]. Steam production from fossil fuel boilers accounts for a significant portion of the total energy use [14, 15]. High-pressure steam is consumed at 5-15 bar and 175°C to 230°C for dissolving gibbsite ores with caustic soda solution, and at 50-100 bar and 325-400 °C for the digestion of boehmite and diaspore ores [16, 17]. This steam is currently supplied from fossil fuel boilers [16, 17]. However, the Bayer process generates significant amounts of waste vapour, including vapour from evaporation (approximately 0.14 bar) and vapour from digestion (approximately ~1 bar). In addition, the calcination stage also releases diluted steam mixed with combustion products, mainly N_2 and CO_2, which further contributes to energy losses [18, 19]. Implementing effective steam recovery technologies to reduce the reliance on fossil fuel steam generation has been identified as one of the potential decarbonisation solutions. However, few studies have conducted a techno-economic analysis of energy efficiency improvements enabled by steam recovery.

Hence, one scope of the study is to explore and evaluate potential steam recovery technologies that enable energy conservation and contribute to low-carbon steam supply.

Steam recovery technologies such as mechanical vapour recompression (MVR) and thermal vapour recompression (TVR) enabling the reuse of low-pressure steam by recompressing it to higher pressure and temperature [20, 21]. Numerous studies have investigated the integration of single-stage MVR or TVR systems in wastewater treatment processes, demonstrating their effectiveness in energy savings [22-27]. However, few studies have developed models for multi-stage MVR or TVR systems and evaluated their integration in alumina refineries. Although a multi-stage MVR configuration has been evaluated by Chatfield [19], detailed understanding of system behaviour remains limited [28]. In addition, no comparative assessments have been conducted against alternative technologies such as TVR or electric boilers which plays a role in decarbonising steam generation. Therefore, this study aims to evaluate the integration of various steam recovery or generation technologies to decarbonise steam supply, and assess the techno- economic performance relative to conventional fossil-fuel boilers.

Calcination, the last step of Bayer process, converting gibbsite to smelter-grade alumina (SGA) at high temperature (~950-1000°C) using fossil fuel combustion [29], accounting for around 30% of total energy use in Australian refineries. This process also releases approximately 0.7 $t_{steam}/t_{Al_2O_3}$ steam, carrying latent energy of approximately 1.7 $GJ/t_{Al_2O_3}$ [30]. However, one of the barriers in steam recovery from calcination is that fossil fuel and air combustion introduces diluents like CO_2 and N_2 together with steam, while simultaneously emitting direct CO_2 emissions. Alternative calcination decarbonisation pathways, including hydrogen combustion or electric calciner, has been proposed to retrofit existing fossil fuel calciners [31]. Retrofitting air calcination to operate under steam environment can avoid the

issue of steam dilution in exit gas stream. However, no studies have evaluated retrofitting a calciner to accommodate either energy sources while simultaneously enabling high-concentration steam recovery. In addition, no studies have compared the calcination performance under steam and air calcination, particularly in terms of cyclone performance, heat utilisation and overall energy consumption. Hence, this study aims to understand such a steam-based calcination flowsheet with integrated steam recovery, and to analyse its performance relative to conventional air calcination.

Retrofitting an existing air-fired calciner to hydrogen combustion in an O_2-steam combustion enables the generation of high-concentration steam for recovery. However, fine entrained particles remain problematic, as existing particulate control systems such as electrostatic precipitator (ESP) or baghouses cannot fully capture solids smaller than 2 µm [32-34]. These particles can cause erosion, thereby negatively affecting the steam recovery system (MVR). To date, no flowsheet has been proposed that integrates a steam cleaning system prior to MVR, nor has the recovery efficiency been comprehensively assessed. Therefore, one objective in the study is to advance the understanding of the integrated steam cleaning and recovery for high-concentration steam recovery from steam calcination.

Through optimisation of steam recovery from both the Bayer process, it is possible to meet 100% of total steam demand. This approach can significantly reduce the reliance on fossil fuel steam generation, thereby lowering energy consumption and emissions. Currently, few studies have evaluated various low-carbon steam supply scenarios through integrating steam recovery from the Bayer process. Hence, the present study aims to meet this need by conducting a techno-economic analysis of alternative steam supply pathways, such as steam recovery from various stages in the Bayer process and steam generation from electric boilers, and benchmarked against fossil fuel boilers

1.2 Significance of the work

This work provides the systematic evaluation of integrating steam recovery as a decarbonising pathway in alumina refineries. By developing process models for multi-stage MVR and TVR systems, the study compares their efficiency against conventional steam generation methods, offering valuable insights into system performance. More importantly, the study estimates a novel retrofittable calciner design capable of accommodating hydrogen in oxygen-steam or electrified calcination under steam environment, thereby increasing the viability of steam recovery from calcination process. Overall, this work advances the understanding of steam recovery technologies and advances the development of a novel retrofittable steam-calcination calciner design with integrated steam recovery.

1.3 Scope and structure of the thesis

This thesis is divided into eight chapters including the introduction and an appendix chapter. The content of each chapter is listed below.

Chapter 2 comprises a comprehensive introduction regarding the Bayer process, with a focus on the digestion and calcination steps, followed by literature review on the potential decarbonisation technologies, including MVR and TVR systems for waste vapour recovery and plausible decarbonising calcination options. This chapter also summarises the research gaps and challenges in integrating steam recovery, as well as the research implications.

Chapter 3, titled “Techno-economic Assessment of Decarbonising Alumina Calcination Using Hydrogen Combustion with Steam Recovery” estimates a novel H_2 in oxygen-steam calcination under steam environment, which enables decarbonised calcination while enhancing the viability of steam recovery. This chapter assesses the calcination performance when hydrogen is used as a fuel, comparing it with current natural gas/air combustion process, with

a focus on the effects of steam environment on the cyclones performance, heat utilisation, and overall energy consumption. Additionally, this study also compares the economic performance of hydrogen combustion with current natural gas-based calcination process, especially the H_2 in oxygen-steam combustion case including the potential value of high-concentration steam.

Chapter 4, titled "Techno-economic Assessment of Integrated Steam Cleaning and Recovery from Alumina Calcination for various decarbonisation scenarios" investigates proposed steam cleaning and recovery system, aiming at overcoming challenges in steam recovery, such as the presence of fine particles and diluent gases. The study also estimates the energy efficiency improvement and economic benefits in steam supplying by integrating steam recovery from calcination.

Chapter 5, titled "Techno-economic Assessment of Multi-stage Mechanical Vapour Recompression (MVR), Thermal Vapour Recompression (TVR) and Integrated TVR-MVR Systems for Net-zero Steam Generation in Alumina Refineries" estimates system efficiencies of the various compression systems when implementing in alumina plants in comparison with traditional natural gas boilers. Additionally, it evaluates the levelised cost of steam for various steam recovery methods and benchmarks them against natural gas boilers.

Chapter 6, titled "Optimisation of Steam Recovery from Calcination and the Bayer circuit using Multi-stage Mechanical Vapour Recompression", estimates the technical and economic viability of various low-carbon steam supply scenarios by integrating steam recovery from various steps and the optimised 100% steam recovery case enabling net-zero steam supply.

Chapter 7 summarises the conclusions of the work. Chapter 8 summarises the recommendations for future work.

Supplementary Appendix for Chapter 4 presents the retrofittable calciner design for fully electrified calcination under a steam environment, together with preliminary process modelling of calcination. It provides indicative data on the exit steam from the calciner under electrified calcination to support the analysis in Chapter 4. References for Chapters are listed at the end of each chapter.

Chapter 2-Literature review

2.1 Bayer process

The Bayer process is for refining alumina from bauxite ore, normally requiring about two tonnes of bauxite to produce one tonne of smelter grade alumina (Al_2O_3) [35]. This process mainly consists of four steps: digestion, clarification, precipitation, and calcination [14], with a global average energy intensity of 15.9 GJ/$t_{Al_2O_3}$ in 2007, decreasing to 10.0 GJ/$t_{Al_2O_3}$ in 2024 [13]. Figure 1 shows the variation in energy intensity in alumina refining across different regions from 2004 to 2024, driven by differences in bauxite ore quality, technologies employed, and fuel types used.

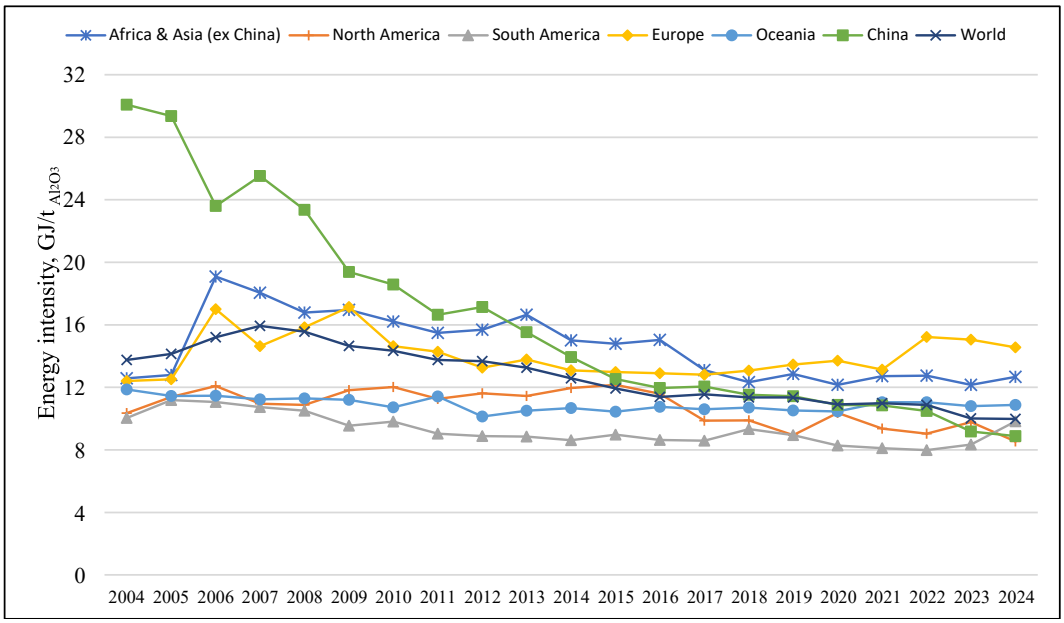


Figure 1. Energy intensity of alumina refining by region for 2004 to 2024 [13].

Digestion

Figure 2 presents the alumina refining process from digestion to calcination. Firstly, the crushed and ground raw material, bauxite ore, is mixed with the caustic soda solution to form a bauxite rich slurry [14]. The slurry is pumped into digestors where the aluminium-containing compound, sodium aluminate, is solubilised and extracted under high-temperature and pressure steam by washing with a hot concentrated sodium hydroxide for several hours [36]. Dissolution of ores with a significant trihydrate bauxite (or gibbsite, ($Al(OH)_3$) content, as shown in

Reaction (1), requires relatively low temperature and pressure of ~145°C and 4-5 bar with Na_2O concentrations of 120-150 g/L, [37]. On the other hand, dissolution of ores containing significant concentration of monohydrate, e.g., boehmite (γ-AlO(OH)) or diaspore (α-AlO(OH)), requires stronger caustic solution (205-245 g/L Na_2O) and higher temperature and pressure of 200°C-250°C and 35 bar, as described in Reaction (2)-(3) [38-40].

Gibbsite ($Al(OH)_3$):

$$Al(OH)_{3(s)} + NaOH_{(aq)} \rightarrow NaAlO_{2(aq)} + 2H_2O_{(l)} \quad (1)$$

Boehmite (γ-AlO(OH)) and diaspore (α-AlO(OH)):

$$\gamma\text{-}AlO(OH)_{(s)} + NaOH_{(aq)} \rightarrow NaAlO_{2(aq)} + H_2O_{(l)} \quad (2)$$

$$\alpha\text{-}AlO(OH)_{(s)} + NaOH_{(aq)} \rightarrow NaAlO_{2(aq)} + H_2O_{(l)} \quad (3)$$

Digestion is one of the greatest consumers of energy in the Bayer process as substantial heating of the slurry is conduced. High temperature and pressure steam are produced via fossil-fuel boilers to heat the slurry indirectly. Historically, and in some modern practice such as the Ma'aden refinery located in Saudi Arabia, bauxite slurry is still heated by direct steam injection [41]. Different digestion technologies are applied depending on the ore quality and refinery design. Atmospheric digestion is in operation in a plant in India for processing gibbsite-rich bauxite ores [41]. Autoclave digestion is the most widely adopted technology globally, operating under pressure leaching conditions [42]. Tube digestion is a particular application of single stream digestion technology that presents strategic advantages for processing mixed grade bauxite ores [43]. Double digestion is employed in certain refineries to separately dissolve the gibbsite and boehmite-rich bauxite ores [41]. After pressurised digestion, the hot slurry passes through multi-stage flash tanks where it is gradually depressurised to atmospheric pressure, causing cooling and flashing water vapour. The vapour is then recirculated to a connected heat exchanger, where it is condensed to provide heat to the incoming slurry. Low-

temperature digestion generally consists of 3-4 depressurisation stages and recuperative heat recovery, while high-temperature digestion typically incorporates 8-12 stages to maximise the heat utilisation [41]. For example, the digestion in Wagerup refinery operates at approximately 150-180°C and processes mainly gibbsite-rich bauxite. After digestion, the slurry is gradually depressurised in 4 stages to atmosphere pressure and discharged at ~110 °C [19]. During the process, a portion of slurry water flashes to water vapour, which is vented through the blow-off flash tank, resulting in heat losses [18, 19]. The discharged slurry is then proceeded to the clarification step.

Clarification

Clarification step separates the insoluble impurities, known as red mud, from the sodium aluminate liquor, termed as "green liquor", through sedimentation in the settling tanks [44]. The clarified liquor then passes through a series of filters to remove any fine impurities.

Precipitation and Evaporation

The green liquor is cooled across multiple precipitator tanks and held for several hours, during which and trihydrate alumina crystals are added to promote gibbsite precipitation [45], as shown in Reaction (4) [14]. The "spent liquor" refers to the remaining liquid after the trihydrate alumina has been precipitated. Heat recovery from green liquor is achieved via heat exchangers, where heat is transferred to the cold "spent liquor". Cooling water is employed to further cool the green liquor and to remove the heat released during the precipitation reaction. The cooling water carries away heat, that, when flashed, can produce low-pressure vapour at 0.14 bar and 52.5 °C [19]. The evaporation step concentrates caustic soda in spent liquor by removing excess water through evaporation. Low-pressure steam is used in this process to heat the spent liquor and evaporating excess water. Similar to digestion process, the liquor passes through multi-stage flash tanks, where it is gradually depressurised, causing water to flash into

vapour. The flashed vapour is then recirculated to a heat exchanger for recuperative heat recovery. This process also releases a substantial amount of low-pressure steam at 0.14 bar and 52.5 °C [14, 15, 46]. The sequence from digestion to precipitation is referred to as the Bayer circuit, with digestion and evaporation constituting the energy-consuming stages, requiring approximately 6.7 GJ/$t_{Al_2O_3}$ energy [12, 19, 29].

$$NaAlO_{2(aq)} + 2H_2O_{(l)} \rightarrow Al(OH)_{3(s)} + NaOH_{(aq)} \quad (4)$$

Calcination

Calcination is the final step in the Bayer process, consuming typically 3 GJ/$t_{Al_2O_3}$ energy in Australian refineries [12]. The trihydrate alumina, known as gibbsite, is calcined in stationary calciners to form smelter grade alumina at high temperature 950~1000°C, as described in Reaction (5) [47]. The calcination reaction occurs in two steps, the dehydroxylation of gibbsite to boehmite (Reaction (6)), followed by the conversion of boehmite to alumina (Reaction (7)). The high temperature calcination in Australian refineries relies largely on natural gas combustion to provide heat, whereas alumina production in China depends heavily on coal [48].

$$Al(OH)_{3(s)} \rightarrow Al_2O_{3(s)} + 3H_2O_{(g)} \quad (5)$$

$$Al(OH)_{3(s)} \rightarrow AlO(OH)_{(s)} + H_2O_{(g)} \quad (6)$$

$$2AlO(OH)_{(s)} \rightarrow Al_2O_{3(s)} + H_2O_{(g)} \quad (7)$$

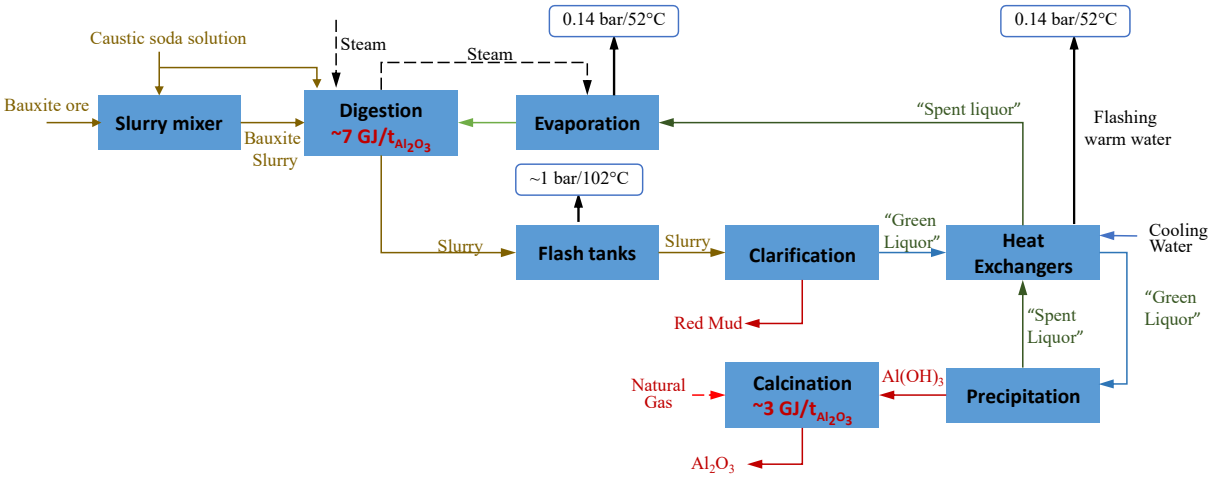


Figure 2. The Bayer process for alumina refining. (adapted from previous work [49])

Calcination technologies

In current refineries, calcination is carried out in stationary calciners, such as Flash Calciner (FF), Circulating Fluidised Bed (CFB) Calciner or Gas Suspension Calciner [50]. Their operations vary depending on the calcination technology. Figure 3 illustrates the current flash calcination process [51], consisting of preheating, main calcination and cooling stages. Firstly, gibbsite with moisture is fed to Cyclone 1 where moisture is removed, and then preheated gibbsite is transported to Cyclone 2 where gibbsite undergoes dehydroxylation to form boehmite, as presented in Reaction (6). Boehmite then enters the main furnace and is converted into alumina, as presented in Reaction (7) [51]. The product, smelter grade alumina, SGA, comprises a complex mixture of transition alumina phases, where γ-alumina is the desired phase, while α-alumina is undesirable. Fuel is injected and combusted with preheated air in the main calciner. A holding vessel is employed to retain the solid for several minutes, ensuring the phase transformation process to form smelter grade alumina. After that, hot gas exits from the top of the holding vessel and directed to Cyclone 2, supplying the heat for pre-calcination. The discharged hot alumina is transported to air cooling cyclones, where the sensible heat in hot alumina is recovered to preheat the injected air. The fluidised bed water cooler is the final cooling step to lower the alumina temperature to approximately 75°C. A

filtration system, such as a baghouse or electrostatic precipitator (ESP), is employed to control the solid emissions, before releasing the exhaust gas from Cyclone 1 to the atmosphere.

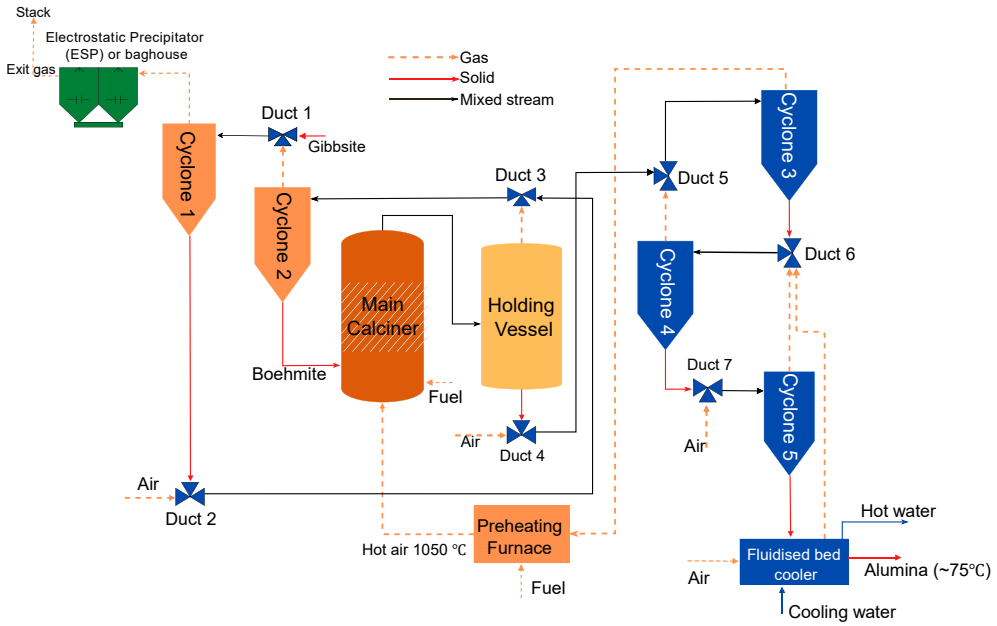


Figure 3. The conventional flash calciner flowsheet. (modified from previous work [41])

Figure 4 presents the Generation 5 CFB calcination flowsheet developed by Outotec [51-53], which consisting of two preheating cyclones, circulating fluidised bed calciner, two cooling cyclones and one large fluidised bed cooler. The preheating stage is similar to flash calcination, where gibbsite is dried and pre-calcined into boehmite in Cyclone 1 and Cyclone 2, respectively, utilising the heat in flue gas from the CFB calciner. The boehmite is converted into smelter grade alumina in the CFB calciner where solid is recirculated to allow sufficient residence time to complete phase transformation. A solid discharge device at the bottom of CFB calciner is used to control the discharge solid mass flow, controlled via a difference pressure measurement to ensure stable inventory in the reactor. To increase the overall heat utilisation efficiency, a portion of boehmite from Cyclone 2 is bypassed and mixed with discharged hot alumina in the external fluidised bed vessel. Solids collected from ESP are returned to the system, ensuring calcination of any gibbsite overflowing from Cyclone 1. Downstream of the reactor, the flowsheet incorporates two cooling cyclones and a large

fluidised bed cooler to recover sensible heat from hot solids for air preheating. Preheated primary air is introduced at the bottom of the CFB calciner for combustion and solids fluidisation, while preheated secondary air is injected downstream of the fuel injection. Fuel is combusted with preheated air and secondary air in two stages to ensure a low formation of NO_x.

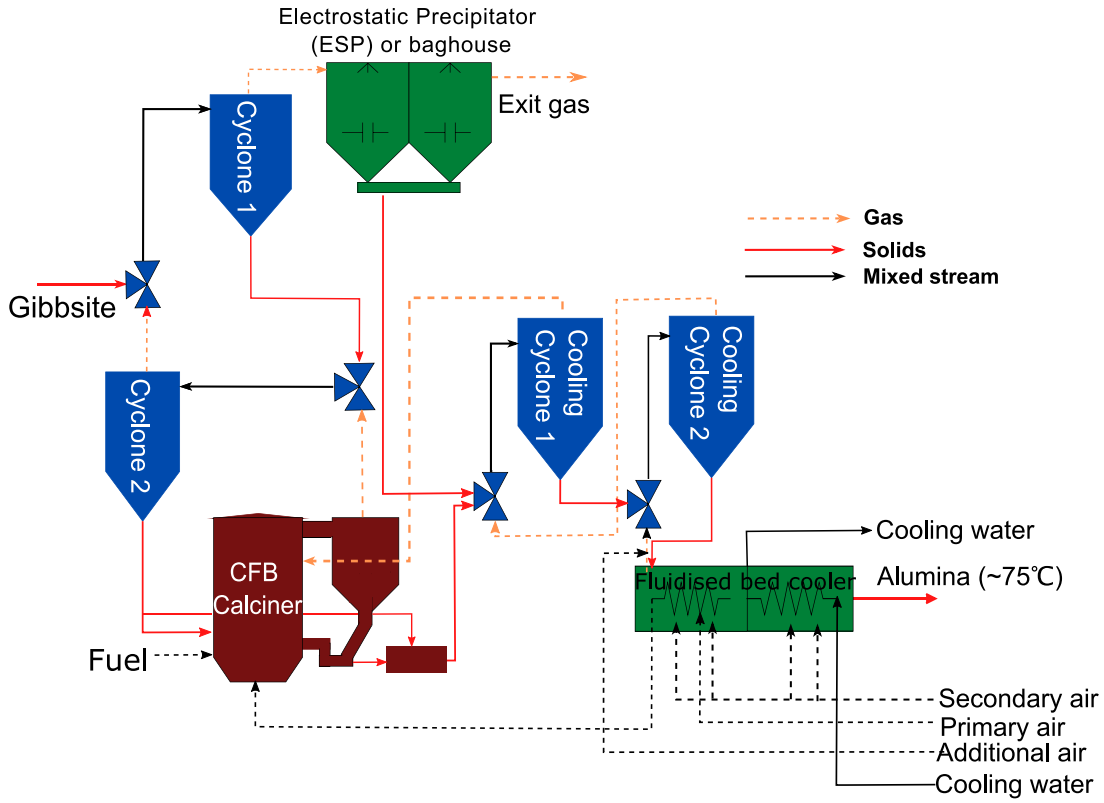


Figure 4. Modern generation 5 CFB calcination flowsheet. (reported from previous work [51, 54])

During the calcination, regardless of the type of calciner used in the refinery, a substantial steam is released together with combustion by-products such as CO_2 and N_2 from the ESP, amounting 0.7 t_{steam}/t_{Al2O3}, with an associated latent energy of approximately 1.7 GJ/t_{Al2O3} [30]. Natural gas is the dominant fuel used in alumina refineries in Australia, although calcination technologies vary across different plants. This study adopts flash calcination as the reference calcination case.

2.2 Waste vapour recovery as a decarbonisation pathway

The waste water vapour within the Bayer process presents a significant energy loss, which offers a potential to improve the energy efficiency by recovering it [29, 31, 55]. In particular, the available low-pressure vapour at sub-atmospheric pressure from precipitation and evaporation stages are estimated to be approximately 0.35 and 0.59 $t_{steam}/t_{Al_2O_3}$ [19], with calculated latent energy of 0.8 and 1.4 $GJ/t_{Al_2O_3}$, respectively, from the study assessing the waste vapour in Australian Wagerup refinery. Vapour at atmospheric pressure is vented from digestion tank, carrying latent energy of 0.4 GJ/t_{Al2O3} [18, 19]. Furthermore, the calcination process also releases diluted steam, which represents another potential steam recovery source. In present operation, high-pressure steam supply for digestion and evaporation usage is typically generated from fossil fuel boilers, such as coal-fired or natural gas-fired boilers [56]. Alternatively, a cogeneration system consisting of a gas turbine coupled with a heat recovery steam generation system, is used in some refineries to produce electricity and steam [19]. The combustion of fossil fuel results in direct CO_2 emissions, accounting for approximately 2/3 of total emissions [57, 58]. Steam recovery powered by renewable electricity offers a potential solution to reduce the reliance on fossil fuel steam generation, thereby cutting the emissions. Although the solution has been identified as one of the potential pathways for future green alumina production, no detailed assessment has been undertaken. One of the scopes of the study is to evaluate the technical and economic feasibility of steam recovery from the Bayer process to achieve energy conservation and CO_2 mitigation in alumina refining.

2.3 Steam recovery or heat recovery technologies

Heat pump (HP) is a key technology that can recover low-grade heat and upgrade to a higher temperature level for reuse [59], playing a significant role in improving energy

efficiency and reducing reliance on fossil fuels in industrial processes. Figure 5 presents the classifications of heat pumps into open-loop and closed-loop systems, distinguished by whether the process vapour itself acts as working fluid [60]. Open-loop systems, such as mechanical vapour recompression (MVR) and thermal vapour recompression (TVR), directly recompress process gas to a higher pressure and temperature [59]. Closed-loop systems employ an independent refrigerant circuit that indirectly recover the heat from heat sources through heat exchangers. This category includes compression heat pumps, in which use mechanical work to drive the heat transfer process, and sorption heat pumps operate by transferring heat through the absorption or adsorption of a refrigerant.

Both open-loop and closed-loop systems have advantages and limitations in their design and operation. Open-loop systems eliminates the need for a dedicated refrigerant circuit, which features simpler configurations and lower capital costs. However, the quality of the process vapour is a critical factor, as solid contamination could cause fouling or mechanical damage to compressor blades in MVR systems. TVR systems are tolerant to particles but are less energy-efficient than MVR. Closed-loop systems operate with sealed refrigerant circuit making them suitable for applications where direct processing of vapour is not practical. But the selection of refrigerant (the working fluids) depends on process temperature and may raise environmental concerns if leakage happens [61]. The capital cost of closed-loop systems is typically higher due to the need for compressors, heat exchangers, and refrigerant management systems.

Given the availability of waste water vapour from the Bayer process and the advantages of open-loop systems, this study focuses on assessing the integration and utilisation of open-loop systems in alumina refining. Although these technologies are mature and already deployed in various industrial sectors for waste heat recovery, few studies have assessed the application

of MVR and TVR systems for steam recovery in alumina refineries, so that the present study aims to evaluate their technical performance and economic feasibility in steam recovery.

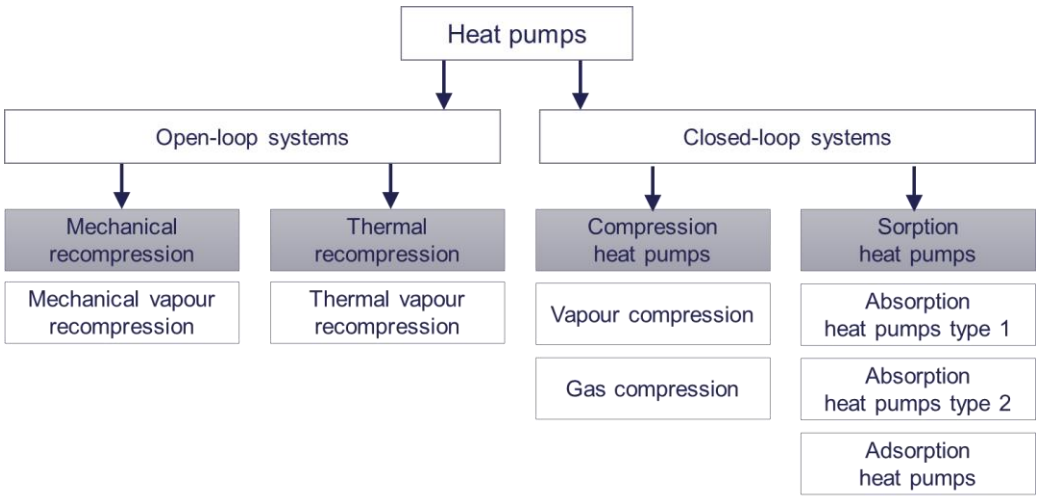


Figure 5. Classification of heat pump technologies [60].

2.3.1 Multi-stage mechanical vapour recompression (MVR)

Mechanical vapour recompression (MVR) increases the temperature and pressure of water vapour through mechanical compression process, which has been identified as one of the potential technologies for steam or heat recovery in alumina refineries [29, 62-64]. MVR has been in use since the 1970s, and is widely employed in distillation, wastewater treatment, and desalination processes [65]. A single-stage MVR system consists of one evaporator coupled with a mechanical compressor. Numerous studies have investigated the utilisation of single- or multi-stage MVR systems in desalination and wastewater treatment processes [22-27]. For example, Dahmardeh et al. [26] modelled the integration of single and two-stage MVR system for treatment of high-salinity wastewater using Aspen Plus. Similarly, Zhou et al. [27] also developed a mathematic model for single-stage MVR system for wastewater desalination. Generally, the system (evaporator) operates under vacuum, with the boiling temperature of approximately 70-85°C, corresponding to sub-atmospheric pressure [26, 27], with the compressor generates the vacuum effect. In the process, single-stage MVR is limited to

compression ratios of about two, which produces a saturation temperature increase of 5-20°C [66, 67]. Carlos et al. [68] developed a model for a modified multistage evaporation system of a chlorine-alkali industrial complex using the three to four stages mechanical vapour recompression configurations, demonstrating that the modified system could reduce steam consumption by around 1%. Their process simulation demonstrated that MVR technology effectively improves overall system efficiency. However, few studies have investigated the MVR integration opportunities in alumina refineries for energy savings.

Given that the required temperature and pressure lift are much higher in alumina refining, for instance, recovering low-pressure waste water vapour of 0.14 bar to 5-15 bar, requiring temperature increasing from 52.5°C to 175°C-230°C [29]. Achieving such a large temperature and pressure lift would require multi-stage MVR system [20, 21, 69], with water injection for desuperheating between each stage to manage the vapour temperature. This desuperheating process for multi-stage operation is essential to maintain the inlet vapour at or near its saturated temperature, reducing compressor electric power load and preventing excessive discharge temperatures [19]. Such a multi-stage MVR configuration has been assessed by Chatfield [19], who demonstrated its potential application at Alcoa's Wagerup alumina refinery in Western Australia. MVR manufacturers have also demonstrated the potential configurations for multi-stage MVR systems [70]. Chatfield examined the implementation of up to 11-stage MVR system for recovering waste vapour from evaporation, precipitation, digestion and calcination steps, with a design pressure of approximately 8.8 bar. The integrated MVR system was estimated to consume approximately 139 MW of electrical power to recover all the waste steam, generating 611 t/hr of steam. This amount exceeds the total steam demand of the refinery by 8%, indicating potential for full steam self-sufficiency by recovery. Technical integration challenges, including the existing refinery infrastructure,

electric power delivery capacity, operating noise and economic feasibility were also included in analysis. However, the study remained high-level, lacking an understanding of the technical details of the MVR systems. Therefore, the present investigation aims to evaluate the system performance in terms of energy use, temperature and pressure increase in compressing process through developing a comprehensive model for multi-stage MVR systems.

2.3.2 Multi-stage thermal vapour recompression (TVR)

Thermal vapour recompression (TVR), also referred to as ejectors, is another widely used method for recompressing steam, requiring high-pressure motive steam to entrain low-pressure steam [71-73]. The majority research of TVR application focus on single-unit integration in desalination and wastewater treatment processes [22-27]. For example, the studies of Zhou et al. [74], Bamardouf et al. [75], Shahzamanian et al. [76] developed mathematical models of integrated TVR distillation process for system efficiency improvement. A novel conceptual design has been proposed to integrate a TVR with the multi-effect evaporation process in the evaporation step in alumina refinery [46]. This concept utilises a TVR to entrain vapour from the flash tanks using boiler-generated motive steam, and reuses the recompressed vapour in evaporation to reduce overall steam demand. However, the pressure ratio achievable with a single-stage TVR is limited, typically less than two [71], which constrains the extent of vapour recompression and the overall potential energy recovery. Robert et al. [71] described a multi-stage TVR system capable of achieving a higher pressure lift. However, its performance and potential implementation in alumina refineries have not yet been comprehensively evaluated. Therefore, the present study aims to develop a mathematic model of multi-stage TVR to estimate the performance in alumina refineries.

2.3.3 System efficiencies and economic analysis

The coefficient of performance (COP) is a key indicator for measuring system efficiency, which is defined as the ratio of thermal energy output to the electrical energy input, as shown in Equation (8) [77, 78]. A review of existing literature highlights several key factors influencing the COP of MVR systems, including the compression ratio, compressor's efficiency, and system design [79]. A single-stage MVR designed for distillation plants, was estimated to achieve a COP of 10 or higher [80]. Similarly, Michael et al**.** [79] evaluated a two-stage MVR system and demonstrated a COP of 7.8 when operating at a compressor efficiency of 70%, underscoring the significant impact of compression stage on overall system performance. Increasing the number of stages generally reduces the COP value due to cumulative compressor work, but it enables higher pressure and temperature lift that are essential in alumina refineries. Existing studies are largely limited to the COP assessment of single- or two-stage MVR systems, with limited studies assessing the multi-stage configurations. Therefore, this study aims to fill this gap by estimating the efficiency performance of the multi-stage MVR systems in the context of alumina refineries.

COP values for TVR systems are rarely reported, making it difficult to assess their system efficiency. Their COP value is inherently dependent on the power input required for motive steam generation, which is typically supplied by boilers, either fossil-fuel-fired or electric boilers. A large amount of motive steam is required in multi-stage TVR systems. Considering the required energy input in motive steam generation, the COP could be lower than that of MVR systems, necessitating further comparison. Furthermore, comparing conventional steam generation (e.g., natural gas boilers) with these emerging steam recovery technologies is also important, offering valuable insights into their system efficiency. Accordingly, this study aims

to meet this need by presenting direct COP comparisons across these technologies for steam production relative to alumina refineries under equivalent process conditions.

$$COP = \frac{\text{Q (Thermal energy output)}}{\text{Q (Electric energy input)}} \quad (8) \quad [77]$$

2.4 Electric boilers as a decarbonisation pathway

Steam generation in alumina refineries typically relies on fossil fuel boilers, such as natural gas-fired or coal-fired boilers. Fossil fuel is combusted with air to produce high-temperature flue gas, which is used to heat the feedwater, evaporate it into steam, and if required, superheat the vapour to the desired conditions. The overall thermal efficiency typically ranges from 75%-90% depending on boiler design and operating conditions [81-84]. Transitioning from natural gas-fired boilers to electric boilers is one of the key decarbonisation pathways for steam generation in alumina refineries, particularly when powered by renewable electricity [29, 85-87]. Electric boilers can achieve near 100% thermal efficiency [88], as they convert electrical energy directly into heat without heat losses from flue gas compared with fossil-fuel boilers [89]. Current commercial electric boiler technologies can achieve steam pressures up to 85 barg [88]. Steam recovery technologies play an important role in waste heat recovery within alumina refineries, as they can significantly reduce the energy required for water evaporation compared with boilers [29]. However, economically, implementing steam recovery systems to capture all waste vapour in the refinery would involve substantial capital investment. For example, according to Chatfield's assessment, approximately 46 compressors are needed to meet the internal steam demand through recovery, resulting in a large installation area and high capital cost of about A$622 million.

Electric boilers play a significant role in decarbonising steam generation in industry. For example, Hasanbeigi et al. [90] investigated electrification opportunities in the US industry and assessed the technical and economic implications of a 100% replacement of fossil-fuel boilers with electric boiler. The study reported a significant 17% energy saving in the full replacement scenario. Zuberi et al. [91] also estimated the technical potential energy and CO_2 reduction by electrifying industrial boilers in the US industry. In another study, Cardenas-Rodriguez et al. investigated the technical and economic performance of steam generation using heavy fuel oil and electric boilers in Brazilian power plant, indicating that electric boilers are more efficient than fossil-fuel fired boiler. Electric boilers also have been identified as a key electrification pathway for steam generation in alumina refineries [29]. For example, the Alunorte alumina refinery in Brazil has recently commenced operation of two new electric boilers to produce steam as part of its efforts to reduce carbon emissions [92]. However, for large steam requirement, their deployment is constrained due to the need for large power supply and electricity delivery infrastructure. Moreover, with the increasing deployment of renewable energy sources, the variability of electricity prices will become a challenge for plants with continuous and constant energy demand [93]. Currently, there is a lack of comprehensive comparative studies assessing various decarbonised steam supply cases in alumina refineries from both technical and economic perspectives, including steam recovery scenarios and steam generation from electric boilers. Hence, the present study aims to meet this need by evaluating various low-carbon steam supply options capable of eliminating the CO_2 emissions related to fossil-fuel-based steam generation.

Economic feasibility analysis is essential for evaluating different strategies for decarbonising steam supply cases relative to fossil fuel steam generation. Steam produced by natural gas boilers benefits from low gas prices, which vary across different regions, for

example, 2.1 US$/GJ in the US, about 10.3 US$/GJ in Europe [94], and 8.6 US$/GJ in Australia in 2024. In contrast, renewable electricity remains comparatively expensive, costing approximately 11-50 US$/GJ, with a levelised cost of electricity (LCOE) ranging from 30 US$/MWh from onshore wind, 40 US$/MWh for solar photovoltaic, 70 US$/MWh for bioenergy and up to 120 US$/MWh for concentrated solar power worldwide [95]. When the costs of electricity transmission infrastructure and the variability of renewable generation are included, the effective price of renewable electricity increases further [96]. The high electricity cost makes the transition to electricity-based steam supply challenging from an economic perspective unless steam recovery systems deliver substantial improvements in energy efficiency. A comparative analysis of the economic viability of the above steam recovery or generation configurations, including milt-stage MVR, TVR, and electric boilers is essential, covering the capital investment, operating costs, and sensitivity to electricity price variations benchmarked against fossil fuel boiler systems. Hence, another objective of this study is to meet this need by comparing the cost of steam across the different configurations.

2.5 Low carbon calcination technologies integrated with steam recovery

In Australian alumina refineries, the calcination stage contributes about 30% of overall energy use and CO_2 emissions during refining, emitting 0.16-0.17 $t_{CO_2}/t_{Al_2O_3}$ [97]. This step also releases steam amounting to 0.7 $t_{steam}/t_{Al_2O_3}$, but it is diluted with roughly 50 wt% non-condensable gas (N_2, CO_2) [30]. Therefore, it poses an opportunity to significantly reduce energy by steam recovery. However, the presence of non-condensable gas complicates the steam compression process. Hence, it is important to retrofit the calcination process to increase steam recovery viability while achieving net-zero carbon calcination. The present investigation aims to meet this need by developing and estimating a retrofittable calcination concept that integrates steam recovery while facilitating low carbon calcination.

2.5.1 Concentrated solar thermal energy

Replacing fossil fuels with alternative renewable energy (e.g. solar thermal energy, hydrogen, electrified heating) [29, 63, 98-100] provides the opportunity to decarbonise the process. Davis et al. [97] analysed the alumina product quality under solar-driven alumina calcination, suggesting that concentrated solar thermal energy (CST) can supply the high-temperature in main calciner and potentially avoids the CO_2 emissions and achieve the even higher quality compared with industrial production. Padilla et al. [101] also investigated the application of CST to reach high temperature upper than 1000°C to obtain alumina from boehmite, demonstrating that concluded that a 10-minutue exposure to solar radiation can produce alumina of the desired quality. However, there are limited studies investigating the retrofitting requirements when employing CST in the calciner and its potential impact on the overall calcination process. Furthermore, the intermittency of solar power would affect the continuous operation of the calcination process, requiring further work to address operational stability and integration challenges.

2.5.2 Pressurised two-stage calcination with steam recovery

Sucech and Mistra have developed a two-stage calcination process that can be retrofitted to Alcoa fluid flash calcination system [102]. In the first stage, hydrate alumina is heated and pre-calcined in a pressurised vessel at 8 bar, converting gibbsite to boehmite. The released steam from the first stage calcination is recovered at 8 bar. The partially calcined solids are then transferred to second stage and calcined by direct heating to 850°C to produce smelter grade alumina. The results show that the final product achieves a specific surface area of 50-80 m^2/g and a loss on ignition (LOI) of less than 1%. Although fossil fuel combustion is still required, the two-stage calcination design enables steam recovery from first stage calcination for direct use in the digestion process without the need for further steam compression.

2.5.3 Hydrogen calcination

Hydrogen combustion is another potential pathway to eliminate direct emissions from fossil fuel combustion in calcination [103-106]. Hydrogen-based alumina calciner project funded by the Australian government is currently underway, aiming to evaluate the use of hydrogen in the alumina calcination process [107]. Yarwun alumina refinery in Australia is conducting a series of tests of the hydrogen calciner to understand the technical feasibility of hydrogen combustion in calcination [108]. However, no detailed assessment report is currently available. Several studies have investigated the economic viability of using hydrogen for heat supply in alumina calcination [109, 110]. For example, Javier et al. [109] performed an economic assessment of hydrogen transition as the decarbonisation strategy in the alumina production. The study provided a broad economic overview of the Bayer process, with results indicating that the economic feasibility of using green hydrogen could be a cost-effective solution when electricity price remains below 45 EUR/MWh. However, the study employs a life-cycle assessment methodology, which remains constrained by high-level system boundaries and has inherent limitations on the depth for evaluating hydrogen use in calcination. Hence, the present study aims to provide a detailed technical assessment of applying hydrogen combustion in the calcination process and an economic analysis evaluating its competitiveness under different hydrogen prices.

Combusting hydrogen with air is a straightforward approach to replace natural gas, as it maintains air as the oxidising agent and carrier gas. Nevertheless, this configuration introduces large amounts of N_2, which dilutes the steam, lowering the steam concentration and complicates the steam recovery. One novel concept proposed by Saw et al. [31] involves conducting hydrogen combustion in an oxygen-steam environment, where the superheated steam is recirculated to transport alumina solids. This configuration enables exiting high-

concentration steam, increasing the viability of steam recovery. To date, no detailed technical analysis has yet been carried out to evaluate the technical and economic feasibility of hydrogen in oxy-steam combustion integrated with a steam recovery system. Therefore, the present study aims to assess such a retrofittable calciner design.

Although transiting from natural gas to hydrogen eliminates carbon emissions associated with fossil fuels combustion [111, 112]. Economic feasibility of applying hydrogen remains challenging due to its high price, which was estimated to be 4-6 US$/kg in 2023-2024 [113-116]. However, recent studies also highlighted that potential decline in electrolysis hydrogen cost as the prices of electrolysers and renewable electricity continue to fall. For example, Longden et al. [114] reported that green hydrogen production costs could drop below 2 US$/kg by 2030 in Australia. Wang et al.[117] also estimated that hydrogen production costs in China could decrease to 2.60 US$/kg between 2020 and 2040. Curcio [118] conducted a comprehensive evaluation of hydrogen production economics across grey, blue, and green hydrogen production. The analysis shows that grey hydrogen, costing approximately 1.5-2.5 US$/kg, remains the lowest cost at present, though its future competitiveness is constrained by carbon pricing obligations. Blue hydrogen, with costs in the range of 2.0-3.50 US$/kg, offers a transitional pathway. Green hydrogen is currently the most expensive, ranging from 3.5-6 US$/kg, and renewable electricity costs below 20-30 US$/MWh are essential for it to achieve cost parity with grey hydrogen. The wide variation in hydrogen price reported in previous studies and limited economic comparisons between hydrogen and natural gas alumina calcination highlights the need for a detailed economic and sensitivity analysis. Carbon capture and storage (CCS) technology captures CO_2 emissions and stores it permanently underground, representing another potential decarbonisation pathway in calcination [119]. However, the current high cost and required scale-up limit its feasibility for deployment [120]. Numerous

studies have estimated the cost of CO_2 capture in fossil fuel power plant. For example, Hayat et al. [121] reported a total CCS of 94-160 US$/t$_{CO2}$ (2024 US$), compromising 86 to 130 US$/t$_{CO2}$ for capture and 24 US$/t$_{CO2}$ for transport and storage on gas-fired power plants. Rubin et al. [122] provided a broader range of 48 to 111 US$/t$_{CO2}$ (2013 US$) for CO_2 capture in natural gas combined cycle (NGCC) power plants. Research on CCS cost in alumina calcination is limited, particularly in comparison with hydrogen pathways for determining the break-even hydrogen price. Hence, this study aims to include such a cost comparison in economic analysis.

2.5.4 Electrified calcination

Electric calciner is another potential strategy to achieve zero direct carbon emissions and enable high-concentration steam recovery [86, 123-125]. Assessment of this pathway is underway. A pilot-scale, Calix's drop-tube electric calciner, located in Victoria, Australia, was developed to test feed gibbsite samples at a rate of 0.06 to 0.144 t/hr, providing valuable insights into the alumina quality under electric calcination [126]. In addition, Alcoa of Australia is conducting pilot trials on electric calcination, with a capacity ranging from approximately 0.2 to 2 t/hr and power requirements ranging from 140 to 1400 kW [127]. These ongoing projects aim to explore the technical feasibility of retrofitting the conventional fossil fuel fired calciner with electrical heating. Considering large capacity of one calciner, above 70 t/hr [54], Electric calciners will need to be scaled up significantly, which will require substantial engineering development and increase the capital investment needed for implementation. These aspects warrant further investigation but are outside the scope of the present study. This study aims to assess the technical viability of steam recovery from electric calcination pathways to understand their integration potential.

2.6 Alumina calcination process under steam environment

2.6.1 The effects of air and steam environments on the calcination performance

Calcination process equipped with several cyclones for solid transportation purpose which play a critical role. It is essential to maintain their stable operation when switching the fuel type and calcination environment. For cyclones efficiency, Shepherd and Lapple's theory [128] indicates that its separation efficiency depends the inlet gas velocity and gas viscosity. It is important to maintain a sufficient gas velocity to carry the particles through the system. Air serves as both the combustion oxidiser and the carrier gas for solid transportation in present calcination operation. Currently, most research considers the air combustion [109, 110], where hydrogen directly replaces natural gas while air continues to be used as the oxidiser. Combusting hydrogen with oxygen-steam offers high-concentration exit steam, but it changes the calcination environment from air to steam. As the gas viscosity of steam differs from that of air, understanding cyclone performance in a steam environment is crucial for predicting separation behaviour.

2.6.2 The effects of steam environment on overall energy consumption

In addition to solids transport, the effect of a steam-rich environment on the heat transfer must also be evaluated. Klett et al. [52] reported that deceased cyclone separation efficiency has a modest impact on total calcination energy consumption. For example, a drop from 100% to 90% separation efficiency in the cooling cyclones increases the fuel consumption by approximately 1.8% due to the reduced presence of solid in the off-gas interfering with the counter-current heat recovery. The heat capacity of steam also differs from that of air, which affects both the heat recovery from hot solids during the cooling stage, and the heat delivery in the preheating zone. This difference would impact overall energy utilisation and energy consumption. Therefore, this thesis aims to evaluate the performance of the calcination process

under air and steam calcination, assessing heat utilisation in the preheating and cooling zones, the performance of cyclones, and the resulting impact on overall energy consumption.

The steam concentration surrounding the solids also play a critical role in determining the dehydroxylation rate of gibbsite [129, 130]. Alumina calcination kinetics of calcination reactions have been investigated by many researchers [16, 131-135]. Candela et al. [131] demonstrated that an increase in surrounding moisture concentration could inhibit the reaction rate of gibbsite to boehmite. Similarly, Saw et al. [16] investigated the reaction kinetics under 80% steam conditions and also demonstrated that steam environment is less favourable for the reaction. These effects would indirectly influence heat utilisation in the preheating zone, thereby affecting the overall calcination energy consumption. Nevertheless, there are limited studies that incorporate reaction kinetics to evaluate their influence on energy use. Therefore, this study aims to meet this need by developing alumina calcination models under both air and steam-based calcination, incorporating available reaction kinetics into the process models to predict the influence of different environments on calcination energy consumption.

2.6.3 The effects of steam environment on alumina quality

Calcination conducted under steam-rich environment can influence several key alumina quality parameters, e.g., loss on ignition (LOI), particle breakage, specific surface area and the phase transition. LOI is used to measure the degree of calcination of SGA, representing the residual hydroxyl content [41]. When alumina dissolves in the electrolyte during aluminium production, the LOI affects the hydrogen fluoride (HF) generation rate, which is toxic and corrosive gas that poses significant health and environment hazards requiring strict control. The higher the LOI content, the higher the HF generation rate [41]. Specific area is another important factor. A higher HF generation requires a greater specific surface area to absorb the HF. However, higher LOI generally corresponds to higher surface area due to the presence of

transition alumina phases. Therefore, modern alumina smelters prefer SGA that has been calcined to achieve an optimal balance. Understanding these parameters under steam calcination is critical for producing SGA that meets industry specifications.

Particle breakage is also important because it affects the particle size distribution (PSD) of SGA. Excessive breakage leads to the formation of fines, which can cause feeding instability in aluminium reduction cells, increased dust emissions, poor flowability, lowering the downstream aluminium production efficiency [35]. Therefore, although outside the scope of this work, understanding the fundamentals of particle breakage, LOI, and specific surface area during calcination remains important.

2.7 Challenges in steam recovery from the calcination process

2.7.1 High-concentration steam recovery from steam calcination

2.7.1.1 Challenges in removing entrained fine particles

One of the objectives of this study is to enable effective steam recovery from the calcination process. The steam calcination pathway enhances steam recovery viability by eliminating N_2 dilution. However, one major limitation is that fine particles entrained in the exit steam poses a significant challenge, despite existing particulate control systems such as electrostatic precipitators (ESP) or baghouses achieving ~99% removal efficiency for particles larger than 2 μm [136, 137]. The baghouse employs fabric filters, where particles are collected on the surface of the filter medium, which is one of the solids control systems used in existing refineries [138, 139]. However, under steam-based calcination, condensation may occur under high relative humidity [137], leading to crusty caking or plugging issue, which could incur periodic maintenance requirements. Electrostatic precipitators use electrical forces to separate the particles from a flowing gas stream by charging the particles while passing through an

electrical field. The particles, either charged positively or negatively, are attracted to the collector plates carrying the opposite charge. The performance of ESPs is highly dependent on loading conditions of the incoming dust and the resistivity of particulates [34, 137], while the effect of steam concentration on particle resistivity remains unknown. The present study assumes that the existing solids-control systems can effectively capture particles greater than 2 μm when the exit gas composition shifts from roughly 50 wt% steam under air calcination to above 99% steam under steam calcination.

The solid concentration in the exit gas stream from calcination is typically controlled to below 50 mg/Nm^3 in alumina refineries, depending on the local environmental regulations [136, 140, 141]. Reported operating data from Queensland alumina Limited (QAL) refinery show particulate emissions ranging from 29-41 mg/Nm^3 [140]. The retained fine particles, particularly those smaller than 2 μm, remain difficult to capture, especially for particle diameters ranging from 0.1 to 1 μm, which are often referred as the "Greenfield gap" [142]. These retained fine particles could potentially damage the blades of MVR compressors [143], as the blades operate at very high rotation speeds [19]. Therefore, a further fine particle removal system for steam cleaning is necessary. To date, no integrated steam-cleaning and recovery concept has been proposed and evaluated. Hence, one objective of the present study is to evaluate such a configuration for recovering high-concentration steam from steam calcination.

2.7.1.2 Integrated steam cleaning and recovery system

To further remove the entrained fine particles less than 2 μm, several advanced particulate control technologies could be implemented such as the water electrostatic scrubber (WES), venturi scrubber, candle filters and steam-hydro scrubber [139, 144]. The WES system uses electrically charged sprayed water droplets to attract and remove fine particles. High

removal efficiency (>90%) for submicron particles (~1 μm) could be achieved and it can operate effectively at high humidity gas conditions [139]. However, the system requires complex design incorporating both a high-voltage field and a liquid-injection system. To date, only pilot-scale demonstration has been reported in 2021 in Italy, with gas flow rate of 1.5 Nm^3/s [145]. The venturi scrubber accelerates the gas velocity through the venturi throat, where the sprayed scrubbing liquid (usually water) contacts with the high-velocity gaseous flow. High collection efficiencies ranging from 50% to 90% could be achieved for sub-particles (0.1~1 μm) depending on the gas velocity [139, 146, 147]. Nevertheless, achieving high collection efficiency causes significant pressure drops, which could potentially incur an energy penalty. Despite this drawback, the venturi scrubber has a simple design and is commercially available for industrial applications. The steam-hydro scrubber employs high-pressure motive steam injection to atomise the scrubbing liquid (usually water) into extremely fine droplets and generate strong turbulence, thereby enhancing fine-particle capture. Despite reported collection efficiencies range from 80% to 90% for the fine particles (0.1-1 μm) [148], industrial deployment remains limited and commercial maturity relatively low. Candle filters are an alternative approach designed to remove fine particles from gas or liquid streams using multiple vertical filter elements [149]. These are porous tubular ceramic or metal filters that allow the fluid passes through them forming a cake on the surface, which is then periodically back-flushed to remove the trapped material.

Given that the high collection efficiency and commercial maturity, the present study considers the integration of a venturi scrubber before the MVR system to further remove fine particles. Accordingly, this study aims to assess the particle removal efficiency of the integrated steam-cleaning system prior to MVR compression. As the pressures drop across the venturi scrubber may incur an energy penalty in addition to energy required for MVR recompression,

this study also aims to understand the energy use associated with steam cleaning and recompression during the steam recovery process.

2.7.2 Heat and steam recovery from the exit gas from air calcination

For diluted steam recovery from air calcination, the combustion by-products, CO_2 and N_2, complicate the recovery process. In digestion, historically, and even in some modern practice such as the Ma'aden refinery located in Saudi Arabia, bauxite slurry is heated by direct steam injection [41]. Although direct contact heating provides high heat transfer coefficient, it requires additional energy input in the evaporation stage to remove the extra condensate associated with the injected steam. In this case, direct steam recovery without gas separation is not technical feasible as the presence of CO_2 in steam would react with caustic soda solution used in digestion. In more modern practice, the slurry is heated indirectly using pipe-in-pipe heaters, where steam condenses on the heat transfer surface and transfers heat through the wall to the slurry [41]. In this case, dilution gas (CO_2) would not react with the caustic solution as it is indirect heating. However, MVR technology for compression is normally processed with nearly pure steam and may require special design for processing mixed gas [80, 150, 151]. In addition, in the indirect pipe-in-pipe heat-transfer processes with bauxite slurry, the non-condensable gases could hinder steam condensation and consequently lower the overall heat-transfer rate. This tendency is supported by simulation studies on film condensation of steam in the presence of non-condensable gases, which report a decrease in average heat transfer coefficients as the air concentration in steam increases from 5% to 45% [152]. Therefore, gas separation is needed when MVR systems compress vapour with high fractions of N_2 and CO_2. Chatfield [19] proposed a configuration that directs the exit gas from the calcination process to a wet scrubber, where water vapour condenses and is then re-evaporated as low-pressure steam in flash tanks. A subsequent multi-stage MVR system is then employed to further recompress

steam. However, this process may lower overall efficiency due to the energy and vapour losses in flash tanks and scrubbers. Although this approach has been proposed, it lacks a comprehensive analysis, particularly on its energy losses and efficiency. Yu et al. [153] also reviewed opportunities for heat and water recovery from alumina calciner stack off-gas, highlighting that this heat in off-gas which is the heat source can be indirectly recovered via heat exchangers to heat the heat sink, such as warm the process condensate (water) or alternatively used as the heat source for a Kalina cycle power generation system. Nevertheless, the majority of the heat in calciner off-gas is embedded as latent heat in its water vapor and indirect heat recovery methods via heat pumps may limit its recovery efficiency. Therefore, this study adopts direct heat recovery via condensation in a scrubber to recover the latent heat in the off-gas, aiming to estimate the steam recovery efficiency of integrated steam separation and recovery process from air calcination, and compares it with the high-concentration steam recovery from steam calcination.

2.8 Steam recovery from both calcination and Bayer circuit

Through optimisation and integration of steam recovery from both alumina calcination and the Bayer circuit, the overall steam demand could potentially be fully met, thereby eliminating reliance on fossil fuel boilers [19]. Achieving full steam recovery may require high capital investment for multi-stage MVR systems and the operating costs are highly sensitive to electricity prices. To date, no study has comprehensively analysed capital costs or electricity price sensitivity of such an optimised steam supply case in comparison with conventional boilers. Hence, the present study aims to advance the understanding of the technical and economic viability of achieving full internal recovery within the Bayer process, compared with other decarbonised steam supply scenarios that combine partial steam recovery from various process steps with boilers for supplementary supply.

2.9 Objectives of the thesis

In light of above literature review, this study aims to assess the techno-economic feasibility of implementing decarbonisation technologies within the Bayer process, with a focus on integrating steam recovery to improve energy efficiency and reduce CO_2 emissions during alumina refining. The objectives are described in each chapter below:

Chapter 3 estimates the techno-economic viability of applying hydrogen combustion in calcination while increasing viability of steam recovery, with the following objectives:

- To estimate a novel retrofittable calciner concept that accommodates hydrogen in oxy-steam combustion while enabling integrated steam recovery.
- To understand the effects of steam-rich environment on calcination performance, such as the cyclone efficiencies, heat utilisation during calcination, and overall energy demand.
- To evaluate the economic feasibility of switching natural gas to hydrogen and the minimum break-even hydrogen prices in comparison with natural gas, with inclusive of the value of steam recovery.

Chapter 4 estimates the integrated steam cleaning and recovery from various calcination scenarios, with the following objectives:

- To evaluate the particle removal efficiency of an integrated venturi scrubber and the resulting reduction in solid concentration prior to MVR system.
- To evaluate the energy consumption in diluted-steam recovery from air-based calcination (natural gas/air and H_2/air combustion) and high-concentration steam recovery from steam-based calcination (electric calcination and H_2 in oxy-steam combustion).
- To assess the potential energy saving and economic viability of decarbonised steam supply scenarios which integrates steam recovery from calcination.

Chapter 5 investigates the technical and economic performance of various steam recovery technologies, with the following objectives:

- To analyse the performance of multi-stage MVR and TVR systems when implementing in alumina refineries for steam recovery through comprehensive process modelling.
- To analyse and compare the COP value among above systems with conventional steam generation methods.
- To evaluate the economic performance of the systems and estimate the break-even renewable electricity prices relative to natural gas.

Chapter 6 assesses the optimised steam recovery from both calcination and the Bayer process, with the following objectives:

a. To estimate the amount of recoverable steam from different steps within the Bayer process.
b. To evaluate the technical and economic feasibility of the optimised steam recovery scenario compared with conventional steam generation from natural gas boilers.

2.10 References

[1] Paris agreement, in The United Nations Framework Convention on Climate Change (UNFCCC). 2015: Paris, France.

[2] Rissman J, Bataille C, Masanet E, Aden N, Morrow III W R, Zhou N, Elliott N, Dell R, Heeren N, and Huckestein B. Technologies and policies to decarbonize global industry: Review and assessment of mitigation drivers through 2070. Applied energy, 2020. 266: p. 114848. https://doi.org/10.1016/j.apenergy.2020.114848.

[3] Zhu L. National carbon emissions from the industry process: Production of glass, soda ash, ammonia, calcium carbide and alumina. Applied Energy, 2016. 166: p. 239-244. https://doi.org/10.1016/j.apenergy.2015.11.005.

[4] Slorach P C and Stamford L. Net zero in the heating sector: Technological options and environmental sustainability from now to 2050. Energy Conversion and Management, 2021. 230: p. 113838. https://doi.org/10.1016/j.enconman.2021.113838.

[5] Fais B, Sabio N, and Strachan N. The critical role of the industrial sector in reaching long-term emission reduction, energy efficiency and renewable targets. Applied Energy, 2016. 162: p. 699-712. https://doi.org/10.1016/j.apenergy.2015.10.112.

[6] The Australian Aluminium Council LTD. Australian Alumina. https://aluminium.org.au/australian-industry/australian-alumina/. 2023 [accessed on 1 July 2025].

[7] Australian Government. Australia's Long-Term Emissions Reduction Plan. https://www.dcceew.gov.au/climate-change/publications/australias-long-term-emissions-reduction-plan. 2023 [accessed on 1 July 2025].

[8] Croucher A, Dean A, Hutley N, Flannery T, Morgan W, Bradshaw S, and Rayner J. Australia's clean industry future: making things here in a net zero world. https://www.climatecouncil.org.au/resources/australias-clean-industry-future-making-things-in-a-net-zero-world/. 2023 [accessed on 6 April 2025].
[9] Australian's emissions projections 2022. https://www.dcceew.gov.au/sites/default/files/documents/australias-emissions-projections-2022.pdf. 2022 [accessed on 6 June 2023].
[10] Gautam M, Pandey B, and Agrawal M. Environmental Carbon Footprints. Butterworth-Heinemann.2018. 197-228.
[11] The Australian Clean Energy Regulator. 2022-23 published data highlights. https://cer.gov.au/markets/reports-and-data/nger-reporting-data-and-registers/2022-23-published-data-highlights. 2023 [accessed on 9 July 2025].
[12] Scarsella A A, Noack S, Gasafi E, Klett C, and Koschnick A. Energy in alumina refining: setting new limits. Light metals 2015, 2015: p. 131-136. https://doi.org/10.1007/978-3-319-48248-4_24.
[13] International Aluminium. Metallurgical Alumina Average Refining Energy Intensity for 2024. https://international-aluminium.org/statistics/metallurgical-alumina-refining-energy-intensity/. 2024 [accessed on 22 Feb 2026].
[14] Tabereaux A T and Peterson R D. Chapter 2.5 - Aluminum Production. Treatise on Process Metallurgy. Elsevier.2014. 839-917.
[15] Henrickson L. The need for energy efficiency in Bayer refining. Essential Readings in Light Metals: Volume 1 Alumina and Bauxite, 2016: p. 691-696. https://doi.org/10.1007/978-3-319-48176-0_96.
[16] Saw W L, Lee L, Ingenhoven P, Chinnici A, Zhang X, Rafique M, Tang Y, Tung D A J, Tsai T C, He Z, Smadi E A, Tian Z F, Lau T, Sun Z, Chin R, Eyk P v, Dally B, and Nathan G. Integrating Concentrating Solar Thermal Energy into the Bayer Alumina Process. https://arena.gov.au/assets/2024/07/Univeristy-of-Adelaide-Integrating-Concentrating-Solar-Thermal-Energy-into-the-Bayer-Alumina-Process-Final-report.pdf. 2023 [accessed on 8 March 2025].
[17] Kelly R, Edwards M, Deboer D, and McIntosh P. New Technology for Digestion of Bauxites. Essential Readings in Light Metals: Volume 1 Alumina and Bauxite, 2016: p. 371-376. https://doi.org/10.1007/978-3-319-48176-0_49.
[18] Pathy S, Misra K, Kumar S S, and Giri U K, Exhaust to Energy: Waste Heat Recovery in Alumina Digesters, in 42nd International ICSOBA Conference. 2024: Lyon, France.
[19] Chatfield R. Mechanical vapor recompression (MVR) for low carbon alumina refining, MVR technical and commercial feasibility studies. https://arena.gov.au/projects/mechanical-vapour-recompression-for-low-carbon-alumina-refining/. 2022 [accessed on 14 June 2024].
[20] Hu B, Wu D, and Wang R. Water vapor compression and its various applications. Renewable and sustainable energy reviews, 2018. 98: p. 92-107. https://doi.org/10.1016/j.rser.2018.08.050.
[21] Ranade V V and Bhandari V M. Industrial wastewater treatment, recycling and reuse. Butterworth-Heinemann.2014.
[22] Hou C, Lin W, Yang L, and Zhang H. Experimental performance evaluation and model-based optimal design of a mechanical vapour recompression system for radioactive wastewater treatment. Energy Conversion and Management, 2022. 252: p. 115087. https://doi.org/10.1016/j.enconman.2021.115087.
[23] O'Shea R, Lin R, Wall D M, and Murphy J D. Assessing decarbonisation pathways in the food and beverage sector: A multi-criteria decision analysis approach. Journal of Cleaner Production, 2022. 371: p. 133534. https://doi.org/10.1016/j.jclepro.2022.133534.
[24] Sharan P and Bandyopadhyay S. Energy integration of multiple-effect evaporator, thermo-vapor compressor, and background process. Journal of Cleaner Production, 2017. 164: p. 1192-1204. https://doi.org/10.1016/j.jclepro.2017.07.041.
[25] Shamet O and Antar M. Mechanical vapor compression desalination technology – A review. Renewable and Sustainable Energy Reviews, 2023. 187: p. 113757. https://doi.org/10.1016/j.rser.2023.113757.
[26] Dahmardeh H, Amiri H A, and Nowee S. Evaluation of mechanical vapor recompression crystallization process for treatment of high salinity wastewater. Chemical Engineering and Processing-Process Intensification, 2019. 145: p. 107682. https://doi.org/10.1016/j.cep.2019.107682.
[27] Zhou Y, Shi C, and Dong G. Analysis of a mechanical vapor recompression wastewater distillation system. Desalination, 2014. 353: p. 91-97. https://doi.org/10.1016/j.desal.2014.09.013.
[28] E. Jaeger D S-J and A. Barry, Integrating Vapor Compression Heat Pumps and Mechanical Vapor Recompression with the Bayer Process, in the 12th International AQW Conference and Exihibition. 2024: Dubai, UAE.

[29] ARENA. A Roadmap for Decarbonising Australian Alumina Refining. https://arena.gov.au/knowledge-bank/a-roadmap-for-decarbonising-australian-alumina-refining/. 2022 [accessed on 15 June 2025].
[30] Mills G, Method for the calcination of aluminium trihvdroxide. 24 October 2007. WO Patent 2008/052249A1. https://patentimages.storage.googleapis.com/30/b9/1d/3e51ae39f87fbb/WO2008052249A1.pdf.
[31] Saw W L, Nathan G J, Chatfield R V, and Haywood R J, Method and Apparatus for Alumina Calcination 2022 17 June 2022. WO2022261726A1. https://patentimages.storage.googleapis.com/b3/bd/c3/d31d8a0f599297/WO2022261726A1.pdf.
[32] Bayless D J, Alam M K, Radcliff R, and Caine J. Membrane-based wet electrostatic precipitation. Fuel processing technology, 2004. 85(6-7): p. 781-798. https://doi.org/10.1016/j.fuproc.2003.11.025.
[33] Jena M C, Mishra S k, and Moharana H S. Effect of Particle Size on Collection Efficiency of ESP and RABH: A Case Study. Aerosol Science and Engineering, 2019. 3: p. 75-87. https://doi.org/10.1007/s41810-019-00045-2.
[34] Douglas D. ESP and assessment. The handbook of English for specific purposes.2012. 367-383.
[35] Seetharaman S. Treatise on Process Metallurgy: Volume 3: Industrial Processes. Elsevier.2024.
[36] Brough D and Jouhara H. The aluminium industry: A review on state-of-the-art technologies, environmental impacts and possibilities for waste heat recovery. International Journal of Thermofluids, 2020. 1: p. 100007. https://doi.org/10.1016/j.ijft.2019.100007.
[37] Bánvölgyi G and Siklósi d P. The improved low temperature digestion (ILTD) process: an economic and environmentally sustainable way of processing gibbsitic bauxites. Essential Readings in Light Metals: Volume 1 Alumina and Bauxite, 2013: p. 362-370. https://doi.org/10.1007/978-3-319-48176-0_48.
[38] Xu B, Smith P, and De Silva L. The Bayer digestion behaviour of transition aluminas formed from roasted gibbsite. International Journal of Mineral Processing, 2013. 122: p. 22-28. https://doi.org/10.1016/j.minpro.2013.04.003.
[39] Songqing G and Zhonglin Y. Preheaters and digesters in the Bayer digestion process. Essential Readings in Light Metals: Volume 1 Alumina and Bauxite, 2016: p. 356-361. https://doi.org/10.1007/978-3-319-48176-0_47.
[40] Wargalla G and Brandt W. Processing of diaspore bauxites. Essential Readings in Light Metals: Volume 1 Alumina and Bauxite, 2016: p. 393-401. https://doi.org/10.1007/978-3-319-48176-0_53.
[41] Raahauge B E and Williams F S. Smelter Grade Alumina from Bauxite: History, Best Practices, and Future Challenges. Springer.2022.
[42] Damaskin A, Suss A, Panov A, Paromova I, Kuznetzova N, Kutkova N, Shipova O, and Kuvyrkina A. Autoclave Desilication of Digested Bauxite Slurry in the Flashing Circuit. Essential Readings in Light Metals: Volume 1 Alumina and Bauxite, 2016: p. 263-267. 10.1007/978-3-319-48176-0_35.
[43] Haneman B, Evolution of Tube Digestion for Alumina Refining, in the 34th ICSOBA conference. 2016: Quebec City, Quebec, Canada.
[44] Xin H, Guo-zhi L, Ting-an Z, Song W, and Long W, Research of Cleaner Production of Alumina and Harmless Utilization of Red Mud, in TMS Annual Meeting & Exhibition 2024. 2024, Springer. p. 99-109.
[45] Hocking M B. Handbook of Chemical Technology and Pollution Control. San Diego: Elsevier Science & Technology.2006.
[46] Chua H T and Rahimi B. Low grade heat driven multi-effect distillation and desalination. Elsevier.2017.
[47] Perander L M, Gasafi E, and Scarsella A, Cost and Energy Efficiency Improvment in Alumina Calcination, in the 12th International AQW Conference and Exihibition. 2024: Dubai, Emirate.
[48] International Aluminium. Metallurgical Alumina Refining Fuel Consumption. https://international-aluminium.org/statistics/metallurgical-alumina-refining-fuel-consumption/?publication=metallurgical-alumina-refining-fuel-consumption. 2024 [accessed on 22 Feb 2026].
[49] Hind A R, Bhargava S K, and Grocott S C. The surface chemistry of Bayer process solids: a review. Colloids and surfaces A: Physicochemical and engineering aspects, 1999. 146(1-3): p. 359-374. https://doi.org/10.1016/S0927-7757(98)00798-5.
[50] Klett C and Perander L. Alumina Calcination: A mature technology under review from supplier perspective. Light Metals 2015, 2015: p. 79-84. https://doi.org/10.1007/978-3-319-48248-4_15.
[51] Perander L, Scarsella, A., Gasafi, E., Schmidt,H.W. CFB Alumina Calciners—New and Future Generation Opportunities for Green Field Refineries. Light Metals 2017, 2017: p. 3-8.
[52] Klett C, Reeb B, Missalla M, and Schmidt H-W. Methods to reduce operating costs in circulating fluidized bed calcination. Light Metals 2011, 2011: p. 125-130. https://doi.org/10.1007/978-3-319-48160-9_22.

[53] Haus S, Borges A, Almeida N, and Duck A. Results of Metso Outotec Calciner Optimizer Operation at CBA Alumina Calcination Plants. Light Metals 2022, 2022: p. 22-30. https://doi.org/10.1007/978-3-030-92529-1_3.
[54] Metso. Schematic illustration of Metso's Generation 5 CFB alumina calciner. https://www.metso.com/portfolio/smelter-grade-alumina-cfb-calcination-plant-solution/. [accessed on 5 June 2025].
[55] Habashi F. A hundred years of the Bayer process for alumina production. Essential Readings in Light Metals: Volume 1 Alumina and Bauxite, 2016: p. 85-93. https://doi.org/10.1007/978-3-319-48176-0_12.
[56] Costa D, Neves R, Melo F, Freitas J, Sousa J, Junior E, and Arcodaci D, Steam Grid Stability Using Advanced Process Control and Real Time Optimization in an Alumina Refinery, in Light Metals 2023, S Broek, Editor. 2023: San Diego, California, USA. p. 196-201.
[57] Climate Change Authority. Industry and Waste. https://www.climatechangeauthority.gov.au/sites/default/files/documents/2024-09/2024SectorPathwaysReviewIndustryandWaste.pdf. 2023 [accessed on 6 July 2025].
[58] Taylor A. Supporting a low emissions future in alumina refining. https://www.minister.industry.gov.au/ministers/taylor/media-releases/supporting-low-emissions-future-alumina-refining. June 2021 [accessed on 9th June 2025].
[59] Gaur A S, Fitiwi D Z, and Curtis J. Heat pumps and our low-carbon future: A comprehensive review. Energy Research & Social Science, 2021. 71: p. 101764. https://doi.org/10.1016/j.erss.2020.101764.
[60] Klute S, Budt M, van Beek M, and Doetsch C. Steam generating heat pumps–Overview, classification, economics, and basic modeling principles. Energy Conversion and Management, 2024. 299: p. 117882. https://doi.org/10.1016/j.enconman.2023.117882.
[61] Ma X, Du Y, Zhao T, Zhu T, Lei B, and Wu Y. A comprehensive review of compression high-temperature heat pump steam system: Status and trend. International Journal of Refrigeration, 2024. 164: p. 218-242. https://doi.org/10.1016/j.ijrefrig.2024.04.024.
[62] Kim C, Kielty J, and Wells I. Decarbonizing Aluminum: Technologies and Approaches to Achieve Zero-Carbon Aluminum. https://www.nrdc.org/sites/default/files/2024-11/Decarbonizing_Aluminum_R%2024-11-A_03.pdf. 2024 [accessed on 12 October 2025].
[63] Scarsella A and Gasafi E. Green Alumina: A Technological Roadmap. Light Metals 2022, 2022: p. 3-10.
[64] Michael Barnes J N, Kushagra Bosamia,, Decarbonisation of the Bayer Process-A Technical Assessment of Enabling Technologies and Process Economics, in the 42nd International ICSOBA Conference. 2024: Lyon, France.
[65] Adamo A, Martín H, Hoz J d l, and Rubio J. A Review of Worldwide Strategies for Promoting High-Temperature Heat Pumps. Applied Sciences, 2025. 15(2): p. 839. doi:10.3390/app15020839.
[66] Bryan W. Hackett. The Essentials of Continuous Evaporation. https://www.aiche.org/resources/publications/cep/2018/may/essentials-continuous-evaporation#:~:text=require%20a%20large%20temperature%20gradient,of%20the%20liquid%20being%20concentrated. 2018 [accessed on 9 June 2025].
[67] Minton P E. Handbook of Evaporation Technology. Elsevier Science.1986.
[68] Keutenedjian Mady C E, Bresciani A E, Paiva J L, de Jardin R N, Guardani R, and de Oliveira S. Thermodynamic assessment of MVR implementation in multistage evaporation plants. Journal of the Brazilian Society of Mechanical Sciences and Engineering, 2018. 40(8): p. 395. 10.1007/s40430-018-1319-x.
[69] Liu G, Yang Q, Zhao Y, Li L, and Wang L. Experimental research on MVR system for industrial wastewater treatment. Desalination and Water Treatment, 2019. 147: p. 99-105. https://doi.org/10.5004/dwt.2019.23537.
[70] PILLER Blowers & Compressors. Multi-Stage Steam Regeneration. https://www.piller.de/fileadmin/media/pdf-files/brochures/Piller-multi-stage-steam-regeneration.pdf. [accessed on 12 November 2024].
[71] Power R B. Steam jet ejectors for the process industries. McGraw-Hill.1994.
[72] Deming Y, Bingqin L, Tao L, and Ming L. Energy saving research on multi-effect evaporation crystallization process of bittern based on MVR and TVR heat pump technology. American Journal of Chemical Engineering, 2020. 8: p. 54-62. https://doi.org/10.11648/j.ajche.20200803.11.
[73] Han Q, Zhang Z, Zhang H, Xue H, Sun W, and Jia L. Multi-ejector system based on multi-ejector optimization control algorithm for energy efficiency improvement and operating condition extension. Applied Thermal Engineering, 2025. 279: p. 127670. https://doi.org/10.1016/j.applthermaleng.2025.127670.

[74] Zhou S, Gong L, Liu X, and Shen S. Mathematical modeling and performance analysis for multi-effect evaporation/multi-effect evaporation with thermal vapor compression desalination system. Applied Thermal Engineering, 2019. 159: p. 113759. https://doi.org/10.1016/j.applthermaleng.2019.113759.
[75] Khalid B, Osman Ahmed H, and Amro Mohammed M. Modelling and Simulation of the Multi-effect/Thermal Vapor Compression Distillation Process. International Journal of Mechanical Engineering and Applications, 2020. 8(4): p. 103-110. https://doi.org/10.11648/j.ijmea.20200804.12.
[76] Shahzamanian B, Varga S, Soares J, Palmero-Marrero A, and Oliveira A. Theoretical performance assessment of a multi-effect distillation system integrated with thermal vapour compression unit running on solar energy. International Journal of Low-Carbon Technologies, 2024. 19: p. 908-921. 10.1093/ijlct/ctae010.
[77] Boltzmann L. Theoretical physics and philosophical problems. Springer.1974. 13-32.
[78] Wiegand G. Mechanical vapor recompression (MVR) solutions in evaporation processes. https://www.gea.com/en/assets/171000/. 2025 [accessed on 10th Jan 2025].
[79] Bantle M, Schlemminger C, Tolstorebrov I, Ahrens M, and Evenmo K, Performance evaluation of two-stage mechanical vapour recompression with turbo-compressors, in the 13th IIR Gustav Lorentzen Conference. 2018: Valencia, Spain.
[80] GEA. Mechanical vapor recompression (MVR) solutions for the economization of distillation. https://www.gea.com/en/assets/304829/. 2023 [accessed on 4 June 2025].
[81] The U.S. Department of Energy. Energy efficiency and industrial boiler efficiency: an industry perspective. https://www.nrel.gov/docs/fy04osti/35106.pdf. 2002 [accessed on 4 July 2025].
[82] Chetan T. Patel, Bhavesh K. Patel, and Vijay K. Patel. Efficiency with different GCV of coal and efficiency improvement opportunity in boiler. International journal of innovative research in science, engineering and technology, 2013. 2(5): p. 1518-1527.
[83] AspenTech. Unit Operations and Reaction Models. https://esupport.aspentech.com/FileAttachment?id=a0g0B00000GfNpB. 2013 [accessed on 11 June 2025].
[84] Barma M, Saidur R, Rahman S, Allouhi A, Akash B, and Sait S M. A review on boilers energy use, energy savings, and emissions reductions. Renewable and sustainable energy reviews, 2017. 79: p. 970-983. https://doi.org/10.1016/j.rser.2017.05.187.
[85] Industrial Decarbonization Roadmap. https://www.energy.gov/sites/default/files/2022-09/Industrial%20Decarbonization%20Roadmap.pdf. 2022 [accessed on 6 June 2025].
[86] Pee A d, Pinner D, Roelofsen O, and Somers K. Decarbonization of industrial sectors: the next frontier. 2018
[87] Farghali M, Osman A I, Mohamed I M, Chen Z, Chen L, Ihara I, Yap P-S, and Rooney D W. Strategies to save energy in the context of the energy crisis: a review. Environmental Chemistry Letters, 2023. 21(4): p. 2003-2039. https://doi.org/10.1007/s10311-023-01591-5.
[88] PARAT. High Voltage Electrode boiler for Steam and Hot water. https://www.parat.no/en/products/industry/parat-ieh-high-voltage-electrode-boiler/. [accessed on 7 June 2025].
[89] Zhang N, Lu X, McElroy M B, Nielsen C P, Chen X, Deng Y, and Kang C. Reducing curtailment of wind electricity in China by employing electric boilers for heat and pumped hydro for energy storage. Applied Energy, 2016. 184: p. 987-994. https://doi.org/10.1016/j.apenergy.2015.10.147.
[90] Ali Hasanbeigi, Lynn Kirshbaum, and Blaine Collison. Electrifying U.S. industry: Technology and process-based approach to decarbonization. https://www.globalefficiencyintel.com/electrifying-us-industry. 2021 [accessed on 22 Feb 2026].
[91] Zuberi M J S, Hasanbeigi A, and Morrow W. Electrification of industrial boilers in the USA: potentials, challenges, and policy implications. Energy Efficiency, 2022. 15(8): p. 70. https://doi.org/10.1007/s12053-022-10079-0.
[92] Hydro. Alunorte starts two new electric boilers, reducing carbon emissions. https://www.hydro.com/en/global/media/news/2025/alunorte-starts-two-new-electric-boilers-reducing-carbon-emissions/. 2025 [accessed on 22 Feb 2026].
[93] Bielefeld S, Cvetković M, and Ramírez A. The potential for electrifying industrial utility systems in existing chemical plants. Applied Energy, 2025. 392: p. 125988. https://doi.org/10.1016/j.apenergy.2025.125988.
[94] Natural gas prices in world data. https://ourworldindata.org/grapher/natural-gas-prices?time=2020..latest. 2025 [accessed on 6 June 2025].
[95] World in Data. Levelized cost of energy for renewables. https://ourworldindata.org/grapher/levelized-cost-of-energy?tab=table&time=2023..latest. 2023 [accessed on 6 June 2025].

[96] Golombek R, Lind A, Ringkjøb H-K, and Seljom P. The role of transmission and energy storage in European decarbonization towards 2050. Energy, 2022. 239: p. 122159. https://doi.org/10.1016/j.energy.2021.122159.
[97] Davis D, Müller,F., Saw,W.L., Steinfeld,A., Nathan,G.J. Solar-driven alumina calcination for CO_2 mitigation and improved product quality. Green Chemistry, 2017. 19(13): p. 2992-3005. https://doi.org/10.1039/C7GC00585G.
[98] Lee L, Ingenhoven P, Tian Z, Sun Z, Chinnici A, Jafarian M, Ashman P, Potter D, and Saw W. Pathways to the use of concentrated solar heat for high temperature industrial processes. Solar Compass, 2023. 5: p. 100036. https://doi.org/10.1016/j.solcom.2023.100036.
[99] Saw W L, Naufal A, Sandoval A B, Beath A, Lovegrove K, van Eyk P, McNaughton R, Bader R, and Nathan G, Technical feasibility of integrating concentrating solar thermal energy in the Bayer alumina process, in SolarPACES 2019. 2019: Daegu, South Korea
[100] Ingenhoven P, Lee L, Saw W, Rafique M M, Potter D, and Nathan G J. Techno-economic assessment from a transient simulation of a concentrated solar thermal plant to deliver high-temperature industrial process heat. Renewable and Sustainable Energy Reviews, 2023. 185: p. 113626. https://doi.org/10.1016/j.rser.2023.113626.
[101] Padilla I, López-Delgado A, López-Andrés S, Álvarez M, Galindo R, and Vazquez-Vaamonde A J. The application of thermal solar energy to high temperature processes: case study of the synthesis of alumina from boehmite. The Scientific World Journal, 2014. 2014(1): p. 825745. https://doi.org/10.1155/2014/825745.
[102] Sucech S W and Misra C. Alcoa Pressure Calcination Process for Alumina. Essential Readings in Light Metals: Volume 1 Alumina and Bauxite, 2016: p. 669-674. 10.1007/978-3-319-48176-0_93.
[103] Neuwirth M, Fleiter T, Manz P, and Hofmann R. The future potential hydrogen demand in energy-intensive industries-a site-specific approach applied to Germany. Energy Conversion and Management, 2022. 252: p. 115052. https://doi.org/10.1016/j.enconman.2021.115052.
[104] Liu W, Zuo H, Wang J, Xue Q, Ren B, and Yang F. The production and application of hydrogen in steel industry. International Journal of Hydrogen Energy, 2021. 46(17): p. 10548-10569. https://doi.org/10.1016/j.ijhydene.2020.12.123.
[105] Zou C, Li J, Zhang X, Jin X, Xiong B, Yu H, Liu X, Wang S, Li Y, and Zhang L. Industrial status, technological progress, challenges, and prospects of hydrogen energy. Natural Gas Industry B, 2022. 9(5): p. 427-447. https://doi.org/10.1016/j.ngib.2022.04.006.
[106] Ramachandran R and Menon R K. An overview of industrial uses of hydrogen. International journal of hydrogen energy, 1998. 23(7): p. 593-598. https://doi.org/10.1016/S0360-3199(97)00112-2.
[107] ARENA. World first hydrogen pilot for low carbon alumina. https://arena.gov.au/news/world-first-hydrogen-pilot-for-low-carbon-alumina/. July 2023 [accessed on 6 April 2025].
[108] Rio Tinto and Sumitomo – Yarwun Hydrogen Calcination Pilot Demonstration Program – Lessons Learnt Report. https://arena.gov.au/knowledge-bank/rio-tinto-and-sumitomo-yarwun-hydrogen-calcination-pilot-demonstration-program-lessons-learnt-report/. 2023 [accessed on 9 March 2025].
[109] Sáez-Guinoa J, Senante I, Pascual S, Llera-Sastresa E, and Romeo L M. Eco-efficiency assessment of carbon capture and hydrogen transition as decarbonisation strategies in alumina production. Journal of Cleaner Production, 2024. 485: p. 144366. https://doi.org/10.1016/j.jclepro.2024.144366.
[110] Mohammed R A. Modeling and Analysis of Power-to-hydrogen based Alumina Hydrate Calcination for Low-carbon Aluminum Making. 2023. Master's Thesis. Khalifa University of Science.
[111] Osman A I, Mehta N, Elgarahy A M, Hefny M, Al-Hinai A, Al-Muhtaseb A a H, and Rooney D W. Hydrogen production, storage, utilisation and environmental impacts: a review. Environmental Chemistry Letters, 2022: p. 1-36. https://doi.org/10.1007/s10311-021-01322-8.
[112] McLellan B, Shoko E, Dicks A, and Da Costa J D. Hydrogen production and utilisation opportunities for Australia. International journal of hydrogen energy, 2005. 30(6): p. 669-679. https://doi.org/10.1016/j.ijhydene.2004.06.008.
[113] Mach T, Calcination apparatus and process using hydrogen. 2023. US20230064514A1. https://patentimages.storage.googleapis.com/17/0c/5d/8cf5d1292a2881/US20230064514A1.pdf.
[114] Longden T, Beck F J, Jotzo F, Andrews R, and Prasad M. 'Clean'hydrogen?–Comparing the emissions and costs of fossil fuel versus renewable electricity based hydrogen. Applied Energy, 2022. 306: p. 118145. https://doi.org/10.1016/j.apenergy.2021.118145.
[115] IEA. The Future of Hydrogen, Report Prepared by the IEA for the G20, Japan. https://www.iea.org/reports/the-future-of-hydrogen. 2019 [accessed on 1 July 2023].
[116] International Energy Agency (IEA). The Future of Hydrogen, Seizing today's opportunities. https://www.iea.org/reports/the-future-of-hydrogen. 2019 [accessed on 1 March 2025].

[117] Wang Y, Wen C, Tu J, Zhan Z, Zhang B, Liu Q, Zhang Z, Hu H, and Liu T. The multi-scenario projection of cost reduction in hydrogen production by proton exchange membrane (PEM) water electrolysis in the near future (2020–2060) of China. Fuel, 2023. 354: p. 129409. https://doi.org/10.1016/j.fuel.2023.129409.
[118] Curcio E. Techno-economic analysis of hydrogen production: Costs, policies, and scalability in the transition to net-zero. International Journal of Hydrogen Energy, 2025. 128: p. 473-487. https://doi.org/10.1016/j.ijhydene.2025.04.013.
[119] Mitterrutzner B, Sovacool B K, Knudsen B R, Bazilian M D, Kim J, Roussanaly S, Tomasgard A, and Griffiths S. Scaling carbon capture and storage (CCS) to gigaton capacity: A multi-dimensional and critical review. International Journal of Greenhouse Gas Control, 2026. 149: p. 104531. https://doi.org/10.1016/j.ijggc.2025.104531.
[120] Intergovernmental Panel on Climate Change. Carbon Dioxide Capture and Storage. https://www.ipcc.ch/site/assets/uploads/2018/03/srccs_wholereport-1.pdf. 2005 [accessed on 8 June 2024].
[121] Hayat M A, Hasan S, and Elshurafa A M. Strategic priorities and cost considerations for decarbonizing electricity generation using CCS and nuclear energy. Energy Reports, 2024. 12: p. 2108-2122. https://doi.org/10.1016/j.egyr.2024.08.017.
[122] Rubin E S, Davison J E, and Herzog H J. The cost of CO_2 capture and storage. International Journal of Greenhouse gas control, 2015. 40: p. 378-400. https://doi.org/10.1016/j.ijggc.2015.05.018.
[123] Mallapragada D S, Dvorkin Y, Modestino M A, Esposito D V, Smith W A, Hodge B-M, Harold M P, Donnelly V M, Nuz A, and Bloomquist C. Decarbonization of the chemical industry through electrification: Barriers and opportunities. Joule, 2023. 7(1): p. 23-41. https://doi.org/10.1016/j.joule.2022.12.008.
[124] Papadis E and Tsatsaronis G. Challenges in the decarbonization of the energy sector. Energy, 2020. 205: p. 118025. https://doi.org/10.1016/j.energy.2020.118025.
[125] Wei M, McMillan C A, and de la Rue du Can S. Electrification of industry: Potential, challenges and outlook. Current Sustainable/Renewable Energy Reports, 2019. 6: p. 140-148. https://doi.org/10.1007/s40518-019-00136-1.
[126] Wheatland M, Fu J, Xia Y, Boot-Handford M, and Sceats M, An Innovative Approach to Smelter-Grade Alumina Calcination Using Renewable Energy, in TMS Annual Meeting & Exhibition 2024. 2024: Orlando, Florida, USA. p. 38-45.
[127] ARENA. Alcoa Renewable Powered Electric Calcination Pilot. https://arena.gov.au/projects/alcoa-renewable-powered-electric-calcination-pilot/. 2022 [accessed on 7 March 2025].
[128] Shephered C and Lapple C. Flow pattern and pressure drop in cyclone dust collectors. Industrial & Engineering Chemistry, 1939. 31(8): p. 972-984. https://doi.org/10.1021/ie50356a012.
[129] Whittington B, Ilievski, D. Determination of the gibbsite dehydration reaction pathway at conditions relevant to Bayer refineries. Chemical Engineering Journal, 2004. 98(1-2): p. 89-97. https://doi.org/10.1016/S1385-8947(03)00207-9.
[130] Vasile B S, Dobra G, Iliev S, Cotet L, Neacsu I A, Surdu V A, Nicoara A I, Boiangiu A, and Filipescu L. Thermally Activated $Al(OH)_3$ Part II—Effect of Different Thermal Treatments. Ceramics, 2021. 4(4): p. 564-575. https://doi.org/10.3390/ceramics4040040.
[131] Candela L, Perlmutter, D.D. Pore structure and kinetics of the thermal decomposition of Al $(OH)_3$. AIChE journal, 1986. 32(9): p. 1532-1545. https://doi.org/10.1002/aic.690320914.
[132] Perić J, Krstulović R, and Vučak M. Investigation of dehydroxylation of gibbsite into boehmite by DSC analysis. Journal of thermal analysis, 1996. 46: p. 1339-1347. https://doi.org/10.1007/BF01979247.
[133] Redaoui D, Sahnoune F, Heraiz M, and Raghdi A. Mechanism and kinetic parameters of the thermal decomposition of gibbsite $Al(OH)_3$ by thermogravimetric analysis. Acta Physica Polonica A, 2017. 131(3): p. 562-565. https://doi.org/10.12693/APHYSPOLA.131.562.
[134] Alex T, Sasi Kumar C, Kailath A J, Kumar R, Roy S, and Mehrotra S. Analysis of mechanically induced reactivity of boehmite using kinetics of boehmite to γ-Al_2O_3 transformation. Metallurgical and Materials Transactions B, 2011. 42: p. 592-603. https://doi.org/10.1007/s11663-011-9494-5.
[135] Boquan Z, Binxiang F, and Xiangcheng L. Dehydration reactions and kinetic parameters of gibbsite. Ceramics International, 2010. 36(8): p. 2493-2498. https://doi.org/10.1016/j.ceramint.2010.07.007.
[136] Mizuno A. Electrostatic precipitation. IEEE Transactions on dielectrics and electrical insulation, 2000. 7(5): p. 615-624. https://doi.org/10.1109/94.879357.
[137] Miller B G. Clean coal engineering technology. Elsevier.2010.

[138] Feng S, Zhong Z, Wang Y, Xing W, and Drioli E. Progress and perspectives in PTFE membrane: Preparation, modification, and applications. Journal of membrane science, 2018. 549: p. 332-349. https://doi.org/10.1016/j.memsci.2017.12.032.
[139] Green D W and Perry R H. Perry's chemical engineers' handbook. McGraw-Hill Education.2008.
[140] Fenger J, Raahauge B E, and Wind C B. Experience with 3x4500 tpd gas suspension calciners (GSC) for alumina. Essential Readings in Light Metals, 2016: p. 664-668.
[141] Jaworek A, Krupa A, and Czech T. Modern electrostatic devices and methods for exhaust gas cleaning: A brief review. Journal of electrostatics, 2007. 65(3): p. 133-155. https://doi.org/10.1016/j.elstat.2006.07.012.
[142] Huang H, Zheng C, and Zhao H. Numerical investigation on non-steady-state filtration of elliptical fibers for submicron particles in the ‘‘Greenfield gap’’range. Journal of Aerosol Science, 2017. 114: p. 263-275. https://doi.org/10.1016/j.jaerosci.2017.09.018.
[143] Howden turbo technology. https://www.chartindustries.com/Products/Compression-Centrifugal-Compressors. [accessed on 1 June 2024].
[144] Gallaer C A and Schindeler J. Mechanical dust collectors. Journal of the Air Pollution Control Association, 1963. 13(12): p. 574-580.
[145] Di Natale F, Carotenuto C, Parisi A, Flagiello D, and Lancia A. Wet electrostatic scrubbing for flue gas treatment. Fuel, 2022. 325: p. 124888. https://doi.org/10.1016/j.fuel.2022.124888.
[146] Das S K and Biswas M N. Studies on ejector-venturi fume scrubber. Chemical Engineering Journal, 2006. 119(2-3): p. 153-160. https://doi.org/10.1016/j.cej.2006.03.019.
[147] Mohan B R, Jain R, and Meikap B. Comprehensive analysis for prediction of dust removal efficiency using twin-fluid atomization in a spray scrubber. Separation and Purification Technology, 2008. 63(2): p. 269-277. https://doi.org/10.1016/j.seppur.2008.05.006.
[148] Meek R L. Control of Particulate Emissions in the Primary Nonferrous Metals Industries. Vol. 1. Environmental Protection Agency.1979.
[149] Letcher T. Comprehensive renewable energy.2022.
[150] PILLER. PILLER Blowers & Compressors. https://www.piller.de/products-services/mvr-blower-piller-blowers-compressors/vapoflex/. [accessed on 12 November 2024].
[151] Energy Efficiency and Conservation Authority. MVR (Mechanical Vapour Recompression) Systems for Evaporation, Distillation and Drying. https://genless.govt.nz/assets/Business-Resources/Mechanical-vapour-recompression-for-evaporation-distillation-drying.pdf. 2019 [accessed on 7 July 2024].
[152] Li S, Wei M, and Wang X. A numerical study on film condensation of steam with non-condensable gas on a vertical plate. Frontiers in Energy Research, 2023. 11: p. 1064067. https://doi.org/10.3389/fenrg.2023.1064067.
[153] Yu S, Gasafi E, Borges A, Grünig J, and Routray P, Heat and Water Recovery from Alumina Calciners Stack Offgas- A Technology Review, in the 12th International AQW Conference and Exihibition. 2024, Dubai, UAE.

Chapter 3

Techno-economic Assessment of Decarbonising Alumina Calcination Using Hydrogen Combustion with Steam Recovery

Preface

Conventional alumina calcination uses natural gas/air combustion to provide high temperature (~950°C) converting gibbsite to smelter-grade alumina (SGA) with steam as the by-product. However, this steam becomes too diluted by combustion products to be economically recovered, even though such recovery is desirable given that the Bayer process requires steam. This chapter investigates hydrogen combustion as a net-zero fuel to natural gas, while also exploring potential to increase the viability of steam recovery from the calcination process by avoiding dilution from combustion products, with a focus on calcination performance, economic feasibility.

Key highlights include:

- The novel hydrogen in oxy-steam calcination concept achieves net-zero emissions while generating high-concentration exit steam.
- Steam-based calcination shows the comparable performance (±1%) of the calcination process such as cyclone separation efficiency, to that for air combustion.
- Steam recovery integration improves the economic viability of hydrogen calcination.

Statement of Authorship

Title of Paper	Techno-economic Assessment of Decarbonising Alumina Calcination Using Hydrogen Combustion with Steam Recovery
Publication Status	☐ Published ☐ Accepted for Publication ☑ Submitted for Publication ☐ Unpublished and Unsubmitted w ork w ritten in manuscript style
Publication Details	Ning S, Nathan G, Ashman P, and Saw W L. Techno-economic Assessment of Decarbonising Alumina Calcination Using Hydrogen Combustion with Steam Recovery. Submitted to Energy Conversion and Management: X, 2025. Under review

Principal Author

Name of Principal Author (Candidate)	Siyun Ning		
Contribution to the Paper	Concept deisgn, Process model development and simulation, Data analysis and interpretation, Drafted the manuscript and acted as corresponding author.		
Overall percentage (%)	65%		
Certification:	This paper reports on original research I conducted during the period of my Higher Degree by Research candidature and is not subject to any obligations or contractual agreements with a third party that would constrain its inclusion in this thesis. I am the primary author of this paper.		
Signature		Date	

Co-Author Contributions

By signing the Statement of Authorship, each author certifies that:

i. the candidate's stated contribution to the publication is accurate (as detailed above);

ii. permission is granted for the candidate in include the publication in the thesis; and

iii. the sum of all co-author contributions is equal to 100% less the candidate's stated contribution.

Name of Co-Author	Graham Nathan		
Contribution to the Paper	Supervision of the work, Concept development, Evaluation and review of the manuscript.		
Signature		Date	

Name of Co-Author			
Contribution to the Paper	Supervision of the work, Concept development, Evaluation and review of the manuscript.		
Signature		Date	2/12/2025

Please cut and paste additional co-author panels here as required.

Name of Co-Author	Woei Lean Saw		
Contribution to the Paper	Supervision of the work, Concept development, Ev pt.		
Signature		Date	

Techno-economic Assessment of Decarbonising Alumina Calcination Using Hydrogen Combustion with Steam Recovery

Siyun Ning [a,b,c], Graham Nathan [b,c,d], Peter Ashman [a,b,c], Woei Lean Saw [a,b,c]

[a] *School of Chemical Engineering, The University of Adelaide, Australia*

[b] *Centre for Energy Technology, The University of Adelaide, Australia*

[c] *Heavy Industry Low-carbon Transition Cooperative Research Centre, Australia*

[d] *School of Electrical and Mechanical Engineering, The University of Adelaide, Australia*

Corresponding author: siyun.ning@adelaide.edu.au

Abstract

This study reports on conditions that enable techno-economic viability from the retrofitting alumina calciners for hydrogen combustion as a decarbonisation strategy, within a novel flowsheet that increases the viability of steam recovery. Three calcination scenarios were evaluated including natural gas in air with CO_2 capture and storage , hydrogen in air and hydrogen in oxygen-steam combustion, the last of which achieves zero direct emissions from calcination while avoiding dilution with nitrogen to increase the viability of steam recovery. These processes were modelled in Aspen plus to assess the calcination performance. The hydrogen/air scenario demonstrates the lowest energy demand for the calcination process at 2.7 GJ/$t_{Al_2O_3}$ (LHV), compared with 2.88 GJ/$t_{Al_2O_3}$ (LHV) for natural gas/air. For the hydrogen and oxy-steam combustion scenario, while the gross energy consumption ranges from 2.89 to 2.96 GJ/$t_{Al_2O_3}$ (LHV), this configuration also offers potential to recover the high-concentration steam for reuse. Energy distribution analysis shows that this higher energy input is attributed to the reduced heat transfer efficiency between recirculation steam and solids in cooling sections and inhibited gibbsite to boehmite reaction in preheating section. Economically, the calculated offset from steam recovery, compared with steam generation via electric boilers, increases the break-even hydrogen price from 2.8 to 3.4 US$/kg for hydrogen in air and hydrogen in oxy-steam cases, relative to natural gas at 7.5 US$/GJ with the inclusion of a carbon capture and storage cost of 179 US$/$t_{CO_2}$.

Keywords: Decarbonisation, Alumina Calcination, Hydrogen Combustion, Techno-economic Analysis, Steam Recovery

1. Introduction

Refining bauxite ore to alumina through the Bayer process requires significant energy, ranging from 8.5 to 14.5 GJ/$t_{Al_2O_3}$ depending on bauxite ore quality, technologies used and fuel types in various regions [1] . The refining process results in an average of 1.2 t CO_2/$t_{Al_2O_3}$ emissions globally [2], though Australian refineries achieve a lower intensity of 0.7 t CO_2/$t_{Al_2O_3}$ [3]. These emissions are nationally significant for major alumina-producing countries. For example, for China, Australia and Brazil, these processes account for approximately 4% [4, 5], 24% [6, 7] and 6% [8], respectively, of scope 1 manufacturing emissions, and 1%, 4% and 1% of the nation's total emissions, respectively. Reducing these emissions is therefore important to the national targets for China [9, 10], Australia [11] and Brazil [12]. Within the Bayer process, steam generation from coal or natural gas-fired boilers for process heat and direct natural gas firing in calcination account for approximately 2/3 and 1/3 of the energy use and total emissions. The calcination process converts gibbsite to smelter-grade alumina (SGA) at high temperature (~950-1000°C) which releases steam during the process, consuming approximately 3 GJ/$t_{Al_2O_3}$ energy [13]. Such temperatures currently necessitate direct combustion of fossil fuels such as oil, coal, and natural gas, with natural gas being the predominant fuel in Australian region [14]. The present study aims to assess alternative low-carbon technologies capable of supplying the high temperatures required for calcination, thereby mitigating the direct emissions from fossil fuel combustion.

The calcination process, as shown in Figure 1, with natural gas injected in preheating furnace and main calciner, where it is combusted with air to provide high temperature. The thermal decomposition of gibbsite to produce Smelter Grade Alumina (SGA) by removal of chemically bound water, , as shown in reaction (1) [15]. Calcination reaction occurs in two steps. Firstly, gibbsite is

converted to boehmite in the preheating cyclone, as shown in reaction (2), after which boehmite is concerted to alumina in the main calciner, as depicted in reaction (3) [16].

$$2\,Al(OH)_3\,(s) \rightarrow Al_2O_3(s) + 3H_2O\,(g) \qquad \Delta H=-101.89\ kJ/mol \qquad (1)\ [17]$$

$$Al(OH)_3(s) \rightarrow AlO(OH)(s) + H_2O(g) \qquad \Delta H=-55.29\ kJ/mol \qquad (2)$$

$$2AlO(OH)(s) \rightarrow Al_2O_3(s) + H_2O(g) \qquad \Delta H=-46.6\ kJ/mol \qquad (3)$$

During alumina calcination, the combustion of natural gas contributes directly CO_2 emissions, and the process vents flue gas containing a significant amount of steam. However, this steam is heavily diluted by a large amount of air and combustion products, making its recovery and reuse in refining process challenging. Given that Bayer process requires high-pressure steam at around 6-8 bar, typically produced from fossil fuel boilers, recovering this wasted steam from calcination is desirable. Therefore, this study aims to assess alternative methods to decarbonise the calcination step, while also exploring potential to increase the viability of steam reuse from the calcination process by avoiding dilution with air and combustion.

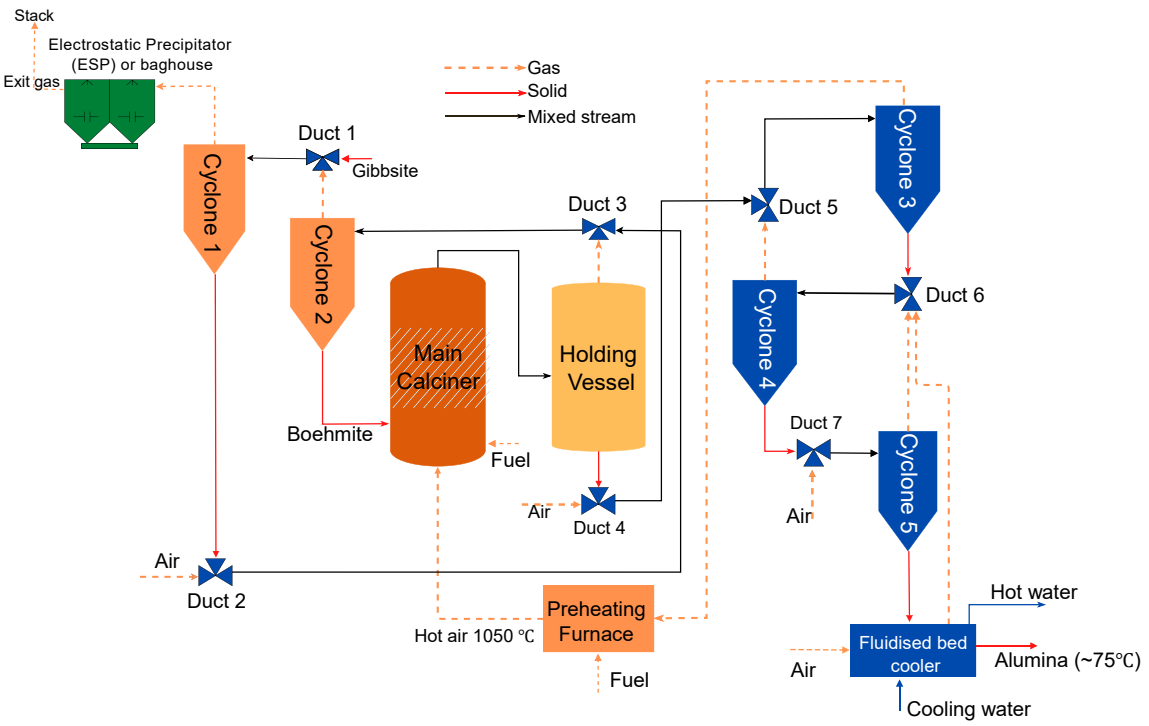


Figure 1. The process flowsheet for the reference conventional flash calciner (adapted from previous work [18]).

Two of the low-carbon calcination options currently under development involving replacing natural gas with either hydrogen or electrical heating, both of which offer the potential to reduce direct

CO_2 emissions from the calcination process [13]. Both of these options offer potential to increase the viability of steam recovery by avoiding dilution gas from natural gas and air combustion, in particular if oxygen is used as the oxidant for the case of hydrogen combustion. Of these two options, the combustion of hydrogen is most advanced. For example, Rio Tinto, one of Australia's leading alumina producers, is presently conducting a series of trials with a hydrogen-fired calciner to assess the technical feasibility of hydrogen-combusted calcination process [19], with the support of the Australian government [20]. However, no techno-economic assessment of the feasibility of these options is currently available for either hydrogen-based or electric calcination. The hydrogen combustion route is easier to implement from the perspective of the calciner, given that relatively few modifications are needed to replace the fuel [21], notwithstanding the need for some development to ensure suitable product quality is maintained, so that the former trial is being undertaken at full scale. In addition, no flowsheet has been reported in the open literature that would allow steam recovery to be made with either energy source. Hence one objective of the present investigation is to propose and evaluate such options.

Each of the options of hydrogen combustion and electrical heating present distinct technical and economic implementation challenges to alumina calcination. For hydrogen combustion to be implemented, the hydrogen must be made available at sufficient scale and cost, which is presently some time away. On the other hand, electric calciners are currently available only at pilot scale, with a capacity approximately 0.2 to 2 t/hr alumina production [22], which is much smaller than the 90 t/hr [23], typical of a large calciner. Hence, electric calciners still require significant scaling and development, potentially increasing capital investment costs, at least for the first versions of the technology. Furthermore, the modifications that are needed for each option can vary significantly from site-to-site, neither of which has been reported in the open literature. Accordingly, the aim of the present investigation is to advance understanding of the various options for integrating hydrogen combustion into alumina calcination these issues through a techno-economic assessment.

During calcination process, injected air serves not only as combustion oxidiser, but also as a carrier gas for transporting solids through the process and as a medium for heat exchange between the gas and solids in the cyclones, as shown in Figure 1. Hence, the development of a retrofittable calciner configuration to accommodate hydrogen must achieve both of these functions. Whilst this is relatively straight-forward for the combustion of hydrogen in air, it is more challenging for the potential configuration in which hydrogen may be combusted in an O_2-steam atmosphere. Changing the fuel from natural gas/air to hydrogen/air must consider impact on flame temperature, volumetric flow-rate, cyclone performance, and heat exchange efficiency in both preheating and cooing stages in calciner circuit, which are crucial to overall calcination performance. However, eliminating the use of air to operate with only hydrogen and oxygen is much more significant, because it must introduce a change to the process flow gases to provide a carrier gas to transport the solids with a similar volumetric flow rate to the original configuration. The logical option is to use superheated steam as the carrier gas and heat exchange medium in hydrogen/O_2-steam calcination, unlocking the potential to discharge nearly pure steam from the stack [24], noting that this requires a modification to the pipe layout. In addition, this requires evaluating the effects of steam-rich atmosphere on the overall calcination process, including cyclone performance and stream temperatures. Given these considerations, the present investigation aims to assess and compare calcination performance when transiting from conventional natural gas/air calcination to either hydrogen/air or hydrogen in oxy-steam combustion.

The reaction environment, particularly the partial pressure of the water vapour surrounding the solids, plays a significant role in determining the rate of gibbsite dehydroxylation reactions (2) and (3) [25]. Studies on the reaction kinetics of gibbsite to boehmite and boehmite to alumina have been reported by numerous researchers, as summarised in Table 1. The reported kinetic parameters, such as activation energy and pre-exponential factors, vary depending on the experiment conditions. Most results have been obtained under a dry atmosphere using thermogravimetric analysis (TGA) to measure the change in mass of a material as a function of time and by use of differential scanning calorimetry (DSC) to measure the heat flow associated with phase transitions as a function of time. The results,

along with the experimental conditions, are presented in Table 1. Saw et al. [26] investigated the reaction kinetics under 80% steam and observed that higher steam concentrations inhibited the reaction rate in the steam calcination environment, consistent with earlier findings [25]. Similarly, Candela [27] also reported that increased steam concentration surrounding the solid can supress the conversion of gibbsite to boehmite. However, no studies to date have integrated reaction kinetics into process models to assess their impact on calcination performance. Given these knowledge gaps, the present study also aims to evaluate the effect of high-concentration steam on the calcination reactions, and its resulted influence on the energy utilisation and consumption, by incorporating kinetic data from the literature.

Table 1: A summary of kinetic parameters reported in the literature for gibbsite calcination.

Gibbsite-boehmite					
Reference	Experiments conditions	Particle size (μm)	Temperature (°C)	Activation energy (KJ/mol)	re-exponential factor (s^{-1})
Peric (1996) [28]	DSC method (20 °C/min) Dry nitrogen atmosphere	/	180-400	133	1.5×10^{9}
Redaoui et al. (2017) [29]	TG/DSC (5-20 °C/min) Dry argon atmosphere	/	246	157.53	7.58×10^{15}
Saw et al. (2023) [26]	80% steam Preheated furnace	60	400	78	7.4×10^{4} ~1.73×10^{5}
Boehmite-alumina					
Zhu et al. (2010) [30]	DSC method (20 °C/min) Dry argon atmosphere	45	450-550	217.24	8.3×10^{13}
Alex et al. (2011) [31]	TG/DSC (5-20 °C/min) Dry argon atmosphere	110	527	211.7	1.12×10^{11}
Saw et al. (2023) [26]	80% steam Preheated furnace	60	650	91.2	2806.0

An economic perspective is also essential when assessing the transition between fuel types. While the current cost of hydrogen produced from the electrolysis using renewable electricity is high, primarily due to the cost of electricity, these costs are projected to reduce into the future, both for electrolysis and decline of electricity price [32, 33]. Recent projections for the price of renewable hydrogen from electrolysis are between 4 to 6 US$/kg in 2023-2024 [34, 35], with a projected decline to 2.5-4.0 US$/kg by 2030 [35, 36]. Further cost reductions to below 2 US$/kg are anticipated by 2050[37, 38]. In addition, a wide range of alternative hydrogen production methods that avoid a reliance on electricity are also under development with significant potential for more substantial cost reductions in the 2050 time-frame, such as solar photo-catalysis, methane pyrolysis, thermochemical water splitting, and bio-derived hydrogen [39]. Notwithstanding carbon capture and storage (CCS)

which captures direct CO_2 emissions and stores it permanently underground represents another potential decarbonisation pathway [40]. The current high cost and scale-up requirement limit its feasibility for deployment [41]. Technologies which reduce emissions through the use of renewable energy offer optional pathways alternative to CCS. Nevertheless, few studies have directly compared these decarbonisation pathways in the context of alumina calcination. Hence, this study aims to compare the associated cost of natural-gas calcination case fitted with CCS against hydrogen-based calcination, while also accounting for the value of nearly pure steam from hydrogen in oxy-steam calcination.

Given the identified knowledge gaps, the present investigation aims to retrofit existing calcination process transiting from natural gas combustion to hydrogen combustion, integrated with high-concentration steam recovery. The study further evaluates the effects of high-concentration steam environment on calcination performance, including calcination reactions and energy utilisation through the integration of literature-based kinetics into process models. Finally, it aims to provide the techno-economic assessment of hydrogen-based calcination with steam recovery in comparison with natural-gas calcination equipped with CCS, thereby providing a critical comparison for evaluating feasible low-carbon pathways for alumina calcination.

2. Methodology

2.1 Calcination case studies

2.1.1 Scenario 1- Alumina calcination with natural gas/air combustion

Figure 1 presents the reference process flowsheet for a conventional flash calciner using natural gas as the gaseous fuel, which is representative of commercial processes [18, 42]. Gibbsite entering the calciner is dried and preheated in Cyclone 1, following which the solids are transported to Cyclone 2, where gibbsite is partially calcined to boehmite, shown in Reaction (2). The corresponding reaction enthalpies are obtained from thermochemical data reported in the literature [17]. The decomposition

of gibbsite is driven by the sensible heat carried by the flue gas from the holding vessel, which provides the necessary thermal energy for the endothermic reaction. Dehydroxylation of boehmite occurs in the main calciner, as described by Reaction (3), requiring high temperature at approximately 950°C [42]. Natural gas is injected into the main furnace and combusted with air to provide the heat to drive this calcination step. Hot combustion gases transport the calcined alumina to the holding vessel to ensure sufficient retention time, typically several minutes, allowing the phase transition process to γ-alumina [18, 43, 44]. In the holding vessel, solids fall to the bottom while gases exit from the top. The separated solids are then transported to cyclones 3-5, where sensible heat in hot solids is recovered to preheat injected air. Some of this air is injected into Duct 2 to transport solids, while additional air is injected into the water-cooled fluidised bed cooler to fluidise the solids and further reduce their temperature to around 75°C. The heated air is directed to the preheating furnace, where it is further heated to 1050°C through natural gas combustion before being supplied to the main furnace. To control the dust emissions, a baghouse (fabric filters) or an electrostatic precipitator (ESP) is used to remove entrained particles in the flue gas before it is released into the atmosphere via the stack.

2.1.2 Scenario 2 - Alumina calcination with hydrogen/air combustion

The only change to the process flowsheet under hydrogen/air combustion from that with natural gas/air combustion (Figure 1) is that, the natural gas is replaced with hydrogen as the input fuel to achieve zero direct emissions from fuel combustion. Only scope 1 emissions from direct fuel combustion are considered, whereas emissions associated with hydrogen production and transport are excluded from the present analysis. In this case, the same input air mass flow is maintained as in natural gas/air combustion to maintain the heat transfer efficiency in preheating and cooling sections. This results in a slight increase in excess air, leading to an oxygen concentration in the exit flue gas of approximately 1% for natural gas/air combustion and 3% for hydrogen/air combustion.

2.1.3 Scenario 3 - Alumina steam calcination under hydrogen/O_2-steam combustion

Figure 2 presents a novel process flowsheet that has been developed previously [24] to enable retrofitting of flash calciner for H_2 combustion in an oxy-steam atmosphere and the recovery of steam. The natural gas is replaced with hydrogen, both in the main furnace and the preheating furnace. After undergoing particle filtration systems, the steam is sent to the first-stage of compression, via a blower, to overcome the pressure losses through the calciner circuit [24]. After the compression, a portion of the steam is recycled to carry solids and establish the atmosphere for oxy-steam combustion. This configuration also introduces additional cyclones (Cyclones 0 and 6), one each for the preheating and cooling stages, to overcome the potential reduction in heat exchange efficiency between the steam and solids relative to that in the original configuration (Figure 1). Superheated steam is returned to Ducts 4 and 9 to recover heat from the discharged hot alumina. Some steam is also recirculated to Duct 3 to transport particles, and to the fluidised bed cooler to fluidise the solids. The recycled steam mass flow is adjusted to maintain similar volumetric flow rates of streams entering the cyclones, ensuring that gas velocities remain consistent with those in natural gas/air calcination. Remaining steam is recovered for reuse in digestion following additional steam recovery processes. Gibbsite is fed and dried in Cyclone 0, after which the solids are transported to Cyclone 1 for preheating, and then to Cyclone 2 where dehydroxylation reaction occurs and gibbsite is partially converted to boehmite. Further decomposition and phase transformations occur in the main calciner and holding vessel at high temperatures (950°C), followed by heat recovery through Cyclones 3 to 6.

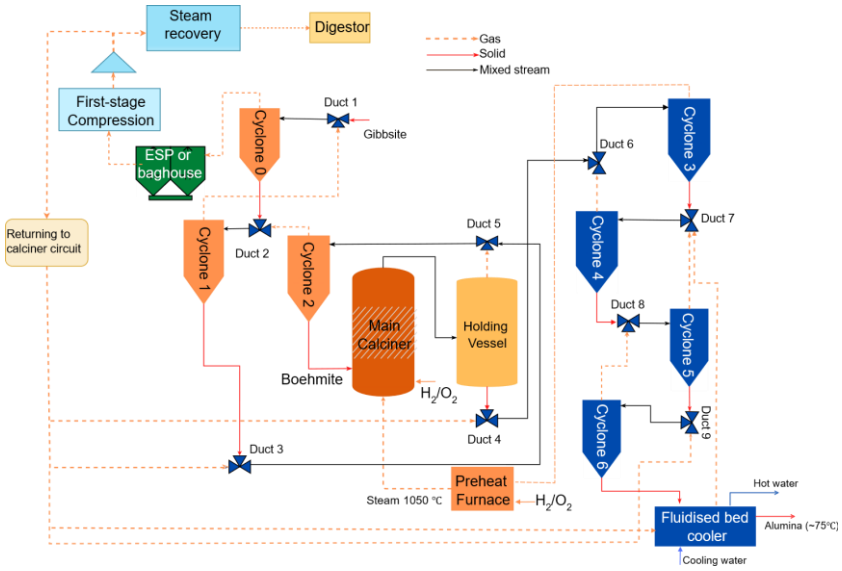


Figure 2.The process flowsheet to achieve steam recovery from flash calcination with H_2 and O_2 that is diluted with recirculated steam before combustion.

2.2 Process modelling

2.2.1 Feed material parameters

The properties of the feed gibbsite, based on the samples from an Australian alumina refinery, together with the natural gas composition are shown in Table 2. The natural gas has a lower heating value of is 47.1 MJ/kg, which lies within the required gas-quality specifications . The total input gibbsite to the calciner is 195.3 t/hr with 6 wt.% of surface moisture, producing 120 t/hr alumina for the calciner.

Table 2: Properties of the gibbsite and natural gas used for the investigation [45].

Natural gas composition	Mole fraction
CH_4 (Methane)	96.85%
C_3H_8 (Propane)	0.16%
C_2H_6 (Ethane)	0.58%
C_4H_{10} (Butane)	0.04%
C_4H_{10} (iso-Butane)	0.04%
C_5H_{12} (Pentane)	0.08%
C_6H_{14} (Hexane)	0.04%
CO_2	2.21%
LHV of natural gas (MJ/kg)	47.1
HHV of natural gas (MJ/kg)	52.1
Moisture of gibbsite (Wt%)	6%
Particle size distribution of gibbsite	(wt%)
0-20 (µm)	2.00%
20-44 (µm)	2.20%
44-74 (µm)	14.90%
74-150(µm)	73.20%
150-180(µm)	7.70%

2.2.2 Process modelling for combustion of natural gas/air (Scenario 1) and hydrogen/air (Scenario 2)

The calcination process, driven by the combustion of either natural gas/air or hydrogen/air (Figure 1), was modelled with the Aspen Plus. An overview of the assumptions made for each unit is provided in Table 3. For modelling some units, such as the main furnace and Cyclone 2, several modelling blocks with different functions were connected. Total heat losses were assumed to be approximately 5% of the total input energy and distributed across each unit, primarily in the main furnace and preheating furnace, with the heat losses distribution in each unit provided in energy distribution flows.

Table 3. The inputs and assumptions used for the process model for the conventional flash calciner (Figure 1).

Unit	Process inputs and assumptions	References
Natural gas/air calcination		
Cyclone1	• A Stairmand-HT type cyclone separator model with assumed diameter of 4 meters. • Shepherd & Lapple calculation method.	[46-48]
Cyclone2	• A Plug Flow reactor connected with a Stairmand-HT type cyclone separator with assumed diameter of 4.5 meters. • Gibbsite-to-boehmite reaction rate is controlled based on kinetics in Redaoui et al. [29] study.	[29, 46, 47]
Preheating furnace	• Natural gas is injected and combusted with air (21 vol% O_2, 79% vol% N_2) to heat the gas stream. • A Stoichiometric reactor model was used, with the outlet temperature set to 1050 °C.Reactions: $CH_4 + 2O_2 \rightarrow CO_2 + 2H_2O$ $C_3H_8 + 5O_2 \rightarrow 3CO_2 + 4H_2O$ $2C_4H_{10} + 13O_2 \rightarrow 8CO_2 + 10H_2O$ $2C_2H_6 + 7O_2 \rightarrow 4CO_2 + 6H_2O$ $C_5H_{12} + 8O_2 \rightarrow 8CO_2 + 10H_2O$ $2C_6H_{14} + 19O_2 \rightarrow 12CO_2 + 14H_2O$	[46]
Main furnace	• A Stoichiometric reactor model simulating natural gas/air combustion, which is connected to a plug flow reactor modelling boehmite-to-alumina reaction with rate-controlled based on kinetic parameters developed by Alex T C (2011) [31]. • Assuming two seconds residence time.	[31, 47]
Holding vessel	• A Continuous Stirred Tank reactor connected with a Swift-HT cyclone with diameter of 6 meters. • Boehmite-to-alumina reaction with rate-controlled based on kinetic parameters developed by Alex T C (2011) [31].	[31, 47]
Cyclone 3	• A Stairmand-HT type cyclone with assumed diameter of 4 meters.	[31, 47]
Cyclone 4	• A Stairmand-HT type cyclone with assumed diameter of 3.8 meters.	
Cyclone 5	• A Stairmand-HT type cyclone with assumed diameter of 3.5 meters.	
ESP	• A Solids separator model, assuming a separation efficiency of 99.9% and a pressure drop of 0.5 kPa [18].	[18, 47]
Fluidised bed cooler	• Uses fluidising air to transport the solids, while cooling water is used to remove heat from hot alumina indirectly. • A heat exchanger using 40°C cold water. • Exported fluidising air temperature is assumed to be average of inlet and outlet solids temperature.	[18, 46]
Hydrogen/air calcination		
Preheating furnace	• A Stoichiometric reactor model. • Reaction: $H_2 + 1/2O_2 \rightarrow H_2O$	
Main furnace	• Assumptions are same with natural gas/air calcination except the fuel combustion.	
Inputs and assumptions of other units are same as for natural gas/air calcination.		

2.2.3 Process model for hydrogen in O_2-steam calcination (Scenario 3)

The process model with hydrogen combustion in O_2-steam was also developed using Aspen Plus. Table 4 presents the process inputs and assumptions made for each of the main units. The configuration of the cyclones, except Cyclones 0 and 6, the ESP and the fluidised bed water cooler, remains unchanged from those developed for Scenarios 2 and 3. Operation temperatures of preheating furnace and main calciner were cross-checked against published calciner operating data [18, 42]. For detailed model validation, such as verifying individual stream temperatures, injected air conditions and cyclones separation efficiencies, the expertise and feedback from industry partners was also incorporated. The attached supplementary document includes the Aspen simulation figures of alumina calcination under three pathways, along with the detailed input parameters.

Table 4: The inputs and assumptions used for the process model for the hydrogen in O_2-steam calcination (Figure 2).

Unit	Process inputs and assumptions	References
Hydrogen in O_2-steam calcination		
Cyclone 1~5	• Cyclone types and diameters of cyclones are same with natural gas combustion scenario. • Gibbsite-to-boehmite reaction rate is controlled based on kinetics in Saw et al. [26] study in Cyclone 2.	[26, 46]
Cyclone 0	• A Stairmand-HT type cyclone with assumed diameter of 4 meters.	[31, 47]
Cyclone 6	• A Stairmand-HT type cyclone with assumed diameter of 3.5 meters.	
Preheating furnace	• Hydrogen is injected and combusted with oxygen to heat the steam stream. • A Stoichiometric reactor model with the outlet temperature set to 1050 °C. • Reaction: $H_2 + 1/2O_2 \rightarrow H_2O$	
Main furnace	• A Stoichiometric reactor model simulating hydrogen combustion, which is connected to a plug flow reactor modelling boehmite-to-alumina reaction with rate-controlled based on kinetic parameters developed by Saw et al. [26].	[26, 46]

2.3 Economic analysis

2.3.1 Capital cost estimation for retrofitting the calciner

The factored estimation method was used to estimate the total capital investment (TCI), which has an inherent uncertainty of approximately 30%. The purchased equipment cost (Cyclones 0 and 6) served as the basis for estimating the cost of both indirect and direct cost items. Installed equipment costs were calculated using an installation factor of 3, applied to account for multiple cyclone installations. Additional direct costs included piping for steam recirculation, the electric control system, and buildings construction. Indirect costs included engineering supervision expenses, home office

expenses, contractor' fees, and contingencies. Ratio factors for estimating cost breakdown were obtained based on solid-fluid processing plants [49], as presented in Table 5. By multiplying the ratio factors with purchased equipment cost, the direct and indirect costs, fixed capital investment and working capital cost were obtained. The capital cost includes only the modifications within the calciner system and does not include upstream infrastructure costs, such as hydrogen production, storage, transportation, or associated manufacturing facilities.

Table 5. Ratio factors [49] used to estimate total capital investment of retrofitting the calciner.

Parameters	Assumed factor number
Direct cost (DC)	
Purchased equipment delivered	E
Purchased-equipment installation for cyclones	E*3
Instrumentation and controls (installed)	0.26*E
Piping (installed)	0.31*E
Electrical systems (installed)	0.10*E
Buildings (including services)	0.29*E
Yard improvements	0.12*E
Service facilities (installed)	0.55*E
Total direct costs	(1.63+3)*E
Indirect cost (IDC)	
Engineering and supervision	0.32*E
Construction expenses	0.34*E
Legal expenses	0.04*E
Contractor's fee	0.19*E
Contingency	0.37*E
Total indirect costs	1.26*E
Fixed capital investment (FCI=DC+IDC)	(2.89+3)*E
Working capital (WC=15% of TCI)	0.15*TCI
Total capital investment(TCI)	FCI+WC

The cost of purchased cyclones required for retrofitting was estimated by Equation (5), in which V_{gas} denotes the inlet gas volumetric flow rate for the cyclone, $C_{cyclone}$ denotes the purchased cost in 2023 US dollars.

$$C_{cyclone} = 17640 \times \left(\frac{V_{gas}}{4.7\ m^3/s}\right)^{0.66} \quad (4)\ [50]$$

2.3.2 Operating cost

2.3.2.1 Levelised cost of decarbonising alumina calcination ($LCOA_C$)

The levelised cost of decarbonising alumina calcination, $LCOA_C$, as shown in Equation (5) , was calculated by focusing on fuel-related cost in the calciner, assuming the calciner has a capacity of 120 t/hr and operates at 90% capacity throughout the year. The retrofitting construction was assumed to be

completed within one year. Maintenance costs for the calciner (M_t) were assumed be fixed at 3% per year of the total retrofitting capital cost. To fairly estimate the alumina calcination cost, the cost of CCS was included in Scenario 1, where electricity demand associated with CO_2 compression and process power represents the primary driver, with the calculation provided in supplementary document. Additionally, Scenario 3 achieves an offset value through steam recovery, quantified by the difference between electric boiler steam generation and steam recovery using multi-stage mechanical vapour recompression (MVR), expressed in Equation (6). The economic offset is driven by the variable electricity cost associated with steam generation (E_{SG}) and steam recirculation and recovery ($E_{SR} + E_B$) for Scenario 3. The generated steam condition was assumed at 200 °C and 8 bar, which is within the typically values of 175-230 °C and 6-8 bar for low-temperature digestion. The steam recovery process using multi-stage MVR was assumed to consume one-third of the power of that required for electric boilers, as reported in the study [21]. The corresponding calculations are provided in supplementary document. A sensitivity analysis was conducted with steam recovery consuming 1/3±10% of power required by electric boilers, to account for uncertainties in recovery process in Scenario 3.

$$LCOA_C = \frac{\sum_{t=1}^{n} \frac{I_t + M_t + GF_t + CCS_t + T_t}{(1+r)^t}}{\sum_{t=1}^{n} \frac{A_t}{(1+r)^t}} \quad (5)$$

$$CD_S = \frac{\sum_{t=1}^{n} \frac{I_{EB} + M_{t-S} + E_{EB} - (I_{SR} + M_{t-S} + E_{SR} + E_B)}{(1+r)^t}}{\sum_{t=1}^{n} \frac{S_t}{(1+r)^t}} \quad (6)$$

$$\text{Net calcination cost} = LCOA_C - CD_S \times \left(\frac{100.9}{120}\right) t_{steam}/t_{Al2O3} \quad (7)$$

I_t	Total Investment in calciner retrofitting (TCI)
M_t	Maintenance expenditures in calciner in year t (3% of I_t)
GF_t	Gaseous fuel (natural gas) costs in year t
CCS_t	Carbon capture, transporting and storage costs in year t
T_t	Hydrogen/oxygen transport costs in year t
I_{EB}	Investment in electric boilers for steam generation
I_{SR}	Investment in steam recovery
M_{t-S}	Maintenance expenditures in steam generation or recovery in year t (3% of I_{EB} or I_{SR})
E_{SG}	Electricity cost in steam generation from e-boiler in year t
E_{SR}	Electricity cost in steam recovery in year t
E_B	Electricity cost in blower to recirculate steam in year t
CD_S	Cost difference via steam recovery or generation in Scenario 3
A_t	Alumina production in year t (120 t/hr capacity)
S_t	Steam amount from Scenario 3 in year t (100.9 t/hr steam recovery rate)
r	Discount rate (10%)
n	Life of the equipment (15Y)

2.3.2.2 Cost of natural gas and CO_2 capture, compression, transport and storage (CCS)

The study assessed sensitivity to the price of natural gas spanning the average prices in United States, United Kingdom, Australia and Netherlands (2019-2023), as summarised in Table 7, ranging from 3.3 US$/GJ to 13.9 US$/GJ. For the natural gas/air calcination, the cost of CCS was included, using 179 US$/$t_{CO2}$ at an electricity price of 70 US$/MWh as the base value, compromising CO_2 capture and compression is 144.1 US$/$t_{CO2}$ and 35 US$/$t_{CO2}$ for transport and storage of compressed CO_2, assuming the alumina plants are located at the South-West of Western Australia. The value of storage cost was adopted from study from Allinson et al. [51], who estimated CO_2 transport and storage costs in the South-West region of Australia at 19-51 US$/$t_{CO2}$, depending on site-specific factors and distance to storage. A sensitivity analysis of CCS cost was conducted for electricity prices ranging from 30 to 100 US$/MWh, yielding a CCS cost range of 123.5-220.8 US$/$t_{CO2}$. This range is broadly in line with the literature, with the cost of CO_2 avoidance ranging from 65-201 US$/$t_{CO2}$ [52, 53]. The integrated carbon capture and compression process for stack flue gas is summarised in supplementary

document, including the technical methodology and economic calculations for the amine-based CO_2 capture system.

2.3.2.3 Cost of hydrogen and oxygen transport, H_2 cost from electrolysis

The reference cost for hydrogen was based on production via water electrolysis using renewable electricity with the estimated costs summarised in Table 6 based on a literature review. A sensitivity analysis was also conducted to assess the impact of hydrogen costs on $LCOA_C$, considering projected variations in hydrogen prices using different production methods. For hydrogen/air and hydrogen/O_2-steam calcination, in addition to the energy costs, the cost of hydrogen and oxygen transport were also included. It was assumed that hydrogen is supplied by a third party and transported via a 200 km pipeline, with a transport cost estimated at approximately 0.26 US$/kg$_{H_2}$, based on IEA estimation [54]. Pure oxygen, considered as a by-product of hydrogen production from electrolysers and was assumed to incur no additional production cost. The transport cost for oxygen was included, estimated at 47 US$/t$_{O_2}$ for transportation via a 200 km pipeline [55]. However, the cost assessment is limited to calciner-related fuel costs, and does not include the additional hydrogen infrastructure costs such as storage, compression, or decompression and distribution systems.

Table 6. Major input parameters for the operating cost analysis for the three scenarios.

Natural gas price worldwide						
Natural gas cost	In Australia	US$/GJ	Average 7.5	2019-2023		[56]
	In Netherlands	US$/GJ	Average 13.9	2019-2023		[57]
	In UK	US$/GJ	Average 11.4	2019-2023		[57]
	In US	US$/GJ	Average 3.3	2019-2023		[57]
H_2 production cost from electrolysis						
	Description	Unit	Value	Reference (or predicted) year		Sources
Hydrogen from electrolysis	Renewable electricity	US$/kg	7.5	2018		[58]
		US$/kg	6.8	2019		[59]
		US$/kg	4.2	2019		[38, 59]
		US$/kg	3.5-6.5	2023		[60]
		US$/kg	2.0	2030		[61, 62]
Cost of H_2 and O_2 transport						
	Description	Unit	Value	Reference Year	Value in 2023	Sources
H_2 transport cost by pipeline	200 KM pipeline	US$/kg$_{H2}$	0.2	2019	0.26	[54]
O_2 transport cost by pipeline	200 KM pipeline	US$/t$_{O2}$	35	2020	47	[55]

3. Results

3.1 Overall calcination performance for the three scenarios

3.1.1 Calculated volumetric flow rates

Table 7 presents the operating conditions including inlet gas volume and temperature of each cyclone and the holding vessel for the three scenarios. In general, the inlet gas volume for Scenario 2 match those for Scenario 1 to within ±4%, with slight differences caused by differences in conditions. For Scenarios 1 and 2, both the inlet gas volume and temperature in Cyclones 3, 4 and 5 are the exactly the same, consistent the same amount of input air. However, the inlet gas volume in Cyclones 1, 2 and the holding vessel are slightly higher for hydrogen/air combustion than for the natural gas/air combustion, consistent with the lower volumetric energy density of hydrogen than natural gas. Similarly, after the combustion reaction in the main calciner, the total molar gas flow rate is higher for hydrogen/air than for natural gas/air, also leading to slightly higher volumetric flow rates at the same operating temperatures in Cyclones 1, 2 and holding vessel. Approximately 62 t/hr of steam is recirculated back to calciner circuit in Scenario 3 . Compared to Scenario 1, the gas volume in Scenario 3 differ by within ±20%, resulted from the variations in operating conditions. Specifically, the gas volume in Cyclones 3 to 5 are estimated 10-20% lower than that for natural gas/air, while the flow rates in Cyclones 1 to 2 are approximately 20% higher. These differences are attributed to the lower density of steam compared to air, resulting in higher gas volumes and corresponding changes in gas velocity throughout the system. For the additional Cyclones 0 and 6, the inlet gas volumetric flow rates are estimated at 86 and 40 m^3/s, respectively. For the case of O_2-steam calcination, maintaining volumetric flow rates comparable to air combustion is challenging, as both the gas molar flow rate and operating temperature influence the actual volume. When alumina calcination occurs in a steam-rich environment (>99%), the temperature profile in each cyclone varies, causing these variations relative to air combustion. The associated temperature differences are discussed in Section 3.1.3.

Table 7. The calculated operating conditions for each cyclone for the three scenarios.

	Solid mole flow (kg/s)	Gas mole flow (kmol/s)	Gas density (kg/m^3)	Gas viscosity (cP)	Inlet gas velocity (m/s)	Temperature (°C)	Inlet gas volumes (m^3/s)
Scenario 1							
Cyclone 1	52.7	2.50	0.68	0.021	19.0	165	85.6
Cyclone 2	43.6	2.32	0.51	0.028	19.1	330	108.0
Holding vessel	34.5	1.68	0.27	0.050	15.8	950	158.0
Cyclone 3	33.6	1.21	0.38	0.043	19.9	716	91.2
Cyclone 4	33.5	1.08	0.48	0.037	15.8	523	65.3
Cyclone 5	33.0	1.04	0.66	0.030	13.1	307	45.3
Scenario 2							
Cyclone 1	52.7	2.57	0.65	0.021	19.6	165	87.3
Cyclone 2	43.5	2.38	0.48	0.028	20.0	330	111.5
Holding vessel	34.5	1.74	0.26	0.051	13.9	950	164.0
Cyclone 3	33.7	1.21	0.38	0.043	19.9	716	91.3
Cyclone 4	33.8	1.08	0.48	0.037	15.8	523	65.4
Cyclone 5	33.0	1.04	0.66	0.030	13.1	307	45.3
Scenario 3							
Cyclone 0	52.7	2.50	0.53	0.015	19.0	167	85.6
Cyclone 1	52.7	2.32	0.39	0.022	23.9	332	107.6
Cyclone 2	43.0	2.32	0.34	0.026	22.0	435	125.1
Holding vessel	34.5	1.78	0.19	0.047	16.5	950	166.4
Cyclone 3	33.8	0.95	0.23	0.040	16.9	782	76.3
Cyclone 4	33.7	0.83	0.25	0.035	14.6	665	50.1
Cyclone 5	33.7	0.79	0.29	0.031	14.5	547	50.1
Cyclone 6	33.2	0.79	0.36	0.024	11.6	389	40.0

3.1.2 Calculated separation efficiency and pressure drop of cyclones

Figure 3(a) presents the calculated separation efficiency of each cyclone for the three calcination scenarios. In general, separation efficiencies for Scenarios 2 and 3 are nearly identical to those in Scenario 1, with variations within ±1%. The calculated separation efficiencies of Cyclones 1 to 5 exceed 97%, of the holding vessel (HV) achieves approximately 93%. Specifically, in Cyclones 1, 2, and HV in Scenarios 2 and 3, the increased inlet gas velocity results in slightly higher separation efficiency (1%), in accordance with the Shepherd and Lapple theory [48]. A higher inlet gas velocity and lower gas viscosity lead to improved separation efficiency. In contrast, for Cyclones 3 to 5, the calculated efficiencies in Scenario 3 are approximately 1% lower than those in Scenario 1, consistent with the lower inlet gas velocity reported in Table 7. The additional Cyclones 0 and 6 achieve efficiencies exceeding 97%, which is attributed to the consistently higher inlet velocities and lower gas viscosity.

Figure 3 (b) presents the calculated pressure drop across each cyclone. Overall, the calculated pressure drops across each cyclone in Scenario 2 is comparable to Scenario 1, resulting in close total pressure losses across calciner circuit of 0.35 bar and 0.34 bar, respectively. For Scenario 3, despite

the inclusion of additional cyclones (Cyclones 0 and 6), the overall pressure drop remains comparable, at approximately 0.34 bar, due to the lower pressure drop across individual cyclones. More specifically, for Scenario 3, the pressure drop across Cyclones 3 to 5 is estimated to be 50% to 70% lower than those for Scenario 1, due to the lower gas density and lower inlets velocity (Table 7), consistent with the principle that pressure drop increases with higher gas density and higher inlet velocities[63].

A reduction in cyclone separation efficiency is expected to result in a slight increase in overall energy consumption, due to the reduced counter-current heat recovery efficiency [64]. A drop in cooling cyclones' separation efficiency from 100% to 90% results in an estimated 1.8% rise in fuel consumption [64]. However, the small variations in cyclone separation efficiency, as shown above, are not expected to significantly influence the overall energy use for the three scenarios. The pressure drop across the calciner circuit must be overcome in Scenario 3 in order to recirculate steam back into the system, resulting in a slightly increase in the electrical power consumption for this scenario. Nevertheless, it is important to note that the performance estimations were derived using Aspen-based mathematical calculations. The behaviour of cyclones under steam-rich environments is not yet fully understood. A more comprehensive understanding of cyclone performance under those conditions would require Computational Fluid Dynamics (CFD) modelling and experimental validation. It is also worth noting that the increased inlet gas velocities for Scenario 3, particularly in Cyclone 1 where it is approximately 20% higher than in Scenario 1, may lead to some increased particle breakage, highlighting the need for further assessment.

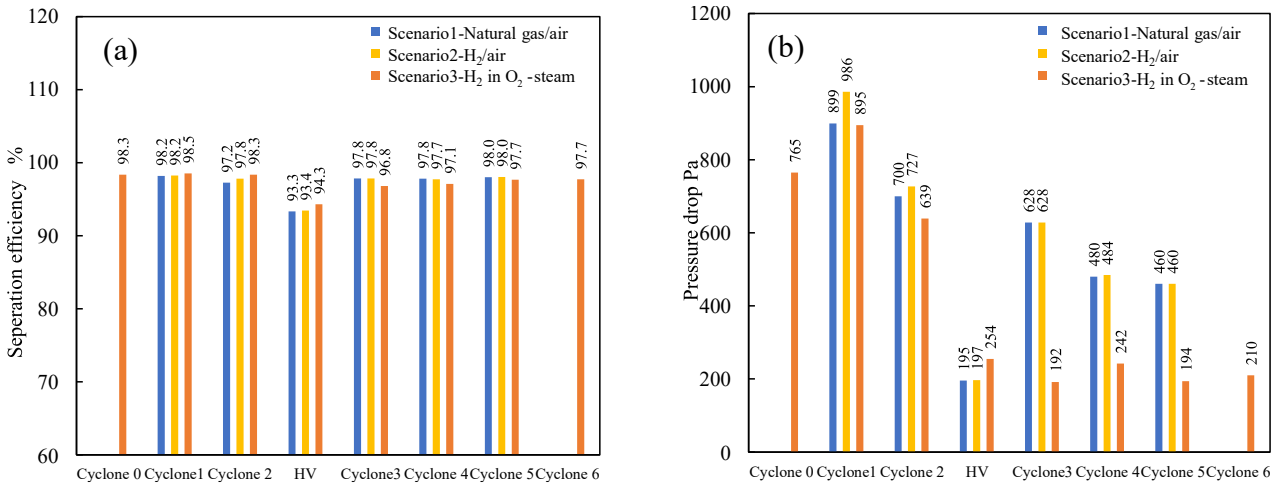


Figure 3. A comparison of the calculated cyclone separation efficiency and pressure drop across each cyclone for the three calcination scenarios.

3.1.3 Stream temperature

Figure 4 presents the calculated stream temperature for the three calcination scenarios. Broadly speaking, hydrogen/air calcination exhibits a similar temperature profile to natural gas/air, including preheating, main and cooling zones. However, hydrogen combustion in oxy-steam yields stream temperatures in Cyclones 1 and 2, as well as Cyclones 3 to 5, that are higher than the natural gas case by some 100°C due to the lower heat transfer efficiency between steam and solid compare with air. The temperatures in the preheat and main calciner zones are maintained at 1050°C and 950°C, respectively, by adjusting the input fuel. The temperature of main calciner is maintained in the range of 950-1000°C to ensure the smelter-grade alumina (SGA) meets the required specifications for LOI **(**Loss on Ignition), specific surface area (SSA), and low α-Al_2O_3 phase content [18]. The preheating furnace is maintained at 1050°C to avoid the formation of α-Al_2O_3, which begins at 1050°C and peaks around 1200°C [65]. Specifically, estimated higher temperature in Cyclones 3-6 is because the higher temperature of returned superheated steam (167 °C) compared to the input air (50°C), which raises the stream temperature after heat exchange in cooling stage. The variations in stream temperatures across the cooling cyclones lead to corresponding differences in heat recovery from the hot solids, which are further discussed in Section 3.2.1.

In the preheating stage, the calculated temperature in Cyclone 2 is approximately 90 °C higher than in Scenario 1, at 434°C and 332°C, respectively. This is because the gibbsite-to-boehmite reaction is inhibited by the steam-rich environment [66, 67], which also reduces the heat transfer from hot gas to gibbsite solid. Simulations under an air-based calcination environment predict 100% conversion, based on the applied kinetic models reported in studies [28, 29]. As a result, more enthalpy is retained in the gas phase, leading to higher gas temperatures in Cyclones 1 and 2 than in Scenarios 1 and 2.

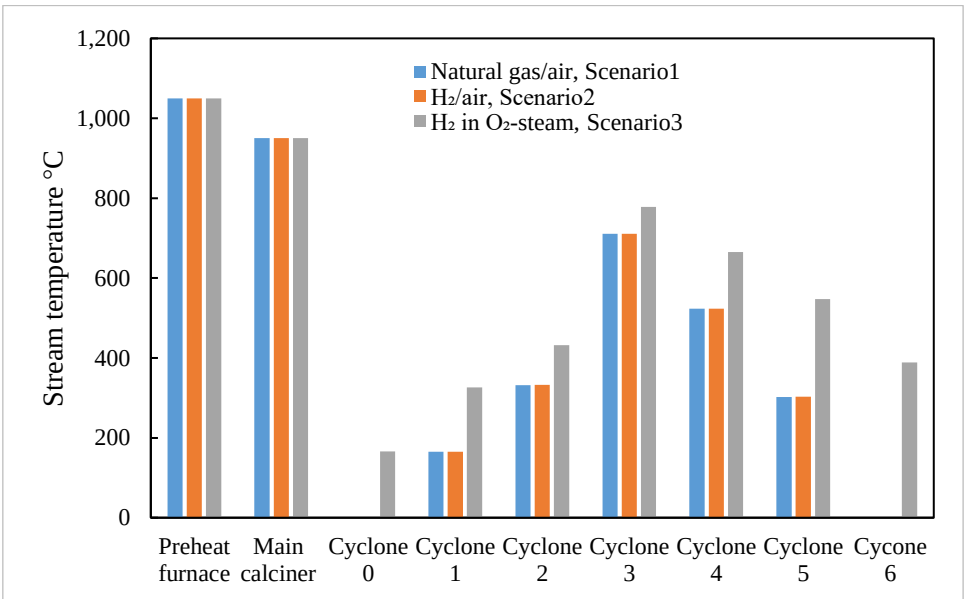
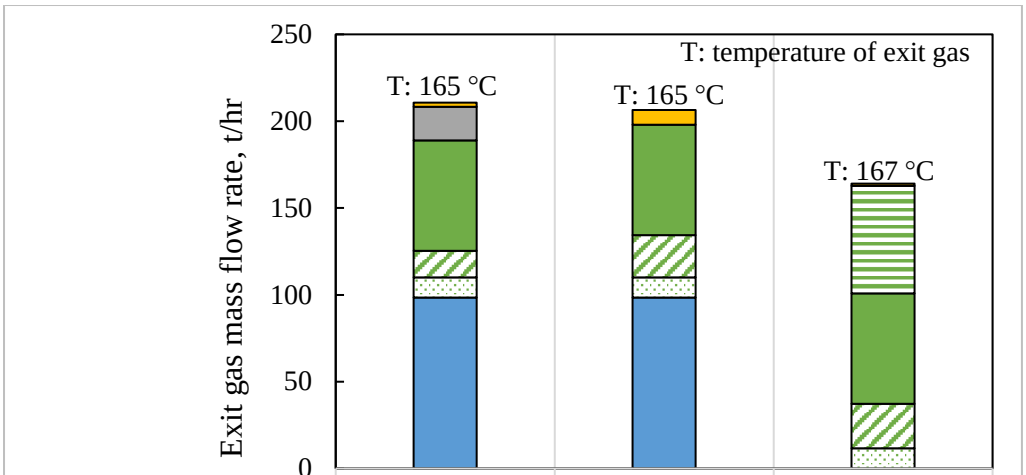


Figure 4. A comparison of the calculated temperature of key process streams for the three calcination scenarios.

3.1.4 Exit flue gas

Figure 5 presents the compositions and mass flow rates of the exit gas for the three calcination scenarios. Scenarios 1 and 2 comprise approximately 47% and 50% N_2, respectively, together with some 40% and 50% of steam, respectively. Recovering steam from the calcination off-gas can potentially reduce steam generation requirement in the refining process, which is desirable. However, this high dilution with nitrogen under air combustion increases the complexity of the recovery process=, as it requires separation of N_2, making direct recovery technically infeasible In contrast, Scenario 3 achieves a high steam concentration at 99.5%, demonstrating inherent capture. Additionally, all direct CO_2 emissions from fuel combustion are eliminated in Scenarios 2 and 3. In Scenario 1, direct emissions are approximately 0.16 t_{CO2}/t_{Al2O3}, corresponding to 19.5 t_{CO2}/hr at a production rate of 120

t/hr alumina. Applying an amine-based CCS system with 90% capture efficiency reduces the residual emissions to 0.016 t_{CO2}/t_{Al2O3} (1.9 t_{CO2}/hr). This reduction requires additional expenditure for CO_2 capture, compression, transport, and storage, with the cost analysis presented in supplementary document. The steam in these gases originates primarily from the calcination reactions (64 t/hr, Reactions (1)-(3)), but also from gibbsite surface moisture (11.7 t/hr) and the products of fuel combustion (natural gas or hydrogen). In total, some 90-98 t/hr (~0.8 t steam/$t_{Al_2O_3}$) of steam is vented through the stack in Scenarios 1 and 2, corresponding to approximately 1.7 GJ/$t_{Al_2O_3}$ in latent energy alone [68]. The potential recovery of this steam is hindered, not only by dilution with N_2, but also by the CO_2 for Scenario 1, which reacts with the caustic soda solution (NaOH) used in digestion. In contrast, the enthalpy flow rate from Scenario 3 is 2.1 GJ/$t_{Al_2O_3}$ from the gas with nearly 99.5% steam (100.9 t/hr steam at 1.06 bar). It should be noted that the present study evaluates direct CO_2 emissions and does not provide a detailed assessment of NO_x formation. Hydrogen/air combustion may lead to higher flame temperatures compared with natural gas, potentially increasing NO_x emissions. Optimisation of burner configuration and nozzles for fuel injection would be required to minimise hot spots and NO_x emissions, necessitating the Computational Fluid Dynamics (CFD) modelling.



	Exit gas Sceanrio 1	Exit gas Scenario 2	Exit gas Scenario 3
O_2	2.3	8.5	1.2
CO_2	19.5	0.0	0.0
Recirculation H_2O			62.0
H_2O from alumina calcinaiton	63.6	63.6	63.6
H_2O from fuel combustion	15.2	24.3	25.6
H_2O from moiture	11.7	11.7	11.7
N_2	98.4	98.4	0.0

Figure 5.The calculated flue gas composition and mass flow rate from the stack for the three calcination scenarios.

3.2 Energy consumption

3.2.1 Calculated energy flow distribution

Figures 6 and 7 presents the calculated energy flow during the calcination process for the three scenarios. Scenarios 1 and 2 have identical energy input, totalling 106.5 MW_{th} (with 22.9 MW_{th} in preheating furnace and 83.6 MW_{th} in main calciner), resulting in the same high heating value energy consumption of 3.19 $GJ/t_{Al_2O_3}$ (HHV). In Scenario 3, total energy input increases by 6.5% to 113.5 MW_{th} (with 26.4 MW_{th} and 87.1 MW_{th} supplied to the preheating furnace and main calciner), resulting increased energy consumption to 3.4 $GJ/t_{Al_2O_3}$ (HHV). This increase is caused by lower heat recovery in the preheating and cooling zones. The calculated energy flow for each stream was based on the reference temperatures indicated at the top of the figures, providing an overview of the energy utilisation during calcination process. The details for the main unit balances are presented in supplementary document. In greater detail, Figure 6 shows that in Scenarios 1 and 2, preheated air delivers 25.3 MW_{th} of heat to the preheating furnace, recovered from hot solids through cyclones 3-5. An additional 22.9 MW_{th} of input energy from natural gas or hydrogen (HHV, based on 25°C heat

value), raises the gas to 1050°C, transferring approximately 47.2 MW_{th} of energy into the main furnace. The fuel input to the main calciner is 83.6 MW_{th} (natural gas or hydrogen) and the incoming boehmite stream contributes another 12.6 MW_{th}, totalling 143.4 MW_{th}. Of this, approximately 30 MW_{th} is consumed by the boehmite-to-alumina reaction, which occurs at temperature above 500°C [16]. Hot gas and solids exit the holding vessel at 950°C, carrying 76.4 MW_{th} and 34.0 MW_{th}, respectively. Heat from hot alumina is recovered via three air cooling cyclones to preheat the air, after which the alumina is cooled to 302°C. It then enters the fluidised bed cooler, where approximately 7.4 MW_{th} is removed by the cooling water, and finally, exits at 75°C with a residual heat of 0.5 MW_{th}. On the hot gas side, gas is directed to Cyclone 2, where the gibbsite-to-boehmite reaction occurs, consuming 31.8 MW_{th} based on a 300°C reaction temperature. After the reaction, hot gas and boehmite are separated, carrying 36.7 MW_{th} and 12.6 MW_{th}, respectively. The boehmite solids are then transported to the main furnace, while the gas is directed to Cyclone 1 to preheat feed gibbsite from 60°C to 165 °C for moisture removal. The heat losses, shown as the green streams, are calculated to be 4.8% of total energy input, mainly occurring in the main furnace and preheating furnace, where they are 1MW_{th} and 3 MW_{th}, respectively.

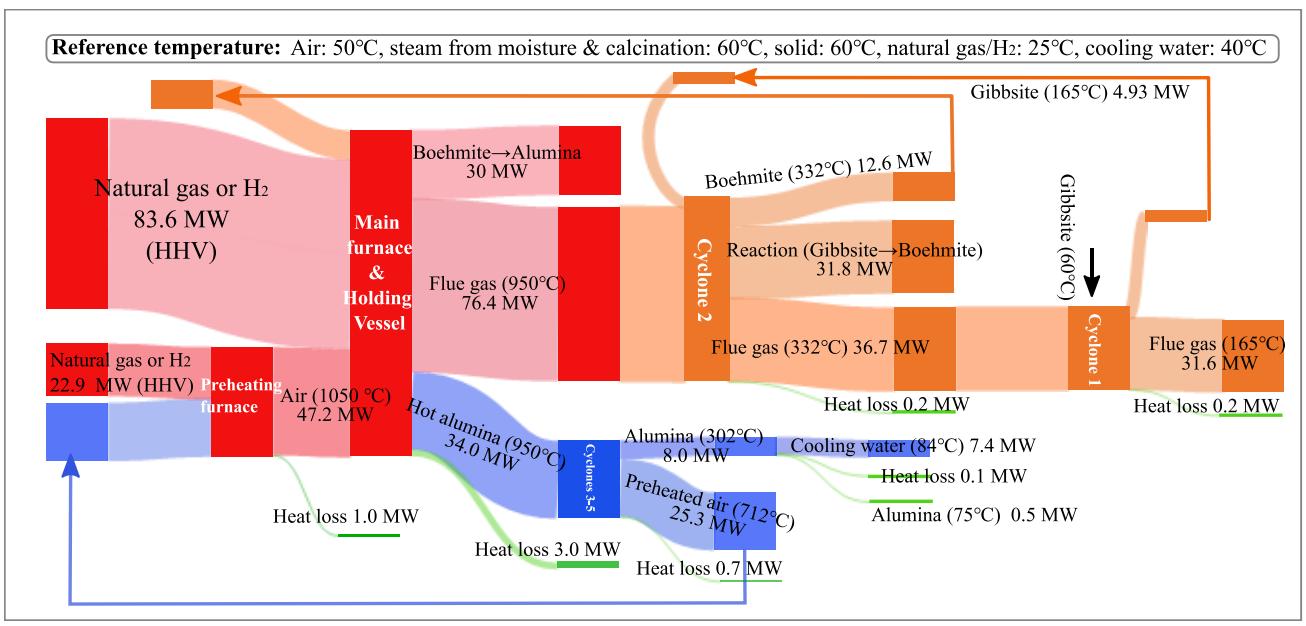


Figure 6. The calculated energy flows for Scenarios 1 and 2 at 120 t/hr alumina production, illustrating the heat recovery, fuel input, reaction heat, and thermal energy distribution across the calciner circuit.

Figure 7 presents the energy flow for Scenario 3, where superheated steam is utilised as the heat exchange medium. Scenario 3 recovers 16% less heat from the hot solids than Scenario 1 in the cooling stage, with 21.8 MW_{th} recovered compared to 25.3 MW_{th} in Scenario 1. To compensate, the energy input (H_2) is increased by 15%, from 22.9 to 26.4 MW_{th} to maintain the same output gas energy of 47.2 MW_{th}. In the main furnace, the total energy input is 151.4 MW_{th} comprising 87.1 MW_{th} from hydrogen (HHV) and 17.1 MW_{th} from the solids, along with 47.2 MW_{th} from hot steam supplied from the preheating furnace. Similar to Scenario 1, approximately 30 MW_{th} is consumed in the boehmite-to-alumina calcination, but there is an additional 8 MW_{th} required to convert the remaining 24% gibbsite from Cyclone 2. The holding vessel discharges 76.4 MW_{th} in hot steam and 34.0 MW_{th} in hot alumina. As discussed above, the lower heat recovery results in a higher heat loss of 10.7 MW_{th} through the cooling water, compared to Scenarios 1 and 2. On the hot gas side, the gibbsite-to-boehmite reaction consumes less energy (23.8 MW_{th}) due to the inhibited reaction, resulting in more thermal energy retained in steam. To better utilise this energy, Cyclone 0 is added to the proposed cycle, achieving an exit steam temperature of 167 °C, which is close to that for Scenario 1. The recirculated steam is assumed to carry no net usable energy, as it is recirculated with minimal temperature change. The overall heat loss is calculated to be 4.8% of total energy input, consistent with Scenario 1. In conclusion, Scenario 3 has a slightly higher overall gross energy consumption due to the reduced heat recovery in the cooling section and incomplete gibbsite conversion in Cyclone 2. However, after the first-stage compression and the return of a portion of the recycled steam for use as carrier gas, the remaining steam remains available for energy recovery.

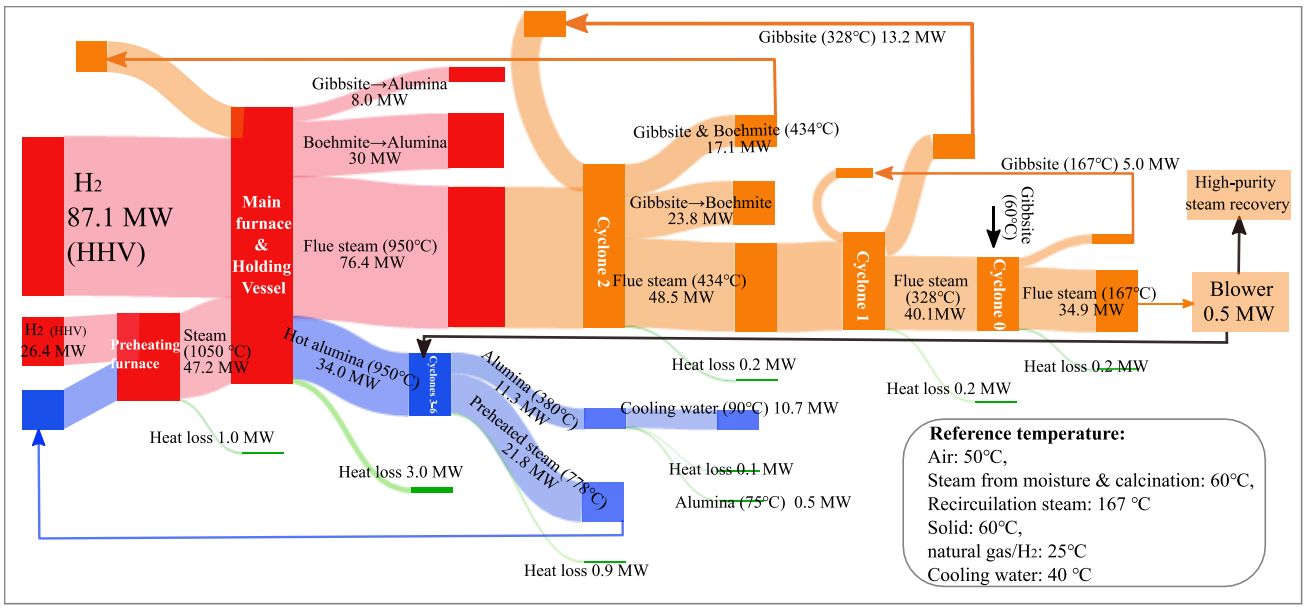


Figure 7. The calculated energy flows for Scenario 3 at 120 t/hr alumina production, illustrating the heat recovery, fuel input, reaction heat, and thermal energy distribution across the calciner circuit.

Figure 8 presents the influence of the conversion of the gibbsite-to-boehmite reaction in Cyclone 2 on the total calculated energy consumption for Scenario 3.The variation in calculated energy use remains within 0.5% across the range, demonstrating an approximately linear relationship. As gibbsite conversion increases, the required energy input to the main furnace decreases accordingly, resulting in lower overall energy consumption. The reaction kinetics of gibbsite pre-calcination in a steam-rich environment play a critical role, indirectly influencing energy consumption as lower conversion in Cyclone 2 leads to suboptimal energy utilisation during preheating.

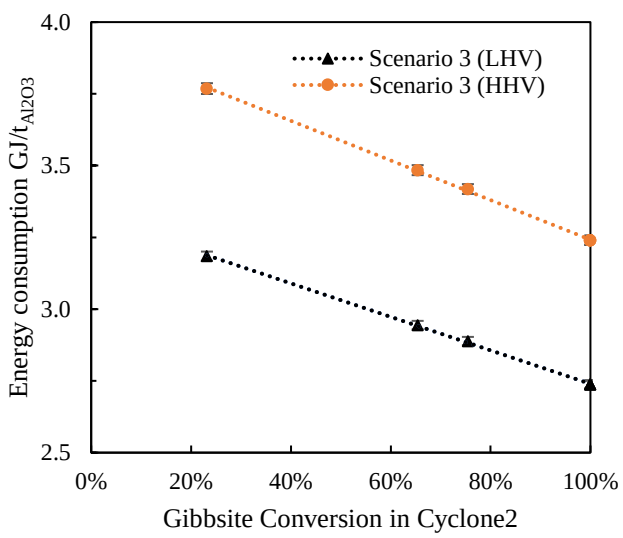


Figure 8. The calculated influence of gibbsite conversion in Cyclone 2 on the overall energy consumption for Scenario 3.

High steam concentration environment in Scenario 3 reduces the heat-recovery efficiency in Cyclones 3-6 compared with the air-combustion case, where air acts as the heat-exchange medium for cooling the hot solids. Even with the addition of an extra cyclone to improve heat recovery, less sensible heat is recovered from the hot solids. Furthermore, in Cyclones 1-2, the heat transfer efficiency is also expected to decrease under high steam concentration conditions. This is primarily because the high steam concentration inhibits the gibbsite to boehmite reactions, resulting in a fraction of unconverted gibbsite being transported to the main calciner as discussed above.3.2.2 Calculated energy consumption

Table 8 presents the calculated energy consumption for the three calcination scenarios. Overall, Scenario 2 has the lowest energy consumption at 2.7 GJ/$t_{Al_2O_3}$ (LHV), compared with 2.88 GJ/$t_{Al_2O_3}$ (LHV) in Scenario 1. Additionally, the calculated overall energy consumption of Scenario 1 was checked with the published operating data of a flash calciner, showing close alignment with the reference value of 2.85 GJ/$t_{Al_2O_3}$ (LHV) [18, 69]. In contrast, Scenario 3 exhibits slightly higher gross energy use, ranging from 2.89 to 2.96 GJ/$t_{Al_2O_3}$ (LHV), which is 0.3%-3% higher than Scenario 1. This increase is indirectly driven by the reduced conversion of gibbsite-to-boehmite in Cyclone 2, at 65%-76%. Consequently, 24%-35% of unconverted gibbsite is carried into the main calciner, requiring additional hydrogen input to achieve complete conversion.

Table 8. The calculated overall energy consumption for each of the three scenarios.

	Unit	Natural gas/air (Scenario 1)	H_2/air (Scenario 2)	H_2 in O_2-steam (Scenario 3)
Total input natural gas	t/hr	7.36	/	/
Total input H_2	t/hr	/	2.69	2.89~2.96
Total input air	t/hr	128.0	128.0	N/A
Total input O_2	t/hr	/	/	24.2~24.8
Al_2O_3 production	t/hr	120.0	120.0	120.0
Gibbsite-to-boehmite conversion in Cyclone 2	%	100%	100%	65%~76%
Overall energy consumption	GJ/t_{Al2O3} (LHV)	2.88	2.70	2.89~2.96
	GJ/t_{Al2O3} (HHV)	3.19	3.19	3.40~3.48

3.3 Economic performance for the three scenarios

3.3.1 Calculated levelised cost of alumina calcination

Figure 9 (a) summarises the calculated levelised cost of alumina calcination ($LCOA_C$) for the three scenarios and Figure 9 (b) presents the cost difference via steam generation from electric boilers or steam recovery in Scenario 3. The nearly pure steam in Scenario 3, approximately 100.9 t/hr is estimated to offset 31 US$/$t_{Al_2O_3}$ compared to direct steam generation via electric boilers at a fixed renewable electricity price of 70 US$/MWh. Sensitivity analysis, assuming that steam recovery via mechanical vapour recompression consumes one-third (±10%) of the power required by electric boilers, results in a cost offset range of approximately 29-33 US$/$t_{Al_2O_3}$, reflecting the marginal economic impact. Overall, Scenario 3 leading to 12-32% lower costs compared to Scenario 2 for the same hydrogen price and a fixed electricity price of 70 US$/MWh [70], driven by the steam recovery offset. Additionally, Scenario 3 demonstrates cost advantages over Scenario 1, achieving 31% lower $LCOA_C$ for a hydrogen price of 2 US$/kg, when CCS costs (179 US$/$t_{CO_2}$) are included and natural gas prices at 7.5 US$/GJ. This makes Scenario 3 cost-competitive at a hydrogen price of 2 US$/kg.

In Scenario 1, CCS costs account for approximately 41-57% of $LCOA_C$, with the cost rising from 21.8-40.6 US$/$t_{Al_2O_3}$ (without CCS) to 50.4-69.2 US$/$t_{Al_2O_3}$ (with CCS). This increase is dominated by electricity consumption, which is critical for both solvent regeneration and CO_2 compression during the capture process. By contrast, in hydrogen scenarios, the cost of hydrogen contributes above 80% of the total calcination cost, making hydrogen price the dominant economic driver. Electricity costs still influence the calcination cost in Scenario 3 indirectly, primarily through their impact on steam recovery costs, which is secondary relative to hydrogen cost. In Scenario 3, capital cost for retrofitting the calciner contributes only ~1% of overall cost. Hydrogen and oxygen transport costs contribute an additional6.4 US$/$t_{Al_2O_3}$ and 9.8 US$/$t_{Al_2O_3}$, respectively. At a high hydrogen price from electrolysis of 4.3 US$/kg [59, 71], based on an electricity price of 70 US$/MWh,

Scenarios 2 and 3 exhibit $LCOA_C$ values of 103.3 and 90.8 US$/$t_{Al_2O_3}$, respectively, which is less cost-effective.

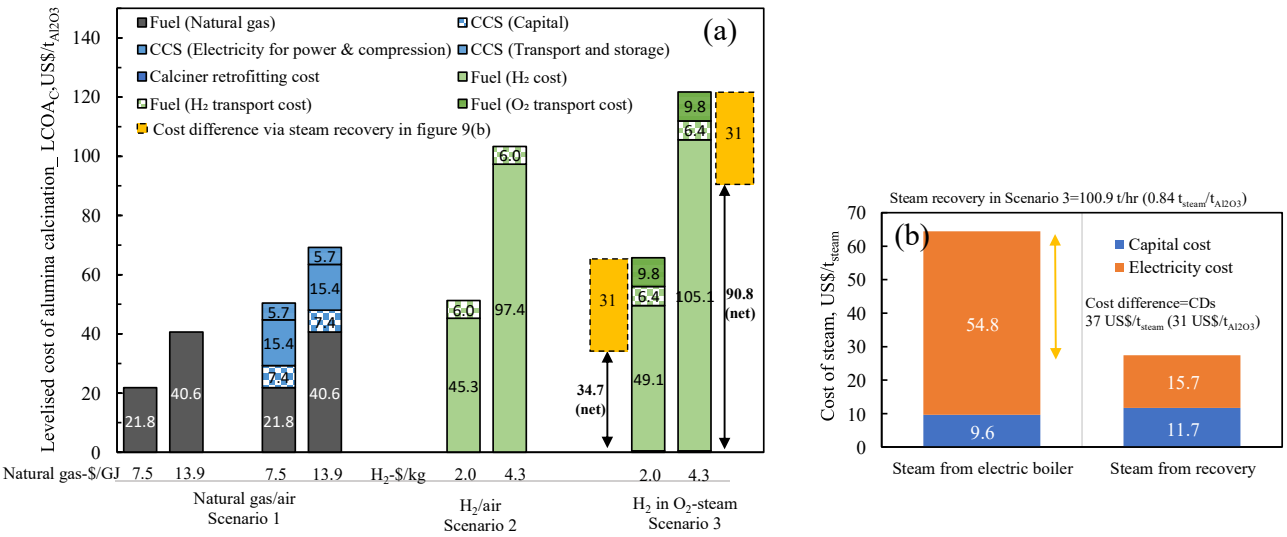


Figure 9 (a) Calculated levelised cost of calcination for the three scenarios, (b) the cost difference via steam recovery or generation in Scenario 3.

3.3.2 Sensitivity analysis in Scenarios 2 and 3

Figure 10 (a) presents the sensitivity of the effects of hydrogen price on the calcination cost in Scenarios 2 and 3, accounting for the value of the recovered steam in Scenario 3. It can be seen that the break-even hydrogen prices for Scenario 2 and Scenario 3are estimated at 2.8 and 3.4 US$/kg, respectively, compared with the natural gas of 7.5 US$/GJ and the inclusion of CCS costs. In contrast, when CCS costs are excluded, the break-even hydrogen price decreases to approximately 1.4 US$/kg for Scenario 2 and 2.0 US$/kg for Scenario 3. Figure 10 (b) presents the calcination cost as a function of natural gas price. At a low projected hydrogen price of 2 US$/kg, Scenario 2 becomes cost-effective when the natural gas price exceeds approximately 8 US$/GJ, whereas Scenario 3 becomes competitive at a significantly lower threshold of around 3 US$/GJ, assuming CCS is included. When CCS costs are excluded, the competitiveness threshold shifts substantially. In this case, Scenario 2 requires a natural gas price above approximately 12 US$/GJ to become cost-effective, while Scenario 3 requires natural gas prices exceeding approximately 17 US$/GJ.

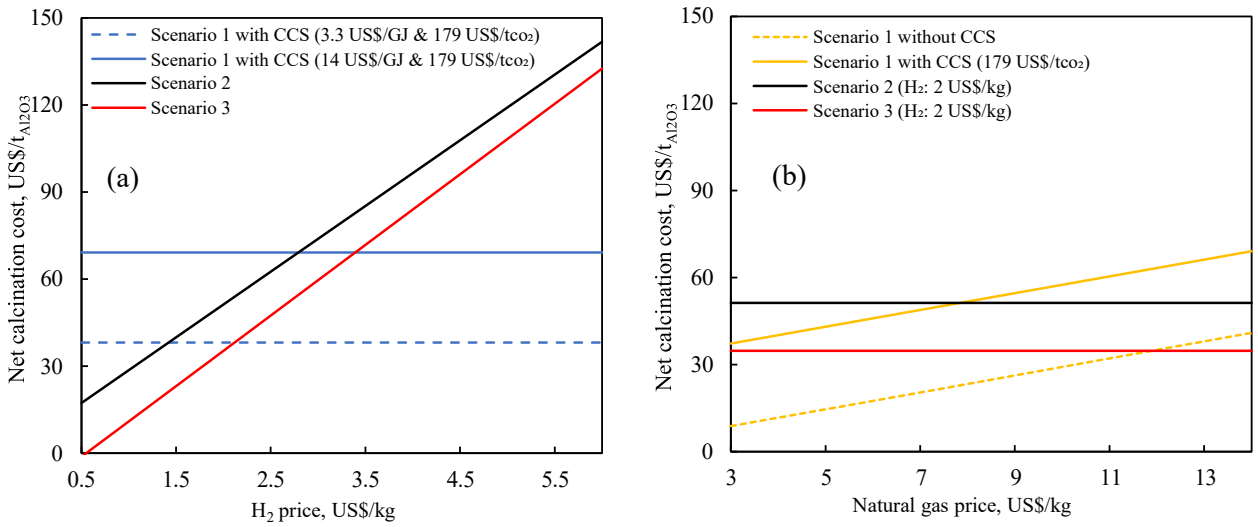


Figure 10. (a) the calculated net calcination cost as a function of hydrogen price, (b) the net cost as a function of natural gas price.

Figure 11 shows the sensitivity of the effects of renewable electricity price on net calcination cost and the corresponding hydrogen price from electrolysis [38, 71]. Overall, renewable electricity prices need to fall below 38 and 42 US$/MWh for Scenarios 2 and 3 to become competitive, respectively, corresponding to hydrogen costs of 2.5-2.7 US$/kg, compared with the elevated natural gas of 14 US$/GJ with CCS cost. Under a low natural gas price scenario of 3 US$/GJ, the required renewable electricity price would need to fall below approximately 5-10 US$/MWh for hydrogen-based calcination to be competitive, indicating that low natural gas prices present a substantial economic barrier to hydrogen deployment. The offset value from steam recovery in Scenario 3 increases as renewable electricity prices rise [38, 72], widening the gap between the Scenario 3 and Scenario 2 curves. However, at lower electricity prices, particularly around 30 US$/MWh, the economic difference between the two scenarios narrows, implying that the additional oxygen transport cost in Scenario 3 is approximately offset by the value from steam recovery.

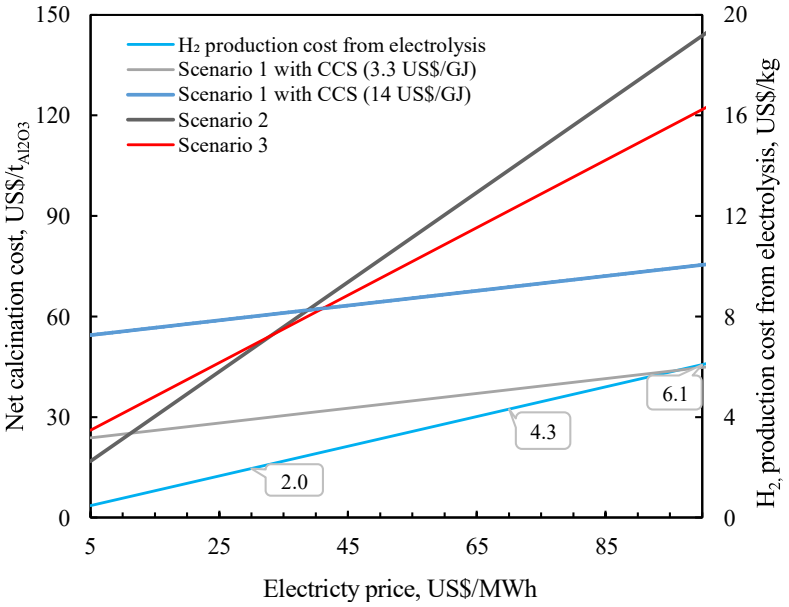


Figure 11. The calculated net calcination cost and hydrogen cost as a function of renewable electricity price for Scenarios 2 and 3.

4. Recommendation for further work

This work analyses the techno-economic performance of alumina calcination when transitioning to hydrogen combustion pathways using ASPEN-based process simulation. Further research is recommended to strengthen the assessment of detailed combustion behaviour. In particular, Computational Fluid Dynamics (CFD) modelling is required to resolve combustion profiles under H_2–air and H_2 in O_2-steam combustion, including the impact on NOx emissions, flame temperature, and spatial temperature profiles within the calciner. Investigation of calcination kinetics under steam-rich environments is also necessary, along with assessment of impacts on alumina quality parameters such as loss on ignition (LOI) and specific surface area. Furthermore, given the potential economic benefit of steam recovery in the H_2 in O_2-steam configuration, further work is needed to investigate its technical and economic feasibility. Additional investigation is also recommended in waste heat recovery from N_2 diluted flue gas under air combustion, considering its high exhaust temperature and potential for improving overall refining process efficiency.

5. Conclusions

This study analyses the techno-economic performance of alumina calcination when transiting from conventional natural gas/air combustion (Scenario 1) to hydrogen-based pathways, including H_2 in air (Scenario 2) and H_2 in an O_2-steam (Scenario 3) calcination. The replacement of natural gas with H_2 in air combustion is calculated to lead to a slightly lower energy consumption of 2.7 GJ/t_{Al2O3} (LHV), relative to 2.88 GJ/t_{Al2O3}. While under H_2 in O_2-steam calcination consumes slightly more energy, at 2.93±0.3 GJ/t_{Al2O3}, due to less efficient heat exchange in superheating recirculated steam and hot solids in cooling stage and inhibited gibbsite-to-boehmite conversion in the preheating stage, a net benefit can still be obtained through the novel configuration that enables the recovery of high-concentration steam. The proposed configuration is also estimated to achieve a comparable performance (±1%) for cyclone separation efficiency to air combustion as it is configured to achieve similar volumetric flow rates and gas velocities. Economically, with CCS included and a natural gas price of 7.5 US$/GJ, the break-even hydrogen prices are 3.4 US$/kg for Scenario 3 and 2.8 US$/kg for Scenario 2. Excluding CCS reduces these thresholds to approximately 2.0 US$/kg and 1.4 US$/kg, respectively. In Scenario 3, steam recovery provides an offset of approximately 31 US$/$t_{Al2O3}$ (relative to electric boiler steam at 70 US$/MWh), which supports the higher break-even hydrogen threshold.

List of Abbreviations

V_{gas}	Inlet gas volumetric flow rate, m_3/s
$LCOA_C$	Levelized cost of alumina calcination, US$/$t_{Al2O3}$
CCS	Carbon capture and storage
MVR	Mechanical vapour recompression
I_t	Total Investment in calciner retrofitting (TCI)
M_t	Maintenance expenditures in calciner in year t
GF_t	Gaseous fuel (natural gas) costs in year t
T_t	Hydrogen/oxygen transport costs in year t
I_{EB}	Investment in electric boilers for steam generation
I_{SR}	Investment in steam recovery
M_{t-S}	Maintenance expenditures in steam generation or recovery in year t
E_{SG}	Electricity cost in steam generation from e-boiler in year t
E_{SR}	Electricity cost in steam recovery in year t
E_B	Electricity cost in blower to recirculate steam in year t
CD_S	Cost difference via steam recovery or generation in Scenario 3, US$/$t_{Steam}$
A_t	Alumina production in year t (120 t/hr capacity)
S_t	Steam amount from Scenario 3 in year t (100.9 t/hr steam recovery rate)

Data Availability Statement

Data will be made available on request.

CRediT Statement

Siyun Ning: Writing – review & editing, Writing – original draft, Methodology, Investigation, Formal analysis, Data curation, Conceptualization. Graham Nathan: Writing – review & editing, Supervision. Peter Ashman: Writing – review & editing, Supervision. Woei Lean Saw: Writing – review & editing, Supervision, Project administration, Funding acquisition.

Acknowledgements

The work is supported by the Heavy Industry Low-carbon Transition Cooperative Research Centre (HILT CRC) which receives funding from its industry, research, and government collaborators, as well as from the Australian Government's Cooperative Research Centres Programme. Siyun Ning acknowledges the financial support provided through an Australian Government Research Training Programme (RTP) Scholarship at the University of Adelaide, along with a supplementary scholarship from HILT CRC. The authors also express their appreciation to industry partners South32 and Alcoa, and sincerely thank David Cochrane and Ray Chatfield for offering valuable industry insights and feedback. Their input played a key role in validating the calcination modelling work.

References

[1] International Aluminium. *Metallurgical Alumina Average Refining Energy Intensity for 2024*. https://international-aluminium.org/statistics/metallurgical-alumina-refining-energy-intensity/. 2024 [accessed on 22 Feb 2026].

[2] Scarsella A A, Noack S, Gasafi E, Klett C, and Koschnick A. *Energy in alumina refining: setting new limits.* Light metals 2015, 2015: p. 131-136. https://doi.org/10.1007/978-3-319-48248-4_24.

[3] Australian Aluminium Council LTD. *Sustainability*. https://aluminium.org.au/sustainability-main/sustainability/. 2024 [accessed on 1 August 2025].

[4] International Energy Agency (IEA). *China*. https://www.iea.org/countries/china#. 2023 [accessed on 12 May 2025].

[5] Qiang W, Peng H, Qinmeng W, and Xueyi G. *Greenhouse gas emissions and future development trends of primary aluminum in China.* Journal of Cleaner Production, 2023. 403: p. 136828. https://doi.org/10.1016/j.jclepro.2023.136828.

[6] Australian Government. *Australia's Long-Term Emissions Reduction Plan*. https://www.dcceew.gov.au/climate-change/publications/australias-long-term-emissions-reduction-plan. 2023 [accessed on 1 July 2025].

[7] Croucher A, Dean A, Hutley N, Flannery T, Morgan W, Bradshaw S, and Rayner J. *Australia's clean industry future: making things here in a net zero world*. https://www.climatecouncil.org.au/resources/australias-clean-industry-future-making-things-in-a-net-zero-world/. 2023 [accessed on 6 April 2025].

[8] International Energy Agency (IEA). *Brazil*. https://www.iea.org/countries/china#. 2023 [accessed on 12 June 2025].

[9] Zhu L. *National carbon emissions from the industry process: Production of glass, soda ash, ammonia, calcium carbide and alumina.* Applied Energy, 2016. 166: p. 239-244. https://doi.org/10.1016/j.apenergy.2015.11.005.

[10] Jinghang X, Yuru G, Jonathan O, Dabo G, and Yuli S. *China carbon emission accounts 2020-2021*. Applied Energy, 2024. 360: p. 122837. https://doi.org/10.1016/j.apenergy.2024.122837.

[11] Zakari A, Khan I, Alvarado R, and Missaoui I. *The impact of renewable energy rebates on environmental sustainability in Australia.* Australasian Journal of Environmental Management, 2024. 31(1): p. 108-125. https://doi.org/10.1080/14486563.2024.2326090.

[12] Raihan A. *The interrelationship amid carbon emissions, tourism, economy, and energy use in Brazil.* Carbon Research, 2024. 3(1): p. 11. https://doi.org/10.1007/s44246-023-00084-y.

[13] Butler C, Maxwell, R.,Graham, P.,Hayward, J. *Australian Industry Energy Transitions Initiative – Phase 1 Report*. https://www.climateworksaustralia.org/resource/australian-industry-energy-transitions-initiative-phase-1-report/. June 2021 [accessed on 1 April 2025].

[14] International Aluminium. *Metallurgical Alumina Refining Fuel Consumption*. https://international-aluminium.org/statistics/metallurgical-alumina-refining-fuel-consumption/?publication=metallurgical-alumina-refining-fuel-consumption. 2024 [accessed on 22 Feb 2026].

[15] Perander L M, Gasafi E, and Scarsella A, *Cost and Energy Efficiency Improvment in Alumina Calcination*, in *the 12th International AQW Conference and Exihibition*. 2024: Dubai, Emirate.

[16] Vasile B S, Dobra G, Iliev S, Cotet L, Neacsu I A, Surdu V A, Nicoara A I, Boiangiu A, and Filipescu L. *Thermally activated Al (OH) 3 Part II—effect of different thermal treatments.* ceramics, 2021. 4(4): p. 564-575. https://doi.org/10.3390/ceramics4040040.

[17] Chen Q and Zeng W. *Calorimetric determination of the standard enthalpies of formation of gibbsite, Al (OH) 3 (cr), and boehmite, AlOOH (cr).* Geochimica et cosmochimica acta, 1996. 60(1): p. 1-5.

[18] Raahauge B E and Williams F S. *Smelter Grade Alumina from Bauxite: History, Best Practices, and Future Challenges*. Springer.2022.

[19] *Rio Tinto and Sumitomo – Yarwun Hydrogen Calcination Pilot Demonstration Program – Lessons Learnt Report*. https://arena.gov.au/knowledge-bank/rio-tinto-and-sumitomo-yarwun-hydrogen-calcination-pilot-demonstration-program-lessons-learnt-report/. 2023 [accessed on 9 March 2025].

[20] ARENA. *World first hydrogen pilot for low carbon alumina*. https://arena.gov.au/news/world-first-hydrogen-pilot-for-low-carbon-alumina/. July 2023 [accessed on 6 April 2025].

[21] ARENA. *A Roadmap for Decarbonising Australian Alumina Refining*. https://arena.gov.au/knowledge-bank/a-roadmap-for-decarbonising-australian-alumina-refining/. 2022 [accessed on 15 June 2025].

[22] ARENA. *Alcoa Renewable Powered Electric Calcination Pilot*. https://arena.gov.au/projects/alcoa-renewable-powered-electric-calcination-pilot/. 2022 [accessed on 7 March 2025].

[23] Haus S, Borges A, Almeida N, and Duck A. *Results of Metso Outotec Calciner Optimizer Operation at CBA Alumina Calcination Plants.* Light Metals 2022, 2022: p. 22-30. https://doi.org/10.1007/978-3-030-92529-1_3.

[24] Saw W L, Nathan G J, Chatfield R V, and Haywood R J, *Method and Apparatus for Alumina Calcination* 2022 17 June 2022. WO2022261726A1. https://patentimages.storage.googleapis.com/b3/bd/c3/d31d8a0f599297/WO2022261726A1.pdf.

[25] Goldberg S, Davis J A, and Hem J D. *The environmental chemistry of aluminum*.2020. 271-331.

[26] Saw W L, Lee L, Ingenhoven P, Chinnici A, Zhang X, Rafique M, Tang Y, Tung D A J, Tsai T C, He Z, Smadi E A, Tian Z F, Lau T, Sun Z, Chin R, Eyk P v, Dally B, and Nathan G. *Integrating Concentrating Solar Thermal Energy into the Bayer Alumina Process*. https://arena.gov.au/assets/2024/07/Univeristy-of-Adelaide-Integrating-Concentrating-Solar-Thermal-Energy-into-the-Bayer-Alumina-Process-Final-report.pdf. 2023 [accessed on 8 March 2025].

[27] Candela L, Perlmutter, D.D. *Pore structure and kinetics of the thermal decomposition of Al (OH)$_3$.* AIChE journal, 1986. 32(9): p. 1532-1545. https://doi.org/10.1002/aic.690320914.

[28] Perić J, Krstulović R, and Vučak M. *Investigation of dehydroxylation of gibbsite into boehmite by DSC analysis.* Journal of thermal analysis, 1996. 46: p. 1339-1347. https://doi.org/10.1007/BF01979247.

[29] Redaoui D, Sahnoune F, Heraiz M, and Raghdi A. *Mechanism and kinetic parameters of the thermal decomposition of gibbsite Al(OH)$_3$ by thermogravimetric analysis.* Acta Physica Polonica A, 2017. 131(3): p. 562-565. https://doi.org/10.12693/APHYSPOLA.131.562.

[30] Boquan Z, Binxiang F, and Xiangcheng L. *Dehydration reactions and kinetic parameters of gibbsite.* Ceramics International, 2010. 36(8): p. 2493-2498. https://doi.org/10.1016/j.ceramint.2010.07.007.

[31] Alex T, Sasi Kumar C, Kailath A J, Kumar R, Roy S, and Mehrotra S. *Analysis of mechanically induced reactivity of boehmite using kinetics of boehmite to γ-Al$_2$O$_3$ transformation.* Metallurgical and Materials Transactions B, 2011. 42: p. 592-603. https://doi.org/10.1007/s11663-011-9494-5.

[32] Bracci J M, Sherwin E D, Boness N L, and Brandt A R. *A cost comparison of various hourly-reliable and net-zero hydrogen production pathways in the United States.* Nature Communications, 2023. 14(1): p. 7391. https://doi.org/10.1038/s41467-023-43137-x.

[33] Singh S K and Tiwari A K. *Solar-powered hydrogen production: Advancements, challenges, and the path to net-zero emissions.* International Journal of Hydrogen Energy, 2024. 84: p. 549-579. https://doi.org/10.1016/j.ijhydene.2024.08.209.

[34] Longden T, Jotzo F, Prasad M, and Andrews R. *Green hydrogen production costs in Australia: implications of renewable energy and electrolyser costs*. https://ccep.crawford.anu.edu.au/publication/ccep-working-paper/17458/green-hydrogen-production-costs-australia-implications. 2020 [accessed on 9 March 2025].

[35] Curcio E. *Techno-economic analysis of hydrogen production: Costs, policies, and scalability in the transition to net-zero.* International Journal of Hydrogen Energy, 2025. 128: p. 473-487. https://doi.org/10.48550/arXiv.2502.12211.

[36] International Energy Agency (IEA). *The Future of Hydrogen, Seizing today's opportunities*. https://www.iea.org/reports/the-future-of-hydrogen. 2019 [accessed on 1 March 2025].

[37] Nnabuife S G, Oko E, Kuang B, Bello A, Onwualu A P, Oyagha S, and Whidborne J. *The prospects of hydrogen in achieving net zero emissions by 2050: A critical review.* Sustainable Chemistry for Climate Action, 2023. 2: p. 100024. https://doi.org/10.1016/j.scca.2023.100024.

[38] Longden T, Beck F J, Jotzo F, Andrews R, and Prasad M. *'Clean'hydrogen?–Comparing the emissions and costs of fossil fuel versus renewable electricity based hydrogen.* Applied Energy, 2022. 306: p. 118145. https://doi.org/10.1016/j.apenergy.2021.118145.

[39] Nnabuife S G, Darko C K, Obiako P C, Kuang B, Sun X, and Jenkins K. *A comparative analysis of different hydrogen production methods and their environmental impact.* Clean Technologies, 2023. 5(4): p. 1344-1380. https://doi.org/10.3390/cleantechnol5040067.

[40] Mitterrutzner B, Sovacool B K, Knudsen B R, Bazilian M D, Kim J, Roussanaly S, Tomasgard A, and Griffiths S. *Scaling carbon capture and storage (CCS) to gigaton capacity: A multi-dimensional and critical review.* International Journal of Greenhouse Gas Control, 2026. 149: p. 104531. https://doi.org/10.1016/j.ijggc.2025.104531.

[41] Intergovernmental Panel on Climate Change. *Carbon Dioxide Capture and Storage*. https://www.ipcc.ch/site/assets/uploads/2018/03/srccs_wholereport-1.pdf. 2005 [accessed on 8 June 2024].

[42] Environmental Protection Agency. *Section 4.8 Operational Report 1. The Bayer Process*. https://epawebapp.epa.ie/licences/lic_eDMS/090151b2806ec707.pdf. 2019 [accessed on 14 March 2025].

[43] Perander L. *Evolution of nano-and microstructure during the calcination of Bayer gibbsite to produce alumina*. 2010. University of Auckland.

[44] Safaei M. *Effect of temperature on the synthesis of active alumina by flash calcination of gibbsite.* Journal of the Australian Ceramic Society, 2017. 53: p. 485-490. https://doi.org/10.1007/s41779-017-0058-2.

[45] AEMO. *The Wholesale Market Gas Quality Monitoring Procedures*. https://www.aemo.com.au/-/media/files/stakeholder_consultation/consultations/gas_consultations/2023/amendments-to-victorian-declared-wholesale-gas-market-and-retail-market/ppc/wholesale-market-gas-quality-monitoring-procedures.pdf. 2024 [accessed on 6 Feb 2026].

[46] Hameed K W. *Chemical Process Simulations using Aspen Hysys*. John Wiley & Sons.2025.

[47] AspenTech. *Unit Operations and Reaction Models*. https://esupport.aspentech.com/FileAttachment?id=a0g0B00000GfNpB. 2013 [accessed on 11 June 2025].

[48] Shephered C and Lapple C. *Flow pattern and pressure drop in cyclone dust collectors.* Industrial & Engineering Chemistry, 1939. 31(8): p. 972-984. https://doi.org/10.1021/ie50356a012.

[49] Peters M S, West R E, and Timmerhaus K D. *Plant design and economics for chemical engineers*. 5th ed. ed. McGraw-Hill chemical engineering series. New York: McGraw-Hill.2003.

[50] Wu W, Jian Z-L, Chou B-Y, You C-Y, and Kuo Y-N. *Process design and techno-economic evaluation of a decarbonized cement production process using carbon capture and utilization.* Processes, 2023. 11(7): p. 2043.

[51] Neal P R, Hou W, Allinson W G, and Cinar Y, *Costs of CO_2 Transport and Injection in Australia*, in *SPE Asia Pacific Oil and Gas Conference and Exhibition*. 2010: Brisbane, Australia.

[52] Hayat M A, Hasan S, and Elshurafa A M. *Strategic priorities and cost considerations for decarbonizing electricity generation using CCS and nuclear energy*. Energy Reports, 2024. 12: p. 2108-2122. https://doi.org/10.1016/j.egyr.2024.08.017.

[53] Dindi A, Coddington K, Garofalo J F, Wu W, and Zhai H. *Policy-Driven Potential for Deploying Carbon Capture and Sequestration in a Fossil-Rich Power Sector.* Environmental Science & Technology, 2022. 56(14): p. 9872-9881. 10.1021/acs.est.1c08837.

[54] International Energy Agency (IEA). *The Future of Hydrogen, Report Prepared by the IEA for the G20, Japan*. https://www.iea.org/reports/the-future-of-hydrogen. 2019 [accessed on 30 April 2025].

[55] Nhuchhen D R, Sit S P, and Layzell D B. *Decarbonisation of cement production in a hydrogen economy.* Applied Energy, 2022. 317: p. 119180. https://doi.org/10.1016/j.apenergy.2022.119180.

[56] *Gas market prices, Australia Energy Regulator*. https://www.aer.gov.au/industry/registers/charts/gas-market-prices. 2024 [accessed on 1 March 2025].

[57] *Natural gas price-world data*. https://ourworldindata.org/grapher/natural-gas-prices?tab=table&time=2020..latest. [accessed on 6 March 2025].

[58] Bruce S, Temminghoff M, Hayward J, Schmidt E, Munnings C, Palfreyman D, and Hartley P. *National hydrogen roadmap*. https://www.csiro.au/en/research/environmental-impacts/fuels/hydrogen/Hydrogen-Roadmap. 2018 [accessed on 20 Jun 2024].

[59] Gielen D, Taibi E, and Miranda R. Hydrogen: A renewable energy perspective. in the 2nd hydrogen energy ministerial meeting. 2019. Tokyo, Japan.https://www.h2knowledgecentre.com/content/policypaper1305.

[60] Council. H. *Hydrogen Insights 2023-The state of the global hydrogen economy, with a deep dive into renewable hydrogen cost evolution*. https://hydrogencouncil.com/wp-content/uploads/2023/12/Hydrogen-Insights-Dec-2023-Update.pdf. 2023 [accessed on 12 June 2024].

[61] International Energy Agency (IEA). *Hydrogen Production and Infrastructure Projects Database, IEA, Paris*. https://www.iea.org/data-and-statistics/data-product/hydrogen-production-and-infrastructure-projects-database. 2024 [accessed on 12 June 2025].

[62] International Energy Agency (IEA). *Global Hydrogen Review 2024*. https://www.iea.org/reports/global-hydrogen-review-2024. 2024 [accessed on 6 June 2025].

[63] Lingjuan W. *Theoretical study of cyclone design*. Texas A&M University.2004.

[64] Klett C, Reeb B, Missalla M, and Schmidt H-W. *Methods to reduce operating costs in circulating fluidized bed calcination.* Light Metals 2011, 2011: p. 125-130. https://doi.org/10.1007/978-3-319-48160-9_22.

[65] Lamouri S, Hamidouche M, Bouaouadja N, Belhouchet H, Garnier V, Fantozzi G, and Trelkat J F. *Control of the γ-alumina to α-alumina phase transformation for an optimized alumina densification.* Boletín de la Sociedad Española de cerámica y vidrio, 2017. 56(2): p. 47-54. https://doi.org/10.1016/j.bsecv.2016.10.001.

[66] Candela L, Perlmutter, D.D. *Kinetics of boehmite formation by thermal decomposition of gibbsite.* Industrial & engineering chemistry research, 1992. 31(3): p. 694-700. https://doi.org/10.1021/ie00003a007.

[67] Lopushan V I, Kuznetsov, G.F., Pletnev, R.N., Kleshev, D.G. *Kinetics of phase transitions of gibbsite during heat treatment in air and in water vapor.* Refractories and Industrial Ceramics, 2007. 48(5): p. 378-382. https://doi.org/10.1007/s11148-007-0099-0.

[68] Mills G, *Method for the calcination of aluminium trihvdroxide*. 24 October 2007. WO Patent 2008/052249A1. https://patentimages.storage.googleapis.com/30/b9/1d/3e51ae39f87fbb/WO2008052249A1.pdf.

[69] Vincent Giroud and Pinoncely A, *Twelve Years Flash Calciner Performance*, in *the 4th International AQW Conference and Exihibition*. 1996: Lyon, France.

[70] Blakers A, Stocks M, Lu B, Cheng C, and Stocks R. *Pathway to 100% renewable electricity.* IEEE Journal of Photovoltaics, 2019. 9(6): p. 1828-1833. https://doi.org/10.1109/JPHOTOV.2019.2938882.

[71] Zun M T and McLellan B C. *Cost projection of global green hydrogen production scenarios.* Hydrogen, 2023. 4(4): p. 932-960. https://doi.org/10.3390/hydrogen4040055.

[72] CSIRO Australia's National Science Agency. *Gen Cost 2023-24*. https://publications.csiro.au/publications/publication/PIcsiro:EP2024-2021. 2023 [accessed on 1 December 2024].

Appendix A for Chapter 3

Capital cost estimation for steam generation via electric boilers and steam recovery via multi-stage mechanical vapour recompression

The factored estimation method was used to estimate the total capital investment (TCI), which has an inherent uncertainty of approximately 30%. The purchased equipment cost served as the basis for estimating the cost of both indirect and direct cost items. Ratio factors for estimating cost breakdown were obtained with consultation with Worley [1], as shown in Table A-2. For the breakdowns, tanks and platework costs covers for boiler feed water pumps, blowdown tanks. Steam piping covers the transportation of steam within the plant. Electrical equipment costs include control and instrument wiring, power wiring, transformers, and associated services. Instrumentation costs cover devices used for process monitoring, measurement, and control.

In present economic analysis, the electric boiler purchase cost is assumed US$ 160 per kW (2024 value) [2, 3], with the installation factor f of 1.53 [4]. Table A-1 presents the reference size and cost of compressors, obtained from open literature. The compressor cost was calculated using Equation (A-1), where C_{refer} is the reference cost, and S_{new} and S_{refer} are the calculated scale in the study and reference scale, respectively.

$$C_{MVR\ compressor} = C_{refer} \times \left(\frac{S_{new}}{S_{refer}}\right)^{0.7} \quad \text{(A-1)}$$

Table A-1. Estimated purchased cost of MVR compressor from open literatures.

Components	Reference cost, C_{refer}	Reference size, S_{refer}	Reference year	Scaling factor	Installation factor, f	Sources
MVR compressors	1.4 NZD M$	3 MW	2019	0.7	1.38	[5]
	3 NZD M$	3 MW	2004	0.7	1.38	[6]
	2.7 USD M$	4.47 MW	1998	0.7	1.38	[7]

Table A-2: Ratio factors used to estimate total capital investment of installing electric boilers.

Parameters	Assumed factor number	
	Electric boilers	**Mechanical vapour recompression**
Direct cost (DC)		
Purchased main equipment	A	A
Purchased-equipment installed	A*1.53	A*1.38
Earthworks	0.01A	0.01A
Concrete	0.05A	0.05A
Structural	0.20A	0.20A
Insulation	0.03A	0.03A
Tanks & Platework	0.04A	0.04A
Piping	0.47A	0.47A
Electrical Equipment	0.33A	0.33A
Instrumentation	0.03A	0.03A
Total direct costs	**(1.16+1.53)A**	**(1.16+1.38)A**
Indirect cost (IDC)		
Project Development allowance	0.06 A	0.06 A
EPCM	0.78 A	0.78 A
Contingency	0.98 A	0.98 A
Total Indirect costs	**1.82 A**	**1.82 A**
Total capital investment (TCI)	**(2.98+1.53) A**	**(2.98+1.38) A**

Process modelling of electric boilers

A heater is used to estimate the energy consumption of electric boilers [8], assuming an inlet water temperature of 40°C and an efficiency of 98% [3, 9]. The calculated energy consumption is 2.78 GJ/t_{steam} from Aspen simulation. Thermodynamic minimum for producing low-pressure saturated steam is calculated at 2.65 GJ/t_{steam} with no losses. When accounting for the realistic operation of electric boilers, such as boiler efficiency (98%), small blowdown with proper operation (1-3%), deaerator losses (~0.5%) [10], the required energy increases to approximately 2.75-2.8 GJ/t_{steam}. This range is consistent with the Aspen result, indicating that the modelled value is thermodynamically and operationally plausible.

Calculation of thermal energy required for steam generation

Feedwater inlet: 40 °C
Boiler efficiency: 98%
Latent heat of vaporisation at 8 bar ($h_{f,g}$): 2.06 MJ/kg
Water specific heat ($C_{p,w}$): 4.18 kJ/kg·°C
Steam specific heat at 170 °C ($C_{p,s}$): 2.5 kJ/kg·°C

1. Heat per kg Steam

Sensible heat = $C_{p,w} \times \Delta T = 4.18\times10^{-3} \times (170–40) = 0.54$ MJ/kg steam
Latent heat = $h_{f,g}$ = 2.05 MJ/kg steam
Sensible heat = $C_{p,s} \times \Delta T = 2.4\times10^{-3} \times (200–170) = 0.06$ MJ/kg steam
Total = 0.54 + 2.05+0.06 = 2.65 MJ/kg steam

References

[1] *Worley, "Discussion on capital cost breakdwon," personal consultation*. https://www.worley.com/. [accessed on 1 June 2023].

[2] Lagendijk J. *An Exploration of the Company Perspective on the Adoption of Industrial Electric Boilers*. https://pure.tue.nl/ws/portalfiles/portal/313517534/1253492_final_version_master_thesis_JSLagendijk.pdf. [accessed on 4 April 2025].

[3] Zuberi M J S, Hasanbeigi A, and Morrow W. *Electrification of industrial boilers in the USA: potentials, challenges, and policy implications.* Energy Efficiency, 2022. 15(8): p. 70. https://doi.org/10.1007/s12053-022-10079-0.

[4] Garrett D E. *Chemical engineering economics*. Springer Science & Business Media.2012.

[5] Energy Efficiency and Conservation Authority. *MVR (Mechanical Vapour Recompression) Systems for Evaporation, Distillation and Drying*. https://genless.govt.nz/assets/Business-Resources/Mechanical-vapour-recompression-for-evaporation-distillation-drying.pdf. 2019 [accessed on 7 July 2024],Chatfield R. *Mechanical vapor recompression (MVR) for low carbon alumina refining, MVR technical and commercial feasibility studies*. https://arena.gov.au/projects/mechanical-vapour-recompression-for-low-carbon-alumina-refining/. 2022 [accessed on 14 June 2024].

[6] Reuben W. Bouman, Scott B. Jesen, Maria L. Wake, and Earl W B. *Process Capital Cost Estimation for New Zealand 2004*. https://books.google.com.au/books?id=_sfzPAAACAAJ. 2005 [accessed on 1 March 2025].

[7] Energy. T U S D o. *Process equipment cost estimation, final report*. https://www.osti.gov/servlets/purl/797810. 2002 [accessed on 8 June 2024].

[8] Hameed K W. *Chemical Process Simulations using Aspen Hysys*. John Wiley & Sons.2025.

[9] Schoeneberger C, Zhang J, McMillan C, Dunn J B, and Masanet E. *Electrification potential of US industrial boilers and assessment of the GHG emissions impact.* Advances in Applied Energy, 2022. 5: p. 100089. https://doi.org/10.1016/j.adapen.2022.100089.

[10] *Industrial combustion boilers*. https://iea-etsap.org/E-TechDS/PDF/I01-ind_boilers-GS-AD-gct.pdf. 2010 [accessed on 6 June 2024].

Appendix B for Chapter 3

Table B-1 summarises the exit-gas composition from the natural-gas/air combustion calcination process.

Table B-1. Exit gas from natural gas/air combustion calcination based on 120 t/hr Al_2O_3 capacity.

Gas volume	m^3/s	87
Temperature	°C	165
Pressure (absolute)	bar	1.06
Flue gas mass fraction		
N_2	%	46.9%
CO_2	%	9.3%
O_2	%	1.1%
H_2O	%	42.8%
Total gas flow	t/hr	210
Density of gas	kg/m^3	0.67

Figure B-1 shows the amine-based CO_2 capture process applied to the exit gas, adapted from a previous study [1]. Stack gas first enters a pre-scrubber cooler to remove particles / and cool to ~35 °C. The cooled gas passes up a packed absorber where 30 wt% amine (MEA) absorbs CO_2. The CO_2 rich amine solution is preheated in a lean/rich heat exchanger and sent to a desorber operating at 2.0 bar. A reboiler, supplied with low-pressure saturated steam generated by electric boilers in this study, regenerates the solvent and releases CO_2. The overhead vapour is condensed to ~35 °C to remove water, after which the CO_2 is sent to four-stage compression with intercooling (air coolers). The compressed CO_2 is delivered at 80 bar and 35 °C for pipeline transport.

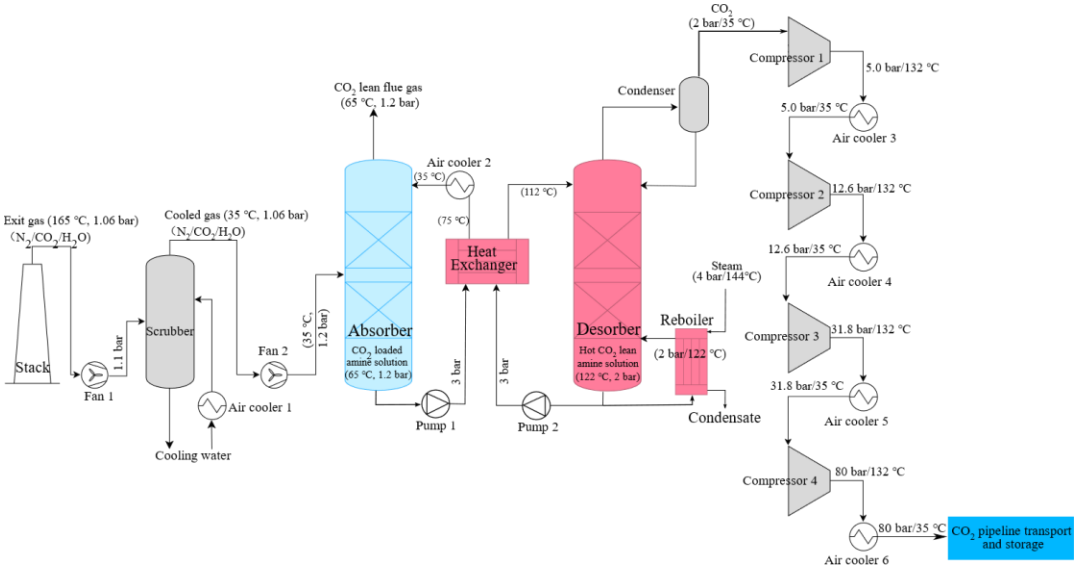


Figure B-1. Schematic illustration of amine-based CO_2 capture process from exit gas.(adapted from previous study [1])

Table B-2 summarises the input parameters for the amine-based CO_2 capture model, including symbols, units, baseline values, and the references cited for each parameter used in the calculations.

Table B-2. Input specifications for the amine-based CO_2 capture.

Parameter	Value	Symbol	Unit	References
MEA (amine) concentration	0.30	wt%	kg/kg	[2]
MEA liquid heat capacity	3.7	$C_{p,L}$	kJ/kg·°C	[3]
Cooled gas heat capacity	1.0	$C_{p,g}$	kJ/kg·°C	
Total heat capacity rate	314.9	C_{tol}	kW/°C	
Lean amine loading	0.20	α_{lean}	mol CO_2/mol MEA	[1, 2]
Rich amine loading	0.50	α_{rich}	mol CO_2/mol MEA	[4]
Loading difference	0.30	$\alpha_{rich} - \alpha_{lean}$	mol CO_2/mol MEA	[1]
Heat of CO_2 absorption	85	ΔH_{abs}	kJ/mol CO_2	[5]
CO_2 capture rate	90		%	[2]
CO_2 captured	17.58		t/hr	
Flue gas temperature at absorber inlet	35		°C	
Lean amine temperature at absorber inlet	35		°C	
Pumps efficiency	70	η	%	[6, 7]
Fans efficiency	70	η	%	[8]
Rich amine pump 1 discharge pressure	3.0		bar(a)	[2]
Lean amine pump 2 discharge pressure	3.0		bar(a)	[2]
Fan 1 discharge pressure	1.1		bar(a)	
Fan 2 discharge pressure	1.2		bar(a)	[1]
The lean/rich amine heat exchange hot-side approach	10		°C	[2]
Condenser temperature	35		°C	[1, 2]
Desorber, condenser pressure	2		bar(a)	[1]
Reboiler duty	3.2	Q_{reb}	GJ/t CO_2	[1]
Low-pressure steam from electric boiler	4 bar/144°C			[1, 9]
Compressors isentropic efficiency	75%			[10]
Assumed pressure ratio per stage (4 stages)	2.51			
Cooling air temperature rise assumed in air cooler	20		°C	
Inlet cooling air temperature	20.5		°C	
Stack pressure blowing air assumed	0.4		KPa	[11-13]

Table B-3 summarises the electrical power consumption of the amine-based CO_2 capture system. The total specific electricity is about 1.36 MWh/$t_{CO2\ captured}$. Power use is dominated by steam generation via the electric boiler (81% of the total), with auxiliaries for fans and pumps contributing 13%, and CO_2 compression accounting for the remaining 6%. For the design case (17.58 t/hr CO_2 capture), this corresponds to approximately 19.7 MW for steam, 3.2 MW for auxiliaries, and 1.6 MW for compression.

Table B-3. Calculated power consumed for the amine-based CO_2 capture.

Parameter	Value	Unit		Fraction
Fan 1	497	KW	Auxiliary: 3162.2 KW	13%
Fan 2	571	KW		
Pump 1	17.6	KW		
Pump 2	9.8	KW		
Fan for air cooler 1	1760	KW		
Fan for air cooler 2	268	KW		
Fan for air cooler 3	9.7	KW		
Fan for air cooler 4	9.7	KW		
Fan for air cooler 5	9.7	KW		
Fan for air cooler 6	9.7	KW		
Compressor 1	390	KW	Compression:1560 KW	6%
Compressor 2	390	KW		
Compressor 3	390	KW		
Compressor 4	390	KW		
Electric boiler for steam generation	19704	KW	Steam: 19704 KW	81%
Steam consumption	1.5	t steam/t CO_2		
Total electric power input in CO_2 capture	24426	KW		
Total electric power input in CO_2 capture	1.39	MWh/t CO_2		

Table B-4 summarises the economic assumptions and calculation of cost of CO_2 capture and compression used for the amine-based CO_2 capture analysis.

Table B-4. Economic analysis assumptions used for economic analysis of the amine-based CO_2 capture.

Parameter	Value	References
Capital cost, million US$/(t/hr CO_2 capture)	3	[1]
Capital cost, million US$	52.7	
Capital cost, US$/t CO_2	46.8	
Renewable electricity price, US$/MWh	70	[14]
Interest rate	10%	
Service lifer, years	15	
Maintenance fee per year	3% of capital	
Cost of CO_2 capture and compression, US$/$t_{CO2}$	144.1	
CO_2 transport and storage cost, US$/$t_{CO2}$	19-51	[15]

Table B-5. Sensitivity analysis for CCS cost (CO_2 capture, compression, transport and storage).

Parameter	Value	References
Electricity price, US$/MWh	30-100	
Interest rate	10%	
Service lifer, years	15	
Maintenance fee per year	3% of capital	
Cost of CO_2 capture and compression, US$/$t_{CO2}$	88.5-185.8	
CO_2 transport and storage cost, US$/$t_{CO2}$	35	[15]
Cost of CCS, US$/$t_{CO2}$	123.5-220.8	

References

[1] Danish Energy Agency. Technology Data for Carbon Capture,Transport and Storage. https://ens.dk/en/analyses-and-statistics/technology-data-carbon-capture-transport-and-storage. 2021 [accessed on 1 August 2024].

[2] Ali, U, et al. Techno-economic process design of a commercial-scale amine-based CO2 capture system for natural gas combined cycle power plant with exhaust gas recirculation. Applied Thermal Engineering, 2016. 103: p. 747-758. https://doi.org/10.1016/j.applthermaleng.2016.04.145.

[3] Concepción, E I, et al. Heat capacities of different amine aqueous solutions at pressures up to 25 MPa for CO2 capture. Journal of Molecular Liquids, 2023. 377: p. 121575. https://doi.org/10.1016/j.molliq.2023.121575.

[4] Putta, K R, et al. CO2 absorption into loaded aqueous MEA solutions: Kinetics assessment using penetration theory. International Journal of Greenhouse Gas Control, 2016. 53: p. 338-353. https://doi.org/10.1016/j.ijggc.2016.08.009.

[5] Vinjarapu, S H B, et al. Heat of absorption of CO2 in 30 wt% MEA with monoethyleneglycol and urea as vapour reduction additives. Energy, 2024. 293: p. 130609. https://doi.org/10.1016/j.energy.2024.130609.

[6] Kaya, D, Çanka Kılıç, F, and Öztürk, H H. Energy efficiency in pumps, in Energy Management and Energy Efficiency in Industry: Practical Examples. In. Springer.2021, p. 329-374.

[7] AspenTech. Unit Operations and Reaction Models. https://esupport.aspentech.com/FileAttachment?id=a0g0B00000GfNpB. 2013 [accessed on 11 June 2025].

[8] The U.S. Environmental Protection Agency. Wet and Dry Scrubbers for Acid Gas Control. https://www.epa.gov/sites/default/files/2021-05/documents/wet_and_dry_scrubbers_section_5_chapter_1_control_cost_manual_7th_edition.pdf. 2021 [accessed on 12 October 2024].

[9] Faramarzi, L, et al. Results from MEA Testing at the CO2 Technology Centre Mongstad: Verification of Baseline Results in 2015. Energy Procedia, 2017. 114: p. 1128-1145. https://doi.org/10.1016/j.egypro.2017.03.1271.

[10] Martynov, S B, et al. Impact of stream impurities on compressor power requirements for CO2 pipeline transportation. International Journal of Greenhouse Gas Control, 2016. 54: p. 652-661. https://doi.org/10.1016/j.ijggc.2016.08.010.

[11] Hill, G B, Pring, E, and Osborn, P D. Cooling towers: principles and practice. Butterworth-Heinemann.2013.

[12] Hensley, J C. Cooling tower fundamentals. Marley Cooling Tower Company Kansas City.1985.

[13] Arya, R K, Verros, G D, and Davim, J P. Compressors and Blowers: Maintenance, Practical Guidance, Energy-Efficient Technologies. Vol. 13. Walter de Gruyter GmbH & Co KG.2025.

[14] Blakers, A, Lu, B, and Stocks, M. 100% renewable electricity in Australia. Energy, 2017. 133: p. 471-482. https://doi.org/10.1016/j.energy.2017.05.168.

[15] Neal, P R, et al. Costs of CO_2 Transport and Injection in Australia. in SPE Asia Pacific Oil and Gas Conference and Exhibition. 2010. Brisbane, Australia.https://doi.org/10.2118/133900-MS. https://doi.org/10.2118/133900-MS.

Chapter 4

Techno-economic Assessment of Integrated Steam Cleaning and Recovery from Alumina Calcination for various decarbonisation scenarios

Preface

Steam generation for the Bayer circuit usage accounts for 60-70% of the total energy consumption and CO_2 emissions in the Bayer process. Recovering steam from the calcination process presents a promising opportunity to improve overall energy efficiency and reduce emissions. However, challenges such as fine particle contamination and flue gas dilution could be a barrier for steam recovery from the calciner circuit technically complex.

Chapter 3 focus on calcination, investigating three calcination scenarios: natural gas/air, hydrogen/air, and hydrogen in oxy-steam, highlighting the potential for high-concentration steam recovery from steam-based calcination and the limitations caused by flue gas dilution in air-based combustion. Chapter 4 addresses the technical barriers in steam recovery by evaluating the feasibility of integrated steam cleaning, diluted-gas separation and recovery from various calcination pathways, with Chapter 3 providing the exit flue gas composition data. Supplementary Appendix for Chapter 4 provides data for fully electrified calcination to support the analysis. This material is placed in the final section of the thesis due to its length and its role as supplementary, preliminary work.

Highlights of this work include:

- The integrated venturi scrubber is estimated to reduce solid concertation in steam below 2.9 mg/Nm^3.
- Steam recovery from various calcination pathways supplies 27-43% of the refinery's total steam demand.
- Integrating steam recovery with existing gas boilers reduces the energy consumption in supplying steam by 21-36%.
- Steam recovery integration improves the economic viability of conventional natural-gas steam generation when CO_2 capture and storage costs are included.

Statement of Authorship

Title of Paper	Techno-economic Assessment of Integrated Steam Cleaning and Recovery from Alumina Calcination for various decarbonisation scenarios
Publication Status	☐ Published ☐ Accepted for Publication ☑ Submitted for Publication ☐ Unpublished and Unsubmitted w ork w ritten in manuscript style
Publication Details	Ning S, Nathan G, Ashman P, and Saw W L. Techno-economic Assessment of Integrated Steam Cleaning and Recovery from Alumina Calcination for various decarbonisation scenarios. Submitted to Chemical Engineering Journal, 2025. Under review

Principal Author

Name of Principal Author (Candidate)	Siyun Ning		
Contribution to the Paper	Concept deisgn, Process model development and simulation, Data analysis and interpretation, Drafted the manuscript and acted as corresponding author.		
Overall percentage (%)	70%		
Certification:	This paper reports on original research I conducted during the period of my Higher Degree by Research candidature and is not subject to any obligations or contractual agreements with a third party that would constrain its inclusion in this thesis. I am the primary author of this paper.		
Signature		Date	

Co-Author Contributions

By signing the Statement of Authorship, each author certifies that:

i. the candidate's stated contribution to the publication is accurate (as detailed above);

ii. permission is granted for the candidate in include the publication in the thesis; and

iii. the sum of all co-author contributions is equal to 100% less the candidate's stated contribution.

Name of Co-Author	Graham Nathan		
Contribution to the Paper	Supervision of the work, Concept development, Evaluation and review of the manuscript.		
Signature		Date	

Name of Co-Author			
Contribution to the Paper	Supervision of the work, Concept development, Evaluation and review of the manuscript.		
Signature		Date	2/12/2025

Please cut and paste additional co-author panels here as required.

Name of Co-Author	Woei Lean Saw		
Contribution to the Paper	Supervision of the work, Concept development, Evaluati ipt.		
Signature		Date	

Chemical Engineering Journal 529 (2026) 173154



Contents lists available at ScienceDirect

Chemical Engineering Journal

journal homepage: www.elsevier.com/locate/cej





Techno-economic assessment of integrated steam cleaning and recovery from alumina calcination

Siyun Ning [a,b,c,*], Graham Nathan [b,c,d], Peter Ashman [a,b,c], Woei Lean Saw [a,b,c]

[a] School of Chemical Engineering, The University of Adelaide, Australia
[b] Centre for Energy Technology, The University of Adelaide, Australia
[c] Heavy Industry Low-carbon Transition Cooperative Research Centre, Australia
[d] School of Electrical and Mechanical Engineering, The University of Adelaide, Australia

ARTICLE INFO

Keywords:
Steam recovery from calcination
Steam cleaning
Decarbonised steam
Multi-stage mechanical vapour recompression
Techno-economic assessment

ABSTRACT

This study evaluates the techno-economic viability of integrated steam recovery from various alumina calcination pathways. A novel recovery flowsheet is developed to enable fine particle removal prior to mechanical vapour recompression (MVR) system, allowing efficient recovery of both diluted and high-concentration steam. Four scenarios were evaluated: recovery of diluted steam from either natural gas/air or H_2/air combustion (Scenarios 1 and 2), and recovery of high-concentration steam from either fully electrified calcination (Scenario 3) or H_2 in oxygen-steam (oxy-steam) combustion (Scenario 4). All the scenarios were modelled in Aspen Plus to assess technical performance, and economic feasibility. Scenario 4 achieves the highest recovery rate at 0.86 t_{steam}/t_{Al2O3}, followed by 0.64 t_{steam}/t_{Al2O3} for Scenario 3 and 0.54–0.55 t_{steam}/t_{Al2O3} for Scenarios 1 and 2. High-concentration steam recovery is more energy efficient, requiring 0.54 GJ/t_{steam} of electricity (9% for particle removal, 91% for compression) compared with 0.71 GJ/t_{steam} (5% for gas separation, 95% for compression) for diluted steam from air-based calcination. Integrating steam recovery from calcination with existing natural gas boilers (the "A" Scenarios) reduces steam-generation energy use by 21–36% and CO_2 emissions by 27–43% relative to a baseline of 6.63 GJ/t_{Al2O3}. Replacing natural gas boilers with electric boilers (the "B" Scenarios) enables zero direct on-site emissions from steam supply and delivers an additional 15% reduction in energy consumption. Economically, Scenario 4A achieves the greatest benefit, lowering the levelised cost of decarbonised steam ($LCOS_B$) by 26% compared with natural gas boilers with carbon capture and storage cost. Overall, the results demonstrate that integrating steam recovery enables substantial improvements in energy efficiency and CO_2 reduction, with high-concentration steam recovery provides superior thermodynamic and economic performance over conventional air-based systems.

1. Introduction

The industrial sector is a major contributor to global greenhouse gas emissions, with energy- and carbon-intensive industries such as cement, steel, aluminium and alumina refining playing a significant role [1–4]. In Australia, alumina refining alone accounts for approximately 24% of scope-1 manufacturing emissions and around 3% of national greenhouse gas emissions [5–7], with a typical carbon intensity of 0.68 t_{CO2}/t_{Al2O3} [8]. Decarbonising alumina refining is therefore critical to advancing broader sustainable industrial production objectives [4,9,10]. Within the Bayer process, steam generation supplied by fossil-fuel-based boilers represents a dominant source of both energy consumption and CO_2 emissions, accounting for approximately 60–70% of the total process energy demand [11]. Consequently, decarbonising steam generation is a key lever for reducing the overall carbon footprint of alumina production. However, the direct substitution of fossil fuels with low-carbon energy sources alone may increase production costs, highlighting the need for alternative approaches. Accordingly, new analyses of innovative process configurations are required that can simultaneously improve process efficiency, reduce emissions, and enhance the economic viability of net-zero alumina production.

The Bayer circuit employs steam at high temperature and pressure to dissolve the alumina hydrate from the ore with a caustic soda solution and precipitate it in a pure form, thereby separating it from the

* Corresponding author at: School of Chemical Engineering, The University of Adelaide, Australia.
E-mail address: siyun.ning@adelaide.edu.au (S. Ning).

https://doi.org/10.1016/j.cej.2026.173154
Received 2 November 2025; Received in revised form 2 January 2026; Accepted 16 January 2026
Available online 19 January 2026
1385-8947/© 2026 The Authors. Published by Elsevier B.V. This is an open access article under the CC BY license (http://creativecommons.org/licenses/by/4.0/).

impurities [12]. The magnitude of the temperature and pressure, together with the details of the process design, depend on the properties of the bauxite, but are typically divided into a higher temperature range for boehmite and a lower temperature range for bauxite options [13]. For digestion of gibbsite-rich bauxite, the pressure and temperature typically range from 6 to 8 bar and 175 °C to 230 °C [14]. This steam consumption is typically 6–7 GJ/t_{Al2O3}, derived from natural gas fossil-fuel fired boilers [15,16]. The calcination step, which is another energy-intensive step, produces steam originating from gibbsite dehydroxylation and fuel combustion. However, this steam is currently vented to atmosphere due to its high dilution with N_2 and CO_2 [14]. Recovering this steam for digestion reuse could potentially reduce the steam generation from natural gas boilers, thereby reducing fossil fuels consumption. Hence, the present study aims to assess the viability of recovering steam from calcination for a typical lower-temperature Bayer circuit, with a view to significantly reducing both CO_2 emissions and energy consumption for the steam generation.

The calcination process converts gibbsite to smelter-grade alumina (SGA), releasing chemically-bound steam at approximately 0.7 t_{steam}/t_{Al2O3}, with an associated latent energy of approximately 1.7 GJ/t_{Al2O3} [17]. Liu [18] presented the potential to utilise this waste heat to heat water via heat exchanger, saving hot water usage, for example in product washing or steam generation. However, no detailed quantitative results were provided to estimate the associated energy reduction. Yu et al. [19] similarly identified that alumina calciner stack off-gas poses itself as a potential for heat and water recovery. Chatfield [20] proposed utilising the off-gas as a steam recovery source, separating steam from N_2 and CO_2 using a scrubber. Chatfield [20] proposed utilising the off-gas as a steam recovery source, separating steam from N_2 and CO_2 using a scrubber. In this approach, steam is first condensed from the flue gas and then re-evaporated to low-pressure steam, followed by mechanical vapour recompression (MVR) to recover and recompress the steam. However, no detailed assessment of the performance of this proposed method has been reported such as the quantity or properties of the recoverable steam from the calciner, thermal energy losses during the condensation or the required electric power input needed for its recovery. Hence one aim of the present investigation is to evaluate this performance.

From the replacement of natural gas/air combustion to alternative net-zero energy sources such as the combustion hydrogen in oxy-steam or electric calcination, offers the potential to significantly increase the viability of steam recovery, as both options avoid dilution with N_2 [14,21]. These approaches have been proposed as key decarbonisation strategies in calcination, enabling net-zero calcination when renewable hydrogen or electricity is used. However, although the two options can yield 0.6–0.8 t_{steam}/t_{Al2O3} of high-concentration steam (>99.5% concentration), the presence of fine particles entrained in the exit steam poses a significant additional challenge. Although existing particulate control systems, such as electrostatic precipitators (ESP) and baghouses can achieve ~99% removal efficiency for particles larger than 2 μm [22,23], typically reducing solid concentrations to below 50 mg/Nm^3 (29–41 mg/Nm^3) [24–28], this is insufficient for use in MVR system. Fine particles can negatively impact the performance and potentially damage the MVR system used in subsequent steam compression [29], so that a highly efficient fine particle removal system is necessary. To date, no integrated steam cleaning and recovery concept has been proposed. Hence, further objectives of the present investigation are to propose and evaluate such a configuration for both the use of electric calcination and for the combustion of hydrogen and oxygen.

Venturi scrubbers are known to be able to achieve a high removal efficiency of fine particles smaller than 2.5 μm and also to operate effectively in steam-rich environments [30–32]. Ali et al., [33] report that the collection efficiency of venturi scrubbers is a function of many variables, such as the particle size, pressure drop. Performance curves [34–36] indicate that they achieve significantly higher particle removal efficiency at a pressure drop of 20 kPa compared to 2.5 kPa, especially for fine particles under 0.1–1 μm diameter [37]. However, despite many studies evaluating the performance of venturi scrubbers varying the particle diameter and pressure drops [38–40], no previous study has been conducted on the particle removal efficiency of venturi scrubber when integrated into a steam recovery process for steam cleaning. Therefore, a further aim is to investigate the particle removal efficiency of an integrated venturi scrubber under different particle size distributions, pressure drops, and solid concentrations in the outlet gases from alumina calcination in either H_2 combustion in oxy-steam or electric calcination, with the goal of achieving high purity steam stream.

The Bayer circuit consumes approximately 2 t_{steam}/t_{Al2O3} [14]. Implementing steam recovery from calcination has the potential to offset a substantial portion of the steam demand from natural gas boilers [20,41]. For carbon mitigation in steam supply, direct replacement of fossil-fuel boilers with electric boilers is another straightforward pathway [14,42–44]. At present, there is a lack of detailed economic assessments comparing alternative steam supply strategies for the Bayer circuit against conventional operation. Such analysis is essential to compare the economic viability of steam recovery systems. Accordingly, the present study aims to meet this need, evaluating the cost competitiveness of various steam supply scenarios including the capital and operating cost.

In light of the identified knowledge gaps, the objectives of the present study are as follows:

1. To develop and evaluate a steam cleaning and recovery flowsheet capable of fine particle removal and steam compression, while recovering high-purity steam from H_2 in oxy-steam combustion or electric calcination pathways.
2. To assess the influence of pressure-drop and particle size distribution on fine particle removal efficiency in an integrated venturi scrubber within the steam recovery configuration.
3. To compare steam recovery performance from alternative calcination processes spanning diluted steam from air-combustion calcination and high-concentration steam from oxy-steam and electric calcination, with regard to the amount of net recoverable steam, enthalpy changes, and energy penalties associated with gas separation and cleaning.
4. To evaluate the techno-economic viability of integrating steam recovery from prospective net-zero calcination configurations compared with a reference natural-gas-fired process, and to estimate the break-even price of renewable electricity price for a range of scenarios.

2. Methodology

2.1. Alumina air-based and steam-based calcination

Fig. 1 illustrates the current flash calcination flowsheet [45], which comprises two preheating stages, a main calcination stage, and a cooling stage. Gibbsite containing free moisture is preheated sequentially in Cyclones 1 and 2 before entering the main furnace, where calcination occurs at high temperature. The discharged hot alumina is then conveyed to air-cooling cyclones, in which its sensible heat is recovered to preheat the injected air. Final cooling is achieved in a fluidised-bed water cooler, reducing the alumina temperature to approximately 75 °C. A particulate control system, such as a baghouse or electrostatic precipitator (ESP), is employed to limit solid emissions prior to releasing the exhaust gas from Cyclone 1 to the atmosphere. Fig. 2 shows the novel calcination process design [21] that can operate via either hydrogen combustion in an oxy-steam environment or fully electric heating. This configuration enables net-zero calcination when renewable energy is available and incorporates integrated steam recovery, using recirculated superheated steam as the carrier gas for solids transport through the calciner. The simplified diagram only depicts the preheating and cooling cyclones as single units. The various calcination scenarios, natural gas/

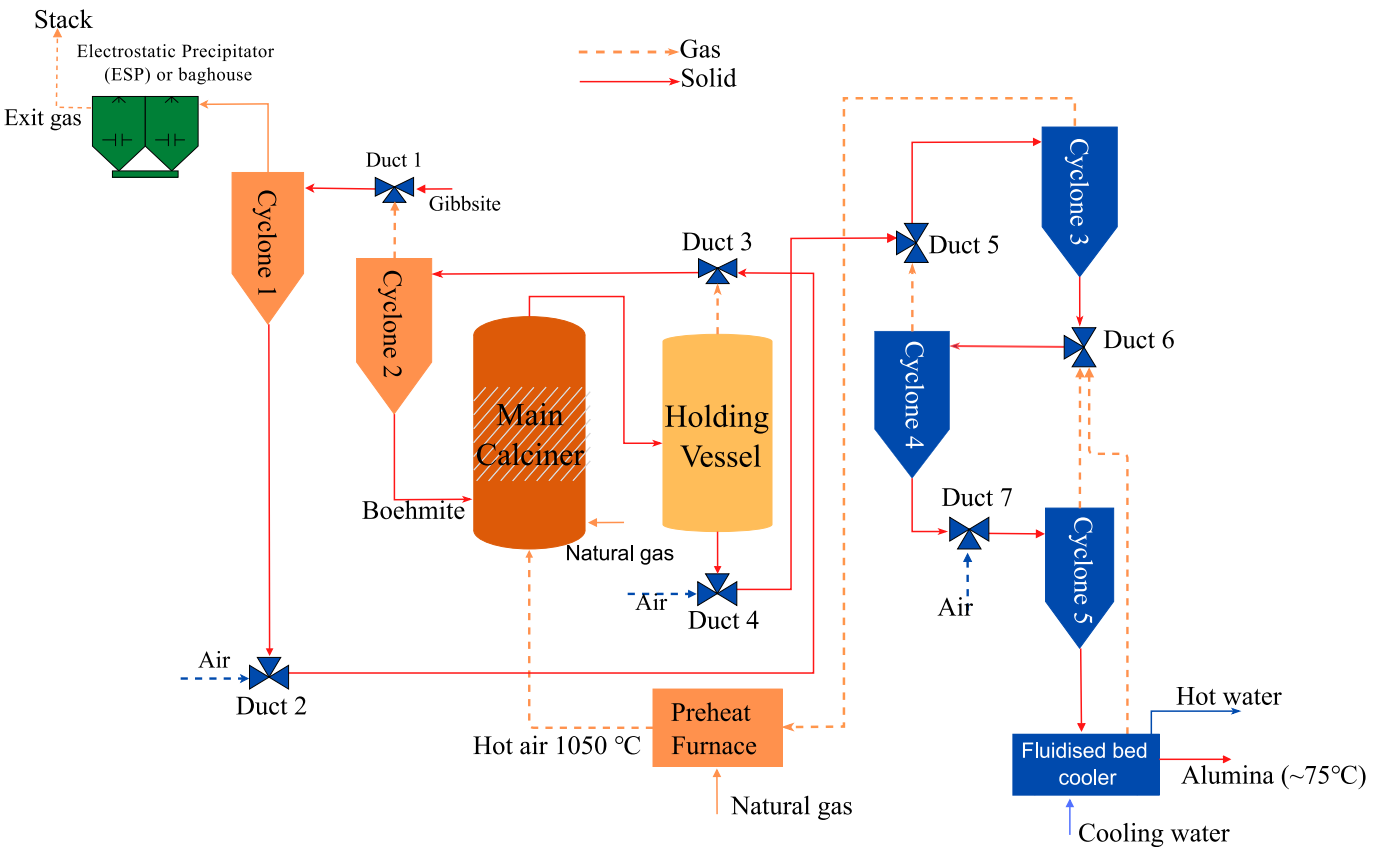


Fig. 1. The conventional flash calciner flowsheet under natural gas/air combustion. (Modified from previous work [47]).

air combustion, H_2/air combustion, H_2 in oxy-steam combustion and fully electrified calcination for 120 t/h alumina capacity were simulated and calculated using Aspen Plus [46].

2.2. Solids concentration in exit gases

The entrained solids concentration at the exit gases after the ESP/baghouse (Fig. 1) is assumed to range from 20 to 50 mg/Nm^3, with a lognormal distribution shown in Eq. (1), representing the particle size distribution by varying the natural logarithm of mean particle size (μ) from −1 to −2 and a standard deviation (σ) from 0.5 to 1. This is based on current design practice in which particle control systems limit solid emissions below 50 mg/Nm^3 [24], or between 5 and 30 mg/Nm^3 [27,28], together with operating data from an Australian alumina plant with emissions in the range of 29–41 mg/Nm^3 [24]. Baghouses typically achieve nearly 100% particles removal larger than 2 μm [26], but efficiency drops for particles smaller than 1 μm. Similarly, ESP shows declined performance for particles in the 0.2–1 μm range [22,23]. Therefore, this study assumes the particle size distribution of the solids leaving the baghouse ranging from 0.01 to 2 μm, as described by Eq. (1).

$$f(x) = \frac{1}{x\sigma\sqrt{2\pi}} e^{-\frac{(\ln x-\mu)^2}{2\sigma^2}} \quad (1)$$

2.3. Steam recovery flowsheets

2.3.1. Integrated spray tower with steam compression process

Fig. 3 presents the integrated gas separation and steam recovery process for recovering diluted steam from an air combustion calciner circuit, which was adapted from previous work [20]. The ESP/baghouse exit gases are first directed by a fan to a spray tower, where cooling water is sprayed from the top and flows counter-currently to the upward gas stream. This enables heat transfer and condensation of water vapour, which is collected at the bottom of the tower. The condensate then passes through a series of filters to remove solids before being pumped to flash tanks. These filters are removable for cleaning and replacement, with a pressure drop of 0.4 kPa across the filters [48,49]. After that, a portion of warm water is evaporated to low-pressure steam in three flash tanks, with a multi-stage MVR system extracting and compressing the steam to 8 bar and 200 °C. To maintain continuous operation, the process water is cooled to 40 °C in a cooling tower and recirculated to the spray tower, while a recirculation tank automatically supplies make-up water as needed.

Table 1 presents the operating conditions of the spray tower used in this study. Two towers were assumed to operate in parallel to cool ESP/baghouse exit gas flow rates of 87–90 m^3/s, as current towers have an operating limit of 47 m^3/s [35]. The inlet spray water is set at 40 °C and the rate is assumed be 2.7 kg per cubic meter of inlet gas [50]. The pressure drop across the tower was calculated to be 0.04 bar, with step-by-step calculation attached in Appendix A, including the diameter, height and capital investment of spray tower.

Table 2 summarises some key operating parameters of the cooling towers assumed to cool water to 40 °C as shown in Figs. 2 and 3, including the cooling range, inlet ambient air temperature, and fan power required to drive the airflow. A forced draft cooling tower was assumed [51,52], with centrifugal fans introducing air into the cooling tower at a typical stack pressure of 0.4 kPa [51–53]. In operation, warm water is sprayed downward while air is forced upward, enabling counter-current contact. A portion of the water evaporates, transferring energy to the steam, while the remaining cooled water is collected at the bottom for reuse. Evaporation occurs due to the vapour pressure difference between the water surface and the air, raising the relative humidity of the air and result in water losses, which needs to be compensated by make-up water.

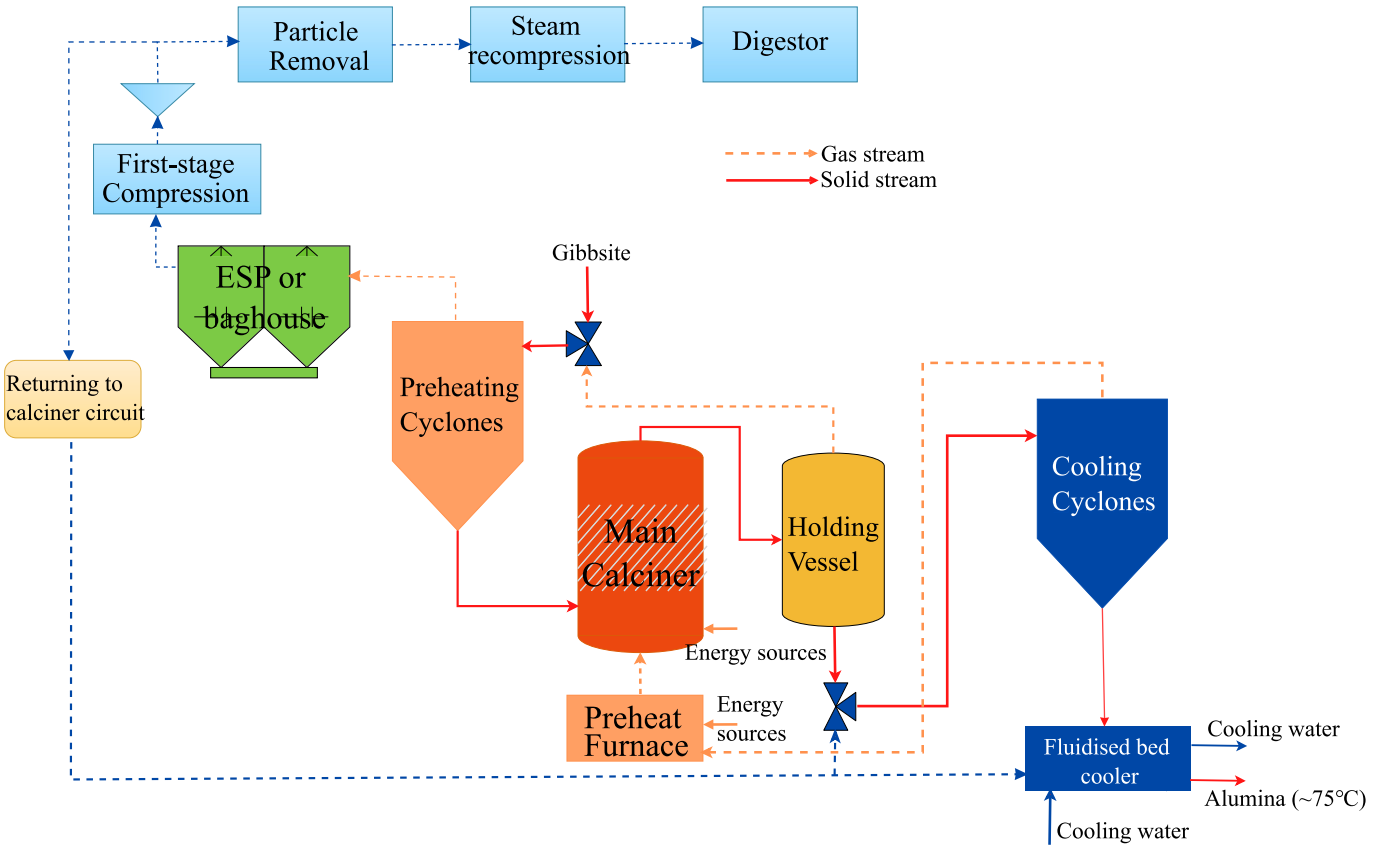


Fig. 2. The process flowsheet to achieve steam recovery from calcination with energy sources (H_2 in oxy-steam combustion or electricity) with recirculated steam as carrier gas.

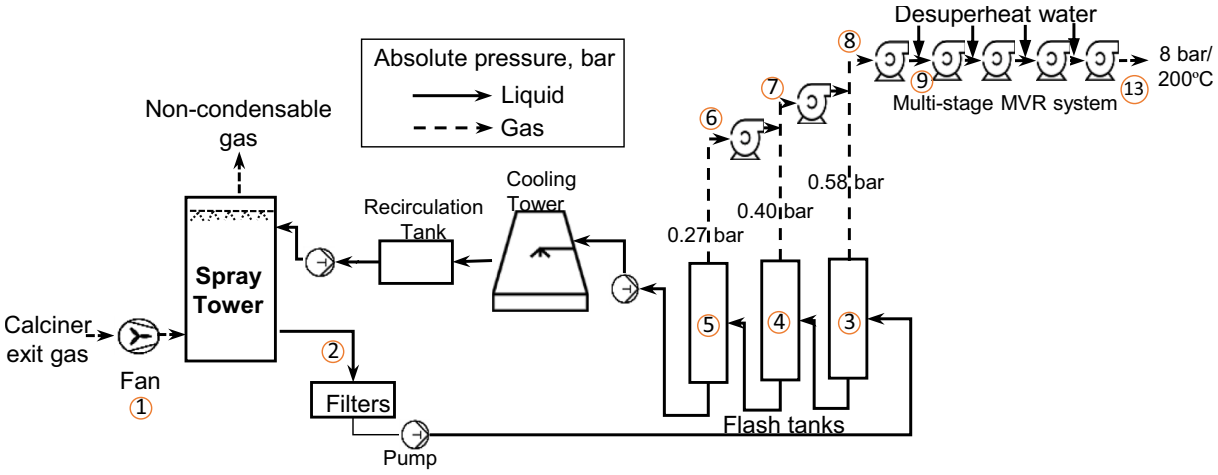


Fig. 3. The steam recovery flowsheet comprising a spray tower, flash tanks and mechanical vapour recompression (MVR) train. (Adapted from previous work [20]).

Table 1
Assumed operating conditions of spray towers.

Calcination pathways		Natural gas/air or H_2/air
Inlet gas volumetric limit [35,50]	m^3/s	47
Scrubber liquid		Water
Scrubber water temperature assumed	°C	40 °C
Liquid to gas ratio [50]	kg/m^3	2.7
Total spray water amount	kg/s	234

The inlet temperature of air is determined by ambient conditions, which was assumed to be 20.5 °C under and 40% relative humidity. The heat exchange between air and water was calculated using Eq. (2) [51], where the heat dissipated from the water equals to the heat gained by the air.

$$L \cdot C_{p(water)} \cdot Cooling\ range = G \cdot (h_2 - h_1) \quad (2)$$

Here, L is the water mass flow rate, C_p is the specific heat of water, and the cooling range is the inlet-outlet water temperature difference. G is the air mass flow rate, determined by liquid to gas ratio (L/G),

Table 2
The key operating conditions for the cooling towers.

Calcination pathways	Natural gas/air or H_2/air	Fully electrified or H_2 in oxy-steam
Cooling water rate (kg/s)	242.5	34.5
Liquid to gas ratio (kg/kg) [55]	0.8	0.8
Inlet water temperature (°C)	67	100
Outlet water temperature (°C)	40	40
Air inlet condition	20.5 °C (under 40% RH, 1.013 bar), moisture content (0.011 kg H_2O/kg air)	
Air inlet enthalpy (kJ/kg)	62 kJ/kg	
Air inlet wet-bulb temperature	30 °C (100% RH)	
Cooling range (°C)	27	60
Air mass flow rate (kg/s)	303	43
Air outlet enthalpy (kJ/kg)	153	270
Air outlet wet-bulb temperature (°C)	38 °C (100% RH) Moisture content (0.044 kg H_2O/kg air)	50 °C (100% RH) Moisture content (0.086 kg H_2O/kg air)
Evaporation rate (kg/s)	10	3.2
Fan power (kW)	144	21
Fan efficiency assumed [36]	70%	70%

assumed to be 0.8 kg/kg to ensure effective contact [54,55]. The values of h_2 and h_1 are the inlet and outlet specific enthalpies of the air (dry air plus water vapour), obtained from the psychrometric chart at the specified temperature and relative humidity [52]. The outlet air is assumed to be saturated (100% RH).

2.3.2. Venturi scrubber and steam compression

Fig. 4 presents the integrated venturi scrubber and steam compression process that was developed to achieve high purity. A portion of superheat steam is recirculated back to the calciner circuit of the electrified or the H_2 in oxy-steam combustion to transport solids and maintain volumetric flow rates comparable to those in natural gas/air calcination. The required recirculated steam flow rates are approximately 84 t/h and 60 t/h for electrified and oxy-steam calciner, respectively. A blower is employed to overcome the pressure drop across the calcination process, compressing the stream to 1.1 bar [53,56,57]. Before entering the venturi scrubber, desuperheat water is injected to cool the steam to near saturation. An induced-draft fan is used to overcome the pressure drop across the scrubber. Spray water is introduced at the throat, where high gas velocity and turbulence enhance droplet-particle interactions, achieving over 50% capture efficiency for submicron particles. The particle-laden condensate collects at the bottom, where it is filtered to remove solids, cooled in a cooling tower, and recirculated via a storage tank with make-up water added to compensate for losses. The cleaned steam exits the scrubber and passes through a four-stage MVR system, where its pressure and temperature are increased to 8 bar and 200 °C.

The separation efficiency of the venturi scrubber was calculated as a function of particle size distribution, expressed as the cumulative collection efficiency for each particle size range in Eq. (3). Here, η is the overall separation efficiency, η_i is the fractional separation efficiency for *ith* particle diameter range, m_i is mass fraction of *ith* particle diameter range, and *i* is the number of particle diameter ranges. The solid separation efficiency of particles in the 0.1–10 μm diameter range at venturi pressure drops between 2.5 and 20 kPa was reported by previous study [34–36]. Table 3 presents the operating condition of the venturi scrubber assumed, including spray water quantity and pressure drop.

$$\eta = \sum_{0}^{i} \eta_i \cdot m_i \ [58] \tag{3}$$

2.4. Steam recovery scenarios

Table 4 presents various scenarios for steam recovery and supply to the Bayer circuit. The reference case represents conventional steam generation method, relying solely on natural gas-fired boilers to generate 2 t_{steam}/t_{Al2O3} steam [20,46]. The electric boiler case represents direct transition from natural gas boilers without steam recovery. Scenarios 1–4 examine alternative steam recovery options from calcination. Each is modelled in two sub-scenarios: "A" uses natural gas boilers to supply any steam shortfall, while "B" uses electric boilers. The scenarios explore different fuel combinations such as natural gas, electricity or both to assess their impact on CO_2 emissions and total energy

Table 3
Operating conditions of the venturi scrubber.

Calcination pathways		Fully electrified	H_2 in oxy-steam
Spray water temperature assumed	°C	40 °C	
Spray water to gas ratio [59]	kg/m^3	0.67	
Inlet gas volume of venturi scrubber	m^3/s	38	46
Spray water mass flow rate	kg/s	25	31
Gas pressure drop	kPa	2.5–20	
Spray nozzle pressure [59]	bar	2.4	

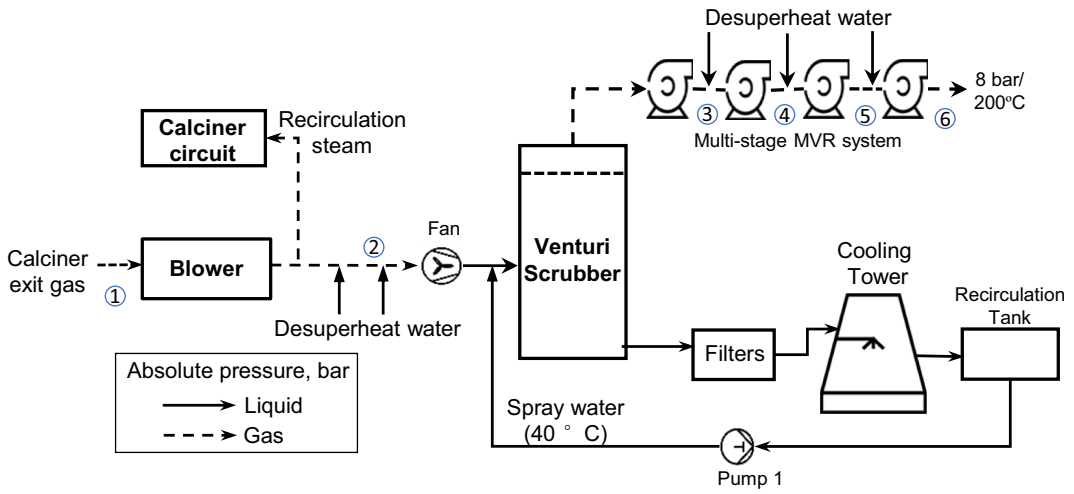


Fig. 4. Integrated venturi scrubber for steam cleaning with steam recovery flowsheet for calcination in high-concentration steam.

Table 4
Steam recovery and supply scenarios to the Bayer circuit.

Steam recovery from various calcination pathways	Boilers for supplementary steam generation
Reference Scenarios	Natural gas boiler with CCS Electric boilers
Scenario 1: Natural gas/air	Scenario 1A: steam recovery (Scenario 1) + natural gas boiler (with CCS) back up Scenario 1B: steam recovery (Scenario 1) + electric boiler back up
Scenario 2: H_2/air	Scenario 2A Scenario 2B
Scenario 3: Fully electrified	Scenario 3A Scenario 3B
Scenario 4: H_2 in oxy-steam	Scenario 4A Scenario 4B

consumption in steam supply.

2.5. Process simulation

The steam recovery flowsheets shown in Figs. 3 and 4 were modelled within the Aspen Plus to analyse industrial process mass and energy balances and support system-level optimisation [60]. An overview of flowsheet model parameters is provided in Table 5. The electric power for fan operation was calculated by Eq. (4), where Q_g is the gas volume flow rate (m^3/s), ΔP is the pressure difference (Pa), and η is the overall efficiency. The pump power for the liquid circuit was calculated using Eq. (5), where L is the liquid flow (m^3/s), ρ_L is the density of the fluid (kg/m^3), ΔP is the pressure difference. The number of compression stages and inter-stage pressure ratios in the MVR system were selected to balance the compressor operability. For a given total pressure lift, distributing compression across multiple stages reduces the per-stage pressure ratio and discharge temperatures. The per-stage compression ratio was limited to 1.76, in line with reported operating constraints for industrial MVR compressors [61–64]. In the diluted steam case, the first and second compressors provide the required vacuum for the flash tanks, operating at compression ratios of 1.48 and 1.45, respectively. Owing to the low inlet vapour pressure, a 7-stage MVR configuration was adopted. In contrast, the high-concentration steam case enters the compressor at a higher pressure and requires a smaller total pressure lift. A 4-stage configuration with similar per-stage pressure ratios was sufficient (Table 5).

Table 5
The inputs and assumptions for the process model for steam recovery (Figs. 3 and 4).

Unit	Process input and assumptions	References
Natural gas boiler	• Steam output at 200 °C and 8 bar. • Efficiency of 82%. • Inlet water temperature of 40 °C.	[64–66]
Electric boiler	• Efficiency of is 98%. • Inlet water temperature of 40 °C.	[67,68]
Fans	• Assumed efficiency of 70%, accounting for both mechanical and motor efficiencies. • Formula: $E_{fan} = \frac{(Q_g) \times \Delta P \times 10^{-3}}{\eta}$ (4)	[36,64,69]
Pumps	• Pumps with assumed the efficiency of 70%, accounting for both flow and mechanical losses. • Formula: $E_{pumps} = \frac{L^* \Delta P \times 10^{-3}}{\eta}$ (5)	[64,70]
Spray tower	•A two-outlet flash block at 1.06 bar with operating condition shown in Table 2.	[36,64]
Flash tanks	•Three by two-outlet flash blocks operated at 0.58, 0.4, and 0.27 bar.	[20]
MVR system	• Desuperheat water is injected at each stage. • 7-stage MVR from 0.27 bar to 8.2 bar. • Isentropic efficiency of compressors of 76%. • Pressure ratio of stage 1: 1.48 • Pressure ratio of stage 2: 1.45 • Pressure ratio of stages 3–5: 1.76 for each stage • Pressure ratio of stage 6: 1.68 • Pressure ratio of stage 7: 1.55	[61–64]
Venturi scrubber	•A two-outlet flash block operated at 1.1 bar with operating condition shown in Table 4.	
Blower	• A compressor with an outlet pressure of 1.1 bar. • Assumed overall blower efficiency of 70%, accounting for both mechanical and motor efficiencies.	[36,69]
MVR system	• 4-stage MVR from 1.1 bar to 8.2 bar. • Pressure ratio of stages 1–2: 1.76 for each stage. • Pressure ratio of stage 3: 1.7 • Pressure ratio of stage 4: 1.42	[61–64]

2.6. Economic analysis

2.6.1. Capital cost estimation for steam recovery

The factor estimation method was used to estimate the total capital investment based on the purchased equipment cost. Table 6 presents the breakdown of factor values, provided in consultation with Worley in Australia, with an inherent uncertainty of approxiately ±30%. The breakdown of direct and indirect costs was estimated using purchased equipment cost as the baseline. Costs for major equipment items including MVR compressors, electric boilers, flash tanks, and cooling towers were estimated using published data from the open literature and adjusted to US$ (2024) by the Chemical Engineering Plant Cost Index (CEPCI). Tables C-3 to C-7 in the supporting documents (Appendix C) summarise the cost estimates for major equipment. The total capital investment (TCI) method was used to estimate the costs for the spray towers and venturi scrubber, following previous work [36,58], including the auxiliary costs for pumps and fans attached in Appendices A and B.

2.6.2. Operating cost

2.6.2.1. Levelised cost of decarbonised steam supply for the Bayer circuit. The alumina refinery is assumed to produce 120 t/h alumina, requiring 240 t/h steam supply the Bayer circuit at a consumption rate of 2 t_{steam}/t_{Al2O3} [14]. The levelised cost of decarbonised steam supply for Bayer circuit, $LCOS_B$, was calculated using Eq. (6). To ensure that the comparison is performed for an equivalent the decarbonised scenario, a cost of CO_2 capture, compression, transport and storage (CCS) was included

Table 6
Ratio factors used to estimate the total capital investment for installation of the steam recovery system.

Parameters	Assumed factor number
Direct cost (DC)	
Purchased main equipment	A
Purchased-equipment installed	A*f
Earthworks	0.01 A
Concrete	0.05 A
Structural	0.20 A
Insulation	0.03 A
Tanks & Platework	0.04 A
Piping	0.47 A
Electrical Equipment	0.33 A
Instrumentation	0.021 A
Total direct costs	**(1.16 + f)A**
Indirect cost (IDC)	
Project Development allowance	0.06 A
EPCM	0.78 A
Contingency	0.98 A
Total indirect costs	**1.82 A**
Total capital investment (TCI)	(2.98 + f) A

for the use of natural gas. The base cost of CCS was calculated to be 179 US$/$t_{CO2}$ captured at an electricity price of 70 US$/MWh. This value comprises 144.1 US$/$t_{CO2}$ for capture and compression, as calculated in Appendix D, and an additional 35 US$/$t_{CO2}$ for transport and storage of compressed CO_2, based on the study by Allinson et al. [71], who estimated CO_2 transport and storage costs in the South-West region of Australia. A sensitivity analysis of CCS cost was conducted for electricity prices ranging from 30 to 120 US$/MWh, yielding a CCS cost range of 124–249 US$/$t_{CO2}$. This range is broadly in line with the literature, with the cost of CO_2 capture cost ranging from 65 to 201 US$/$t_{CO2}$ [72,73].

The $LCOS_B$ was calculated as the cost of supplying steam only, excluding differences in calcination process costs associated with natural gas, hydrogen, or electricity. The capital and operating costs of the calcination process (hydrogen oxy-steam calcination, natural gas/air or hydrogen/air calcination, and fully electrified calcination) were not included, as these technologies are at different stages of development and their costs are highly site-specific and therefore fall beyond the boundary of this study. Nevertheless, the results provide useful inputs for future integrated techno-economic assessments of low-carbon alumina refining (Table 7).

$$LCOS_B = \frac{\sum_{t=1}^{n} \frac{TCI_t + M_t + G_t + C_t + E_t}{(1+r)^t}}{\sum_{t=1}^{n} \frac{A_t}{(1+r)^t}} \quad (6)$$

2.6.2.2. Renewable electricity price assumption. The reference value for the average price of renewable electricity was assumed to be 70 US $/MWh, consistent with modelling by Andrew et al. [74] for a 100% renewable electricity supply in the Australian market. A sensitivity analysis was then carried out to examine the impact of electricity price over the range 30 to 120 US$/MWh. This spans the global range of 2023 levelised cost of electricity (LCOE) for sources spanning onshore wind, concentrated solar power, offshore wind, bioenergy, geothermal, hydropower, and standalone solar photovoltaic [75].

2.6.2.3. Natural gas price. Natural gas price sensitivity was assessed using 2019–2023 averages for the United States, United Kingdom, Australia, and the Netherlands, ranging from 3.3 US$/GJ to 13.9 US $/GJ [76,77]. The average Australian price of 7.5 US$/GJ over this period is taken as the reference value in this study.

3. Results and discussion

3.1.1. Exit gases from calcination pathways

Table 8 presents the composition, temperature, pressure, flow-rate of the exit gases from the calciner, which provide a comparative basis for evaluating the steam recovery potential of each calcination scenario. For combustion with natural gas/air and H_2/air calcination, N_2 constitutes nearly half of the exhaust flue gas, with a dilution level of approximately 47%. For steam calcination under fully electrified and H_2 in oxy-steam combustion, high-concentration steam is generated.

Table 7
Assumptions for the levelised cost of decarbonised steam supply for the Bayer circuit.

TCI (investment expenditures in year t)	The construction is within 1 year
M_t, Operating and maintenance expenditures in year t	3% of TCI
G_t, Cost in natural gas in year t	7.5 US$/GJ gas price
C_t, Cost of CO_2 capture and storage in year t	179 US$/$_{CO2}$
E_t, Cost of renewable electricity in year t	70 US$/MWh
A_t, Alumina production in year t	With 90% operating time per year, 120 t Al_2O_3/h capacity
r, Discount rate	10%
n, Life of the system	15

Table 8
The calculated properties of the exit gases from the calciner for the four calcination scenarios, based on 120 t/h Al_2O_3 capacity.

Calcination pathways		Natural gas/air	H_2/air	Fully electrified	H_2 in oxy-steam
Gas volume	m^3/s	87	90	85	85
Temperature	°C	165	165	176	167
Pressure (absolute)	bar	1.06	1.06	1.06	1.06
Gas components (mass fraction)					
N_2	%	46.9%	47.9%	0%	0%
CO_2	%	9.3%	0%	0%	0%
O_2	%	1.1%	4.2%	0%	0.8%
H_2O	%	42.8%	47.9%	100.0%	99.2%
Total gas flow	t/h	210	205	159	163
Density of gas	kg/m^3	0.67	0.64	0.52	0.53

3.1.2. Calculated particle removal efficiency of the integrated venturi scrubber

Fig. 5(a)–(d) presents the calculated particle removal efficiency of the integrated venturi scrubber and the outlet solid concentration for various particle size distribution (PSD) and inlet solid concentrations. In general, at a higher steam stream pressure drop of 20 kPa, the estimated efficiency exceeds 94%, reducing the outlet solid concentration to 1.2–2.9 mg/Nm^3. Fig. 4(a) and (b) presents the probability distribution and cumulative fraction of particle sizes for $-1 < \mu < -2$ and $0.5 < \sigma < 1$. For $\mu = -2$ and $\sigma = 0.5$, the PSD spans between 0.01 μm and 0.5 μm, indicating a narrow range of fine particles. Fig. 3(c) and (d) shows the effects of pressure drops and PSD on the calculated solid removal efficiency and outlet solid concentration. For a spray pressure drop of 2.5 kPa, the calculated efficiency decreases significantly from 87% to 18% as the log mean particle size μ decreases from 0 to −2. This reduction is due to the low removal efficiency (<10%) of submicron particles (0.1–1 μm) under low-pressure conditions [78]. The resulting outlet solid concentration ranges from 16 to 40 mg/Nm^3, exceeding the recommended threshold of <5 mg/Nm^3, or even lower based on internal discussions with MVR manufacturers [79]. However, with a higher steam stream pressure drop of 20 kPa, the separation efficiency consistently high at 94–100% for all PSD's, to achieve outlet solids concentrations of 1.2 and 2.9 mg/Nm^3. This highlights the need for higher pressure drops of the gaseous stream in integrated venturi scrubber to maintain good separation efficiency for fine particles, despite the higher fan energy required to overcome it.

3.2. Energy consumption for steam recovery

3.2.1. Enthalpy change in steam recovery processes

Fig. 6 presents the enthalpy changes in recovering diluted from both the case of air-combusted calcination and from the high-concentration steam from H_2 in oxy-steam or electrified calcination, highlighting the differences in two steam recovery processes. The use of high-concentration steam avoids unnecessary condensation and re-evaporation steps in diluted steam recovery, thereby avoiding enthalpy loss and greatly lowering energy demand. It thereby also greatly reduces the number of stages in the process.

The initial enthalpy of diluted steam from natural gas/air and H_2/air calcination is calculated to be 1320–1457 kJ/kg, which is much lower than the 2810 kJ/kg of high-concentration steam. In the diluted steam case, condensation in the spray tower reduces enthalpy to ~420 kJ/kg and temperature to 102 °C. This condensation is necessary for re-evaporation and subsequent compression but results in additional energy losses, as discussed in Section 3.2.2. Re-evaporation of low-pressure steam from three flash tanks results in lower steam pressure and temperature compared with high-concentration steam, thereby increasing

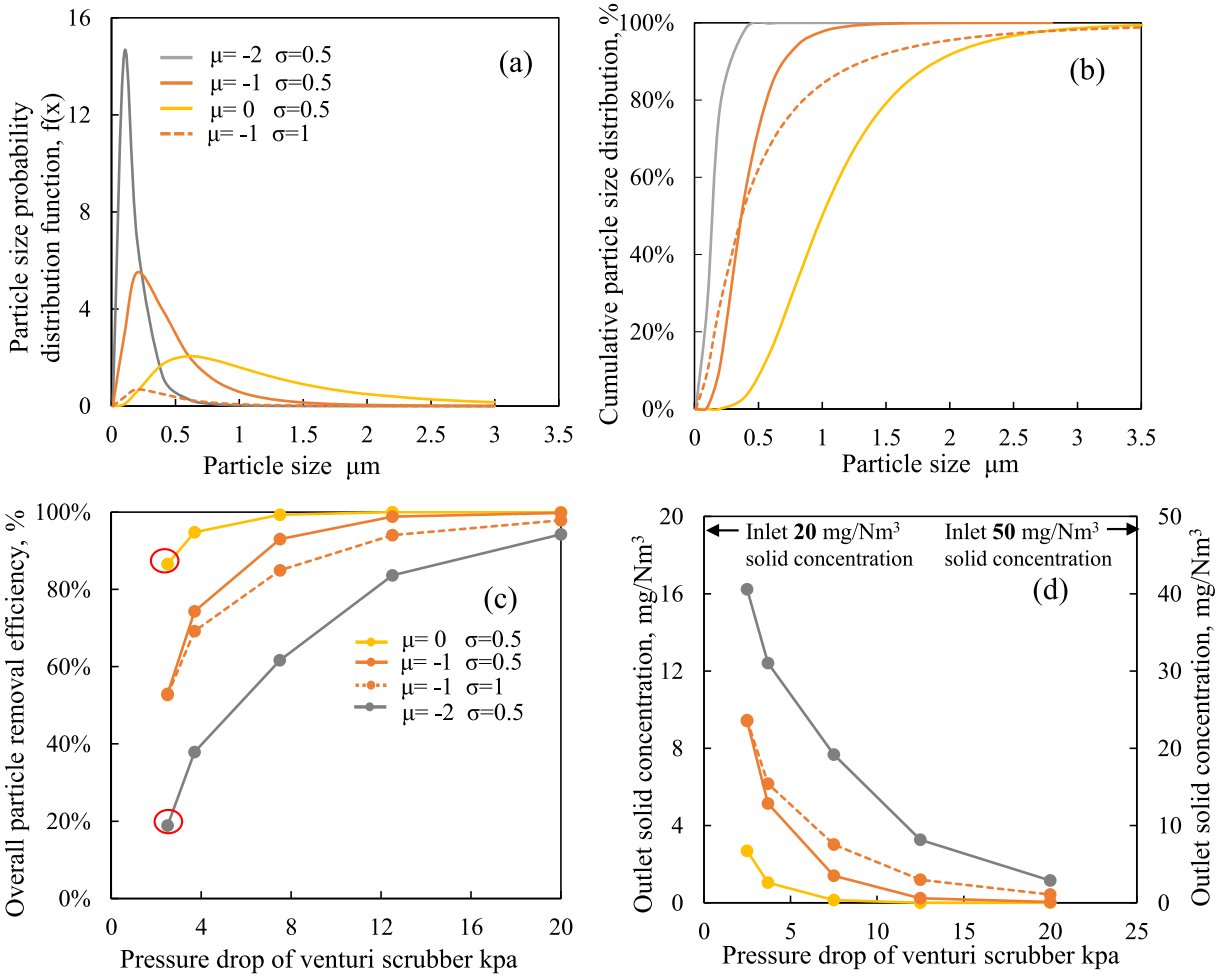


Fig. 5. The calculated performance of the venturi scrubber system for the various scenarios showing (a) particle size probability distributions; (b) particle size cumulative fraction curves; (c) the effects of PSD and pressure drops of steam stream on the calculated particle removal efficiency; (d) the corresponding calculated outlet solids concentration.

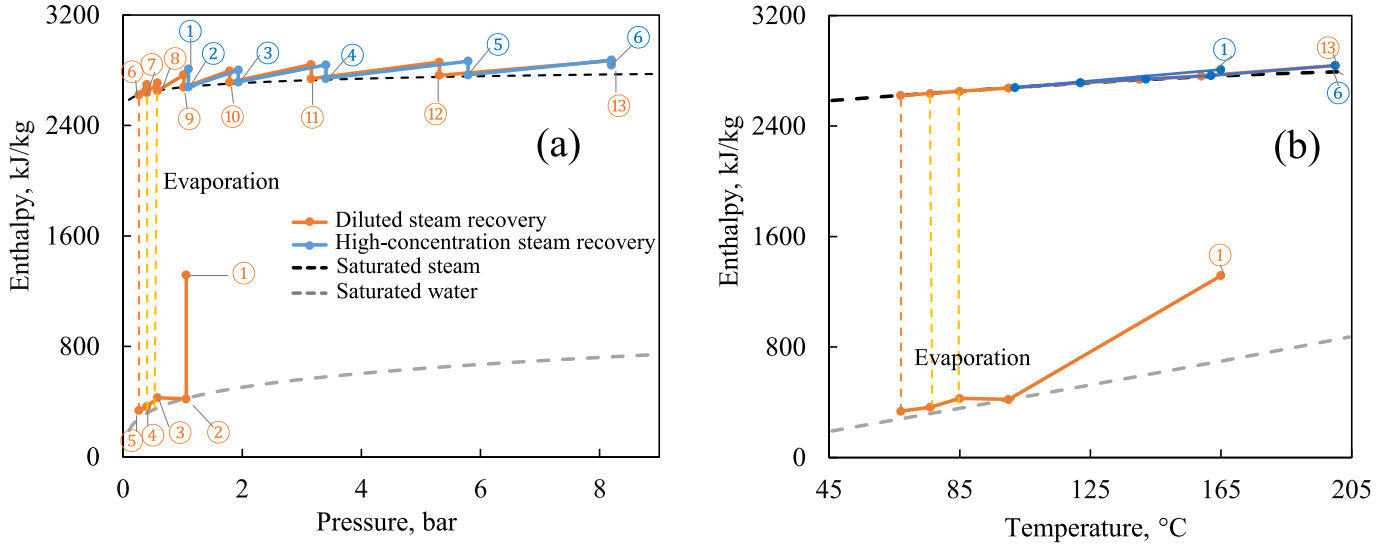


Fig. 6. Enthalpy changes in recovering steam for both the diluted gases from air-combusted calcination and for the high-concentration steam from H_2 in oxy-steam or electrified calcination, showing data on both (a): Enthalpy-Pressure(h-p) diagram, (b): Enthalpy-Temperature(h-T) diagram. Refer to Figs. 2 and 3 for the corresponding locations in the cycle diagrams for the states shown here.

the compression ratio and requiring more MVR stages. Consequently, a 7-stage MVR system is needed to compress the steam to 8 bar and 200 °C. In contrast, the recovery from high-concentration steam (Scenarios 3–4) avoids these losses. This system only needs one venturi scrubber, instead of the tower and three flash tanks, and achieves the pressure with only 4-stages of MVR to achieve the same temperature and pressure. In this way it avoids the need for condensation and re-evaporation, thereby improving recovery efficiency.

3.2.2. Mass balance and energy flows through steam recovery

Fig. 7 presents the mass flow balance through steam recovery for Scenarios 1 and 4. Overall, the recovery of high-concentration steam from fully electrified and H_2-oxy-steam combustion (Scenarios 3 and 4) achieves approximately 94% of the exit steam. For Scenario 4, the total steam flow is 162.8 t/h, comprising 62 t/h of recirculated steam and 100 t/h available for recovery (excluding a small portion of O_2). Excluding losses in the venturi scrubber, 93.3 t/h of cleaned vapour is directed to the MVR system for further compression. In contrast, recovery of diluted steam from natural gas/air or H_2/air calcination achieves a lower recovery rate of 62%, due to losses in the flash vessels. For Scenario 1, the flue gas flow contains 90 t/h of steam, of which 55.6 t/h is directed to MVR system for further compression.

Fig. 8 presents the calculated flows of energy through the various steam recovery processes. Overall, energy losses from condensation in flash tanks are much higher in Scenarios 1 and 2, accounting for 43% of flue gas energy, compared with 14% in venturi scrubber in Scenarios 3 and 4, due to greater losses in spray towers and flash tanks than in the venturi scrubber. For Scenario 1, the flue gas carries 67.1 MJ/s of energy, of which 1.28 MJ/s is lost to non-recoverable N_2 and CO_2 in the spray tower. The remaining energy is recovered through condensation, with the hot water directed to three flash tanks where 37.5 MJ/s of energy is evaporated as steam and fed to the MVR system, while 28.8 MJ/s is lost. Following evaporation step, the MVR system, with a 12.2 MJ/s electrical power input, compresses this steam, yielding an outlet steam with a total energy value of 49.7 MJ/s. In addition, flashing water to low-pressure steam increases the overall compression ratio, requiring 7-stage as noted above. Scenario 2, with H_2/air combustion yields a slightly higher steam content in the flue gas, resulting in a marginal increase in energy output of 50.5 MJ/s.

Scenario 4, which recovers high-concentration steam from H_2 in oxy-steam combustion, achieves the highest energy recovery, producing 78.8 MJ/s of outlet steam. A total of 74.2 MJ/s is directed to the venturi scrubber for recovery, with a portion recirculated to the calciner circuit, about 10% higher than the diluted gas in Scenario 1. Approximately 10.0 MJ/s is lost due to the condensation in the venturi scrubber. The remaining 65.2 MJ/s of steam energy is compressed in a four-stage MVR system, requiring 13.6 MJ/s of power. Scenario 3, based on fully electrified calcination, achieves a lower net heat recovery of 59.0 MJ/s per calciner (120 t/h Al_2O_3 capacity). As for Scenario 4, it requires steam recirculation to the calciner circuit to transport solids and maintain volumetric flow rates comparable to those for natural gas/air calcination. As there are no combustion products in fully electrified calcination, a greater recirculation volume is required to match gas flow, with estimated recirculated steam rates of approximately 84 t/h and 62 t/h for Scenarios 3 and 4, respectively. Overall, Scenario 4 achieves the highest energy recovery, surpassing Scenarios 1 and 2 by 37% and Scenario 3 by 25%, though it requires greater power input in MVR system.

3.2.3. Energy consumption and recoverable steam

Fig. 9 presents the energy consumption distribution and recoverable steam quantity for the four calcination pathways. Scenario 4 achieves the highest recovery at 103 t/h, consistent with the recoverable energy

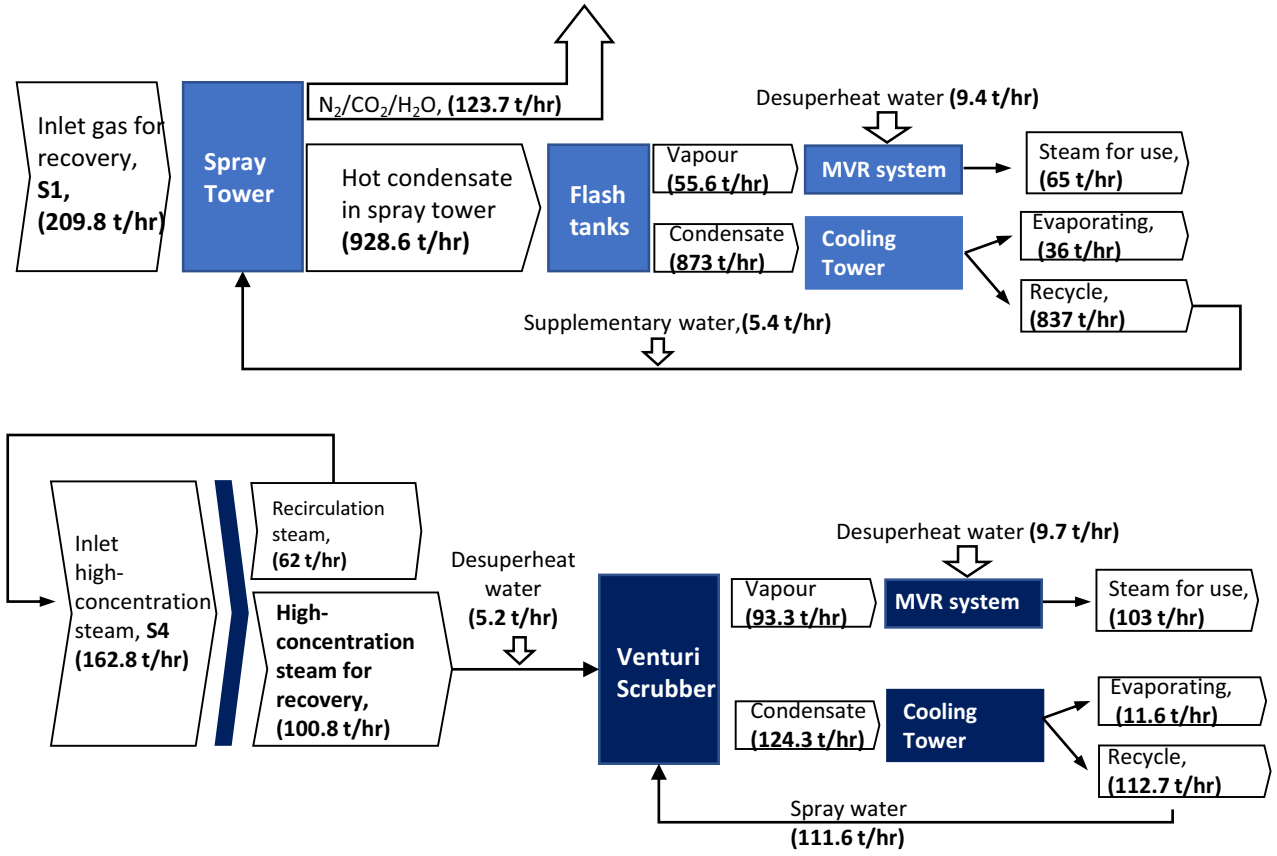


Fig. 7. Mass flow balance in recovering diluted steam from natural gas/air combustion and high-purity steam from H_2 in oxy-steam calciner based on 120 t/h alumina calciner capacity.

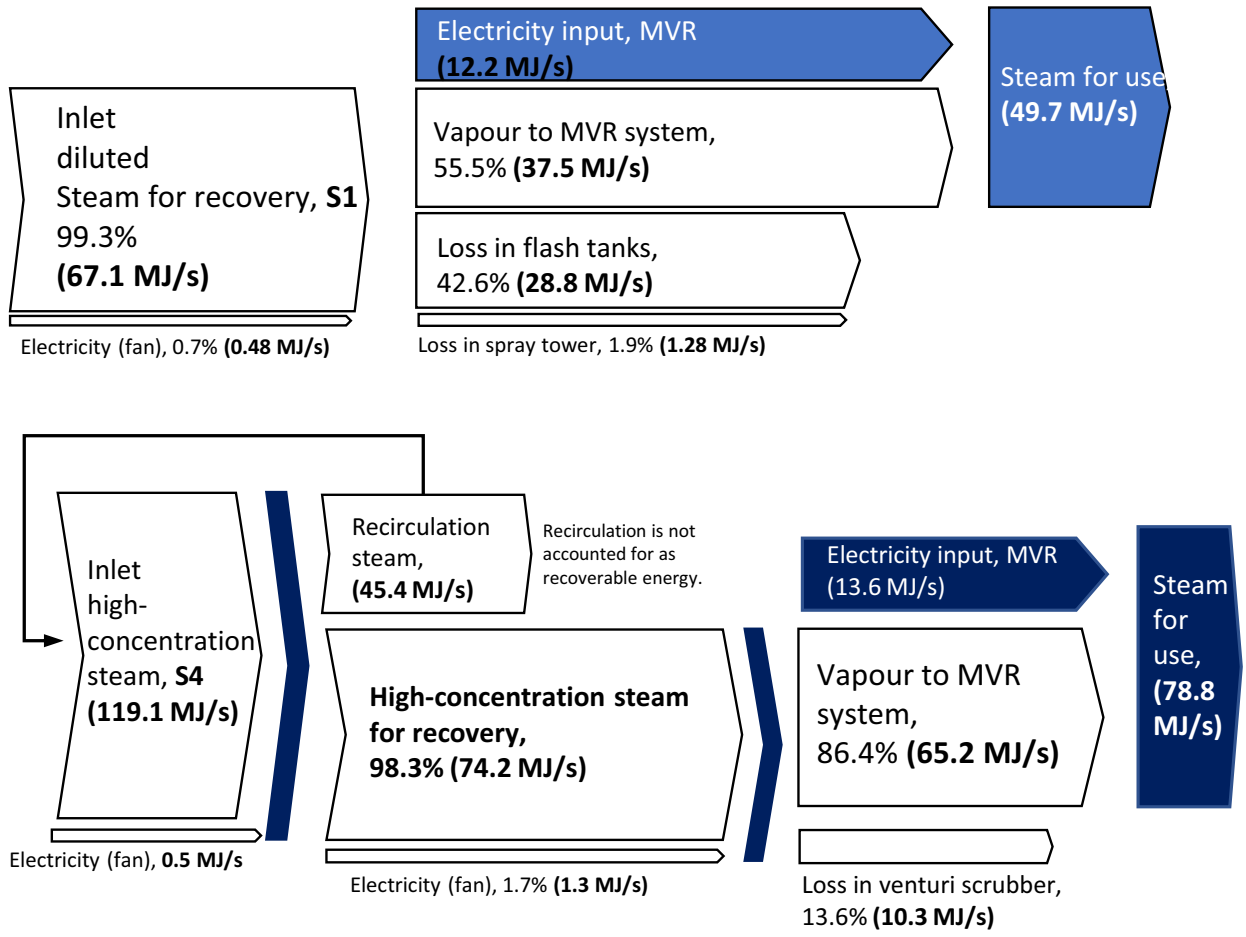


Fig. 8. Energy flows in recovering diluted steam from natural gas/air combustion (Scenario 1) and high-purity steam from H_2 in oxy-steam combustion (Scenario 4) based on 120 t/h alumina calciner capacity.

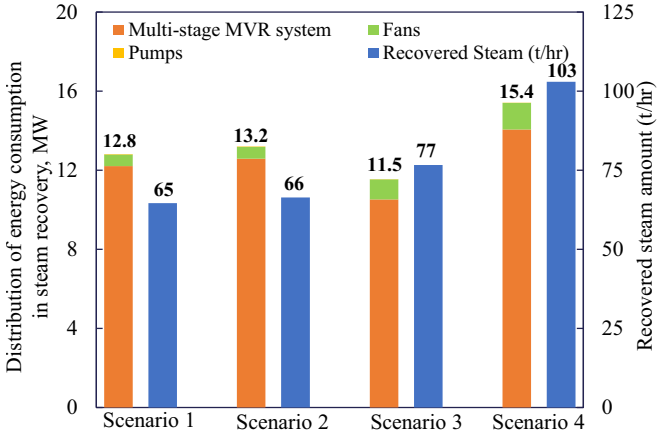


Fig. 9. The distribution of energy consumption and quantity of recovered steam for Scenarios 1 to 4.

shown in Fig. 6. Its total electric power demand is 15.4 MJ/s, which is14–17% higher than Scenarios 1 and 2, and 25% higher than Scenario 3, driven mainly by the MVR system (13.6 MJ/s). The fans, blower (1.8 MW) and pumps (0.006 MW) contribute marginally to the energy consumption. For Scenarios 1 and 2, about 95% of the total energy is consumed by the MVR system, with the remaining 5% required for gas separation due to the higher-pressure duty of compressing low-pressure evaporated steam. For Scenarios 3 and 4, the MVR system accounts for ~91% of the total energy use, with fans contributing the remaining 9% due to the steam pressure drop of 0.2 bar in the venturi scrubber. Scenarios 1 and 2 achieve net steam recovery of approximately 65–66 t/h per calciner, limited by the flash vessels as discussed above. Scenario 3 delivers a lower net steam recovery of 77 t/h than Scenario 1, as does not generate any combustion products.

Fig. 10 presents the energy consumption required for steam production or recovery for the four scenarios. In general, recovering high-

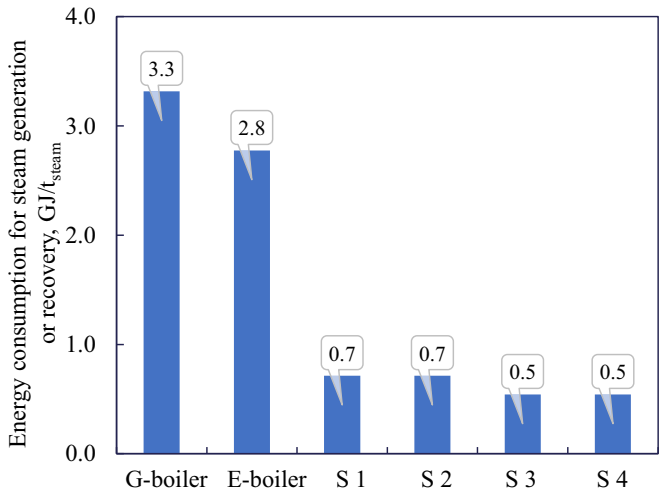


Fig. 10. The energy consumption required for the steam generation or recovery processes in Scenarios 1 to 4. (S1-S4: Scenarios 1 to 4).

concentration steam from H_2 in oxy-steam combustion and fully electrified calcination exhibits significantly higher efficiency, requiring a much lower energy input of 0.54 GJ/t_{steam}. In contrast, recovering diluted steam consumes 31% higher energy, requiring energy input of 0.71 GJ/t_{steam}. This is because condensation and re-evaporation steps in flash tanks and flashing water to low-pressure steam increases overall steam compression ratio, as discussed above. In addition, compared to steam generation from boilers, steam recovery configurations show substantial less energy consumption, conserving 79–84% energy per ton of steam relative to natural gas boilers and 75–81% relative to electric boilers. With the integration of steam recovery process from calciner, the need for boiler-generated steam can be reduced and its impact on energy consumption in steam supply for the Bayer circuit is presented in Section 3.3.

3.3. Energy consumption in steam supply for the Bayer circuit in Scenarios 1A to 4B

Fig. 11(a) presents the recoverable steam and the additional steam supplied by boilers for Scenarios 1 to 4. Overall, Scenario 4 recovers 0.86 t_{steam}/t_{Al2O3} from the calciner, enabling the replacement of 43% of boiler-generated steam and resulting in a 36% energy reduction compared to solely relying on natural gas boilers. For the reference case, approximately 6.63 GJ/t_{Al2O3} is consumed to generate 2 t_{steam}/t_{Al2O3} at 200 °C and 8 bar, emitting 0.36 t_{CO2}/t_{Al2O3} emissions. Scenarios 1 and 2 achieves 0.54–0.55 t_{steam}/t_{Al2O3} recovery rate, thereby offsetting 27% of the boiler-generated steam. Scenario 3, in comparison, meets 32% of the steam demand through recovery.

Fig. 11(b) presents the energy consumption and associated CO_2 emissions for the steam supply to the Bayer circuit for Scenarios 1A to 4B. Integrating steam recovery with the exiting natural gas boilers is expected to reduce energy use to 4.25 GJ/t_{Al2O3} for Scenario 4A and 5.23 GJ/t_{Al2O3} for Scenarios 1 and 2A, corresponding to reductions of 36% and 21%, respectively. They also achieve a 27% and 43% emissions reduction due to their decreased reliance on natural gas boilers. Further replacing natural gas boilers with electric boiler achieves an additional 15% energy reduction due to the higher efficiency of the boiler. Scenario 4B demonstrates the lowest energy use at 3.64 GJ/t_{Al2O3}, corresponding to a 45% reduction relative to the reference case of natural gas boilers. Furthermore, zero CO_2 emissions can be achieved when renewable electricity sources are used. Within the defined system boundary considering on-site steam-supply operations only, the "B" scenarios achieve zero direct CO_2 emissions when renewable electricity is used.

In addition, the proposed scenarios demonstrate substantial CO_2 avoidance potential. Total CO_2 emissions in on-site steam-supply operations are reduced from 0.37 t_{CO2}/t_{Al2O3} to 0.26–0.27 t_{CO2}/t_{Al2O3}, corresponding to a 27% reduction in emissions associated with steam generation in Scenario 1,2 A. Further reduction is achieved in Scenario 4A, where CO_2 emissions decrease further to 0.21 t_{CO2}/t_{Al2O3}, reflecting a 43% reduction. Replacing natural gas boilers with electric boilers enables zero direct on-site CO_2 emissions from steam supply. While renewable electricity is considered, upstream emissions associated with electricity generation or transport are not included. These results highlight the substantial energy savings and carbon reduction potential of integrating high-efficiency steam recovery systems in alumina refining.

3.4. Economic analysis

3.4.1. Levelised cost of decarbonised steam supply

Fig. 12 presents the distribution of levelised cost for the scenarios of decarbonised steam ($LCOS_B$), accounting for steam production and recovery, but not including the costs of the calcination process itself, which could influence the alumina production economics. It can be seen that by offsetting 43% of the steam from natural gas boilers, Scenarios 4A reduces $LCOS_B$ by 26% to 81.7 US$/$t_{Al2O3}$ compared to the reference case at 110.2 US$/$t_{Al2O3}$, while Scenarios 1,2A and 3A achieve 12% and 19% reductions by offsetting 27% and 32% steam from gas boilers, respectively, for the reference price of natural gas (7.5 US$/GJ), CCS cost (179 US$/t_{CO2}), and renewable electricity price (70 US$/MWh). When operating solely on natural gas boilers, fuel and CCS contribute 46% and 54% of total costs, respectively. As boiler steam demand decrease due to steam recovery, these shares drop to 37% (natural gas) and 45% (CCS) in Scenarios 1 and 2A, and further to 35% and 42% in Scenario 4A. In parallel, the higher steam recovery rate increases the cost share for steam recovery from 18% in Scenarios 1,2A to 23% in Scenario 4A. Within the steam recovery-related costs, capital expenditure accounts for approximately 10–13% of the total cost, while pumps and fans operating cost contribute around 1%.

Transitioning from natural gas to electric boilers reduces energy consumption, but it is less cost-effective at a renewable electricity of 70 US$/MWh. The $LCOS_B$ increases to 128.8 US$/$t_{Al2O3}$ (16% CAPEX, 84% electricity) when generating steam solely from electric boilers. Integrating steam recovery from the calciner enhances cost-effectiveness, with Scenarios 1B and 2B reducing costs by 14% and Scenario 4B by up to 28% compared with solely electric boilers. However, total CAPEX for electric boilers and recovery systems rises to 20–24% of total cost due to the additional steam recovery investment. Overall, the "B" scenarios have 13–17% higher costs than the corresponding "A" Scenarios. For the "B" scenarios, electricity price is the primary cost driver, whereas in "A" Scenarios, costs are more sensitive to the combined effects of natural gas, CCS, and electricity prices, as shown in the sensitivity analysis.

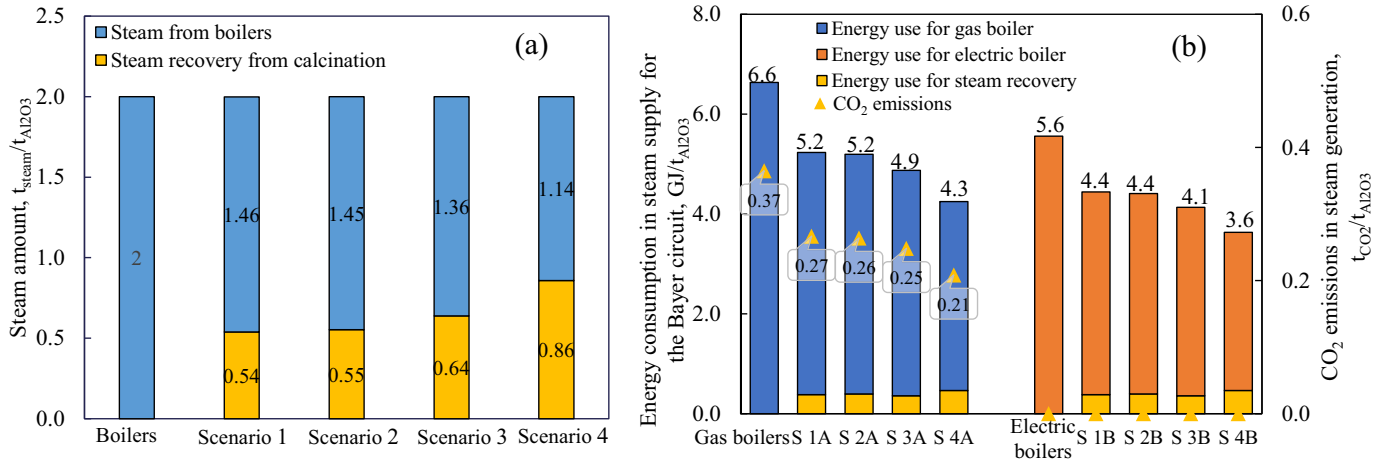


Fig. 11. The steam quantity from recovery and generation (a) and energy consumption (b), CO_2 emission in steam supply for the Bayer circuit for Scenarios 1A to 4B.

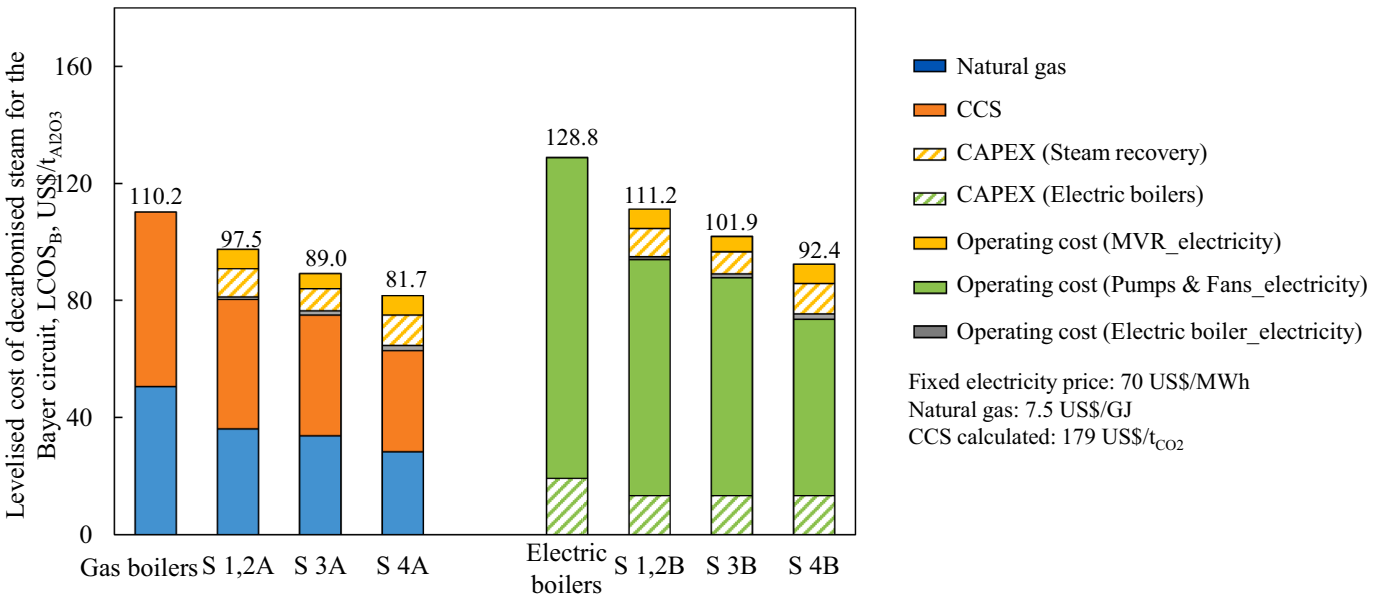


Fig. 12. The distribution of levelised cost of production or recovery of decarbonised steam for Scenarios 1A to 4B, ignoring any differences in the cost of the alternative calcination processes.

3.4.2. *Sensitivity analysis for the LCOS$_B$*

Fig. 13 presents the calculated LCOS$_B$ as a function of the cost of natural gas price for Scenarios 1A to 4A, employing natural gas boilers. The LCOS$_B$ increases linearly with higher natural gas prices for "A" Scenarios, with Scenario 4A remaining the most cost-effective option across the price range. As gas price increasing from 3 to 14 US$/GJ, the LCOS$_B$ rises from approximately 64.0 to 105.7 US$/t$_{Al2O3}$ in Scenario 4A with CCS contributing 34.6 US$/t$_{Al2O3}$. This represents a 19–31% reduction compared with natural gas boilers, with LCOS$_B$ increasing from 79.6 to 152.6 US$/t$_{Al2O3}$ under the same conditions, with CCS contributing 59.7 US$/t$_{Al2O3}$. Scenarios 1, 2A, and 3A fall in between, offering intermediate pathways in the cost competitiveness. Gas price remains the dominant factor, while steam recovery mitigates overall sensitivity to natural gas price fluctuations. In contrast, electric boilers are less cost-effective at 70 US$/MWh electricity price than the other scenarios. It achieves cost parity with natural gas boilers with CCS is achieved when gas price exceeds 10.4 US$/GJ.

Fig. 14(a) and (b) presents the effects of electricity price on the calculated LCOS$_B$ for "A" and "B" Scenarios. For the "A" Scenarios, the impact of electricity price is less significant than that of "B" as expected, although the relationship for each is linear. For reference case of natural gas boilers, as the electricity price increases from 30 to 120 US$/MWh, the cost of CCS rises from 124 to 249 US$/t$_{CO2}$, consequently increasing the LCOS$_B$ by 41.1 US$/t$_{Al2O3}$, from 91.1 to 132.2 US$/t$_{Al2O3}$. For the "A" Scenarios, the same electricity price increase raises the LCOS$_B$ by 35–39 US$/t$_{Al2O3}$. In contrast, for electric boilers, the impact is more pronounced, with the LCOS$_B$ increasing by approximately 137 US $/t$_{Al2O3}$.

For "B" Scenarios, the LCOS$_B$ rises by 91–111 US$/t$_{Al2O3}$ across the same electricity price range, showing a more pronounced effect compared with the "A" Scenarios. Cost parity with natural gas boilers (with CCS) is achieved when electricity prices fall to approximately 102 US$/MWh for Scenario 4B, with a 7.5 US$/GJ natural gas price. In comparison, the break-even electricity prices for Scenario 3B and Scenario 1,2B are less favourable, at 82 US$/MWh and 68 US$/MWh, respectively. For electric boilers, cost parity with natural gas is only achieved when electricity prices fall to around 52 US$/MWh. The results indicate that Scenario 4B is the most cost-effective across the electricity price range due to its combination of high steam recovery rates. The "B" Scenarios gain more benefit from lower electricity prices, while the "A" Scenarios benefit more from low natural gas prices.

Fig. 15 compares the LCOS$_B$ between Scenario 4A and Scenario 4B. It can be seen that the break-even electricity prices vary between approximately 30 and 91 US$/MWh, depending on the natural gas prices from 3 to 14 US$/GJ. In particular, at a natural gas price of 7.5 US $/GJ, the "B" Scenario becomes cheaper than the "A" Scenario when electricity prices fall below 52 US$/MWh. At a lower natural gas price of 3 US$/GJ, renewable electricity prices need to drop below approximately 30 US$/MWh for the "B" scenario to remain cost-competitive. The comparison provides an economic perspective between transitioning decarbonised steam supply for the Bayer circuit to a fully renewable electricity-powered process versus retaining natural gas boilers including CCS with steam recovery. In the short term, low natural gas price remains attractive, although the application of CCS introduces challenges associated to CO_2 transport and storage. In the long term, with projected declines in renewable electricity costs and the development of supporting energy infrastructure, a fully electrified steam supply presents a sustainable option.

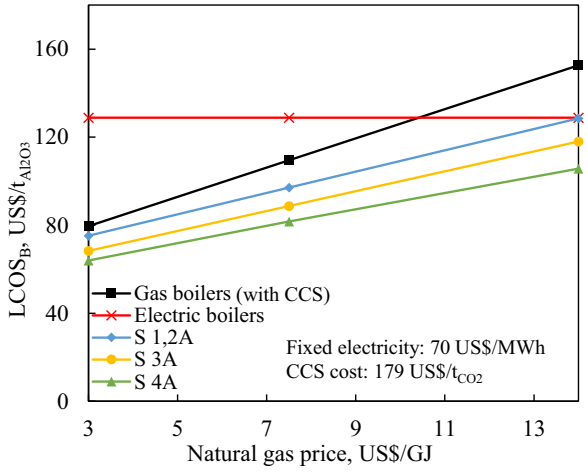


Fig. 13. The calculated levelised cost of decarbonised steam (LCOS$_B$) as a function of natural gas price for Scenarios 1A to 4A, in comparison with the reference case for gas and electric boilers.

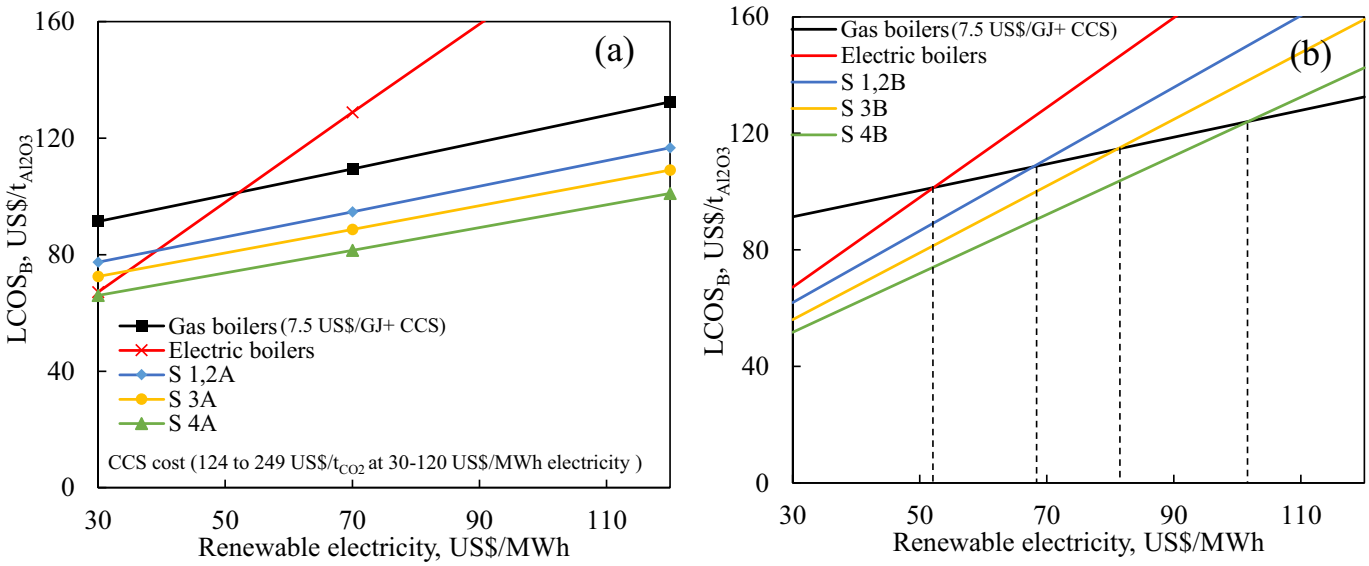


Fig. 14. The calculated levelised cost of decarbonised steam ($LCOS_B$) as a function of renewable electricity for "A" Scenarios and "B" Scenarios, in comparison with the reference case for gas and electric boilers.

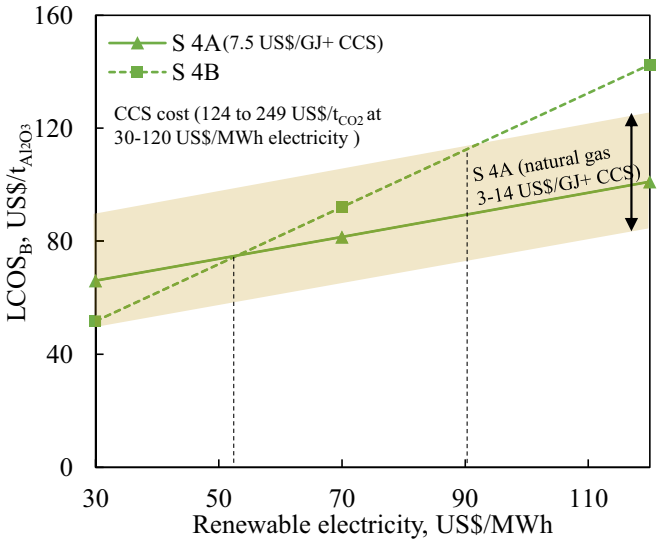


Fig. 15. Comparison of the levelised cost of decarbonised steam ($LCOS_B$) between Scenario 4A and 4B.

3.5. Discussion

The results demonstrate that the steam concentration of the calciner off-gas is a critical determinant of recovery efficiency, compression duty, and overall system performance. Recovery of diluted steam in Scenarios 1 and 2 requires substantially higher compression duty than recovery of high-concentration steam in Scenarios 3 and 4. In addition, separation of non-condensable gases introduces significantly higher energy losses, amounting to approximately 46% in Scenarios 1 and 2 compared with 14% in Scenarios 3 and 4. As a result, the quantity of recoverable steam is lower for diluted off-gas, offsetting approximately 27% of steam demand, whereas high-concentration steam recovery offsets up to 43%. Although effective particulate control remains essential, it requires a venturi scrubber pressure drop of 20 kPa.

From an energy and emissions perspective, integrating steam recovery from either air-based or steam-based with existing natural gas boilers reduces steam-generation energy use by 21–36%, providing a meaningful pathway to improve refinery efficiency and reduce CO_2 emissions. Economically, although steam recovery from steam-based calcination offers greater cost benefits in steam supply, upstream costs and emissions associated with hydrogen and electricity supply fall outside the defined system boundary and have not been considered in this study. Inclusion of these factors in future whole-of-plant techno-economic analyses will be important to fully evaluate deployment potential.

4. Conclusions

This study investigated the potential to improve the energy efficiency and economic viability of decarbonising alumina refining by integrating steam recovery from both air-based calcination (natural gas/air and hydrogen/air) and steam-rich calcination pathways (fully electrified and hydrogen oxy-steam combustion). For diluted steam, an integrated gas-separation and 7-stage mechanical vapour recompression (MVR) configuration was applied. In contrast, high-concentration steam recovery employs a venturi scrubber for particulate control combined with a four-stage MVR system. The integrated particle-cleaning system was calculated to achieve outlet solid concentrations below 2.9 mg/Nm^3 at high pressure drop of 20 kPa prior to MVR.

The results indicate that steam recovery from calcination corresponds to approximately 27% of the Bayer circuit steam demand from air-based calcination and 32%–43% for steam-based calcination, with energy consuming 0.71 GJ/t_{steam} and 0.54 GJ/t_{steam}, respectively. This integration is estimated to reduce the energy use for steam production by 21–36% when retaining existing natural gas boilers ("A" Scenarios) for supplementary steam supply. Replacing natural gas boilers with electric boilers ("B" Scenarios) enables a further 15% reduction and achieves zero direct on-site CO_2 emissions from steam supply. Economically, the levelised cost of decarbonised steam is estimated to decrease by 10–24% relative to a reference case using natural gas boilers with carbon capture and storage (7.5 US$/GJ with 179 US$/t$_{CO2}$ CCS), ignoring any differences in the cost of the alternative calcination processes.

CRediT authorship contribution statement

Siyun Ning: Writing – review & editing, Writing – original draft, Methodology, Investigation, Formal analysis, Data curation, Conceptualization. **Graham Nathan:** Writing – review & editing, Supervision. **Peter Ashman:** Writing – review & editing, Supervision. **Woei Lean**

Saw: Writing – review & editing, Supervision, Project administration, Funding acquisition.

Declaration of competing interest

The authors declare that they have no known competing financial interests or personal relationships that could have appeared to influence the work reported in this paper.

Acknowledgements

The work is supported by the Heavy Industry Low-carbon Transition Cooperative Research Centre (HILT CRC) which receives funding from its industry, research, and government collaborators, as well as from the Australian Government's Cooperative Research Centres Program. Siyun Ning acknowledges the financial support provided through an Australian Government Research Training Program (RTP) Scholarship at the University of Adelaide, along with a supplementary scholarship from HILT CRC. The authors also express their appreciation to Worley in Australia for offering valuable industry insights and feedback on the economic assessment and capital cost estimation.

Appendix A. Supplementary data

Supplementary data to this article can be found online at https://doi.org/10.1016/j.cej.2026.173154.

Data availability

Data will be made available on request.

References

[1] Q. Du, Q. Li, C. Lu, M. Ma, L. Bai, The impact of combining differentiated carbon tax and emissions trading system on the construction sector: based on the industry linkage perspective, Energ. Buildings 347 (2025) 116230, https://doi.org/10.1016/j.enbuild.2025.116230.
[2] S. Lin, Y. Wang, L. Li, Y. Lei, S. Wu, Y. Wang, F. Yang, Z. Wang, Y. Cui, The cost and benefit of synergistic emission reduction of CO2 and non-CO2 greenhouse gases in the industrial sector in the context of carbon neutrality, J. Clean. Prod. 525 (2025) 146551, https://doi.org/10.1016/j.jclepro.2025.146551.
[3] A. Sharma, S. Sayed, S. Seethamraju, S. Bandyopadhyay, Decarbonization measures for the Indian aluminum sector, Process Integr. Optim. Sustainability 9 (5) (2025) 1891–1906, https://doi.org/10.1007/s41660-025-00537-4.
[4] S. Zhu, C. Gao, K. Song, M. Chen, F. Wu, X. Li, An assessment of environmental impacts and economic benefits of multiple aluminum production methods, J. Clean. Prod. 370 (2022) 133523, https://doi.org/10.1016/j.jclepro.2022.133523.
[5] A. Croucher, A. Dean, N. Hutley, T. Flannery, W. Morgan, S. Bradshaw, J. Rayner, Australia's Clean Industry Future: Making Things here in a Net Zero World, 2023.
[6] Australian's Emissions Projections. https://www.dceeew.gov.au/sites/default/files/documents/australias-emissions-projections-2022.pdf, 2022 (accessed on 6 June 2023).
[7] M. Gautam, B. Pandey, M. Agrawal, Chapter 8-carbon footprint of aluminum production: emissions and mitigation, Environmental Carbon Footprints Industrial Case Studies. (2018) 226–228.
[8] Australian Aluminium Council LTD, Sustainability. https://aluminium.org.au/sustainability-main/sustainability/, 2024 accessed on 1 August 2025.
[9] 2022–23 published data highlights, https://cer.gov.au/markets/reports-and-data/nger-reporting-data-and-registers/2022-23-published-data-highlights, 2023. accessed on 12 June 2024.
[10] L. Zhu, National carbon emissions from the industry process: production of glass, soda ash, ammonia, calcium carbide and alumina, Appl. Energy 166 (2016) 239–244, https://doi.org/10.1016/j.apenergy.2015.11.005.
[11] A. Furlong, B. Hogan, D. Hilla, *Enabling Improved Waste Heat Recovery in Digestion for Energy and Carbon Footprint Reduction*, in *the 42nd International ICSOBA Conference*, Lyon, France, 2024.
[12] R. Den Hond, I. Hiralal, A. Rijkeboer, Alumina yield in the Bayer process past, present and prospects, in: D. Donaldson, B.E. Raahauge (Eds.), Essential Readings in Light Metals: Volume 1 Alumina and Bauxite, Springer International Publishing, Cham, 2016, pp. 528–533.
[13] J. Metson, in: R. Lumley (Ed.), *2 - Production of Alumina*, in Fundamentals of Aluminium Metallurgy, Woodhead Publishing, 2011, pp. 23–48.
[14] ARENA, A Roadmap for Decarbonising Australian Alumina Refining. https://arena.gov.au/knowledge-bank/a-roadmap-for-decarbonising-australian-alumina-refining/, 2022 (accessed on 15 June 2025).
[15] H.-G. Schwarz, S. Briem, P. Zapp, Future carbon dioxide emissions in the global material flow of primary aluminium, Energy 26 (8) (2001) 775–795, https://doi.org/10.1016/S0360-5442(01)00032-9.
[16] M. Gautam, B. Pandey, M. Agrawal, Carbon footprint of aluminum production: emissions and mitigation, in: Environmental Carbon Footprints, Elsevier, 2018, pp. 197–228.
[17] G. Mills, Method for the Calcination of Aluminium Trihydroxide, 24 October 2007. WO Patent 2008/052249A1, https://patentimages.storage.googleapis.com/30/b9/1d/3e51ae39f87fbb/WO2008052249A1.pdf.
[18] L. Yingying, L. Laishi, L. Xinqin, B. Ruisheng, Recovering waste-heat and water from alumina Calciner gas, in: M. Hyland (Ed.), Light Metals 2015, Springer International Publishing, Cham, 2016, pp. 69–71.
[19] S. Yu E. G, A. Borges, J. Grünig, P. Routray, Heat and water recovery from alumina calciners stack offgas- a technology review, in: Proceedings of the 12th International AQW Conference and Exihibition, 2024. https://aqw.com.au/component/zoo/?task=callelement&format=raw&item_id=597&element=7a9fb9aa-c8cf-4e64-8a22-71d6f4c3ca3b&method=download.
[20] R. Chatfield, Mechanical Vapor Recompression (MVR) for Low Carbon Alumina Refining, MVR Technical and Commercial Feasibility Studies. https://arena.gov.au/projects/mechanical-vapour-recompression-for-low-carbon-alumina-refining/, 2022 accessed on 14 June 2024.
[21] W.L. Saw, G.J. Nathan, R.V. Chatfield, R.J. Haywood, Method and Apparatus for Alumina Calcination 2022, 17 June 2022. WO2022261726A1, https://patentimages.storage.googleapis.com/b3/bd/c3/d31d8a0f599297/WO2022261726A1.pdf.
[22] D.J. Bayless, M.K. Alam, R. Radcliff, J. Caine, Membrane-based wet electrostatic precipitation, Fuel Process. Technol. 85 (6–7) (2004) 781–798, https://doi.org/10.1016/j.fuproc.2003.11.025.
[23] M.C. Jena, S. Mishra, k, and Moharana H S., Effect of particle size on collection efficiency of ESP and RABH: a case study, Aerosol Sci. Eng. 3 (2019) 75–87, https://doi.org/10.1007/s41810-019-00045-2.
[24] J. Fenger, B.E. Raahauge, C.B. Wind, Experience with 3 x 4500 TPD gas suspension Calciners (GSC) for alumina, in: D. Donaldson, B.E. Raahauge (Eds.), Essential Readings in Light Metals: Volume 1 Alumina and Bauxite, Springer International Publishing, Cham, 2016, pp. 664–668.
[25] A. Jaworek, A. Krupa, T. Czech, Modern electrostatic devices and methods for exhaust gas cleaning: a brief review, J. Electrostat. 65 (3) (2007) 133–155, https://doi.org/10.1016/j.elstat.2006.07.012.
[26] A. Mizuno, Electrostatic precipitation, IEEE Trans. Dielectr. Electr. Insul. 7 (5) (2000) 615–624, https://doi.org/10.1109/94.879357.
[27] S.W. Sucech, C. Misra, *Alcoa Pressure Calcination Process for Alumina*, in Essential Readings in Light Metals: Alumina and Bauxite, Inc, In. John Wiley & Sons, 2013, pp. 669–676.
[28] Metso, Emissions in alumina calcination. https://www.metso.com/insights/blog/mining-and-metals/emissions-in-alumina-calcination/, 2019 (accessed on 30 July 2024).
[29] Howden Turbo Technology. https://www.chartindustries.com/Products/Compression-Centrifugal-Compressors, 2017 (accessed on 1 June 2024).
[30] S.K. Das, M.N. Biswas, Studies on ejector-venturi fume scrubber, Chem. Eng. J. 119 (2–3) (2006) 153–160.
[31] B.R. Mohan, R. Jain, B. Meikap, Comprehensive analysis for prediction of dust removal efficiency using twin-fluid atomization in a spray scrubber, Sep. Purif. Technol. 63 (2) (2008) 269–277, https://doi.org/10.1016/j.seppur.2008.05.006.
[32] B.G. Miller, Clean Coal Engineering Technology, Elsevier, 2010.
[33] M. Ali, Y.C. Qi, K. Mehboob, A review of performance of a venturi scrubber, Res. J. Appl. Sci. Eng. Technol. 4 (19) (2012) 3811–3818.
[34] L.K. Wang, N.C. Pereira, Y.-T. Hung, Air Pollution Control Engineering 1st Edition ed., vol. 1, Humana press, 2004.
[35] W.T. Davis, A.J. Buonicore, Air Pollution Engineering Manual, 2nd Edition ed, Wiley, New York, 2000.
[36] The U.S. Environmental Protection Agency, Wet and Dry Scrubbers for Acid Gas Control. https://www.epa.gov/sites/default/files/2021-05/documents/wet and dry scrubbers section 5 chapter 1 control cost manual 7th edition.pdf, 2021 accessed on 12 October 2024.
[37] H. Huang, C. Zheng, H. Zhao, Numerical investigation on non-steady-state filtration of elliptical fibers for submicron particles in the "greenfield gap"range, J. Aerosol Sci. 114 (2017) 263–275, https://doi.org/10.1016/j.jaerosci.2017.09.018.
[38] M. Ali, C. Yan, Z. Sun, H. Gu, K. Mehboob, Dust particle removal efficiency of a venturi scrubber, Ann. Nucl. Energy 54 (2013) 178–183, https://doi.org/10.1016/j.anucene.2012.11.005.
[39] R. Cao, H. Wang, R. Gong, Z. Jiang, H. Zhang, J. Zhu, Y. Song, Pressure drop model of gas-liquid phase for Venturi scrubber in fog-annular flow, Chem. Eng. Res. Des. 205 (2024) 748–762, https://doi.org/10.1016/j.cherd.2024.04.036.
[40] S. Viswanathan, Modeling of Venturi scrubber performance, Ind. Eng. Chem. Res. 36 (10) (1997) 4308–4317, https://doi.org/10.1021/ie970235s.
[41] A.A. Scarsella, S. Noack, E. Gasafi, C. Klett, A. Koschnick, Energy in alumina refining: setting new limits, Light Met. 2015 (2015) 131–136, https://doi.org/10.1007/978-3-319-48248-4_24.
[42] Industrial Decarbonization Roadmap. https://www.energy.gov/sites/default/files/2022-09/Industrial%20Decarbonization%20Roadmap.pdf, 2022 (accessed on 6 June 2025).

[43] A.D. Pee, D. Pinner, O. Roelofsen, K. Somers, Decarbonization of Industrial Sectors: The Next Frontier. https://www.mckinsey.com/~/media/mckinsey/business%20functions/sustainability/our%20insights/how%20industry%20can%20move%20toward%20a%20low%20carbon%20future/decarbonization-of-industrial-sectors-the-next-frontier.pdf, 2018 (accessed on 6 June 2025).
[44] M. Farghali, A.I. Osman, I.M. Mohamed, Z. Chen, L. Chen, I. Ihara, P.-S. Yap, D. W. Rooney, Strategies to save energy in the context of the energy crisis: a review, Environ. Chem. Lett. 21 (4) (2023) 2003–2039, https://doi.org/10.1007/s10311-023-01591-5.
[45] L. Perander, A. Scarsella, E. Gasafi, H.W. Schmidt, CFB alumina Calciners—New and future generation opportunities for green field refineries, in: Light Metals 2017. In, Springer, 2017, pp. 3–8.
[46] N. Siyun, N. Graham, A. Peter, L.S. Woei, *Technical Assessment of Steam Recovery from Alumina Calcination for Sustainable Bauxite Digestion* in *43rd International Conference and Exhibition ICSOBA 2025*, Nanning, China, 2025.
[47] B.E. Raahauge, F.S. Williams, Smelter Grade Alumina from Bauxite: History, Best Practices, and Future Challenges, Springer, 2022.
[48] M. Kamiński, J.M. Gac, P. Sobiech, P. Kozikowski, T. Jankowski, Pressure drop dynamics during filtration of mixture aerosol containing water, oil, and soot particles on nonwoven filters, Polymers 15 (7) (2023) 1787, https://doi.org/10.3390/polym15071787.
[49] K.-M. Yao, M.T. Habibian, C.R. O'Melia, Water and waste water filtration. Concepts and applications, Environ. Sci. Technol. 5 (11) (1971) 1105–1112, https://doi.org/10.1021/es60058a005.
[50] The United State Environmental Protection Agency, Air Pollution Control Technology Fact Sheet. https://www.epa.gov/air-emissions-monitoring-knowledge-base/air-pollution-control-technology-fact-sheet-permanent-total, 2003 accessed on 9 July 2025.
[51] G.B. Hill, E. Pring, P.D. Osborn, Cooling Towers: Principles and Practice, Butterworth-Heinemann, 2013.
[52] J.C. Hensley, Cooling Tower Fundamentals, Marley Cooling Tower Company, Kansas City, 1985.
[53] R.K. Arya, G.D. Verros, J.P. Davim, Compressors and Blowers: Maintenance, Practical Guidance, Energy-Efficient Technologies, Walter de Gruyter GmbH & Co KG, 2025.
[54] S.P. Fisenko, A.I. Petruchik, A.D. Solodukhin, Evaporative cooling of water in a natural draft cooling tower, Int. J. Heat Mass Transf. 45 (23) (2002) 4683–4694, https://doi.org/10.1016/S0017-9310(02)00158-8.
[55] A.H.N. Khalifa, *Thermal and exergy analysis of counter flow induced draught cooling tower.* International journal of current, Eng. Technol. (2015) 2868.
[56] B.D. Baloni, S.A. Channiwala, S.N.R. Harsha, Design, development and analysis of centrifugal blower, J. Inst. Eng. India Ser. C 99 (2018) 277–284, https://doi.org/10.1007/s40032-017-0356-z.
[57] C. Hariharan, M. Govardhan, Improving performance of an industrial centrifugal blower with parallel wall volutes, Appl. Therm. Eng. 109 (2016) 53–64, https://doi.org/10.1016/j.applthermaleng.2016.08.045.
[58] The United States Environmental Protection Agency, Section 6: Particulate Matter Controls. https://www.epa.gov/sites/default/files/2020-11/documents/cs6ch2.pdf, 2002 accessed on 1 August 2024.
[59] EPA, Air Pollution Control Cost Manual. https://www.epa.gov/sites/default/files/2020-07/documents/c_allchs.pdf, 2002 (accessed on 1 July 2024).
[60] M.F.U. Hasnain, H.O. Ali, S. Aziz, P.M. Kouotou, M. Waqas, S.M.A. Naqvi, M. H. Athar, M. Ammar, I. Shah, D.-W. Jung, Optimization and techno-economic analysis of catalytic gasification of wheat straw biomass using ASPEN PLUS model, Arab. J. Chem. 17 (7) (2024) 105821, https://doi.org/10.1016/j.arabjc.2024.105821.
[61] PILLER, PILLER Blowers & Compressors. https://www.piller. de/products-services/mvr-blower-piller-blowers-compressors/vapoflex/, 2024 (accessed on 12 November 2024).
[62] Atlas Copco, Mechanical Vapor Recompression Key to Steam Energy Upgrade within a Polyolefin Plant, in: https://www.atlascopco.com/gas-and process/en/pressure-points-blog/mechanical-vapor-recompression-key-to-steam energy-upgrade-within-a-polyolefin-plant, 2021 accessed on 12 November 2024.
[63] S. Klute, M. Budt, M. van Beek, C. Doetsch, Steam generating heat pumps–overview, classification, economics, and basic modeling principles, Energ. Conver. Manage. 299 (2024) 117882, https://doi.org/10.1016/j.enconman.2023.117882.
[64] AspenTech, Unit Operations and Reaction Models. https://esupport.aspentech.com/FileAttachment?id=a0g0B00000GfNpB, 2013 (accessed on 11 June 2025).
[65] The U.S. Department of Energy, Energy efficiency and industrial boiler efficiency: an industry perspective. https://www.nrel.gov/docs/fy04osti/35106.pdf, 2002 (accessed on 4 July 2025).
[66] Chetan T. Patel, Bhavesh K. Patel, Vijay K. Patel, Efficiency with different GCV of coal and efficiency improvement opportunity in boiler, Int. J. Innov. Res. Sci. Eng. Technol. 2 (5) (2013) 1518–1527.
[67] C. Schoeneberger, J. Zhang, C. McMillan, J.B. Dunn, E. Masanet, Electrification potential of US industrial boilers and assessment of the GHG emissions impact, Adv. Appl. Energy 5 (2022) 100089, https://doi.org/10.1016/j.adapen.2022.100089.
[68] M.J.S. Zuberi, A. Hasanbeigi, W. Morrow, Electrification of industrial boilers in the USA: potentials, challenges, and policy implications, Energ. Effic. 15 (8) (2022) 70, https://doi.org/10.1007/s12053-022-10079-0.
[69] F.P. Bleier, Fan Handbook: Selection, Application, and Design, McGraw-Hill, 2018.
[70] D. Kaya, F. Çanka Kılıç, H.H. Öztürk, Energy efficiency in pumps, in: Energy Management and Energy Efficiency in Industry: Practical Examples. In, Springer, 2021, pp. 329–374.
[71] P.R. Neal, W. Hou, W.G. Allinson, Y. Cinar, *Costs of CO_2 Transport and Injection in Australia*, in *SPE Asia Pacific Oil and Gas Conference and Exhibition*, Brisbane, Australia, 2010.
[72] M.A. Hayat, S. Hasan, A.M. Elshurafa, Strategic priorities and cost considerations for decarbonizing electricity generation using CCS and nuclear energy, Energy Rep. 12 (2024) 2108–2122, https://doi.org/10.1016/j.egyr.2024.08.017.
[73] A. Dindi, K. Coddington, J.F. Garofalo, W. Wu, H. Zhai, Policy-driven potential for deploying carbon capture and sequestration in a fossil-rich power sector, Environ. Sci. Technol. 56 (14) (2022) 9872–9881, https://doi.org/10.1021/acs.est.1c08837.
[74] A. Blakers, B. Lu, M. Stocks, 100% renewable electricity in Australia, Energy 133 (2017) 471–482.
[75] World in Data, Levelized Cost of Energy for Renewables. https://ourworldindata.org/grapher/levelized-cost-of-energy?tab=table&time=2023..latest, 2023 (accessed on 6 June 2025).
[76] Gas market prices, Australia Energy Regulator. https://www.aer.gov.au/industry/registers/charts/gas-market-prices, 2024 (accessed on 1 March 2025).
[77] Natural Gas Price-World Data. https://ourworldindata.org/grapher/natural-gas-prices?tab=table&time=2020..latest, 2024 (accessed on 6 March 2025).
[78] L.K. Wang, N.C. Pereira, Y.-T. Hung, K.H. Li, Air Pollution Control Engineering vol. 1, Springer, 2004.
[79] Piller, "Discussion on the MVR Performance," Personal Email Consultation. https://www.piller.com/, 2024 (accessed on 1 June 2024).

Chapter 5

Techno-economic Assessment of Multi-stage Mechanical Vapour Recompression (MVR), Thermal Vapour Recompression (TVR) and Integrated TVR-MVR Systems for Net-zero Steam Generation in Alumina Refineries

Preface

Chapter 4 focuses on addressing key barriers such as fine particle removal and flue gas dilution to recover steam from calciner. Mechanical vapor recompression (MVR) is used to raise steam pressure and temperature after steam clean-up. MVR system is highly sensitive to fine particles, thereby effective particle removal is essential.

Steam compression is a critical step to raise steam pressure and temperature. This chapter compares various steam compression technologies from both technical and economic perspectives. It evaluates the performance of mechanical vapor recompression (MVR) and thermal vapor recompression (TVR) and integrated TVR-MVR systems as low-emission alternatives to conventional steam generation.

Highlights of this chapter include:

- MVR systems provide the highest efficiency, achieving 73-85% energy savings with a COP of 3.2-5.7, relative to natural gas boilers.
- Integrated TVR-MVR configurations reduce system complexity and operational risks while maintaining competitive performance, achieving ~54% energy savings, delivering a COP of 1.9.
- Multi-stage TVR systems are less viable, offering only 20-43% energy savings with a COP of 1.0-1.4.

Statement of Authorship

Title of Paper	Techno-economic Assessment of Multi-stage Mechanical Vapour Recompression (MVR), Thermal Vapour Recompression (TVR) and Integrated TVR-MVR Systems for Net-zero Steam Generation in Alumina Refineries
Publication Status	☐ Published ☐ Accepted for Publication ☐ Submitted for Publication ☑ Unpublished and Unsubmitted w ork w ritten in manuscript style
Publication Details	Ning S, Saw W L., Ashman P, and Nathan G. Techno-economic Assessment of Multi-stage Mechanical Vapour Recompression (MVR),Thermal Vapour Recompression (TVR) and Integrated TVR-MVR Systems for Net-zero Steam Generation in Alumina Refineries. Writen in manuscript style, 2025

Principal Author

Name of Principal Author (Candidate)	Siyun Ning		
Contribution to the Paper	Concept deisgn, Process model development and simulation, Data analysis and interpretation, Drafted the manuscript and acted as corresponding author.		
Overall percentage (%)	70%		
Certification:	This paper reports on original research I conducted during the period of my Higher Degree by Research candidature and is not subject to any obligations or contractual agreements with a third party that would constrain its inclusion in this thesis. I am the primary author of this paper.		
Signature		Date	

Co-Author Contributions

By signing the Statement of Authorship, each author certifies that:

i. the candidate's stated contribution to the publication is accurate (as detailed above);

ii. permission is granted for the candidate in include the publication in the thesis; and

iii. the sum of all co-author contributions is equal to 100% less the candidate's stated contribution.

Name of Co-Author	Woei Lean Saw		
Contribution to the Paper	Supervision of the work, Concept development, Evaluation and review of the manuscript.		
Signature		Date	

Name of Co-Author			
Contribution to the Paper	Supervision of the work, Concept development, Evaluation and review of the manuscript.		
Signature		Date	2/12/2025

Please cut and paste additional co-author panels here as required.

Name of Co-Author	Graham Nathan		
Contribution to the Paper	Supervision of the work, Concept development, the manuscript.		
Signature		Date	

Techno-economic Assessment of Multi-stage Mechanical Vapour Recompression (MVR), Thermal Vapour Recompression (TVR) and Integrated TVR-MVR Systems for Net-zero Steam Generation in Alumina Refineries

Siyun Ning[1,2,3] , Woei Lean Saw[1,2,3], Peter Ashman[1,2,3], Graham Nathan [2,3,4]

[1] *School of Chemical Engineering, Adelaide University, Australia*

[2] *Centre for Energy Technology, Adelaide University, Australia*

[3] *Heavy Industry Low-carbon Transition Cooperative Research Centre, Australia*

[4] *School of Electrical and Mechanical Engineering, Adelaide University, Australia*

Corresponding author: siyun.ning@adelaide.edu.au

Abstract

The study reports a techno-economic assessment of various integrated steam recovery configurations in alumina refining process, including multi-stage MVR (mechanical vapour recompression), multi-stage TVR (thermal vapour recompression), and integrated TVR-MVR system, aimed at achieving a decarbonised or net-zero steam production relative to fossil fuel boilers. Steam recovery from waste vapour at 1.1 bar/102°C and 0.14 bar/52.5°C to 8 bar/ 200°C were simulated in Aspen Plus/MATLAB and validated with mathematical models. Results show that the multi-stage MVR system achieves the highest efficiency, delivering a COP (coefficient of performance) of 5.7 for an inlet pressure of 1.1 bar, corresponding to an 85% energy savings relative to natural gas boilers which consumes 3.3 GJ/t_{steam} with an efficiency of 82%. The integrated TVR-MVR has a lower COP of 1.9 for an inlet pressure of 0.14 bar, corresponding to roughly 54% energy reduction relative to natural gas boilers. In contrast, multi-stage TVR systems show lower technical viability, with COP of 1.4 at 1.1 bar inlet pressure and COP of 1.0 at 0.14 bar inlet pressure. Economically, steam recovery via MVR remains competitive with natural gas boilers with CCS cost over an electricity price range of 30-120 US$/MWh, even when the natural gas prices are as low as 3 US$/GJ. By comparison, the integrated TVR-MVR system requires a break-even electricity price below 34 US$/MWh, while the TVR system requires prices below 30 US$/MWh under the same conditions.

Key words: net-zero steam, steam recovery, multi-stage MVR, multi-stage TVR, alumina refining decarbonisation

1. Introduction

Steam generation for process heat in alumina refining process, currently produced from fossil-fuel boilers or co-generation systems, typically accounts some of 70% of CO_2 emissions from alumina refining [1-4]. The resulted direct CO_2 emissions are approximately 0.56 $t_{CO_2}/t_{Al_2O_3}$ if natural gas boilers are used, 0.64 $t_{CO_2}/t_{Al_2O_3}$ for coal boilers, and 0.44 $t_{CO_2}/t_{Al_2O_3}$ for gas turbine cogeneration systems [5]. In low-temperature digestion Bayer process, high-pressure steam particularly at 6-13 bar and 175°C-230°C is consumed [6]. While it is now becoming technically viable to produce this steam from electric boilers powered with renewable electricity, exploring alternative methods such as open-cycle heat pumps that offer significant higher efficiency in electrifying steam generation by waste heat recovery is also significant. Such an option is plausible as a substantial waste steam is presently vented from the Bayer circuit at some 102 °C from digestion and at approximately 52.5 °C and 0.14 bar from precipitation and evaporation steps [7, 8]. Therefore, the overall objective of the present investigation is to evaluate the viability of recovering these sources of vapour to generate high-pressure steam through steam recovery technologies while eliminating the direct CO_2 emissions from fossil fuel steam generation.

Mechanical vapour recompression (MVR) and thermal vapour recompression (TVR), also known as ejectors, can be used to compress vapour to a higher pressure and temperature [9, 10], and are classified as open-loop systems heat pump systems [7, 11, 12]. Numerous studies have investigated the integration of TVR and MVR systems in industrial applications, with the majority of studies focusing on single-stage integration in the desalination and wastewater treatment processes, e.g., studies from Dahmardeh et al. [13], Zhou et al. [14], [13], Bamardouf et al. [15] and Shahzamanian et al. [16]. Novel conceptual designs integrate a

single-stage MVR or TVR with the multi-effect evaporation system in the alumina refinery's evaporation step [17]. However, the achievable pressure ratio with a single-stage TVR or MVR is limited, typically to less than two [18, 19], having a saturation temperature increase of 5-20°C [20, 21]. It constrains the extent of vapour utilisation as high-pressure steam is needed for the alumina refining. Multi-stage MVR or TVR systems are needed to achieve sufficiently pressure and temperature increase. For multi-stage TVR, Robert et al. [18] described a multi-stage TVR system capable of achieving a higher steam pressure ratio. Nevertheless, the performance and implementation of such a system in alumina refineries have not been comprehensively evaluated. Chatfield et al. [5] assessed the implementation of an up to 11-stages of MVR for recovering waste vapour from the Bayer process. The study demonstrated its potential application at the Australian Wagerup alumina refinery, and identified the integration challenges, such as infrastructure limitations and electricity delivery capacity. However, no detailed understanding of such a multi-stage MVR system, which are complex and multi-component, such as the temperature and pressure rise per stage. Such details are important given the wide range of MVR single-stage compression components and systems from various suppliers. For example, Thermosag India Ltd. [22] offer MVR systems with a saturated steam temperature rise of approximately 8-20 °C in a single stage. Similarly, Piller's VapoFlex technology delivers a temperature rise of around 11 °C per stage, while the VapoMaxX configuration can achieve temperature lifts of around 20 °C per stage [23]. In terms of pressure performance, the Howden SG series is reported to achieve single-stage pressure ratios of up to two [24], although the associated temperature rise has not been reported. To date, no studies have evaluated the pressure and temperature rise in multi-stage MVR systems when applied in steam recovery processes. Also, no comparative assessments have been made against with multi-stage TVR systems. For this reason, the present study aims to evaluate the performance of compression using such systems in alumina plants.

While MVR systems are highly energy-efficient, they are also constrained by low tolerance to particles, requiring rigorous steam cleaning before recompression, and also have a limited volumetric flow capacity of up to 170 m^3/s [25]. Also, multi-stage MVR systems are capital intense and the system requires a large installation footprint. The study by Chatfield [5] indicated that ~46 compressors would be needed to recover 611 t/hr steam. At the same time, although MVR technology is reliable, operating with many stages introduces challenges such as anti-surge control during start-up, significantly reducing overall system reliability [5]. In contrast, TVR systems are particle-tolerant, capable of handling large gas volumes, and relatively inexpensive [18], but their reliance on high demand of motive steam decreases the system efficiency. Given the advantages and limitations of the two methods, integrating TVR and MVR may offer a potential method to increase the viability of steam recovery in alumina plants. Such a hybrid system offers a reduced number of MVR stages and improve the operational stability, although this improvement must be traded off against by a lower overall efficiency. No previous studies have proposed or evaluated such a configuration. Therefore, the study aims to meet this need by developing a model and evaluating the viability of such hybrid options.

The coefficient of performance (COP) is a key indicator used to evaluate system efficiency and is defined as the ratio of thermal energy output to electrical energy input, as shown in Equation (1) [26]. Several key factors influencing the COP of MVR systems are the compression duty, compressor's efficiency, and system design [27, 28].

$$\mathrm{COP} = \frac{\mathrm{Q\ (Thermal\ energy\ output)}}{\mathrm{Q\ (Electric\ energy\ input)}} \qquad (1)\ [26]$$

An integrated single-stage MVR with a distillation system can achieve a COP of 10 or higher [28]. Michael et al. [27] reported a COP of 7.8 for a two-stage MVR operating at a compressor efficiency of 70%. In a pilot project from Dutch government [29], a two-stage MVR system

compressed steam from 4 bar to 13.5 bar, yielding an overall COP of 7.5, underscoring the significant impact of compression stages on overall system performance. Although the performance of single and two-stage MVR systems has been reported, multi-stage configurations remain unexplored, leaving a notable gap in understanding MVR systems. Hence, the present study aims to estimate the COP value of multi-stage MVR. The COP for TVR systems are rarely explored, but depends on the power input required for motive steam generation. Likewise, the COP value of an integrated TVR-MVR system depends on both the energy consumption for the motive steam generation and the work of mechanical compression work. There is a lack of a study reporting such system efficiencies under conditions of relevance to the Bayer circuit. Hence, further objective is to evaluate the potential viability of hybrid TVR-MVR systems in steam recovery under such conditions.

Economic viability study is also essential to justify investment for decarbonising steam supply cases relative to fossil fuel steam generation. A comparative assessment of the relative viability of MVR, TVR, and TVR-MVR configurations should consider differences in capital investment, operating costs, and energy consumption. Such comparisons should also be made relative to fossil fuel steam generation, such as natural gas boilers which benefit from low gas prices, ranging from 3 to 14 US$/GJ across different regions [30]. In contrast, renewable electricity for decarbonised steam supply is more expensive, costing approximately 11-50 US$/GJ, with a levelised cost of electricity (LCOE) ranging from 30 US$/MWh from onshore wind, 40 US$/MWh for solar photovoltaic, 70 US$/MWh for bioenergy and up to 120 US$/MWh for concentrated solar power worldwide [31]. These costs increase further when accounting for renewable electricity delivery and storage [32]. The cost disparity poses an economic barrier to shifting toward electricity-based steam supply unless steam recovery systems provide substantial gains in energy efficiency. Despite this, there is a lack of comprehensive studies comparing the capital and operating costs of these recovery

technologies with those of traditional natural gas boilers. Hence, a further aim of the present study is to fill this gap by comparing the economic viability of these systems, in comparison with the use of traditional natural gas boilers.

In light of the identified gaps, this study aims to develop comprehensive process models to evaluate the performance of multi-stage mechanical vapour recompression (MVR) and thermal vapour recompression (TVR) systems for application in alumina refineries. The study further compares the performance of a novel integrated TVR–MVR configuration with standalone TVR and MVR systems. In addition, the coefficient of performance (COP) of the three proposed steam recovery systems is assessed. Finally, the economic viability of these steam recovery technologies is evaluated by benchmarking the levelised cost of steam against conventional natural gas boilers.

2. Methodologies

2.1 Assumptions for waste water vapour from the Bayer process

Figure 1 presents the available water vapour from the digestion, evaporation and precipitation steps in the Bayer process, with the conditions adapted from prior studies [5, 33]. Two conditions of currently vented vapour were selected, namely 1.1 bar/102°C and 0.14 bar/52.5°C, while the target outlet steam condition of 8 bar/200°C was selected, which is typical steam requirement for low-temperature digestion of gibbsite-rich bauxite [5, 34]. Medium-pressure vapour is released from flash tanks in the digestion step. Low-pressure vapour is generated by flashing warmed cooling water in precipitation and from the progressive heating of the liquor in the evaporation stage [5].

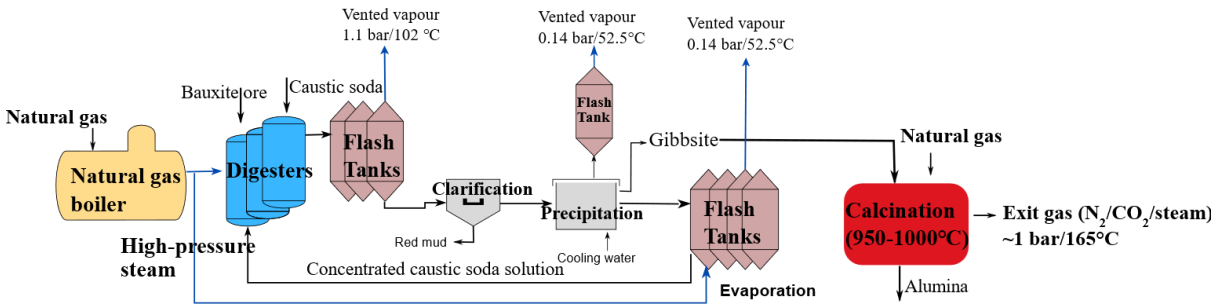


Figure 1. The typical conditions of the vapour that is presently vented from the Bayer process, and offer potential for recovery.

2.2 Steam recovery systems

Figure 2 presents the proposed multi-stage MVR, TVR and integrated TVR-MVR configurations for steam recovery that were assessed here. For steam recovery from calcination using MVR, the removal of entrained alumina particles and diluted gases (N_2 and CO_2) to a purity necessary prior to MVR system for reliable operation was assumed to be achievable by adapting the flash system proposed by Alcoa [5], which has been modelled by our previous work [35]. An 8-stage MVR system is shown as an example, although the exact number of stages depends on the inlet and outlet steam pressures. In the first two stages, compressors are arranged in parallel to handle the large volume of low-pressure waste steam (at 0.14 bar) due to the volumetric capacity limit of individual units (170 m^3/s). Desuperheat water is injected at each stage to reduce the specific volume before the next stage of compression. Two compressor types are considered in this study: low-speed compressors(e.g. Howden's centrifugal Turbo Fan) , with a pressure ratio below 1.45 and a capacity of up to 170 m^3/s [25]; and high-speed compressors capable of pressure ratios up to 2, which are typically used when the volumetric flow rate is less than approximately 120 m^3/s [5]. The system was modelled using Aspen Plus software to evaluate its performance for various inlet and outlet steam conditions.

The multi-stage TVR system operates by entraining low-pressure inlet steam using high-pressure motive steam, which is assumed to be supplied by electric boilers powered by renewable electricity. The number of stages is determined by the overall compression duty and by the performance characteristics of each ejector. Configurations with three or more stages

were evaluated, with a 6-stage TVR flowsheet presented as an example. The quantity and pressure of motive steam were selected to suit the system's compression ratio, based on available information [18, 36]. The process was simulated using MATLAB to estimate motive steam requirements, including both pressure and flow rate.

The integrated TVR-MVR system was developed for compressing low-pressure steam (0.14 bar), employing TVR for the first two-stages of compression. It can be seen that this typically halves the number of MVR units.

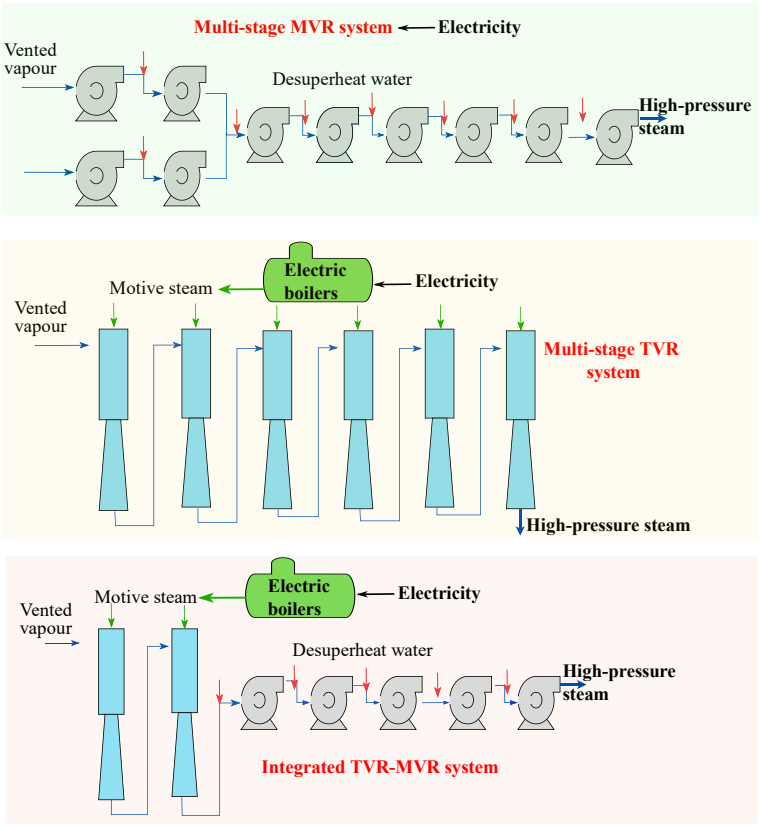


Figure 2. An example of equivalent configurations of multi-stage MVR, TVR and integrated TVR-MVR systems for steam recovery compatible with electrification.

2.3 Process simulation for multi-stage TVR

The mathematical model for the TVR system was developed using MATLAB, as defined in Equations (2)-(10), describing the fluid flow and pressure changes across each ejector stage. Figure 3 shows schematic of Stage 1 and Stage 2 ejector. F_0 is the mass flow of waste vapour entrained into the first stage. Er_1 and Er_i are the entrainment ratio for the first and ith stage, respectively, defined as the ratio of the mass flow of suction vapour to that of motive vapour.

Cr_1 and Cr_i are the compression ratio of the first and i[th] stage, respectively, defined as the ratio of outlet pressure to suction pressure. Pr_1 *and* Pr_i are defined as the ratio of the suction pressure to the motive pressure for the first and i[th] stage. F_{m1} and F_{mi} are the mass flow of motive steam for the first and i[th] stage. P_{m1} and P_{mi} denote the motive steam pressure for the first and i[th] stage. P_1 and P_i represent the outlet vapour pressure after first and i[th] stage. The i[th] value represents the stage number of TVR systems. The values of the ejector's compression ratio Cr, entrainment ratio Er ratio, and pressure Pr were extracted from design curves for optimum single-stage ejector from Perry's chemical engineering handbook [36].

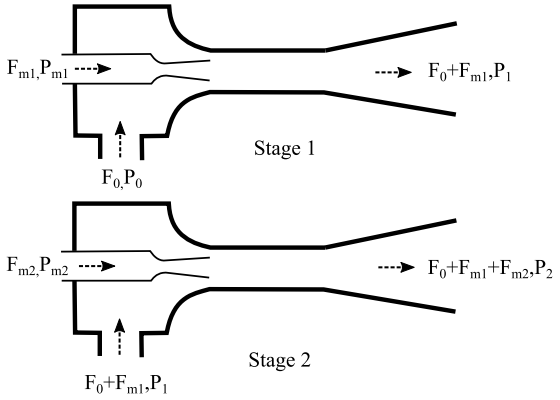


Figure 3. Schematic of the stage 1 and 2 ejectors.

$$F_{m1} = \frac{F_0}{Er_1} \quad \text{Stage 1} \quad (2)$$

$$F_{m2} = \frac{F_0 + F_{m1}}{Er_2} \quad \text{Stage 2} \quad (3)$$

$$F_{mi} = \frac{F_0 + F_{m(i-2)} + F_{m(i-1)}}{Er_i} \quad (i = 3,4,5,6\ldots14) \quad \text{Stage 3 to stage i} \quad (4)$$

$$P_{m1} = \frac{P_0}{Pr_1} \quad \text{Stage 1} \quad (5)$$

$$P_{m2} = \frac{P_1}{Pr_2} \quad \text{Stage 2} \quad (6)$$

$$P_{mi} = \frac{P_{i-1}}{Pr_i} \quad (i = 3,4,5,6\ldots14) \quad \text{Stage 3 to stage i} \quad (7)$$

$$P_1 = P_0 \cdot Cr_1 \quad \text{Stage 1} \quad (8)$$

$$P_2 = P_1 \cdot Cr_2 \quad \text{Stage 2} \quad (9)$$

$$P_i = P_{(i-1)} \cdot Cr_i \quad (i = 3,4,5,6\ldots14) \quad \text{Stage 3 to stage i} \quad (10)$$

$$\mathrm{COP}_T = \frac{(F_0 + \sum_{i=1}^{i} F_{mi}) \cdot \mathrm{h_{out}}}{W_{EB}} \quad (11)$$

The most energy-efficient configuration, characterised by the lowest total motive steam consumption (sum of F_{mi}), was obtained through iterative simulations. The overall system

performance, COP_T was calculated as the ratio of thermal output to the combined electrical power input of electric boilers for motive steam generation, shown in Equation (8). To ensure feasibility, the motive steam pressure constraint is set at 84 bar, aligning with the capabilities of current commercial electric boiler technology [37].

2.4 Process simulation for multi-stage MVR and integrated TVR-MVR

The multi-stage MVR and integrated TVR-MVR systems were developed within Aspen Plus, with Table 1 summarising the parameters assumed in the process model.

Table 1. Overview of the process simulation parameters employed in steam recovery or generation processes via Aspen Plus.

	Blocks and assumptions used in process simulation	**References**
Natural gas boilers, Electric boilers	• Outlet steam temperature =200 °C and pressure =8 bar, typical of low-temperature digestion. • Assumed efficiency of 82 % for natural gas boilers. • Assumed efficiency of 98% for electric boilers. • A heater is used to heat the inlet water (40 °C). • The CO_2 emissions was calculated based on pure methane (CH_4) combustion.	[38-42]
Multi-stage MVR	• A compressor is connected to a flash block, with desuperheat water injected at each stage of the compression process. • For multi-stage MVR, the units are arranged in series. • Isentropic efficiency of compressors =76 %. • Compression ratio of low-speed compressors is assumed to range from 1.3-1.45. • Compression ratio of high-speed compressors is assumed to range from 1.45 to 2. • Desuperheat water is injected to maintain inlet steam temperature 5 °C above saturation in high-speed compressors and at saturation temperature in low-speed compressors.	[5, 12, 23-25, 43]
Integrated TVR-MVR	• Performance of first and second TVR units: $Er = 4, Cr = 1.44, \mathrm{A} = 100, Pr = 0.042$ • Followed by multi-stage MVR simulated in Aspen plus.	[36]
Note: All pressures are absolute. The simulation is based on an outlet steam flow of 100 t/hr.		

2.4.1 Mathematic models for MVR-systems and integrated TVR-MVR system

The multi-stage MVR compression processes were also calculated with Equations (12)-(22) to validate the models developed by Aspen Plus. The compression process follows the thermodynamic principles of adiabatic compression, with the ideal case assumed to be isentropic. Here, T_0 and P_0 represent the inlet waste water vapour temperature and pressure, while T_i denotes the discharge temperature after stage i^{th} compression stage. The actual power for the compressor at stage i, W_i, was calculated with Equation (15) and the total electric power input for the MVR systems (W_{TM}) was obtained by summing all stage powers shown in Equation (20). Desuperheat water is injected before each compression stage to desuperheat the

discharge temperature T_i to or near the saturation temperature, thereby avoiding excessively high specific volume that would result in higher electrical power consumption. The mass flow rate of injected desuperheat water, $m_{D,i}$, introduced before stage $(i+1)$, was calculated with Equation (16). For integrated TVR-MVR systems, the first and second stages were calculated using Equations (2)-(10), while the subsequent MVR stages were evaluated using the following Equations. The coefficient of performance for the MVR system, COP_M, was calculated as the ratio of thermal output to electrical power input of the MVR compressors. For TVR-MVR system, COP_{T-M} was calculated as the ratio of thermal output to the combined electrical power input of both the MVR system and the electric boilers for motive steam generation, as presented in Equation (22).

$$T_i = T_{i-1} + \frac{T_{i-1}\cdot[(\frac{P_i}{P_{i-1}})^{\frac{k-1}{k}}-1]}{\eta_{is}} \quad (12)$$

$$h_i = h_{i-1} + C_P \cdot T_{i-1} \cdot [(\frac{P_i}{P_{i-1}})^{\frac{k-1}{k}}\text{-}1]/\eta_{is} \quad (13)$$

$$\Delta h_i = C_P \cdot T_{i-1} \cdot [(\frac{P_i}{P_{i-1}})^{\frac{k-1}{k}}\text{-}1]/\eta_{is} \quad (14)$$

$$W_i = m_{i-1} \cdot \Delta h_i \quad (15)$$

$$m_{D,i} = m_{i-1} \cdot \frac{h_i - h_{tar-i}}{h_i - h_w} \quad (16)$$

$$m_i = m_{i-1} + m_{D,i} \quad (17)$$

$$\Delta T_{C-i} = T_i - T_{i-1} \quad (18)$$

$$\Delta T_{tar-i} = T_{tar-i} - T_{i-1} \quad (19)$$

$$W_{TM} = \sum_{i=1}^{i} W_i \quad (20)$$

$$COP_M = \frac{m_{out} \cdot h_{out}}{W_{TM}} \quad (21)$$

$$COP_{T-M} = \frac{m_{out} \cdot h_{out}}{W_{TM} + W_{EB}} \quad (22)$$

2.5 Economic analysis

2.5.1 Capital cost estimation

The total capital investment for installing steam recovery was estimated using the factor method, for which the breakdown of the purchased major equipment, including concrete, structural, piping for transporting steam, electrical equipment, and instrumentation, shown in

Table 2. An uncertainty of ±30% is adopted to reflect the typical accuracy range of techno-economic assessments, where capital and operating costs were estimated using scaling correlations and literature data [44]. Detailed purchase cost and installation factor for the TVR, MVR, and electric boiler systems are presented in Appendices A and B.

Table 2. Ratio factors used to estimate the total capital investment of installing steam recovery.

Parameters	**Assumed factor number**
Direct cost (DC)	
Purchased main equipment	A
Purchased-equipment installed	A*f
Earthworks	0.01A
Concrete	0.05A
Structural	0.20A
Insulation	0.03A
Tanks & Platework	0.04A
Piping	0.47A
Electrical Equipment	0.33A
Instrumentation	0.021A
Total direct costs	**(1.16+f)A**
Indirect cost (IDC)	
Project Development allowance	0.06 A
EPCM	0.78 A
Contingency	0.98 A
Total Indirect costs	**1.82 A**
Total capital investment (TCI)	(2.98+f) A

2.5.2 Levelised cost of decarbonised steam

The levelised cost of steam (LCOS) was calculated with Equation (23). A reference natural gas price of 7.5 US$/GJ was used representing the current Australia gas price [45], with sensitivity analysis undertaken over the range 3-14 US$/GJ span average prices in the United States, United Kingdom, and the Netherlands (2019-2023) [30]. A reference for decarbonised steam generation costs was calculated to be 179 US$/$t_{CO_2}$ based on carbon capture and storage (CCS) for natural gas boilers using a post-combustion capture approach. A renewable electricity of 70 US$/MWh was selected as the baseline [46]. This is assumed to qualify for net-zero production certification standards, so that addressing the lifecycle emissions of the renewable energy is beyond the scope of the present analysis. A sensitivity analysis was then conducted over the range 30-120 US$/MWh for the renewable electricity [31]. The CO_2 emissions evaluated in this work correspond solely to on-site steam production. Indirect emissions attributable to electricity supply chains are outside the boundary and therefore not considered.

$$LCOS = \frac{\sum_{t=1}^{n} \frac{TCI_t + M_t + G_t + C_t + E_t}{(1+r)^t}}{\sum_{t=1}^{n} \frac{S_t}{(1+r)^t}} \quad (23)$$

TCI (Investment expenditures)	The construction is completed within 1 year
M_t , Operating and maintenance expenditures in year t	3% of TCI
G_t, Cost in natural gas in year t	3-14 US$/GJ gas price
C_t, Cost of CO_2 capture and storage (CCS) in year t	Calculated at 179 US$/$t_{CO2}$ [35]
E_t, Cost of renewable electricity in year t	30-120 US$/MWh
S_t, steam production in year t	Based on 100 t/hr generation or recovery rate
r , Discount rate	10%
n , Life of the system	15

3. Results

3.1 Multi-stage TVR

Figure 4 presents that the number of TVR stages significantly influences the total motive steam demand. With inlet pressure of 1.1 bar, as the number of stages increases from three to six, the total motive-to-inlet steam ratio decreases from 8 to 2.7 t_{motive}/t_{inlet}. This trend is because higher compression ratio per stage requires either greater motive steam quantity or higher motive steam pressure [37]. A 6-stage TVR system is the optimal configuration as it achieves the minimum required motive steam amount. Similarly, with inlet pressure of 0.14 bar, a minimum of a 4-stage TVR system is needed to achieve the high overall compression duty. However, this configuration requires an exceptionally high total motive steam ratio of 38 t_{motive}/t_{inlet}, highlighting its significant dependence on external steam supply. A 12-stage TVR configuration is the optimal solution, reducing the ratio from 38 to 13 t_{motive}/t_{inlet}.

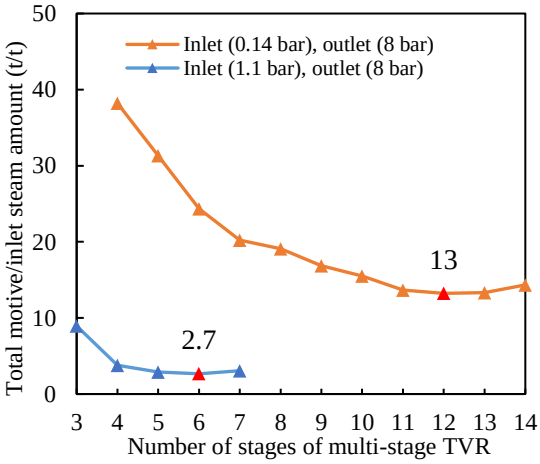


Figure 4. Ratio of total motive to initial steam of different numbers of multi-stage TVR systems.

Figures 5 (a) and (b) presents the calculated temperature and pressure profiles, as well as the motive steam requirements for the optimum TVR systems. For the 6-stage TVR system, steam pressure rises gradually from 1.1 to 8 bar, with a compression ratio per stage of 1.3-1.45. Correspondingly, the pressure required for the motive steam increases from 26 bar to 80 bar. While the temperature rises per stage ranges from 11 to 25 °C, all of which fall within manageable limits. For compressing steam from 0.14 bar to 8 bar, the optimised 12-stage TVR configuration evenly distributes the compression duty, with motive steam pressure gradually increasing from 2 to 80 bar.

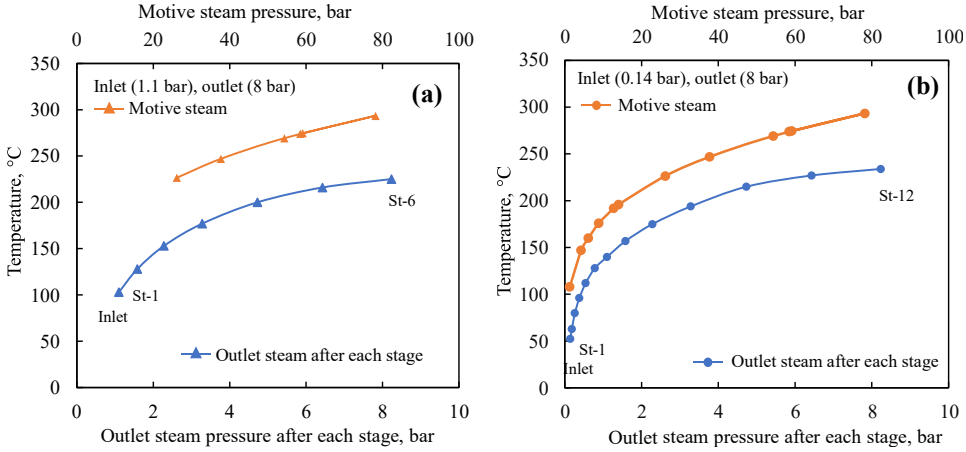


Figure 5. Temperature and pressure change and motive steam requirements calculated for optimised systems with (a) 6-stages TVR and (b) 12-stages TVR.

Figures 6 (a) and (b) present the motive-to-inlet steam ratio, energy consumption for motive steam generation and the COP value for multi-stage TVR systems. The 6-stage TVR system exhibits a COP value of 1.4, requiring a total of 1.9 GJ/t_{steam} to generate the motive steam from electric boilers. This corresponds to an outlet-to-inlet steam ratio of 3.7, with 2.7 units of motive steam per unit of inlet steam. The 12-stage TVR system has an even lower COP of 1, together with an energy demand of 2.6 GJ/t_{steam} for motive steam generation. The outlet-to-inlet steam ratio increases significantly to 12.9, as the cumulative effect of the 12 stages drives substantially higher motive steam requirements. An increase in motive steam flow rate greatly raises steam generation energy demand and reduces overall system efficiency. To fairly

benchmark efficiency across different steam generation and recovery methods, a COP comparison is provided in Section 3.4.

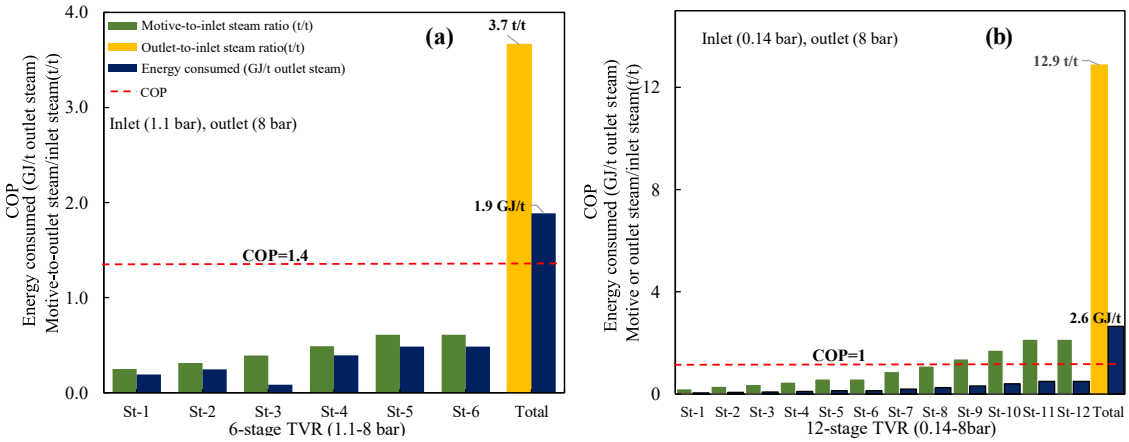


Figure 6. The calculated values of motive-to-inlet steam ratio, energy consumption and COP for the optimal steam recovery systems employing (a) 6-stage TVR and (b) 12-stage TVR.

3.2 Multi-stage MVR

Figure 7 (a) presents the temperature-pressure rise during the compression process in the multi-stage MVR system for various inlet and outlet steam conditions. The case with a low inlet pressure vapour (0.14 bar) requires 8 compression stages to reach the outlet of 8 bar. The steam temperature increases significantly after each compression stage, noting that the desuperheat water is injected before each stage. For the 0.14 bar inlet pressure, the first four low-speed stages achieve a pressure ratio of ~1.45 per stage, with a saturation temperature rise of 10-14°C per stage. The subsequent high-speed compressors provide a higher compression ratio up to two, leading to a temperature rise 19-23 °C per stage. The case with an inlet steam pressure of 1.1 bar leads to a significant reduction in the overall compression duty. Under these conditions, only a 4-stage MVR system is required to achieve an outlet pressure of 8 bar, using a combination of low-speed and high-speed compressors. When operating with only low-speed compressors layout, an 11-stage compression train is required for an inlet pressure of 0.14 bar, while approximately 6-stages is needed for an inlet pressure of 1.1 bar. Figure 6 (b) presents the outlet-to-inlet steam ratios with water injection after each stage. Overall, with outlet pressure of 8-bar, the cumulative water injection increases the ratio to 1.11 and 1.26 for inlet

pressures of 0.14 bar and 1.1 bar, respectively. These values provide a useful basis for selecting the inlet vapour flow to meet a given outlet steam requirement.

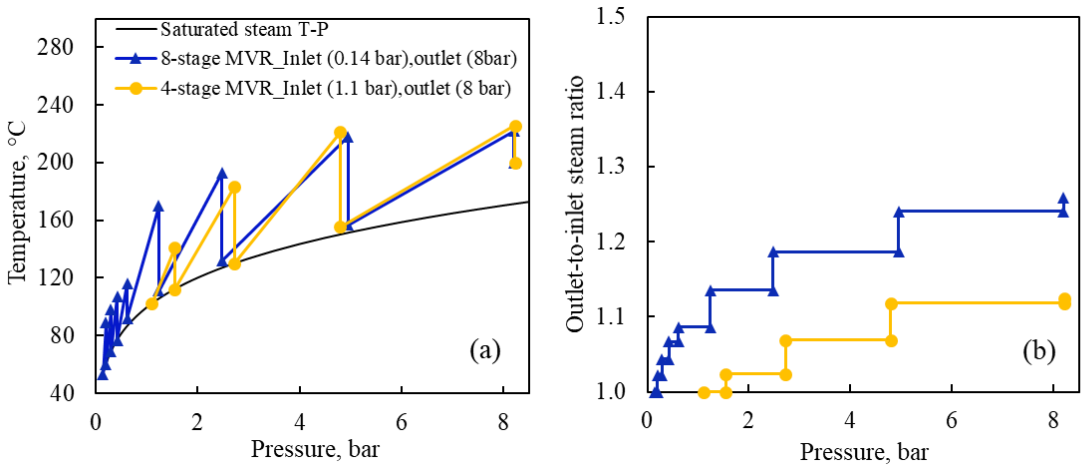


Figure 7. The calculated dependence on pressure rise through the multi-stage MVR systems with water injection after each stage (a) temperature rise, and (b) outlet-to-inlet-steam ratio.

3.3 Integrated TVR-MVR system

Figures 8 (a) and (b) present the equivalent calculated values of temperature-pressure rise and the outlet-to-inlet steam ratio changes for the hybrid TVR-MVR systems when compressing steam from 0.14 bar to 8 bar. For the first and second stages, TVR raises the steam temperature by 16-17 °C with high-pressure motive steam. The subsequent MVR provides a higher compression ratio up to two, leading to a temperature rise of approximately 20°C per stage. With the addition of motive steam and water injection after each stage , the outlet-to-inlet steam ratio increases to 1.92, which is lower than that of multi-stage TVR but higher than that of MVR system. Compared with a 8-stage MVR system operating at 100 t/hr with a total of 10 MVRs, an integrated 2-stage TVR and 5-stage MVR configuration halves the number of MVR units to 5, significantly lowering both capital equipment requirements and system complexity. This configuration also has the potential to reduce the installation footprint by approximately 50%, as estimated in Appendix C. It also significantly increasing system reliability, both through lower dependence on the failure of individual MVR unit and through reduced risk of surging during start-up when steam flow is insufficient [5]. When considering practical implications, it is important to consider the available vapour fluctuation from the

alumina refining process and the operating risk. In MVR systems, individual compressor failure presents operational challenges and the anti-surge issues during start-up may occur when steam flow is fluctuated and insufficient [5]. With more stages of compressors, the risk of surge can be exacerbated due to the increased complexity of multiple compression stages. The integration lowers system complexity and operational risks by reducing the number of stages, while incorporating TVR in the initial stages ensures sufficient steam supply from the motive steam. Therefore, quantifying the operational risks associated with multi-stage MVR and integrated TVR-MVR systems is important, which is limited in this study.

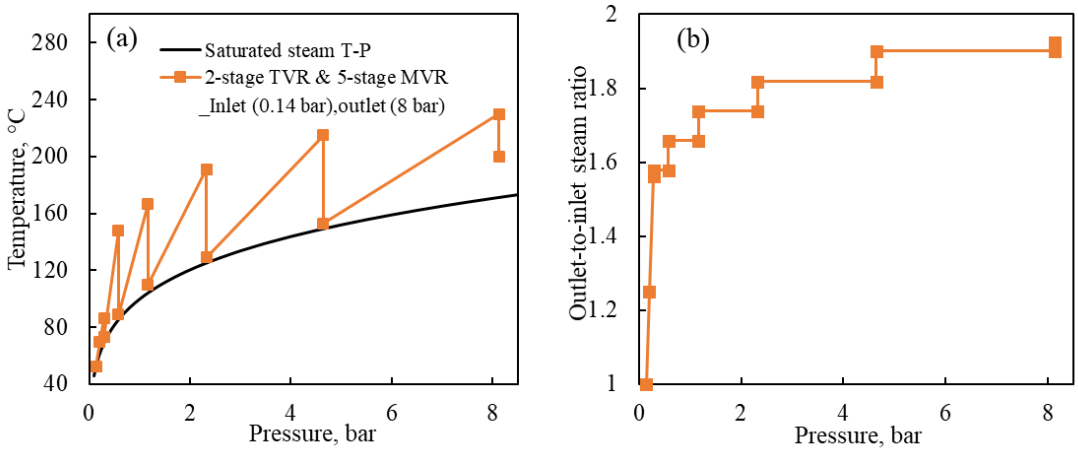


Figure 8. The calculated (a) temperature and pressure rise and (b) outlet-to-inlet-steam ratio through the integrated TVR-MVR system.

3.4 Energy consumption and system efficiency

Figure 9 presents the calculated values of energy consumption and COP for the various steam generation and recovery configurations. Overall, the MVR systems have the lowest energy consumption and highest COP value. For the inlet vapour pressure of 1.1 bar, it requires 0.5 GJ/t_{steam} energy, achieving a COP of 5.7. In contrast, the TVR system consumes about four times more energy, with a COP of 1.4. Both systems outperform natural gas boilers, leading to energy reduction by 85% and 42%, respectively. For the inlet vapour pressure of 0.14 bar, the MVR system requires 0.9 GJ/t_{steam} energy for recompressing and maintains high COP of 3.2. This corresponds to a reduction in energy use by 73% relative to the natural gas boilers. The integrated TVR-MVR system represents an intermediate option, with a COP of 1.9 and some

55% energy savings relative to natural gas boilers. The 12-stage TVR system exhibits a relatively low COP close to that of electric boilers (~1) and achieves 21% energy reduction compared with than natural gas boilers, indicating limited system efficiency.

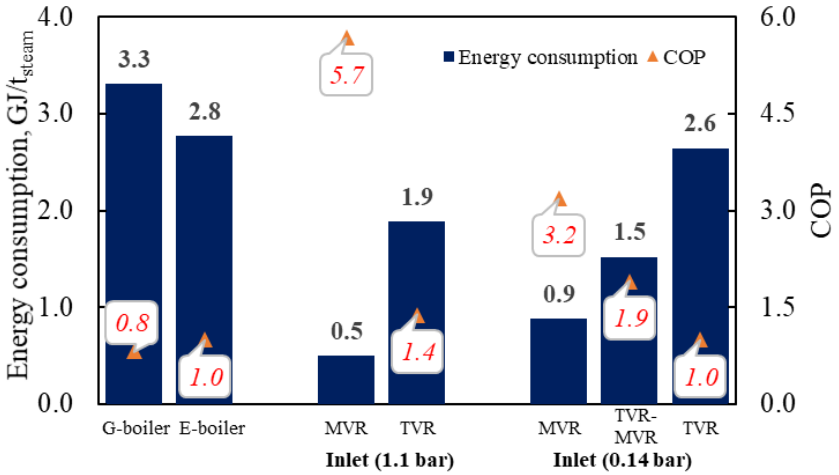


Figure 9. A comparison of the calculated energy consumption and COP (or efficiency) for the various steam generation or recovery systems.

3.5 Economic results

Figure 10 presents the calculated levelised cost of decarbonised steam (LCOS) for various steam generation or recovery systems. The LCOS for the reference case of natural gas boilers with CCS is calculated to be 55.1 US$/$t_{steam}$, with the carbon capture and storage cost contributing 30 US$/$t_{steam}$ alone. Relative to the baseline, the multi-stage MVR systems demonstrate the greatest cost reduction potential, lowering the LCOS by 65% and 39% when recovering steam from 1.1 bar and 0.14 bar, respectively, corresponding to LCOS at 19.1 and 33.6 US$/$t_{steam}$. These estimates for the reference case assume 70 US$/MWh for renewable electricity, 7.5 US$/GJ for natural gas, and 179 US$/$t_{CO2}$ for CCS. The capital cost of the MVR system increases by 74% from 9.5 to 16.5 US$/$t_{steam}$ for the inlet pressure of 1.1 bar and 0.14 bar, caused by the increased required stages, accounting for approximately 50% of the LCOS. In contrast, the capital cost of the TVR system does not change significantly with changes in inlet pressure and is estimated to be 8-10 US$/$t_{steam}$, with 99% of cost attributed to the electric boilers investment for motive steam generation. Compared with natural gas boilers with CCS, steam recovery via multi-stage TVR system achieves apprxoimately18% cost reduction for an

inlet pressure of 1.1 bar, while the LCOS increases by 10% for an inlet pressure of 0.14 bar. The integrated TVR-MVR system provides a modest cost saving of 14% relative to natural gas boilers, with the LCOS at 47.4 US$/$t_{steam}$. Electric boilers cost 64.4 US$/$t_{steam}$ in steam generation, reflecting the high electricity costs. However, they offer significant advantages such as operational simplicity and may improve their competitiveness should electricity prices decline in the future as anticipated. With higher inlet steam quality, the MVR system is estimated to become competitive with natural-gas boilers without CCS, with steam recovery costing 19.1 US$/$t_{steam}$, compared with 25.1 US$/t_{steam} for natural gas boilers at 7.5 US$/GJ gas price.

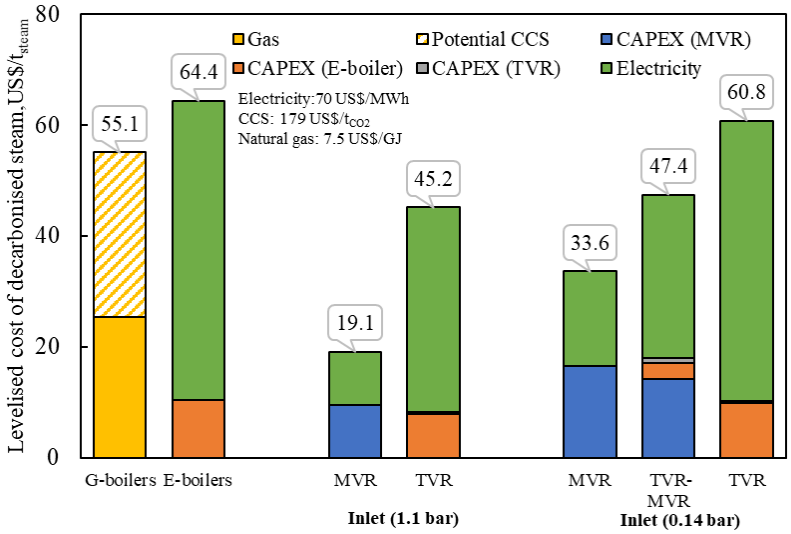


Figure 10. The calculated values of levelised cost of decarbonised steam (LCOS) for various reference case of steam generation or recovery systems.

Figure 11 presents the calculated LCOS as a function of renewable electricity price. For natural gas boilers with CCS, the estimated LCOS increases from 31 to 87 US$/$t_{steam}$ as gas prices rise from 3 to 14 US$/GJ. When CCS is included, the CCS cost ranges from 124 to 249 US$/$t_{CO_2}$, corresponding to electricity price of 30-120 US$/MWh in the economic analysis [35], reflecting the electricity intensity during CO_2 capture and compression. The CCS cost contributes 20-41 US$/$t_{steam}$ to the LCOS. Among all steam recovery methods, the multi-stage MVR system remains cost-effective relative to natural gas boilers with CCS across the electricity range, even for low gas prices of 3 US$/GJ. In contrast, the multi-stage TVR system

requires electricity prices below 52 US$/MWh to compete with 3 US$/GJ natural gas price at 1.1 bar inlet pressure, and break-even price decreases to 30 US$/MWh at 0.14 bar inlet pressure. The integrated TVR-MVR system has a break-even price of 34 US$/MWh for the inlet pressure of 0.14 bar. Electric boilers are the most expensive of the electrified options, exhibiting nearly overlapping LCOS curves with the TVR system at 0.14 bar inlet vapour pressure, requiring a break-even electricity price of 30 US$/MWh.

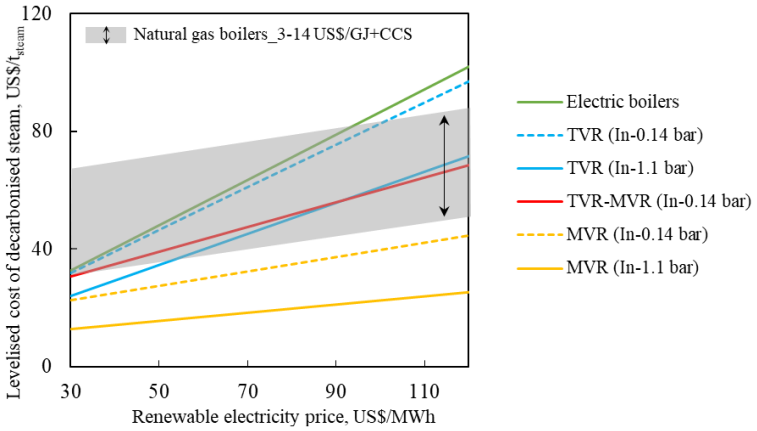


Figure 11. The calculated levelised cost of decarbonised steam (LCOS) as a function of renewable electricity price for various steam generation or recovery systems and the two inlet pressures for recovered steam.

4. Conclusions

Steam recovery via multi-stage MVR, TVR and hybrid TVR-MVR systems were assessed from technical and economic perspectives, in comparison with natural gas boilers. MVR achieves the greatest energy and cost reduction. When recompressing water vapour to 8 bar, the MVR system achieves about 85% energy reduction for an inlet pressure of 1.1 bar, delivering a COP of 5.7, and approximately 73% for an inlet pressure of 0.14 bar, corresponding to a COP of 3.2, compared with natural gas boilers. In contrast, the integrated TVR-MVR configuration achieves a modest energy saving of 55% for inlet vapour at 0.14 bar, delivering a COP of 1.9. Multi-stage TVR system demonstrates lower efficiency, leading to approximately 42% energy savings for 1.1 bar inlet vapour pressure (COP=1.4), and about 21% for an inlet pressure of 0.14 bar (COP=1.0) relative to natural gas boilers. From an economic perspective, steam recovery via MVR can be cost-competitive with natural gas boilers with

CCS over an electricity price range of 30-120 US$/MWh, even when the natural gas price is as low as 3 US$/GJ. The integrated TVR-MVR configuration is estimated to reach cost parity at an electricity price of approximately 34 US$/MWh for 0.14 bar inlet pressure and 3 US$/GJ gas price, while offering advantages in reduced system complexity. In comparison, multi-stage TVR systems require a break-even electricity price of approximately 52 US$/MWh to compete with natural gas boilers at a gas price of 3 US$/GJ for an inlet pressure of 1.1 bar, while the break-even threshold decreases to around 30 US$/MWh for an inlet pressure of 0.14 bar.

Nomenclature

F_0	kg/s	Mass flow of suction steam in the first stage
F_{m1}	kg/s	Mass flow of motive steam for the first stage
F_{mi}	kg/s	Mass flow of motive steam for the ith stage
Er_1		Entrainment ratio in the first stage
Er_i		Entrainment ratio in the ith stage
P_0		Pressure of suction steam in the first stage
P_1		Pressure of outlet steam after stage 1
P_i		Pressure of outlet steam after stage i
P_{m1}		Pressure of motive steam for the first stage
P_{mi}		Pressure of motive steam for the ith stage
Pr_1		Ratio of the suction pressure to the motive pressure for the first stage
Pr_i		Ratio of the suction pressure to the motive pressure for the ith stage
Cr_1		Compression ratio for the first and ith stage
Cr_i		Compression ratio for the ith stage
T_i	K	Discharge temperature after stage i
T_{tar-i}	K	Target temperature after stage i after desuperheat water injection
T_0	K	Inlet steam temperature
P_i	bar	Discharge pressure after stage i
P_0	bar	Inlet steam pressure
h_i	kJ/kg	Steam enthalpy of steam at T_i temperature
h_{tar-i}	kJ/kg	Steam enthalpy of steam at T_{tar-i} temperature
h_0	kJ/kg	Inlet steam enthalpy
C_P	kJ/(kg·k)	Steam heating capacity
k		Heat capacity ratio, C_p/C_v, equal to 1.3 for steam
W_i	kW	Calculated input electric power for stage i
W_{TM}	kW	Total input electric power for MVR compressors
$m_{D,i}$	kg/s	Injected desuperheat water before stage $(i+1)$
m_i	kg/s	Inlet steam mass flow rate for stage $(i+1)$
m_{out}	kg/s	Final outlet steam mass flow rate
W_{EB}	kW	Total input electric power for electric boilers
COP_M		COP for multi-stage MVR system
COP_{T-M}		COP for integrated TVR-MVR system
COP_T		COP for multi-stage TVR system

Acknowledgements

The work is supported by the Heavy Industry Low-carbon Transition Cooperative Research Centre (HILT CRC) which receives funding from its industry, research, and government collaborators, as well as from the Australian Government's Cooperative Research Centres Program. Siyun Ning acknowledges the financial support provided through an Australian Government Research Training Program (RTP) Scholarship at the University of Adelaide, along with a supplementary scholarship from HILT CRC.

5. References

[1] Yang Ni and Yingwei Bai, *Digestion-Evaporation Combined Process in Alumina Refinery*, in *the 37th international ICSOBA Conference*. 2019: Krasnoyarsk, Russia.

[2] Songqing G and Zhonglin Y. *Preheaters and digesters in the Bayer digestion process.* Essential Readings in Light Metals: Volume 1 Alumina and Bauxite, 2016: p. 356-361. https://doi.org/10.1007/978-3-319-48176-0_47.

[3] Seetharaman S. *Treatise on Process Metallurgy: Volume 3: Industrial Processes*. Elsevier.2024.

[4] Tabereaux A T and Peterson R D. *Chapter 2.5 - Aluminum Production*. Treatise on Process Metallurgy. Elsevier.2014. 839-917.

[5] Chatfield R. *Mechanical vapor recompression (MVR) for low carbon alumina refining, MVR technical and commercial feasibility studies*. https://arena.gov.au/projects/mechanical-vapour-recompression-for-low-carbon-alumina-refining/. 2022 [accessed on 14 June 2024].

[6] Brough D and Jouhara H. *The aluminium industry: A review on state-of-the-art technologies, environmental impacts and possibilities for waste heat recovery.* International Journal of Thermofluids, 2020. 1: p. 100007. https://doi.org/10.1016/j.ijft.2019.100007.

[7] E. Jaeger D S-J and A. Barry, *Integrating Vapor Compression Heat Pumps and Mechanical Vapor Recompression with the Bayer Process*, in *the 12th International AQW Conference and Exihibition*. 2024: Dubai, UAE.

[8] Mach T, *Energy Consumption in talalhe Bayer Process*, in *the 12th International AQW Conference and Exihibition*. 2024: Dubai, UAE.

[9] Hu B, Wu D, and Wang R. *Water vapor compression and its various applications.* Renewable and sustainable energy reviews, 2018. 98: p. 92-107. https://doi.org/10.1016/j.rser.2018.08.050.

[10] Ranade V V and Bhandari V M. *Industrial wastewater treatment, recycling and reuse*. Butterworth-Heinemann.2014.

[11] Gaur A S, Fitiwi D Z, and Curtis J. *Heat pumps and our low-carbon future: A comprehensive review.* Energy Research & Social Science, 2021. 71: p. 101764. https://doi.org/10.1016/j.erss.2020.101764.

[12] Klute S, Budt M, van Beek M, and Doetsch C. *Steam generating heat pumps–Overview, classification, economics, and basic modeling principles.* Energy Conversion and Management, 2024. 299: p. 117882. https://doi.org/10.1016/j.enconman.2023.117882.

[13] Dahmardeh H, Amiri H A, and Nowee S. *Evaluation of mechanical vapor recompression crystallization process for treatment of high salinity wastewater.* Chemical Engineering and Processing-Process Intensification, 2019. 145: p. 107682. https://doi.org/10.1016/j.cep.2019.107682.

[14] Zhou Y, Shi C, and Dong G. *Analysis of a mechanical vapor recompression wastewater distillation system.* Desalination, 2014. 353: p. 91-97. https://doi.org/10.1016/j.desal.2014.09.013.

[15] Khalid B, Osman Ahmed H, and Amro Mohammed M. *Modelling and Simulation of the Multi-effect/Thermal Vapor Compression Distillation Process.* International Journal of Mechanical Engineering and Applications, 2020. 8(4): p. 103-110. https://doi.org/10.11648/j.ijmea.20200804.12.

[16] Shahzamanian B, Varga S, Soares J, Palmero-Marrero A, and Oliveira A. *Theoretical performance assessment of a multi-effect distillation system integrated with thermal vapour compression unit running on solar energy.* International Journal of Low-Carbon Technologies, 2024. 19: p. 908-921. 10.1093/ijlct/ctae010.

[17] Chua H T and Rahimi B. *Low grade heat driven multi-effect distillation and desalination*. Elsevier.2017.

[18] Power R B. *Steam jet ejectors for the process industries*. McGraw-Hill.1994.

[19] Giampaolo T. *Compressor handbook: principles and practice*. River Publishers.2010.

[20] Bryan W. Hackett. *The Essentials of Continuous Evaporation*. https://www.aiche.org/resources/publications/cep/2018/may/essentials-continuous-evaporation#:~:text=require%20a%20large%20temperature%20gradient,of%20the%20liquid%20being%20concentrated. 2018 [accessed on 9 June 2025].

[21] Minton P E. *Handbook of Evaporation Technology*. Elsevier Science.1986.

[22] Ltd. T I P. *Mechanical Vapour Recompression (MVR) Evaporator Manufacturers*. https://thermosag.com/mechanical-vapour-recompression-mvr-evaporator-manufacturers/. [accessed on 1 Octorber 2025].

[23] PILLER. *PILLER Blowers & Compressors*. https://www.piller.de/products-services/mvr-blower-piller-blowers-compressors/vapoflex/. [accessed on 12 November 2024].
[24] *Howden Centrifugal Blowers*. https://www.chartindustries.com/Products/Centrifugal-Blowers. [accessed on 11 July 2025].
[25] *Howden turbo technology*. https://www.chartindustries.com/Products/Compression-Centrifugal-Compressors. [accessed on 1 June 2024].
[26] Boltzmann L. *Theoretical physics and philosophical problems*. Springer.1974. 13-32.
[27] Bantle M, Schlemminger C, Tolstorebrov I, Ahrens M, and Evenmo K, *Performance evaluation of two-stage mechanical vapour recompression with turbo-compressors*, in *the 13th IIR Gustav Lorentzen Conference*. 2018: Valencia, Spain.
[28] GEA. *Mechanical vapor recompression (MVR) solutions for the economization of distillation*. https://www.gea.com/en/assets/304829/. 2023 [accessed on 4 June 2025].
[29] Atlas Copco. *Mechanical Vapor Recompression key to steam energy upgrade within a polyolefin plant*. https://www.atlascopco.com/gas-and-process/en/pressure-points-blog/mechanical-vapor-recompression-key-to-steam-energy-upgrade-within-a-polyolefin-plant. 2021 [accessed on 12 November 2024].
[30] *Natural gas prices in world data*. https://ourworldindata.org/grapher/natural-gas-prices?time=2020..latest. 2025 [accessed on 6 June 2025].
[31] *World in Data. Levelized cost of energy for renewables*. https://ourworldindata.org/grapher/levelized-cost-of-energy?tab=table&time=2023..latest. 2023 [accessed on 6 June 2025].
[32] CSIRO Australia's National Science Agency. *GenCost 2022-23*. https://www.csiro.au/-/media/EF/Files/GenCost/GenCost2022-23Final_27-06-2023.pdf. 2023 [accessed on 6th July 2025].
[33] Klett C and Perander L. *Alumina Calcination: A mature technology under review from supplier perspective*. Light Metals 2015, 2015: p. 79-84. https://doi.org/10.1007/978-3-319-48248-4_15.
[34] Saw W L, Naufal A, Sandoval A B, Beath A, Lovegrove K, van Eyk P, McNaughton R, Bader R, and Nathan G. *Technical feasibility of integrating concentrating solar thermal energy in the Bayer alumina process.* AIP Conference Proceedings, 2020. 2303(1)10.1063/5.0029572.
[35] Ning S, Nathan G, Ashman P, and Saw W L. *Techno-economic assessment of integrated steam cleaning and recovery from alumina calcination.* Chemical Engineering Journal, 2026. 529: p. 173154. https://doi.org/10.1016/j.cej.2026.173154.
[36] Green D W and Perry R H. *Perry's chemical engineers' handbook*. McGraw-Hill Education.2008.
[37] PARAT. *High Voltage Electrode boiler for Steam and Hot water*. https://www.parat.no/en/products/industry/parat-ieh-high-voltage-electrode-boiler/. [accessed on 7 June 2025].
[38] ARENA. *A Roadmap for Decarbonising Australian Alumina Refining*. https://arena.gov.au/knowledge-bank/a-roadmap-for-decarbonising-australian-alumina-refining/. 2022 [accessed on 15 June 2025].
[39] The U.S. Department of Energy. *Energy efficiency and industrial boiler efficiency: an industry perspective*. https://www.nrel.gov/docs/fy04osti/35106.pdf. 2002 [accessed on 4 July 2025].
[40] Chetan T. Patel, Bhavesh K. Patel, and Vijay K. Patel. *Efficiency with different GCV of coal and efficiency improvement opportunity in boiler.* International journal of innovative research in science, engineering and technology, 2013. 2(5): p. 1518-1527.
[41] Schoeneberger C, Zhang J, McMillan C, Dunn J B, and Masanet E. *Electrification potential of US industrial boilers and assessment of the GHG emissions impact.* Advances in Applied Energy, 2022. 5: p. 100089. https://doi.org/10.1016/j.adapen.2022.100089.
[42] Zuberi M J S, Hasanbeigi A, and Morrow W. *Electrification of industrial boilers in the USA: potentials, challenges, and policy implications.* Energy Efficiency, 2022. 15(8): p. 70. https://doi.org/10.1007/s12053-022-10079-0.
[43] Hocking M B. *Handbook of chemical technology and pollution control*. Elsevier.2016.
[44] Garrett D E. *Chemical engineering economics*. Springer Science & Business Media.2012.
[45] *Gas market prices, Australia Energy Regulator*. https://www.aer.gov.au/industry/registers/charts/gas-market-prices. 2024 [accessed on 1 March 2025].
[46] Blakers A, Lu B, and Stocks M. *100% renewable electricity in Australia.* Energy, 2017. 133: p. 471-482. https://doi.org/10.1016/j.energy.2017.05.168.

Appendix A for Chapter 5

The size factors of TVR were calculated with Equation (A-1) and (A-2) [1]. Table A-1 presents the calculated size factor and estimated cost, based on previous study [1]. Table A-2 presents the size factor for 12-stage TVR system.

$$\text{Dryairequivalent(DAE)} = \frac{suction\ load\ of steam(t/hr) \cdot 2205}{0.8 * 0.96} \quad \text{(A-1) [1]}$$

$$\text{Size factor}_{(\text{ejector})} = \frac{DAE}{Suction\ pressure\ (bar) \cdot 750} \quad \text{(A-2) [1]}$$

Table A-1. The size factors and purchased cost of 6-stage TVR system. (inlet pressure of 1.1 bar and outlet pressure of 8 bar, 100 t/hr outlet steam mass flow rate)

	Suction steam in TVR (t/hr)	Suction pressure (bar, absolute)	Size factor	Purchased cost in 1992 US$ with stainless steel material	Cost in 2024 US $
Stage 1	27.2	1.1	103	30,000	67,039
Stage 2	34.1	1.6	82	26,000	58,101
Stage 3	42.6	2.3	71	22,000	49,162
Stage 4	53.2	3.3	62	20,000	44,693
Stage 5	66.5	4.7	54	18,000	40,223
Stage 6	83.2	6.4	50	18,000	40,223

Table A-2. The size factors and purchased cost of 12-stage TVR system. (inlet pressure of 0.14 bar and outlet pressure of 8 bar, 100 t/hr outlet steam mass flow rate)

TVR	Suction steam in TVR (t/hr)	Suction pressure (bar, absolute)	Size factor	Purchased cost in 1992 US$ with stainless steel material	Cost in 2024 US $
Stage 1	7.81	0.14	214	46,000	102,793
Stage 2	9.38	0.18	197	40,000	89,385
Stage 3	11.72	0.26	171	36,000	80,447
Stage 4	14.65	0.38	149	34,000	75,978
Stage 5	18.31	0.54	129	32,000	71,508
Stage 6	22.89	0.78	112	31,000	69,274
Stage 7	27.47	1.10	96	27,000	60,335
Stage 8	34.33	1.58	83	26,000	58,101
Stage 9	42.92	2.28	72	22,000	49,162
Stage 10	53.64	3.28	63	20,000	44,693
Stage 11	67.06	4.73	54	18,000	40,223
Stage 12	83.82	6.43	50	18,000	40,223

Appendix B for Chapter 5

Cost estimation for MVR

Table B-1 presents the reference size and cost of compressors, obtained from open literature. The compressor cost was calculated using Equation (B-1), where C_{refer} is the reference cost, and S_{new} and S_{refer} are the calculated scale in the study and reference scale, respectively.

$$C_{MVR\ compressor} = C_{refer} \times (\frac{S_{new}}{S_{refer}})^{0.7} \quad \text{(B-1)}$$

Table B-1. Estimated purchased cost of compressor from open literatures.

Components	Reference cost, C_{refer}	Reference size, S_{refer}	Reference year	Scaling factor	Installation factor, f	Sources
MVR compressors	1.4 NZD M$	3 MW	2019	0.7	1.38	[2, 3]
	3 NZD M$	3 MW	2004	0.7	1.38	[4]
	2.7 USD M$	4.47 MW	1998	0.7	1.38	[5]

Cost estimation for electric boilers

The electric boiler purchase cost is assumed US$ 160 per kW (adjusted to 2024 value) [6, 7], with the installation factor f of 1.53 [8]. Based on give estimations of 50~160 US$/kW for the e-boiler itself in year 2018, for capacities between 2.9 MW and 73 MW [7].

Appendix C for Chapter 5

Installation footprint estimation for multi-stage MVR and integrated TVR-MVR

Size estimation for MVR

The operating boundaries for compressors used in MVR systems are defined by an impeller diameter up to 2.2 m (86 inches), capable of handling a steam volumetric flow rate of 170 m^3/s, with a gas velocity of 45 m/s [9]. The estimated impeller diameter (D) for each stage is calculated by Equation (C-1), where V (m^3/s) represents the inlet steam volumetric flow. The L/D (length to impeller diameter) ratios of compressors is assumed at 3.8, and the specific W/D (width to impeller diameter) ratios is assumed at 2.5 [10]. However, it is important to note that factor ratios may vary depending on design specifications and manufacturer standards.

$$D = \sqrt{\frac{V \cdot 4}{45 \cdot \pi}} \qquad \text{(C-1)}$$

Size estimation for TVR

The TVR size factor was determined using Equations (A-1) and (A-2), which define the suction diameter, with the ejector length generally about ten times this diameter, as reported in the book Steam Jet Ejectors for the Process Industries (p. 312, figure 10.1) [1].

Footprint estimation of systems

The estimated footprint of the MVR system depends significantly on the layout arrangement and the operating mass flow rates [3]. The installation footprint and number of compressor units were estimated for multi-stage TVR and integrated TVR–MVR systems, operating at outlet steam flow rates of 100 t/hr and 200 t/hr. Figure C-1 presents an example of the optimised layout arrangement for an 8-stage MVR system, adopted from previous study [3]. As steam pressure increases, its volume decreases, leading to a smaller impeller size and, consequently, a more compact compressor. The space between each stage is assumed to be equivalent to the average width of two compressors to ensures operation safety.

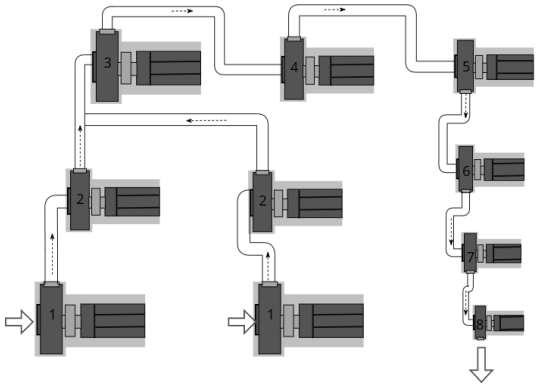


Figure C-1. An example of layout arrangement of 8-stage MVR system based on previous study [3].

Table C-1 presents the estimated installation footprint and number of units for multi-stage MVR and integrated TVR-MVR system. Overall, integrating a two-stage TVR in the initial stages reduces the MVR stages by three, thereby decreasing the installation area by approximately 50%. For an 8-stage MVR system, two parallel compressors are required in the first two stages to handle the high steam volume, giving a total of 10 compressors and an estimated footprint of 566 m^2 at an operating rate of 100 t/hr. At a higher steam demand of 200 t/hr, two

trains of 8-stage MVR systems could be installed, each operating at 100 t/hr steam capacity. In the integrated system, incorporating two-stage TVR reduces the number of compressors from 10 to 5 at 100 t/hr, lowering the footprint by about 50%.

Table C-1. Estimated installation footprint and number of units for multi-stage MVR and integrated TVR-MVR systems.

8-stage MVR system (inlet steam pressure of 0.14 bar and outlet of 8 bar)					
Inlet steam mass flow rates (t/hr)	Outlet steam mass flow rates (t/hr)	Number of compressors			Estimated installation area (m^2)
79	100	10 (1 train)			566 m^2 (21.7*26)
159	200	2*10 (1 train)			2*566 m^2
Integrated TVR-MVR system (2-stage TVR and 5-stage MVR) (inlet steam pressure of 0.14 bar and outlet of 8 bar)					
		Number of compressors	Number of TVRs	Number of E-boilers	Estimated installation area (m^2)
52	100	5 (1 train)	2	2	282 m^2 (17.1*16.5)
104	200	2*5 (1 train)	2	2	2*282 m^2

References

[1] Power R B. *Steam jet ejectors for the process industries.[Glossary included]*. 1994

[2] Energy Efficiency and Conservation Authority. *MVR (Mechanical Vapour Recompression) Systems for Evaporation, Distillation and Drying*. https://genless.govt.nz/assets/Business-Resources/Mechanical-vapour-recompression-for-evaporation-distillation-drying.pdf. 2019 [accessed on 7 July 2024].

[3] Chatfield R. *Mechanical vapor recompression (MVR) for low carbon alumina refining, MVR technical and commercial feasibility studies*. https://arena.gov.au/projects/mechanical-vapour-recompression-for-low-carbon-alumina-refining/. 2022 [accessed on 14 June 2024].

[4] Reuben W. Bouman, Scott B. Jesen, Maria L. Wake, and Earl W B. *Process Capital Cost Estimation for New Zealand 2004*. https://books.google.com.au/books?id=_sfzPAAACAAJ. 2005 [accessed on 1 March 2025].

[5] Energy. T U S D o. *Process equipment cost estimation, final report*. https://www.osti.gov/servlets/purl/797810. 2002 [accessed on 8 June 2024].

[6] Lagendijk J. *An Exploration of the Company Perspective on the Adoption of Industrial Electric Boilers*. https://pure.tue.nl/ws/portalfiles/portal/313517534/1253492_final_version_master_thesis_JSLagendijk.pdf. [accessed on 4 April 2025].

[7] Zuberi M J S, Hasanbeigi A, and Morrow W. *Electrification of industrial boilers in the USA: potentials, challenges, and policy implications.* Energy Efficiency, 2022. 15(8): p. 70. https://doi.org/10.1007/s12053-022-10079-0.

[8] Garrett D E. *Chemical engineering economics*. Springer Science & Business Media.2012.

[9] *Howden turbo technology*. https://www.chartindustries.com/Products/Compression-Centrifugal-Compressors. [accessed on 1 June 2024].

[10] Brun K and Kurz R. *Compression machinery for oil and gas*. Gulf Professional Publishing.2018.

Chapter 6

Optimisation of Steam Recovery from Calcination and the Bayer circuit using Multi-stage Mechanical Vapour Recompression

Preface

Key results from Chapter 4 shows that steam recovery from calcination can meet up to 42% of the steam demand in the Bayer circuit. Chapter 5 assesses various steam recovery technologies and highlights that multi-stage mechanical vapor recompression (MVR) offers the highest energy efficiency among the proposed configurations evaluated.

Beyond calcination, waste low-pressure vapour from the Bayer circuit can also be recovered to further offset steam demand. This chapter therefore assesses the technical and economic potential of achieving up to 100% steam supply from recovery.

Highlights of this chapter include:

- 100% steam demand can be met via steam recovery, 43% from calcination (e.g. H_2 in oxygen-steam combustion), and the remaining 57% from the Bayer circuit.
- The optimised steam recovery scenario reduces energy use by up to 79%, enabling zero-carbon steam supply powered by renewable electricity.

Statement of Authorship

Title of Paper	Techno-economic Assessment of Steam Recovery from Calcination and the Bayer circuit using Multi-stage Mechanical Vapour Recompression
Publication Status	☐ Published ☑ Accepted for Publication ☐ Submitted for Publication ☐ Unpublished and Unsubmitted w ork w ritten in manuscript style
Publication Details	Ning S, Nathan G, Ashman P, and Saw W L, Techno-economic Assessment of Steam Recovery from Calcination and the Bayer circuit using Multi-stage Mechanical Vapour Recompression Paper. In the 155th TMS Annual Meeting & Exhibition, San Diego, California, USA, 15th- 19th March 2025.

Principal Author

Name of Principal Author (Candidate)	Siyun Ning		
Contribution to the Paper	Concept deisgn, Process model development and simulation, Data analysis and interpretation, Drafted the manuscript and acted as corresponding author.		
Overall percentage (%)	65%		
Certification:	This paper reports on original research I conducted during the period of my Higher Degree by Research candidature and is not subject to any obligations or contractual agreements with a third party that would constrain its inclusion in this thesis. I am the primary author of this paper.		
Signature		Date	25/11/2025

Co-Author Contributions

By signing the Statement of Authorship, each author certifies that:

i. the candidate's stated contribution to the publication is accurate (as detailed above);

ii. permission is granted for the candidate in include the publication in the thesis; and

iii. the sum of all co-author contributions is equal to 100% less the candidate's stated contribution.

Name of Co-Author			
Contribution to the Paper	Supervision of the work, Concept development, Evaluation and review of the manuscript.		
Signature		Date	

Name of Co-Author			
Contribution to the Paper	Supervision of the work, Concept development, Evaluation and review of the manuscript.		
Signature		Date	2/12/2025

Please cut and paste additional co-author panels here as required.

Name of Co-Author	Woei Lean Saw			
Contribution to the Paper	Supervision of the work, Concept development, Evalu	anuscript.		
Signature			Date	

Optimisation of Steam Recovery from Calcination and the Bayer Circuit Using Multi-stage Mechanical Vapour Recompression

Siyun Ning, Graham Nathan, Peter Ashman, and Woei Lean Saw

Abstract

The present study evaluates the technical and economic feasibility of recovering vented vapour from the Bayer circuit (evaporation, precipitation, and digestion steps) and calcination as a decarbonisation strategy for alumina refining, using Aspen Plus, compared with conven- tional natural gas boilers. Results show that 100% of steam supply for Bayer circuit usage can potentially be met via internal recovery: 43% from calcination (H_2 in oxygen-steam combustion), 9% from digestion, 37% from evaporation, and 11% from precipitation. An esti- mated 79% reduction in energy consumption for steam supply is plausible with full (100%) steam recovery, rela- tive to steam generation from gas boilers. Economically, compared with boilers at a gas price of 7.5 US$/GJ including a cost of carbon capture and storage (CCS) of 179 US$/$t_{CO2}$, the full steam recovery scenario is esti- mated to reduce the levelised cost of decarbonised steam for the Bayer circuit ($LCOS_B$) by 50% at a fixed 70 US$/MWh electricity price, dropping from 110.2 to 55.1 US$/$t_{Al2O3}$. The capital cost of multi-stage mechanical vapour recompression (MVR) is the dominant component (50%) of the $LCOS_B$ in this scenario, while renewable electricity remains the primary operating cost driver. A sensitivity analysis indicates that, with natural gas at 7.5 US$/GJ and no CCS, cost parity is achieved when electricity prices fall below 60 US$/MWh; with CCS, electricity-based steam recovery is cost-competitive for costs above 30 US$/MWh.

Keywords

Steam recovery · Bayer circuit · Calcination · Net-zero steam · Multi-stage MVR

Introduction

Alumina production via the Bayer process typically consumes around 10.5 GJ/t_{Al2O3} energy, of which approximately 70% is attributed to steam generation from natural gas boilers for the Bayer circuit [1–3]. High-pressure steam is used, whose requirements depend on the bauxite type. Gibbsite ores, digested at lower temperatures (175–230 °C, 5–15 bar), require less energy-intensive conditions than boehmite or diaspore ores (325–400 °C, 50–100 bar) [4]. Substantial quantities of waste vapour are released from the Bayer circuit, owing to its low pressure and/or concentration which make recovery challenging. Nevertheless, this presents a significant energy loss with significant potential for energy efficiency improvement if the waste vapour, along with its heat, can be recovered [4–6]. Present cycles typically vent some 2.2 GJ/t_{Al2O3} in the form of latent heat in the low-pressure steam at 0.14 bar and 52.5 °C from the digestion to precipitation steps [1, 7, 8]. In addition, medium-pressure vapour at 1.1 bar and 102 °C is vented from the digestion tank, carrying latent energy of 0.4 GJ/t_{Al2O3} [3, 9]. This steam is presently generated from water using natural gas or electric boilers, the water and energy for which could be substantially reduced were effective steam recovery approaches to be identified. Similarly, vapour is also vented from the calcination step, which is the last step of Bayer process, that converts gibbsite to alumina, releasing chemically bound water. Hence the overall aim of the paper is to evaluate the techno-economic potential of configurations for which steam recovery is plausible.

S. Ning (✉) · G. Nathan · P. Ashman · W. L. Saw
The University of Adelaide, North Terrace Campus, Adelaide, SA, Australia
e-mail: siyun.ning@adelaide.edu.au

Heavy Industry Low-Carbon Transition Cooperative Research Centre (HILT CRC), Adelaide, SA, Australia

G. Nathan
e-mail: graham.nathan@adelaide.edu.au

P. Ashman
e-mail: peter.ashman@adelaide.edu.au

W. L. Saw
e-mail: woei.saw@adelaide.edu.au

© The Minerals, Metals & Materials Society 2026

R. Seno (ed.), *Light Metals 2026*, The Minerals, Metals & Materials Series, https://doi.org/10.1007/978-3-032-13832-3_17

Recent work has proposed two retrofittable calcination pathways, employing either hydrogen combustion or electrified calcination under a steam environment, with potential to generate high-concentration steam for recovery [4, 5] while eliminating calcination-related emissions. These pathways are estimated to recover 0.6–0.8 t_{steam}/t_{Al2O3} steam, equating to 1.4–1.8 GJ/t_{Al2O3} of latent energy. The amount of steam available from both the calcination and Bayer circuit, it is possible to satisfy is greater than the steam demand in the Bayer circuit, making recovery a desirable target. However, the technical and economic barriers to implementing this cost effectively are sufficiently great that no systems to achieve this recovery have ever been implemented [4]. Hence, the study aims to advance the understanding of the technical and economic viability of achieving full internal recovery within the Bayer process.

Mechanical vapour recompression (MVR) systems increase the temperature and pressure of low-pressure steam with mechanical compression, offering potential to contribute to recovery of vented vapour. However, mechanical compression requires steam of sufficient purity and quality to avoid damage to the blades, requiring careful process design. A multi-stage MVR configuration has been proposed for recovery from the Bayer circuit by Chatfield [9], while Furlong et al. [10] also demonstrated its potential to decarbonise steam generation for meeting the steam demand through recovery has the potential to reduce some 70% of total CO_2 emissions from alumina production [9, 11, 12], aligning with global targets for net-zero emis- sions by 2050–2070 [13–16]. However, a comprehensive techno-economic assessment of plausible systems for steam recovery from both calcination and Bayer circuit is still lacking. Achieving full steam recovery from Bayer process may incur high capital investment, particularly for multi-stage MVR, while operating costs are sensitive to electricity prices. No studies have comprehensively analysed capital costs or electricity price sensitivity in comparison with conventional boilers. Therefore, this study aims to evaluate the economic feasibility of plausible configurations for steam recovery from Bayer process.

In light of these gaps, this study aims to evaluate the technical and economic viability of plausible configurations for steam recovery to achieve a net-zero steam supply for the Bayer circuit. The specific objectives are:

1. To evaluate the technical viability of novel configurations for sufficient steam recovery from both the calcination and Bayer circuit using steam clean-up and multi-stage MVR systems to meet total steam demand.
2. To estimate potential energy savings and CO_2 reductions from eliminating the need for steam generation for the Bayer circuit from the proposed systems for internal steam recovery.
3. To evaluate the capital and operating costs of full internal recovery in comparison with conventional gas boilers, with and without carbon capture, compression, transport, and storage (CCS).

Methodology

Steam Sources from the Bayer Process

For the steam recovery simulations, we used vapour conditions for the relevant Bayer steps from prior studies [9, 17]. These values are typical, although actual values vary for each plant due to differences in vapour conditions and mass flow rates.

- Digestion waste vapour: 1.1 bar absolute, 102 °C, ~0.16 t_{steam}/t_{Al2O3} [17].
- Precipitation low-pressure vapour: 0.14 bar absolute, 52 °C, ~0.35 t_{steam}/t_{Al2O3} [9].
- Evaporation low-pressure vapour: 0.14 bar absolute, 52 °C, ~0.59 t_{steam}/t_{Al2O3} [9].
- Diluted steam from natural gas or H_2/air calcination: 1.06 bar absolute, 165 °C, ~0.75–0.8 t_{steam}/t_{Al2O3}.
- High-purity steam from H_2 in oxy-steam and fully electrified calcination: 1.06 bar absolute, 167 °C, 0.6–0.8 t_{steam}/t_{Al2O3}.
- The steam consumption in Bayer circuit is assumed at two t_{steam}/t_{Al2O3} [9].
- The steam supply condition is assumed to be 8 bar and 200 °C for the low-temperature digestion case.

As shown in Fig. 1, the digestion step uses high-pressure steam and caustic soda to dissolve bauxite and form a sodium aluminate solution [18, 19]. The process incorpo- rates multi-stage flash tanks to utilise the thermal energy efficiently, but the last tank vents a small amount of vapour at approximately 102 °C [9]. Following digestion, the clar- ification step separates the insoluble solids (red mud) from the green liquor that carries dissolved aluminium species, which is not a primary source of recoverable steam [20, 21]. Next, the green liquor proceeds to the precipitation step, where gibbsite (aluminium hydroxide) is crystallised by cooling it to approximately 75~100 °C using cooling water [9]. The steam source from this step is generated by flashing the warmed cooling water, together with the evaporated steam typically at 0.14 bar and 52 °C [9]. After precipitation, the spent liquor is recycled to the evapora- tion step, where additional water is evaporated to concen- trate the solution for reuse in digestion. This releases an

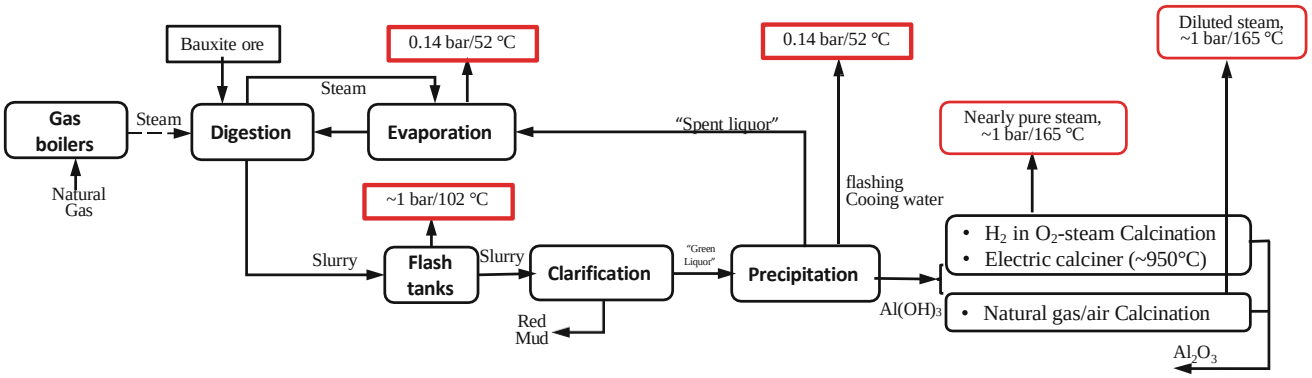


Fig. 1 Vented waste vapour sources in the Bayer process (adapted from previous work [4, 9, 19])

additional 0.59 t_{steam}/t_{Al2O3} low-pressure steam [9]. The calcination step generates steam from gibbsite dehydra- tion reaction and fuel combustion, converting gibbsite to alumina. Under conventional natural gas/air combustion, the exhausted steam is diluted by ~ 50% N_2, yielding ~0.75–0.8 t_{steam}/t_{Al2O3}. Under H_2 in oxy-steam combustion or electrification calcination in steam environment, can be configured to produce high-concentration steam in the range of 0.6–0.9 t_{steam}/t_{Al2O3}, from the process modelling results of calcination using Aspen Plus in previous work. A novel configuration is investigated to remove fine particles (typically < 2 μm) that are generated from the calcination process and persist even after particulate control systems such as electrostatic precipitators (ESP) or baghouses. This employs a gas separation and steam-cleaning systems prior to the MVR unit, with flowsheets developed and analysed. Similarly, vapour from the digestion tanks may present same challenge comparable to calcination vapour, owing to its contact with bauxite slurry and the potential entrainment of solids, impurities, and non-condensable gases. This also requires further investigation and are not yet included at this stage.

Table 1 summarises the steam supply scenarios analysed in this study. LD-0 represents the reference case, in which all steam is generated from natural gas boilers. LD-1 and LD- 3 consider steam recovery from different calcination pathways. LD-4 includes steam recovery from both H_2 oxy-steam calcination and digestion. LD-5 represents scenarios where low-pressure steam is recovered from evaporation and precipitation. For LD-1 and LD-5, supplementary steam is supplied from natural gas boilers when the recovered steam is insufficient. LD-6 represents the optimised case, integrating steam recovery from H_2 oxy-steam calcination, digestion, evaporation, and precipitation.

Table 1 Steam supply scenarios for the Bayer circuit

Steam supply scenarios	Steam recovery from various steps	Steam from boilers
LD-0	N/A	Natural gas boilers
LD-1	Natural gas/air or H_2/air combustion calcination	Natural gas boilers for supplementary steam generation
LD-2	Fully electrified calcination	
LD-3	H_2 in oxy-steam combustion calcination	
LD-4	H_2 in oxy-steam calcination + digestion	
LD-5	Evaporation + precipitation	
LD-6	H_2 in oxy-steam calcination + digestion + evaporation + precipitation	N/A

Steam Recovery Process Simulation from Different Steps

The steam recovery processes from different steps were modelled using Aspen Plus. An overview of the parameters assumed is summarised in Table 2.

Economic Analysis

Capital Cost Estimation for Steam Recovery

The total capital investment was estimated using the factor method based on purchased equipment costs, with an inherent uncertainty of ±30%. Table 3 presents the breakdown of factor values, provided in consultation with Worley. The breakdown includes tanks and platework for boiler feedwater pumps, blowdown tanks, and MVR water injection

Table 2 Overview of Aspen Plus process simulation parameters in steam recovery processes based on 120 t/hr Al_2O_3 production and 240 t/hr steam supply in Bayer circuit

	Blocks and assumptions used
Natural gas boilers	• Outlet steam temperature = 200 °C and pressure = 8 bar, typical of low-temperature digestion [4] • Assumed efficiency of 82% [22, 23] • A heater is used to heat the inlet water (40 °C)
MVR system	• A compressor is connected to a flash block, with desuperheated water injected at each stage of the compression process • For multi-stage MVR, the units are arranged in series • Isentropic efficiency of compressors = 76% [24–26] • Compression ratio of low-speed compressors is assumed to range from 1.3 to 1.45 [9, 24, 27] • Compression ratio of high-speed compressors is assumed to range from 1.5 to 2 [9, 24, 27]
Steam sources	
Precipitation evaporation	• An 8-stage MVR system was modelled to compress steam from 0.14 bar to 8 bar
Digestion	• A 4-stage of MVR was implemented to compress steam from ~ 1 bar to 8 bar
Natural gas/air calcination	• An integrated spray tower with 7-stage MVR system for diluted N_2 and CO_2 separation and vapour recompression [9]
H_2 in oxygen-steam combustion/electrified calcination	• An integrated particle cleaning unit and 4-stage MVR system for fine particle removal and vapour recompression

Note All pressures are absolute

Table 3 Ratio factors used to estimate the total capital investment for installing steam recovery

Parameters	Assumed factor number
Direct cost (DC)	
Purchased main equipment	A
Purchased-equipment installed	A*f
Earthworks	0.01A
Concrete	0.05A
Structural	0.20A
Insulation	0.03A
Tanks and Platework	0.04A
Piping	0.47A
Electrical Equipment	0.33A
Instrumentation	0.021A
Total direct costs	**(1.16 + f)A**
Indirect cost (IDC)	
Project Development allowance	0.06 A
EPCM	0.78 A
Contingency	0.98 A
Total indirect costs	**1.82 A**
Total capital investment (TCI)	(2.98 + f) A

pumps. Steam piping is required for all scenarios to transport steam. Purchased equipment costs were sourced from literature as shown in Table 4 and adjusted to 2024 US$ using the scaling factor equation shown in Eq. 1. In this equation, C_r and S_r present the reference cost and size in literature, $\boldsymbol{n}$ is the scaling factor, and C and S present the cost and size in the study.

$$C = C_r \times \left(\frac{S}{S_r}\right)^n \quad (1)$$

Levelised Cost of Decarbonised Steam Supply in Bayer Circuit

The levelised cost of decarbonised steam supply in the Bayer circuit, $LCOS_B$, per ton of alumina, was calculated with Eq. 2, using the assumptions shown in Table 5. To esti- mate decarbonised steam generation costs, a carbon capture and sequestration (CCS) cost of 179 US$/$t_{CO2}$ was applied for gas boilers using a post-combustion capture approach [31, 32]. An amine-based CO_2 capture process was simu- lated with 90% capture efficiency [33]. The CO_2 capture and compression was calculated to be 144.1 US$/$t_{CO2}$, and transport and sequestration of compressed CO_2 contribute 35 US$/$t_{CO2}$ [34], assuming the alumina plants are located at the South-West of Western Australia. A sensitivity anal- ysis was conducted over 30–120 US$/MWh for renewable electricity [35] to assess the impact on steam and CCS costs, with a 70 US$/MWh as the baseline [36]. The natural gas prices were varied over the range 3–14 US$/GJ, with a 7.5 US$/GJ Australian baseline, to assess impacts on steam supply cost [37].

Table 4 Estimated purchased cost of key components from open literature

Components	Reference cost, C_r	Reference size, S_r (MW)	Reference year	Scaling factor, n	Installation factor, f	Sources
MVR compressors	1.4 NZD M$	3	2019	0.7	1.38	[9, 28]
	3 NZD M$	3	2004	0.7	1.38	[29]
	2.7 USD M$	4.47	1998	0.7	1.38	[30]

Table 5 Assumptions for the levelised cost of decarbonised steam supply for Bayer circuit

TCI (Investment expenditures in year t)	The construction is within 1 year
M_t, Operating and maintenance expenditures in year t	3% of TCI
G_t, Cost in natural gas in year t	7.5 US$/GJ
C_t, Cost of CCS in year t	179 US$/$t_{CO2}$ (under 70 US$/MWh electricity price)
E_t, Cost of renewable electricity in year t	70 US$/MWh
A_t, Alumina production in year t	120 t/hr with 90% operating
r, Discount rate	10%
n, Life of the system	15

$$LCOS_B = \frac{\sum_{t=1}^{n} \frac{TCI_t + M_t + G_t + C_t + E_t}{(1+r)^t}}{\sum_{t=1}^{n} \frac{A_t}{(1+r)^t}} \quad (2)$$

Results

Technical Results

Steam Supply Scenarios in the Bayer Circuit

Figure 2 presents the calculated distribution of sources for the steam supply for the series of scenarios, each of which satisfies the steam demand for the Bayer circuit (low-temperature digestion case). This shows that 100% steam usage can be met through internal vapour recovery, for the LD-6 case. The sources for this steam are 43% from calcination with H_2 in oxy-steam combustion, 9% from digestion, 37% from evaporation, and 11% from precipitation. Alternatively, vapour could be recovered from the Bayer circuit or calcination separately, supplemented by existing gas boilers. Scenarios LD-1 to LD-3 incorporate steam recovery from the calcination process, including natural gas/air or H_2/ air combustion, electrified or H_2 in oxy-steam combustion. These are calculated to meet 27%, 32%, and 43% of total demand, respectively. Steam recovery from evaporation and precipitation is estimated to meet 37 and 22% of the total demand, respectively, shown in LD-5.

Energy Consumption in Various Steam Supply Scenarios

Figure 3 compares energy consumption for each of the steam supply scenarios, together with the associated CO_2 emissions. It can be seen that both the energy consumption and CO_2 emissions decrease with an increase in the extent of steam recovery. The case with full internal recovery scenario is calculated to reduce energy required for steam supply by 79%, also enabling zero CO_2 emissions where the need for gas boilers is removed. For Scenario LD-3, with ~ 42% of steam met from H_2 in oxy-steam calcination, energy consumption drops by 36% to 4.25 GJ/t_{Al2O3}. For Scenario LD-5, ~58% of total steam supplied from evaporation and precipitation vapour recovery is calculated to reduce energy use by 43%, lowering it to 3.74 GJ/t_{Al2O3}. Similarly, retaining gas boilers for supplementary steam supply results in CO_2 emissions ranging from 0.15 to 0.27 t_{CO2}/t_{Al2O3} in LD-1 to LD-5. It is also observed that recovering steam from the calciner has a more substantial impact compared to recovery from evaporation and precipitation, due to high steam pressure and temperature, although additional steps are required to clean the steam.

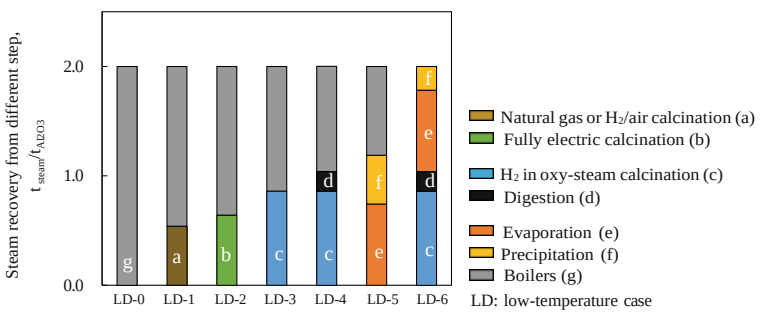


Fig. 2 The distribution of sources for the steam recovery for the various steam supply scenarios (see Table 1), each of which meets 100% steam demand for the Bayer circuit

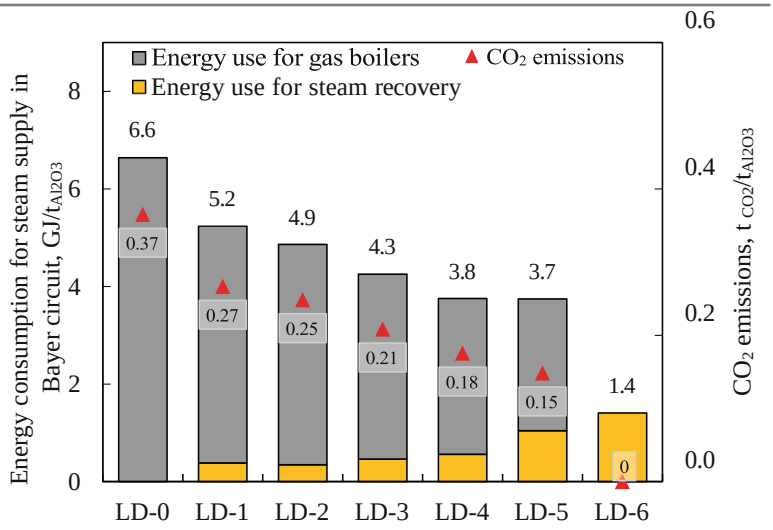


Fig. 3 Distribution of energy consumption, together with CO_2 emissions, for the various steam supply scenarios to the Bayer circuit

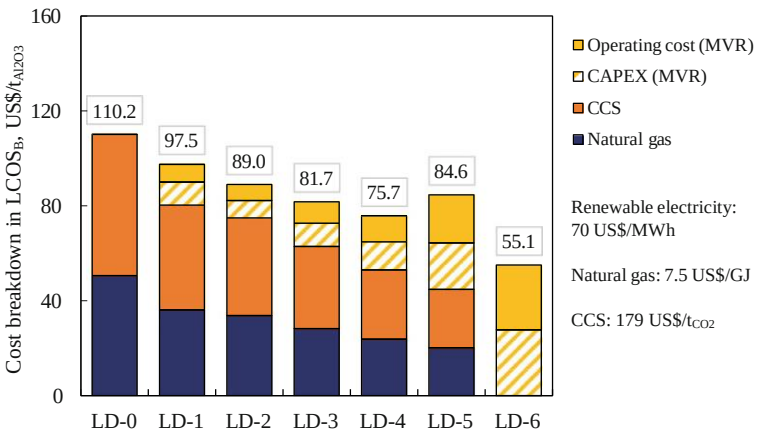


Fig. 4 Calculated $LCOS_B$ for the various steam supply scenarios to the Bayer circuit, ignoring any differences in the cost of the alternative calcination processes

Economic Results

Figure 4 presents the cost breakdown in $LCOS_B$ for the various steam supply scenarios. The calculated $LCOS_B$ decreases gradually from 110.2 to 55.1 US$/$t_{Al2O3}$ with increased steam recovery rates. A 50% cost reduction is estimated for the case with full steam recovery and for a fixed electricity price of 70 US$/MWh. However, this cost reduction is accompanied by a significant increase in capital investment, rising from 9.7 (for LD-1) to 27 US$/$t_{Al2O3}$ (for LD-6), which increases its share from 10 to 50% of total cost, due to the additional infrastructure required for the MVR systems. For Scenario LD-5, with 59% of the total steam recovered from evaporation and precipitation, the $LCOS_B$ decreases by 23% from the baseline, indicating a modest cost advantage from low-pressure vapour recovery.

Sensitivity Analysis

Figure 5 presents the impact on the $LCOS_B$ of changes to the gas price to the gas boilers, in comparison with the 100% internal recovery scenario LD-6. For gas boilers, the $LCOS_B$ increases proportionally with the natural gas price, ranging from 21 to 94 US$/$t_{Al2O3}$ across the gas prices from 3 to 14 US$/GJ without CCS. The baseline 179 US$/$t_{CO2}$ CCS cost contributes a further 59 US$/$t_{Al2O3}$, raising the $LCOS_B$ to 80–153 US$/$t_{Al2O3}$. For a fixed electricity price of 70 US$/ MWh, LD-6 is more cost-effective than gas boilers without CCS once gas exceeds 8.5 US$/GJ. When including the CCS cost, LD-6 remains cost-effective across the entire gas price range, delivering 26–64% lower cost.

Figure 6 presents the $LCOS_B$ as a function of renewable electricity price for the full internal recovery scenario. The $LCOS_B$ is calculated to increase proportionally with the electricity price, ranging from 39 to 75 US$/$t_{Al2O3}$ across 30– 120 US$/MWh electricity price. For comparison, a gas boiler at 7.5 US$/GJ without CCS yields 50.6 US$/$t_{Al2O3}$. Rela- tive to this benchmark, electricity-based steam achieves cost parity when electricity prices are below 60 US$/MWh. When CCS is included, based on the cost assumptions reported above, the CCS cost varies from 124 to 249 US$/$t_{CO2}$ over 30–120 US$/MWh, which reflects the electricity intensity of CO_2 capture process, and contributes an additional 41–82 US$/$t_{Al2O3}$. Compared with the CCS-inclusive benchmark,

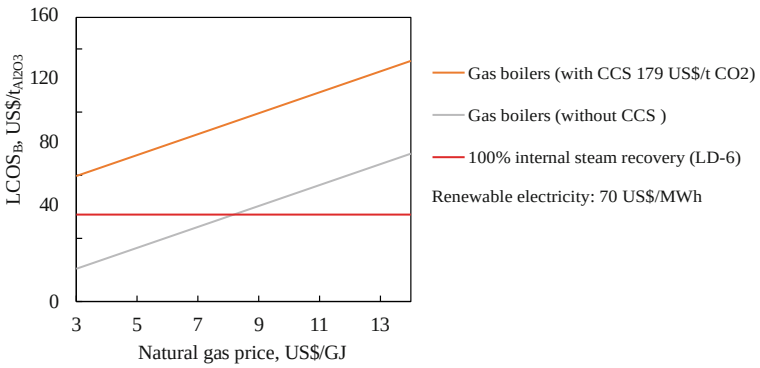


Fig. 5 Calculated $LCOS_B$ as a function of natural gas price and CCS cost in comparison with the full internal steam recovery scenario

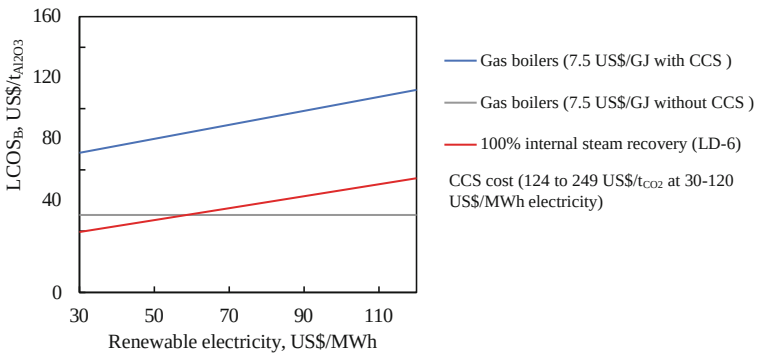


Fig. 6 Calculated levelised cost of steam for the Bayer circuit as a function of renewable electricity price for the scenario with 100% internal steam recovery in comparison with gas boilers

internal recovery is cost-competitive over the full electricity price range considered.

Conclusions

Integrating steam recovery from both the Bayer circuit and calcination has been calculated to be able to meet 100% of steam demand for Bayer circuit, although some of the assumptions are yet to be verified at commercial scale. Full steam recovery is estimated to decrease energy consumption for the steam generation by 79%, down to 1.4 GJ/t_{Al2O3} for a typical low-temperature Bayer circuit. This configuration also enables the elimination of CO_2 emissions through the transition from fossil fuel-based steam generation to renewable electricity-based steam recovery. Economically, full steam recovery is estimated to reduce the cost of decarbonised steam by 50% for the case of a fixed electricity price of 70 US$/MWh, natural gas of 7.5 US$/GJ, and CCS of 179 US$/t_{CO2}. Sensitivity analyses indicate that electricity- based steam is cost-competitive with unabated gas for the case in which electricity prices are below 60 US$/MWh at a gas price of 7.5 US$/GJ without CCS, and remains cost-competitive over gas with CCS for electricity prices above 30 US$/MWh.

Acknowledgements This work was supported by the Heavy Industry Low-Carbon Transition Cooperative Research Centre (HILT CRC), with funding provided by its industry, research, and government partners, as well as the Australian Government's Cooperative Research Centre Program.

References

1. Alton T. Tabereaux, et al., (2014) Chapter 2.5—Aluminum Production. Treatise on Process Metallurgy. Elsevier Ltd. pp. 839–917.
2. Xuan Lian, et al., (2025) Life Cycle Assessment of Alumina Production by the Bayer Process. JOM 77 (4):2221–2225. https://doi.org/10.1007/s11837-025-07181-w.
3. Santunu Pathy, et al., (2024) Exhaust to Energy: Waste Heat Recovery in Alumina Digesters. Paper presented at the 42nd International ICSOBA Conference, Lyon, France, 27–31 October 2024.
4. ARENA, (2022) A Roadmap for Decarbonising Australian Alumina Refining. https://arena.gov.au/knowledge-bank/a-roadmap-for-decarbonising-australian-alumina-refining/. Accessed on 15 June 2025
5. Woei Lean Saw, et al., (2022) Method and Apparatus for Alumina Calcination US Patent 2024308868-A1. 17 June 2022.
6. Fathi Habashi, (2016) A hundred years of the Bayer process for alumina production. Essential Readings in Light Metals: Volume 1 Alumina and Bauxite. Springer. P85–93.
7. Lawrie Henrickson, (2016) The need for energy efficiency in Bayer refining. Essential Readings in Light Metals: Volume 1 Alumina and Bauxite:691–696.https://doi.org/10.1007/978-3-319-48176-0_96.

8. Hui Tong Chua, et al., (2017) Low grade heat driven multi-effect distillation and desalination. Elsevier.
9. Ray Chatfield, (2022) Mechanical vapor recompression (MVR) for low carbon alumina refining, MVR technical and commercial feasibility studies. https://arena.gov.au/projects/mechanical-vapour-recompression-for-low-carbon-alumina-refining/. Accessed on 14 June 2023
10. Andrew Furlong, et al., (2024) Enabling Improved Waste Heat Recovery in Digestion for Energy and Carbon Footprint Reduction. Paper presented at the 42nd International ICSOBA Conference, Lyon, France, 27–31 October 2024.
11. Rahman Saidur, (2011) Energy savings and emission reductions in industrial boilers. Thermal science 15 (3):705–719.https://doi.org/10.2298/tsci091014046s.
12. Jinghua Fang, et al., (1999) Coal utilization in industrial boilers in China—a prospect for mitigating CO2 emissions. Applied Energy 63 (1):35–52.https://doi.org/10.1016/S0306-2619(99)00011-2.
13. Jan Maurice Bödeker, et al., (2010) Aluminium and renewable energy systems–prospects for the sustainable generation of electricity and heat. https://citeseerx.ist.psu.edu/document?repid=rep1&type=pdf&doi=77e625686fe58aca72860a933ff779ff8ec0ba99. Accessed on 6 June 2024.
14. Amit Roy, (2024) Towards net-zero steam production: challenges and solutions for industrial decarbonisation. Master, Lahti University of Technology LUT
15. Ashleigh Croucher, et al., (2023) Australia's clean industry future: making things here in a net zero world. https://www.climatecouncil.org.au/resources/australias-clean-industry-future-making-things-in-a-net-zero-world/. Accessed on 6 April 2025.
16. Bin Lu, et al., (2021) A zero-carbon, reliable and affordable energy future in Australia. Energy 220:119678.https://doi.org/10.1016/j.energy.2020.119678.
17. Cornelis Klett, et al., (2015) Alumina Calcination: A mature technology under review from supplier perspective. Light Metals 2015:79–84.https://doi.org/10.1007/978-3-319-48248-4_15.
18. Metson J.B., et al., (2006) Evolution of microstructure and properties of SGA with calcination of Bayer gibbsite. Light Metals (Warrendale, PA, United States):89–93.
19. James Metson, (2011) Production of alumina. Fundamentals of aluminium metallurgy. Elsevier. pp 23–48.
20. György Bánvölgyi, et al., (2013) The improved low tempera- ture digestion (ILTD) process: an economic and environmentally sustainable way of processing gibbsitic bauxites. Essential Readings in Light Metals: Volume 1 Alumina and Bauxite. Springer. pp 362–370.
21. Yang Ni, et al., (2019) Digestion-Evaporation Combined Process in Alumina Refinery. Paper presented at the Proceedings of the 37th international ICSOBA Conference, 2019.
22. The U.S. Department of Energy, (2002) Energy efficiency and industrial boiler efficiency: an industry perspective. https://www.nrel.gov/docs/fy04osti/35106.pdf. Accessed on 4 July 2025.
23. Chetan T. Patel, et al., (2013) Efficiency with different GCV of coal and efficiency improvement opportunity in boiler. International journal of innovative research in science, engineering and technology 2 (5):1518-1527.
24. PILLER, PILLER Blowers & Compressors. https://www.piller.de/products-services/mvr-blower-piller-blowers-compressors/vapoflex/. Accessed on 12 November 2024
25. Atlas Copco, (2021) Mechanical Vapor Recompression key to steam energy upgrade within a polyolefin plant. https://www.atlascopco.com/gas-and-process/en/pressure-points-blog/mechanical-vapor-recompression-key-to-steam-energy-upgrade-within-a-polyolefin-plant. Accessed on 12 November 2024.
26. Sven Klute, et al., (2024) Steam generating heat pumps–Overview, classification, economics, and basic modeling principles. Energy Conversion and Management 299:117882. https://doi.org/10.1016/j.enconman.2023.117882.
27. Howden turbo technology. https://www.chartindustries.com/Products/Compression-Centrifugal-Compressors. Accessed on 1 June 2024.
28. Energy Efficiency and Conservation Authority, (2019) MVR (Mechanical Vapour Recompression) Systems for Evaporation, Distillation and Drying. https://genless.govt.nz/assets/Business-Resources/Mechanical-vapour-recompression-for-evaporation-distillation-drying.pdf. Accessed on 7 July 2024.
29. Reuben W. Bouman, et al., (2005) Process Capital Cost Estimation for New Zealand 2004. https://books.google.com.au/books?id=_sfzPAAACAAJ. Accessed on 1 March 2025.
30. The United State Department of Energy., (2002) Process equipment cost estimation, final report. https://www.osti.gov/servlets/purl/797810. Accessed on 8 June 2024.
31. Edward S Rubin, et al., (2015) The cost of CO_2 capture and storage. International Journal of Greenhouse gas control 40:378–400.https://doi.org/10.1016/j.ijggc.2015.05.018
32. Muhammad Adnan Hayat, et al., (2024) Strategic priorities and cost considerations for decarbonizing electricity generation using CCS and nuclear energy. Energy Reports 12:2108–2122. https://doi.org/10.1016/j.egyr.2024.08.017.
33. Danish Energy Agency, (2021) Technology Data for Carbon Capture, Transport and Storage. https://ens.dk/en/analyses-and-statistics/technology-data-carbon-capture-transport-and-storage. Accessed on 1 August 2024.
34. P. R. Neal, et al., (2010) Costs of CO_2 Transport and Injection in Australia. Paper presented at the SPE Asia Pacific Oil and Gas Conference and Exhibition, Brisbane, Australia, 2010.
35. (2023) World in Data. Levelized cost of energy for renewables. https://ourworldindata.org/grapher/levelized-cost-of-energy?tab=table&time=2023..latest. Accessed on 6 June 2025
36. Andrew Blakers, et al., (2017) 100 % renewable electricity in Australia. Energy 133:471–482. https://doi.org/10.1016/j.energy.2017.05.168
37. Natural gas price-world data. https://ourworldindata.org/grapher/natural-gas-prices?tab=table&time=2020..latest. Accessed on 6 March 2025

Chapter 7-Conclusions

This study advances the understanding of steam recovery integration in the Bayer process, contributing to the development of low-carbon alumina production.

7.1 Applying hydrogen combustion in calcination while increasing the viability of steam recovery

The cyclones performance, heat utilisation, and overall energy consumption when replacing natural gas with hydrogen, particularly in oxygen-steam calcination was assessed, which enhances the viability of high-concentration steam recovery from calcination. Results indicate that hydrogen/air combustion demonstrates the lowest energy consumption at 2.7 GJ/$t_{Al_2O_3}$ (LHV), compared to 2.88 GJ/$t_{Al_2O_3}$ (LHV) for natural gas/air combustion. In the hydrogen in oxygen-steam combustion, energy consumption ranges from 2.89 to 2.96 GJ/$t_{Al_2O_3}$ (LHV). This is primarily attributed to reduced heat transfer efficiency between superheated steam and solids in the cyclones, along with inhibited pre-calcination reactions under a steam environment. It was also found that cyclone separation efficiencies remained above 97%, comparable to those under air combustion, when recirculated steam was used as the carrier gas to maintain similar volumetric flow rates. Economically, the break-even hydrogen price was calculated to range from 1.4 to 2.8 US$/kg under H_2/air combustion to compete with natural gas/air combustion with carbon capture and storage (CCS) cost (3-14 US$/GJ plus 179 US$/t_{CO_2} CCS). In contrast, for H_2 in oxygen-steam scenario, the break-even hydrogen price ranged from 2.2 to 3.4 US$/kg if this steam was recovered relative to steam generation via electric boilers at fixed renewable electricity price 70 US$/MWh. It should be noted that costs related to hydrogen handling, infrastructure, storage, compression, distribution, and safety measures fall outside the defined system boundary and are therefore not included in the analysis.

7.2 Integrated steam cleaning and recovery from various calcination scenarios

The techno-economic feasibility of recovering diluted and high-concentration steam from the calcination step was estimated. Results show that steam recovery from natural gas/air (Scenario 1) and H_2/air (Scenario 2) calcination yields 0.54~0.55 t_{steam}/t_{Al2O3}, with 0.71 GJ/t_{steam} energy use, of which 5% is allocated to gas separation. Fully electrified (Scenario 3) and H_2 in oxygen steam calcination (Scenario 4) achieve higher recovery rates of 0.64 and 0.86 t_{steam}/t_{Al2O3}, respectively, with lower energy consumption of 0.54 GJ/t_{steam}, with 9% for gas cleaning and 91% for steam compression. The recovered steam amount from calcination was estimated to offset 27%-43% of the total steam demand currently generated by natural gas boilers, corresponding to a 21-36% reduction in energy consumption for steam generation. Economically, the calculated levelised cost of decarbonising steam for the Bayer Circuit ($LCOS_B$) (normalised per tonne of alumina) was expected to decrease by 10%-24% compared with natural gas boilers with CCS (7.5 US$/GJ with 179 US$/t_{CO2} CCS) at a fixed electricity price of 70 US$/MWh, excluding any differences in the cost of the alternative calcination processes.

7.3 Comparison of various steam compression technologies

Various steam recovery technologies, including multi-stage MVR, multi-stage TVR, and proposed integrated TVR-MVR were assessed in terms of their systems efficiency when integrated in alumina refineries. Multi-stage MVR achieves the greatest energy conservation and cost reduction. Recompressing vapour to 8 bar, the MVR system achieves about 85% energy reduction for an inlet pressure of 1.1 bar, delivering a COP of 5.7, and approximately 73% for an inlet pressure of 0.14 bar, corresponding to a COP of 3.2, compared with natural gas boilers. In contrast, the integrated TVR-MVR configuration achieves a modest energy

saving of 55% for inlet vapour at 0.14 bar, delivering a COP of 1.9. Multi-stage TVR system offers lower efficiency, achieving around 42% energy savings for an inlet pressure of 1.1 bar (COP=1.4), and about 21% for an inlet pressure of 0.14 bar (COP=1.0) relative to natural gas boilers. From an economic perspective, steam recovery via MVR can be cost-competitive with natural gas boilers equipped with CCS over an electricity price range of 30-120 US$/MWh, even when the natural gas price is as low as 3 US$/GJ. However, quantifying the operational risks associated with system complexity and practical implication, for example, integrated TVR-MVR systems lowers system complexity by reducing the MVR stages is limited in this study, requiring further detailed assessment.

7.4 Optimisation of steam recovery from the Bayer circuit and calcination

Finally, the study considered integrating steam recovery from both calcination and Bayer circuit using MVR systems and estimated the various decarbonised steam supply scenarios. Results demonstrate that 100% of steam supply for Bayer circuit usage can potentially be met via internal recovery: 43% from calcination (H_2 in oxygen-steam combustion), 9 % from digestion, 37% from evaporation, and 11% from precipitation. An estimated 79 % reduction in energy consumption for steam supply is plausible with optimised steam recovery case, relative to steam generation from gas boilers. Economically, compared with boilers at a gas price of 7.5 US$/GJ including a cost of carbon capture and storage (CCS) of 179 US$/$t_{CO_2}$, the full steam recovery scenario was estimated to reduce the levelised cost of decarbonising steam for the Bayer circuit ($LCOS_B$) by 50% at a fixed 70 US$/MWh electricity price, dropping from 110.2 to 55.1 US$/$t_{Al2O3}$. A sensitivity analysis indicates that, with natural gas at 7.5 US$/GJ and no CCS, cost parity is achieved when electricity prices fall below 60 US$/MWh; with CCS, electricity-based steam recovery is cost-competitive for costs above 30 US$/MWh. The present study optimises steam recovery from both the calcination process and the Bayer circuit.

However, the availability of recoverable vapour may vary across different alumina refineries depending on plant operating conditions. These variations may introduce uncertainty in the assumptions adopted in this modelling study, requiring further investigation.

Chapter 8-Future work recommendation

The present study estimated the techno-economic feasibility of steam recovery integration within the Bayer process. Further studies are recommended to build on this work considering some of the limitations of the process modelling. Aspen Plus was used to simulate the calciner, assessing changes in stream temperature, cyclone performance and overall energy consumption. However, other impacts are also relevant and important when transitioning from natural gas/air combustion to hydrogen, such as combustion behaviour and potential effects on product quality, which cannot be captured through Aspen plus simulation. Computational Fluid Dynamic (CFD) process modelling and experimental work are recommended to understand the combustion behaviour including the impact on NO_x emission, spatial flame behaviour and stability when transiting to hydrogen/air combustion. In addition, considering the higher flame temperature of hydrogen combustion, additional retrofitting may be required to avoid material embrittlement and overheating, along with fuel nozzles modifications for adequate mixing to minimise the NO_x emissions. From an economic perspective, the cost for hydrogen storage, compression and decompression, distribution, and associated safety-control systems are outside the scope, which are important and should be incorporated in future work. It is also noted that the impact of steam on alumina quality, e.g. LOI (loss on ignition), specific surface area, particle breakage, porosity has not been assessed. This highlights the need for further experimental work on alumina calcination under steam-rich conditions. Furthermore, it is observed in process modelling the pre-calcination reaction may be inhibited under a steam-rich environment, indirectly affecting the energy consumption in calcination. To better understand this influence, conducting experimental studies on the reaction kinetics under steam conditions is necessary. Further retrofitting needs to be considered to address the potential inhibition of

the pre-calcination. One possible approach is a two-stage calcination configuration, in which a first-stage reactor is introduced to enable the use of renewable heat sources. This first stage could be implemented using a Calix drop tube reactor or a fluidised bed reactor, allowing for a complete gibbsite to boehmite conversion. These options represent areas for further investigation.

Other than hydrogen calcination, electric calcination could be explored as a potential decarbonisation pathway. However, large scale implementation remains challenging due to scaling up and uncertainties in heat transfer efficiency. It is therefore recommended to investigate plausible electric calciner technologies from both technical and economic perspectives in future work. Steam cleaning and recovery from calcination was investigated in this study as an effective particle control system is essential to ensure the steam quality before entering the multi-stage mechanical vapour recompression system. Alternative steam cleaning technologies may be considered other than venturi scrubber considered in the study, such as water electrostatic scrubbing (WES), candle filters and steam-hydro scrubbers for capturing fine particles. Further investigation in the potential integration of other steam cleaning technologies is recommended, along with experimental work to evaluate the steam cleaning efficiency, steam quality prior to multi-stage MVR system.

Process modelling in steam recovery process in this study assumes constant recoverable steam from the calciner. However, real refinery operation includes several calciners operate simultaneously, and one calciner taken offline for maintenance activities may impact the recoverable steam for recovery. To supply continuous steam, supplementary steam from generation units, e.g., electric boilers, natural gas boilers, to compensate for fluctuations in the steam recovery supply is necessary. Future work is recommended to address this issue by evaluating the system under practical operating conditions. Fluctuations in steam availability

may also affect the operational availability and performance of the MVR system, as inlet vapour variation can impact compressor stability and lifetime. Therefore, further evaluation of multi-stage MVR performance under dynamic operating conditions, supported by experimental studies, is recommended. Multi-stage MVR, multi-stage TVR, and the integrated TVR-MVR were assessed in the study, which are all open-loop heat pump systems. The closed-loop systems operate with a sealed refrigerant circuit, where the waste heat in vapour is recovered and transferred through evaporation and condensation of the refrigerant. Given that the potential contamination of the vapour from the Bayer process, indirect heat recovery using closed loop systems may be a plausible alternative to explore without the need of vapour cleaning. Therefore, it's suggested that waste heat recovery research could explore the integration of closed-loop systems in Bayer process, along with a techno-economic analysis against open-loop systems.

In addition to recover steam from calcination, recovering steam from evaporation, precipitation is also assessed in this study to meet the total steam consumption. However, one of the limitations is that the modelling assumes a constant steam consumption. In reality, steam consumption varies over time due to redundancy and maintenance requirements within the Bayer circuit, which also affects the availability of waste steam. Therefore, a more detailed whole plant analysis that incorporates the dynamic steam consumption profile will be necessary to fully assess the integration of steam recovery at refinery scale. In addition, the thesis is focused on low-temperature digestion, which has relatively lower steam pressure requirement (5-15 bar). However, high-temperature digestion requires much higher steam pressure (50-100 bar), which is not technically feasible for MVR or TVR systems. Further studies are recommended to explore alternative steam generation or technologies capable of meeting the higher-pressure requirements of high-temperature digestion.

Electrifying the steam generation and calcination process offers a pathway for decarbonisation. However, due to the substantial increase in electricity demand, factors such as electricity price, share of renewable electricity, and the infrastructure investment are critical. Further research is needed to establish a high-level transition roadmap that builds on the findings in this study to quantify the infrastructure investment and electricity demand needed for low-carbon transition pathways.

Supplementary Appendix for Chapter 4

Process Modelling for Retrofitting Alumina Calcination for Fully electrification

Preface

This chapter provides supplementary data on fully electrified calcination, including the amount of exit steam condition to support the analysis presented in Chapter 4.

Process Modelling for Retrofitting Alumina Calcination for fully electrification

Abstract

This chapter evaluated the technical feasibility of retrofitting the Calix electric calciner technology into CFB calciner as a low-carbon alternative calcination to conventional natural gas/air combustion. The retrofitted configuration utilises recirculated superheated steam as the carrier gas, enabling comparable volumetric flow rates to the conventional system. As a result, cyclone separation performance is preserved, with efficiencies exceeding 97%. Energy consumption was assessed under E-calciner wall temperatures from 900°C to 1100°C, with electric power demands estimated at 70-83 MW for the e-calciner and 12-20 MW for the electric gas heater under assumed 90% overall heating efficiency. This results in an overall energy consumption of 2.73~2.86 GJ/t_{Al2O3} for electric calcination.

1. Introduction

Decarbonising high-temperature industrial processes using electric calcination technologies has been proposed as a promising pathway [1, 2]. Calix's flash electric calcination technology is one of the approach which are applicable in alumina refining, cement manufacturing, and steel production [3, 4]. The core technology is utilising an indirect heating method where minerals descend through the electric reactor tubes, with gases released during this process exiting from the top of the tube. A notable integration of this technology is the LEILAC (Low Emissions Intensity Lime and Cement) project [3, 5], which allows for the capture of released CO_2 from the top, significantly simplifying carbon capture. The core flash electric calcination technology developed by Calix is also applicable to alumina calcination. In this process, steam released during calcination exits from the top of the reactor as a pure stream, which can be efficiently recovered and reused within the system [6]. However, this technology

is currently limited to pilot-scale testing. A pilot-scale electric calciner located in Victoria, was designed to test feed gibbets samples at a rate of 0.06 to 0.144 t/hr [6]. The system is used to evaluate the quality of calcined samples based on parameters such as loss on ignition (LOI), surface area, and the absence of undesirable α-alumina phases. Tests have been conducted across a wall temperature from 900 to 1120 °C, demonstrating promising results in producing high-quality alumina. However, there is no studies evaluating the technical viability of the potential in retrofitting with full-scale alumina calcination. Conventional alumina calciners, such as flash or circulating fluidised bed (CFB) systems, rely on natural gas/air combustion. In these designs, air serves both as a combustion medium and as a transport agent for moving particles through the process. In contrast, Calix's electric calcination technology delivers heat indirectly via externally heated reactor walls, removing direct combustion in calciner. To support particle transport and maintain volumetric flow rates comparable to those in conventional calcination processes, superheated steam exiting the system is redirected back into the calcination stage, where it functions as the carrier gas [7]. This introduces a pure steam environment, which differs from air environment. Therefore, this study aims to evaluate the technical feasibility of retrofitting existing alumina calcination processes with Calix's flash electric calcination technology integrated with steam recovery and assess the calcination performance, with a particular focus on quantifying the exit steam from the calcination pathway.

2. Methodology

2.1 Retrofitted fully electrified calcination integrated with calix technology

Figure S1 shows the retrofitted electrified configuration. The boehmite solids separated from Cyclone 2 are conveyed to the top of the electric calciner. Figure S2 presents Calix's pilot-scale electric flash calcination reactor. To integrate it into the existing alumina calcination process, the conventional main furnace is replaced by the calix electric calciner. Given the

capacity limitations of a single large-scale electric calciner, achieving industrial throughput may require the use of multiple drop-tube reactors, whereas current demonstrations typically illustrate only a single reactor for conceptual representation. The calcined alumina exits from the bottom of the reactor, while the generated steam exits from the top. Air is not introduced into the system, and instead, a portion of the exiting steam is recycled as the carrier gas to maintain volumetric flow rates comparable to those in conventional air-based calcination. The recycled steam mass flow is adjusted to ensure consistent gas velocities entering the cyclones, preserving cyclone performance and separation efficiency. Remaining steam is directed to digestion step following a steam recovery process. Due to the pressure drop caused by the cyclone system, a first-stage compression step, utilising either a blower or steam ejector, is used to support continuous steam circulation. Additionally, an electric steam heater is employed to raise the temperature of steam entering Cyclone 2, supplying the thermal energy required for the preheating stage. Under a pure steam environment, the conversion of gibbsite to boehmite may be inhibited [8-10]. An additional Cyclone 1.1 is introduced to enhance the heat transfer efficiency between particles and steam in preheating stage.

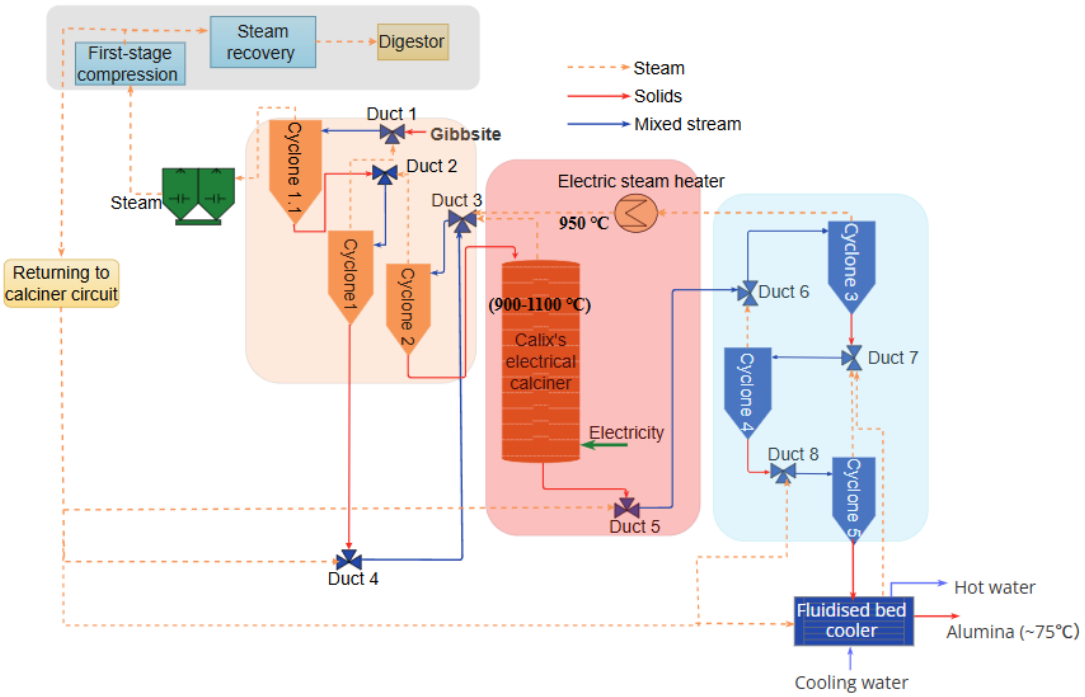


Figure S1. Retrofitted alumina calcination with Calix electric calciner technology.

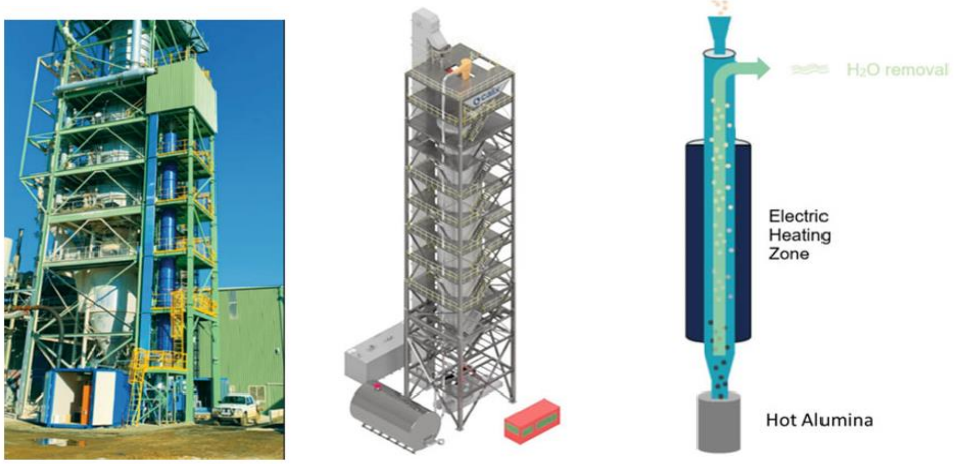


Figure S2. Calix's pilot electric flash calcination reactor. [6]

2.2 Process modelling

The calcination process under fully electrified calcination, as shown in Figure 1 was modelled in the Aspen Plus, with Figure S3 presenting the developed model. A summary of the key parameter assumptions for each unit operation is provided in Table S1. Gas-solid separation efficiency and cyclone pressure drops were calculated using the Shepherd & Lapple method [11, 12]. The total heat losses were estimated at approximately 4% of the total energy input and were distributed proportionally across the system, with the majority attributed to the main furnace and the preheating furnace.

Table S1. Process modelling parameters assumptions for retrofitted electrified calcination

	Retrofitted fully electrified calcination
Electrical steam heater	• Simulated by a heater, with the temperature setting from 900 to 1100°C. varying the outlet temperature to see the effects on overall calcination. • With a typical 95% efficiency [13].
Calix electrical calciner	Simulated by connected Rstoic model and components separator model • A Rstoic reactor model was used to simulate boehmite to alumina, with the outlet temperature varied between 900°C and 1100°C, consistent with the temperature range in pilot-scale experiments[6]. • Components separator was used to separate solids and gas
Cyclone 1.1	• Simulated using a Stairmand-HT type cyclone • The diameter of the cyclone was set to 4 meters
Cyclone 2	• Same simulation method was applied as for Cyclone 2 in the conventional calcination case. • Reaction kinetics for the boehmite-to-alumina transformation under steam environment were based on the model developed by Saw, L.W., and T.C. Tsai et al.[10]. With expected conversion of approximately 66-76% under steam environment.

- Parameter setting of other units is same with natural gas/air calcination in chapter 3.
- The Calix electric calciner is modelled with an assumed efficiency ranging from 90% to 98% to evaluate its impact on overall energy consumption.

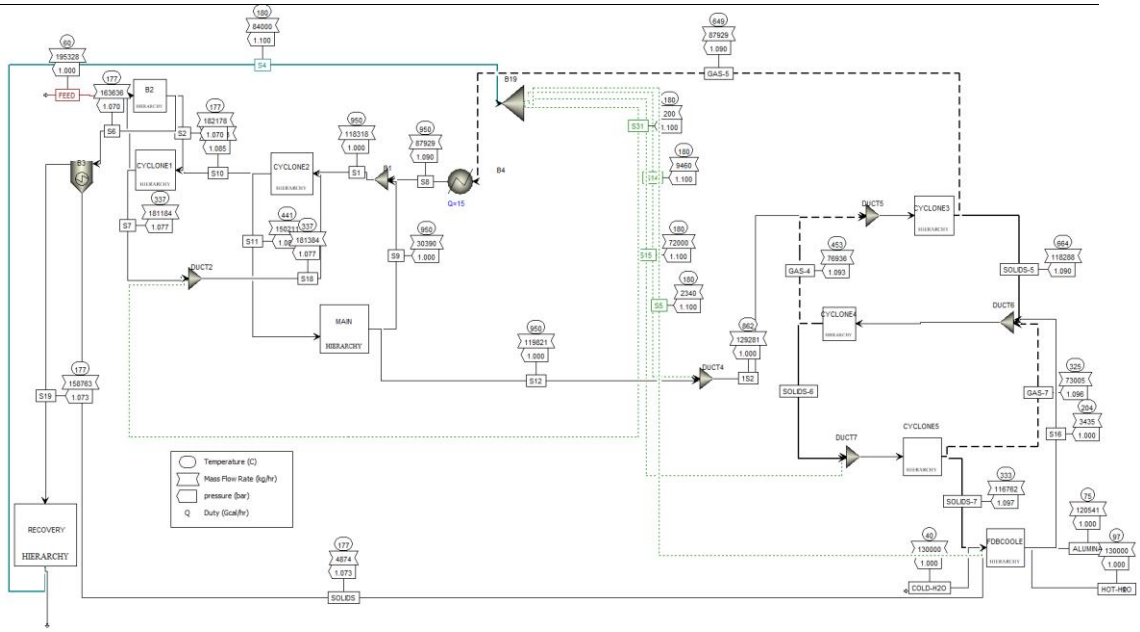


Figure S3. Aspen Process model of electrified calcination

3. Results

3.1 Technical results

Figure S4(a) presents the electric capacity required of the electric calcination system. A moderate increase in total electric power input is observed as the E-calciner wall temperature rises from 900°C to 1100°C, increasing from 90 MW to 95 MW. This increase is attributed to a higher load on the E-calciner. From the pilot experiment data [6], the flash electric calciner operating at 900°C enables the production of alumina with a relatively high specific surface area (SSA) of 120-140 m^2/kg, although it results in a loss on ignition (LOI) of approximately 3%. In contrast, increasing the wall temperature to 1050-1100°C reduces the LOI to below 1%,

but lowers the SSA to 60-80 m^2/kg, indicating a trade-off between the product quality. The specific energy consumption increases with wall temperature, from 2.73 to 2.86 GJ/t_{Al2O3}, reflecting reduced efficiency due to greater thermal losses at higher wall temperatures. A modest overall heating efficiency of 90% is assumed in this analysis. As shown in figure S4(b), higher wall temperatures also lead to raised exit steam temperature from 171°C to 194°C. Figure S4(c) presents the exit pure, comprising 84 t/hr of recirculated steam acting as the carrier gas, and 76 t/hr (0.63 t/t_{Al2O3}) of recoverable steam, offering significant potential for direct steam recovery.

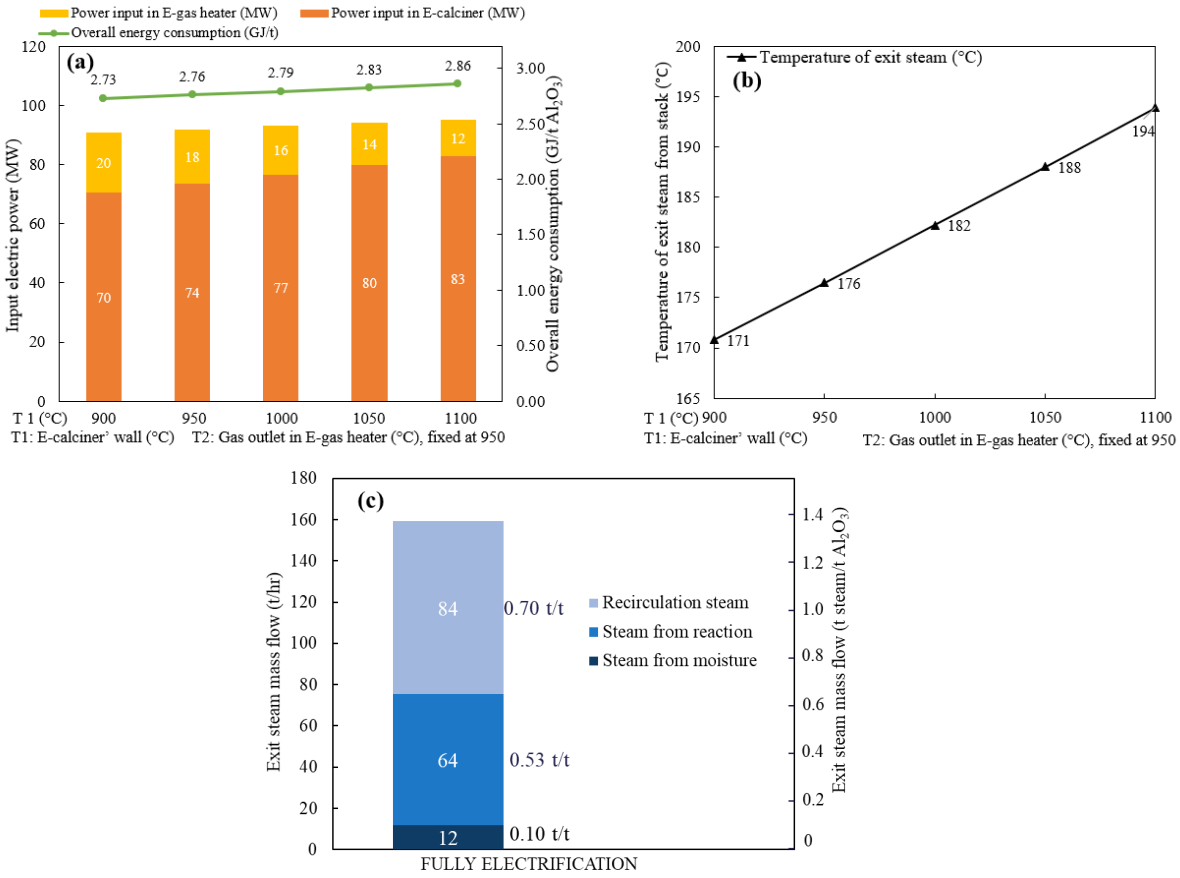


Figure S4. Calculated electric power consumption (a), exit pure steam temperature (b) and amount (c) under varied e-calciner wall temperature.

3.2 Comparison of calcination process performance

Figure S5(a) compares the volumetric gas flow rates across each cyclone for the conventional natural gas calcination system and the retrofitted fully electrified calcination. The

results present the closely matched flow rates, with only minor differences observed at Cyclones 1 and 2. The holding vessel (HV is removed in the electrified system due to the Calix electric calciner's design, which separates gas and solids vertically, with gases exiting from the top and solids discharged from the bottom. Cyclones 3 to 5 exhibit close flow behaviour, with steam recirculation. Figure S5(b) presents the separation efficiencies of cyclones, all of which maintain comparable efficiencies exceeding 97% under electrified calcination and natural gas/air combustion.

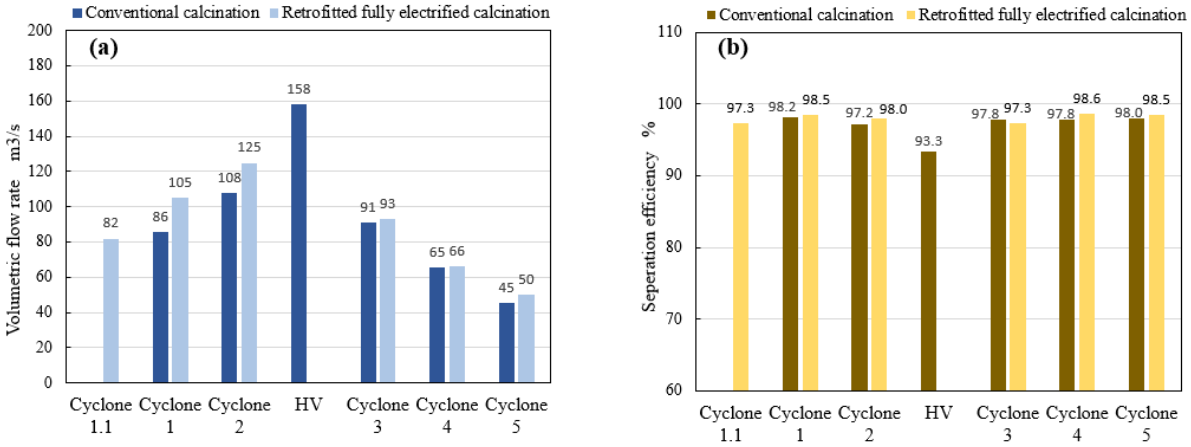


Figure S5. The volumetric flow rates (a) and calculated separation efficiency (b) of cyclones in conventional natural gas/air and retrofitted fully electrified calcination.

3.3 Effects of heating efficiency and gibbsite conversion in Cyclone 2 on energy consumption

Figure S6 illustrates the influence of gibbsite conversion rate and E-calciner heating efficiency on the overall energy consumption. Gibbsite-to-boehmite conversion has a significant effect on the system's power demand. Based on current reaction kinetics, a gibbsite conversion rate of approximately 66%~76% is expected in Cyclone 2 under a pure steam atmosphere, in contrast to the 100% conversion typically achieved under air-based calcination. This observation suggests that steam may inhibit the transformation process, in agreement with experimental findings [8]. However, the available kinetic data is primarily derived from low heating rate experiments and low temperature, which differs from operating conditions of industrial calciners under high-temperature, rapid-heating. Therefore, a sensitivity was

conducted, showing that varying the gibbsite conversion rate from 100% to 0% leads to an increase in overall energy consumption, rising from 2.6 GJ/$t_{Al_2O_3}$ to 3.2 GJ/$t_{Al_2O_3}$. Simultaneously, the heating efficiency of the E-calciner also has a significant impact on power consumption. For instance, at a representative gibbsite conversion rate of 76%, the specific energy consumption decreases from 2.76 GJ/$t_{Al_2O_3}$ at 90% efficiency to 2.58 GJ/$t_{Al_2O_3}$ at 98% efficiency. As the significant impact of heating efficiency, further research is recommended to develop a detailed heat transfer model between the solid particles and the heated wall, with the aim of accurately estimating the overall heating efficiency from electricity to particles in the calciner.

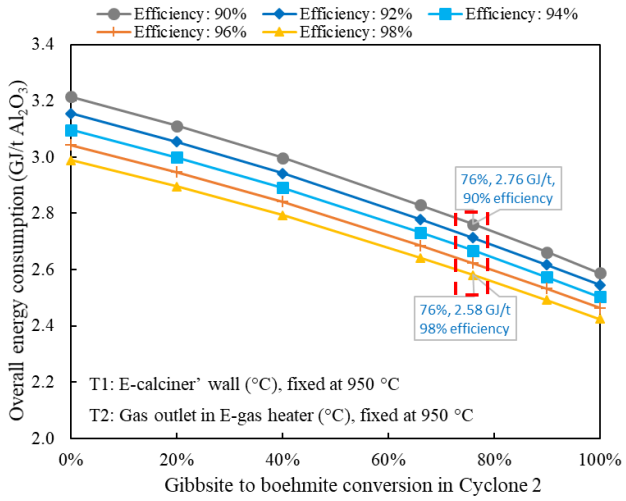


Figure S6. Effects of heating efficiency of E-calciner and gibbsite conversion on overall energy consumption.

5. Conclusions and recommended further work

The fully electrified system demonstrates comparable overall energy consumption to conventional natural gas/air combustion, with values of 2.76 GJ/$t_{Al_2O_3}$ under an operating temperature of 950°C for both the E-calciner (assumed 90% heating efficiency) and E-gas heater (95% efficiency). Overall energy demand is sensitive to E-calciner heating efficiency. Increasing the heating efficiency from 90% to 98% can yield a potential energy saving of up to 0.2 GJ/$t_{Al_2O_3}$. Furthermore, despite differences in carrier gas composition (air vs. recirculated

steam), the volumetric gas flow rates through the cyclone stages remained similar in both systems, resulting in comparable separation efficiencies consistently above 97%.

The chapter presents a preliminary process modelling for retrofitting alumina calcination for fully electrification by integrating Calix technology. One of missing content is to estimate the potential scaling challenge of Calix drop-tube reactor. For example, heat transfer efficiency between solid and wall of the scaled-up reactor. It is recommended to develop a detailed heat transfer model between wall and solids of the reactor. In addition, the large power requirement of the electric calciner, up to 80 MW, poses a significant technical barrier. Partial electrification of the calcination process is recommended for future research, offering a more practical pathway to decarbonisation.

6. References

[1] Michael Barnes J N, Kushagra Bosamia, Decarbonisation of the Bayer Process – A Technical Assessment of Enabling Technologies and Process Economics, in the 42nd International ICSOBA Conference. 2024: Lyon, France.

[2] ARENA. A Roadmap for Decarbonising Australian Alumina Refining. https://arena.gov.au/knowledge-bank/a-roadmap-for-decarbonising-australian-alumina-refining/. 2022 [accessed on 15 June 2025].

[3] Limited A. Next Generation Carbon Capture Technology. https://assets.publishing.service.gov.uk/media/6294923ce90e07039e31b777/aecom-next-gen-carbon-capture-technology-technoeconomic-analysis.pdf. 2022 [accessed on 8 July 2025].

[4] Engineering C. CALIX – Zero Emissions Steel Technology (ZESTY). https://arena.gov.au/assets/2024/05/Calix-Zesty-Tech-%E2%80%93-Zero-Emissions-Iron-and-Steel-study-and-final-reports.pdf. 2024 [accessed on 9 October 2025].

[5] Hills T P, Sceats M, Rennie D, and Fennell P. LEILAC: Low cost CO2 capture for the cement and lime industries. Energy procedia, 2017. 114: p. 6166-6170.

[6] Wheatland M, Fu J, Xia Y, Boot-Handford M, and Sceats M, An Innovative Approach to Smelter-Grade Alumina Calcination Using Renewable Energy, in TMS Annual Meeting & Exhibition 2024. 2024: Orlando, Florida, USA. p. 38-45.

[7] Saw W L, Nathan G J, Chatfield R V, and Haywood R J, Method and Apparatus for Alumina Calcination 2022 17 June 2022. WO2022261726A1. https://patentimages.storage.googleapis.com/b3/bd/c3/d31d8a0f599297/WO2022261726A1.pdf.

[8] Candela L, Perlmutter, D.D. Kinetics of boehmite formation by thermal decomposition of gibbsite. Industrial & engineering chemistry research, 1992. 31(3): p. 694-700. https://doi.org/10.1021/ie00003a007.

[9] Stacey M. Kinetics of decomposition of gibbsite and boehmite and the characterization of the porous products. Langmuir, 1987. 3(5): p. 681-686.

[10] Saw W L, Lee L, Ingenhoven P, Chinnici A, Zhang X, Rafique M, Tang Y, Tung D A J, Tsai T C, He Z, Smadi E A, Tian Z F, Lau T, Sun Z, Chin R, Eyk P v, Dally B, and Nathan G. Integrating Concentrating Solar Thermal Energy into the Bayer Alumina Process. https://arena.gov.au/assets/2024/07/Univeristy-of-Adelaide-Integrating-Concentrating-Solar-Thermal-Energy-into-the-Bayer-Alumina-Process-Final-report.pdf. 2023 [accessed on 8 March 2025].

[11] Stairmand C J. The design and performance of cyclone separators. Trans. Inst. Chem. Engrs., 1951. 29: p. 356-362.

[12] Shephered C and Lapple C. Flow pattern and pressure drop in cyclone dust collectors. Industrial & Engineering Chemistry, 1939. 31(8): p. 972-984. https://doi.org/10.1021/ie50356a012.
[13] Micropyretics Heaters International (MHI). Electric Airtorch. https://mhi-inc.com/electric-airtorch-process-gas-heaters-industrial-heat-decarbonize/. [accessed on 6 June 2025].